EFFECT OF FREE STREAM TURBULENCE ON BOUNDARY LAYER TRANSITION

Mohamed Salah Eldin
ABDEL-KAREEM

Department of Aeronautics,
Imperial College of Science and Technology

A Thesis Submitted for the Degree of
Doctor of Philosophy of the University of London

December, 1978

ABSTRACT

This is an experimental study of the effect of free stream grid turbulence with intensity of 0.01 - 0.06 on the position of transition and the development of the laminar-transitional boundary layer over the surface of a flat plate. Transition is found to correlate with a modified Taylor's parameter of the form:-

$$\frac{u}{U}\left(\frac{\theta}{L_x}\right)^{1/6}$$

The plate thickness and the geometry of the leading edge are found to play an important role in determining the position of transition.

The mean velocity profiles are found to have a wavy shape with a tendency to develop a point of inflexion just prior to breakdown.

Averages of the different turbulent quantities are also reported together with the development of different terms in the turbulent energy equation throughout the range studied.

Finally, a comparative study of oscillograph plots of hot-wire output and their respective power spectra, together with an experimental study of the statistics of the turbulent burst formation within the range of the experiment are presented. The suggestion is made that the free stream turbulence may play a major role in interfering with the instability processes of the laminar boundary layer only during the early stages of the latter's development over the surface of the plate where the turbulent energies of both regions are still of comparable magnitudes. Prior to transition, the turbulent energy in the free stream seems to be only a small fraction of that already in the developing boundary layer.

بسم الله الرحمن الرحيم

الحمد لله الذى هدانا لهذا و ما كنا

لنهتدى لولا أن هدانا الله

In the name of God, Most Gracious,

Most Merciful

Praise be to God, who hath guided us to this,

never could we have found guidance, had it not

been for the guidance of God.

ACKNOWLEDGEMENTS

The author would like to express his thanks to his supervisor, Dr. J. M. R. Graham, for the many stimulating discussions and the numerous helpful suggestions which he has made in the course of the present study.

I would also like to thank the members of the academic staff (at the Aeronautics Department, Imperial College) who helped in various ways especially Dr. H. Mahgoub and Mr. I. Shabaka for the many helpful discussions we had together whilst the study was in progress.

I would also like to express my thanks to Mr. J. Beasley, Mr. J. Coles, Mr. T. Lye and Mr. C. P. McAra for the careful construction of the models used, to Mr. M. L. Eals for his patient care of the electronic equipment used and to Mr. J. O'Leary for taking the photographs.

Finally, a special mention of Mrs. H. A. Bastin for typing the thesis so efficiently and at a very high speed (in contrast with my low speed stuff), a thing that had a favourable effect on my blood pressure during the final stages of producing the thesis.

LIST OF CONTENTS

		Page
ABSTRACT		ii
ACKNOWLEDGEMENTS		iv
LIST OF CONTENTS		v
LIST OF SYMBOLS		x
LIST OF ABBREVIATIONS		xi
CHAPTER 1	INTRODUCTION	1
CHAPTER 2	MEASURING EQUIPMENT AND TECHNIQUES	16
2.1	Wind Tunnel	16
2.2	Traverse Gear	16
2.3	Model	18
2.4	Velocity Measurement	23
2.4.1	Using the Pitot Tube	23
2.4.2	Using the Hot-Wire Anemometer	23
2.5	Pressure Measurements	27
2.5.1	Static Pressure Measurements	27
2.5.2	Total Pressure Measurements	29
2.6	Skin Friction Measurements	29
2.7	Free-Stream Turbulence Generation	30
2.8	Detection of Place of Transition	31
2.9	Analogue Signal Recording and Digitisation	35
2.9.1	Analogue Signal Recording	35
2.9.2	Analogue Signal Digitisation	36
2.10	Sound Pressure Measurements Using Electronic Apparatus	39
2.11	Alignment of Plate With Flow Direction	39

		Page
CHAPTER 3	DATA PROCESSING TECHNIQUES AND THE UNDERLYING THEORETICAL BASES	41
3.1	Determination of the Mean (Longitudinal) and the Fluctuating Turbulent Quantities	41
	3.1.1 From the Output of a U-Wire	41
	3.1.2 From the Output of an X-Wire	42
	3.1.3 From the Output of a Double-Wire	43
3.2	Determination of the Mean Velocity Component Normal to the Plate Inside the Boundary Layer	45
3.3	Computation of the Different Terms in the Turbulent Energy Equation	46
3.4	Determination of the Boundary Layer Parameters	51
3.5	Determination of the Position of the First Measuring Station Relative to the Wall	52
3.6	Burst Intermittency Detection	55
3.7	The Power Spectral Analysis	59
3.8	Estimation of the Convection Velocity for the Disturbances of Different Wave Numbers Inside a Boundary Layer	61
3.9	The Static Pressure Distribution Around the Nose-Plate Combination Using the Potential Flow Theory	69
3.10	Determination of the Longitudinal Integral Length Scale of Turbulence (L_x)	70
3.11	Data Smoothing	72
CHAPTER 4	GENERAL PROPERTIES OF THE FLOW FIELD IN THE EXPERIMENT	73
4.1	The Sound Pressure Level Inside the Tunnel	73
4.2	Temperature Drift Inside the Tunnel Due to Prolonged Tunnel Operation	75
4.3	Static Pressure Distribution Over the Plate	77
4.4	The Nature of the Flow Behind the Turbulence Producing Grids	79

		Page
4.5	The Longitudinal Integral Scale of Grid Produced Turbulence	83
4.6	Changes in the Characteristics of the Mean and the Fluctuating Velocity Profiles Through the Laminar Boundary Layer Induced by Changes in the Plate Thickness	84
4.7	Homogeneous Turbulent Flow Past the Flat Plate	85
CHAPTER 5	PARAMETERS AFFECTING TRANSITION OF A LAMINAR BOUNDARY LAYER OVER A FLAT PLATE	90
5.1	Introduction	90
5.2	Effect of Free Stream Turbulence on Transition	91
5.2.1	Effect of the Free Stream Turbulence Intensity ($\sqrt{\overline{u^2}}/U$)	91
5.2.2	Effect of the Integral Length Scale (L_x)	93
5.2.3	Transition Parameter	94
5.3	Effect of Change in the Plate Thickness on Transition	98
5.3.1	Effect of Changes in the Free Stream Turbulence Characteristics Induced by Changes in the Plate Thickness on Transition	98
5.3.2	Effect of Changes in the Plate Thickness on Transition as Reflected Through the Induced Changes in the Pressure Distribution Over the Nose Section	100
CHAPTER 6	LAMINAR-TRANSITIONAL BOUNDARY LAYER BENEATH A TURBULENT FREE STREAM	111
6.1	Introduction	111
6.2	The Laminar-Transitional Boundary Layer Beneath a Free Stream Turbulence of Different Intensities and Length Scale	112
6.2.1	The Wall Friction Measurements	112
6.2.2	The Mean Velocity Profiles	114

			Page
	6.2.3	The Boundary Layer Parameters	119
		(a) The Boundary Layer Thickness (δ)	119
		(b) The Boundary Layer Shape Factor (H)	120
		(c) The Wall Shear Stress Coefficient (C_f)	121
	6.2.4	The Streamwise Turbulent Velocity Profiles	122
6.3	The Development of the Laminar-Transitional Boundary Layer Beneath a Turbulent Free Stream of Nearly Constant Intensity		124
	6.3.1	The Mean Velocity Distribution in the Working Section Over the Plate	125
	6.3.2	The Distribution of Wall Shear Stress Over the Plate	125
	6.3.3	The Mean Velocity Profiles Throughout the Boundary Layer	126
	6.3.4	The Development of the Profiles of the Turbulent Velocity Components Along the Plate	131
	6.3.5	The Development of the Turbulent Kinetic Energy ($\overline{q^2}$) Inside the Boundary Layer Along the Plate Surface	133
	6.3.6	The Development of the Reynolds Stress ($\overline{uv}$) Profiles Through the Laminar Transitional Layer	134
	6.3.7	The Triple Products of the Turbulent Velocity Components in the Laminar-Transitional Layer	136
	6.3.8	The Evolution of the Turbulent Energy Within the Laminar-Transitional Layer	138
CHAPTER 7	MECHANICS OF TRANSITION		146
7.1	Introduction		146
7.2	Hot-Wire Oscillogram Records Throughout the Laminar-Transitional Boundary Layer		146
7.3	Statistical Study of Burst Formation Within a Boundary Layer		152

		Page
7.4	Development of the Energy at Different Wave Numbers Within the Laminar-Transitional Boundary Layer Beneath a Turbulent Free Stream of Varying Intensity	155
7.5	Development of the Energy at Different Wave Numbers Within the Laminar-Transitional Boundary Layer Beneath a Turbulent Free Stream of Nearly Constant Intensity	158
CHAPTER 8	CONCLUDING REMARKS	165
APPENDIX I	COMPUTER ROUTINE FOR THE BURST INTERMITTENCY DETECTION	172
APPENDIX II	INVESTIGATION OF THE EFFECT OF THE INTENSITY AND THE LENGTH SCALE OF THE FREE STREAM TURBULENCE ON THE LAMINAR BOUNDARY LAYER OVER A FLAT PLATE; A MODIFICATION OF TAYLOR'S PARAMETER	175
REFERENCES		179
FIGURES		192

LIST OF SYMBOLS

b	Half the minor axis of an ellipse.
C_f	Skin friction coefficient.
C_p	Pressure coefficient.
F	Function.
f	Frequency.
g	Gravitational acceleration.
I	Moment of inertia.
L	Integral length scale of turbulence.
ℓ	Length scale of the large eddies.
M	Grid mesh size.
P	Pressure.
$\overline{q^2}$	Turbulent kinetic energy.
R	Reynolds number.
T	Temperature.
t	Plate thickness.
U, u	Mean and fluctuating velocity components in the x-direction.
V, v	Mean and fluctuating velocity components in the y-direction.
w	Fluctuating velocity component in the z-direction.
x	Streamwise direction.
y	Direction normal to the plate surface.
z	Spanwise direction.

Greek

α	Incidence.
γ	Intermittency.
δ	Boundary layer thickness.
ϵ	Viscous dissipation.

η	Length scale of the smallest eddies.
λ, Λ	Pohlhausen parameter $\frac{\theta^2 \text{ (or } \delta^2)}{\mu U} \cdot \frac{\partial P}{\partial x}$
μ	Viscosity.
ν	Kinematic viscosity.
θ	Boundary layer momentum thickness.
π	3.1415 9265.
ρ	Density.
τ	Time.
ω	Wave number.

Subscript

G	Grid.
n	Nose section.
T	Transition.
x	Distance to leading edge.
θ	Boundary layer momentum thickness.

List of Abbreviations

BL	Boundary Layer.
FFT	Fast Fourier Transform.
FST	Free Stream Turbulence.
KE	Kinetic Energy.
LBL	Laminar Boundary Layer.
LE	Leading Edge.
PG	Pressure Gradient.
Re	Reynolds number.
R_{x_T}	Reynolds number of Transition $\left\{\frac{U_\infty x_T}{\nu}\right\}$.
R_{θ_T}	Reynolds number of Transition $\left\{\frac{U_\infty \theta_T}{\nu}\right\}$.

TBL	Turbulent Boundary Layer.
TE	Trailing Edge.
2D	Two-dimensional.
3D	Three-dimensional.

CHAPTER 1

INTRODUCTION

Ever since the time of Reynolds, about a hundred years ago when the transition of the pipe flow was first detected, until now, this subject has preoccupied many workers in the field of fluid mechanics. In fact, the increasing efforts which have been and are being devoted to the study of this phenomenon, have up until now served to demonstrate the complexity of this process of transition. So much so that it can rightly be said that transition seems to be less understood now than it has seemed to the workers in the field say forty years ago. The truth of this statement is demonstrated by the fact that the research during the past forty years has not only revealed an increasing number of factors that may simultaneously affect the process of transition in an unpredictable way, but it has also persuaded some investigators to keep their minds open to the possibility that "the mechanism and the modes of transition might after all not be unique" (Morkovin, 1978).

We now realise that boundary layer transition is very sensitive to parameters which may not necessarily affect the average properties of the laminar boundary layer or the turbulent boundary layer, e.g. small velocity fluctuations, wall vibrations, low level sound field, wall waviness, leading edge irregularities, small isolated roughness elements and in the case of supersonic speeds, entropy fluctuations and temperature spottiness may also be added. There are also other parameters which may leave their marks on the average properties of the laminar boundary layer or the turbulent boundary layer such as high intensity free stream turbulence and pressure gradient.

The problem is that most of these factors are quite hard to measure and they are likely to be present with varying degrees in nearly

all the experimental and practical flow situations where their effects may accumulate in different and non-linear ways.

In an attempt to sift such numerous factors, Morkovin (1958) argues that one should keep in mind the possibilities of multiple responsibility and dominant responsibility of the flow features promoting transition.

By the late forties, it was widely believed that, depending on the amount of disturbance in the free stream, two existing theories explained adequately most of the processes involved in the transition of boundary layers.

The first theory regards the laminar boundary layer as a medium capable of "natural oscillations" around its mean. Approximate calculations of such oscillatory motions were feasible by linearising the governing Navier-Stokes equations into the form known as the Orr-Sommerfield equations and finding their eigenvalues. The solutions are known as the Tollmien-Schlichting waves.

The theory went on to say that small disturbances in the flow would tend to excite these Tollmien-Schlichting waves and would amplify or damp according to the value of the Reynolds number, and once the amplification had started, the disturbance would absorb energy from the mean flow until they caused the final breakdown of the laminar flow into turbulence.

Schubauer et al (1948) confirmed experimentally (using the vibrating ribbon technique) the existence of the Tollmien-Schlichting waves in the laminar boundary layer before transition with free stream turbulence of intensity 0.02%*. They also observed that in the case of

---

* In fact, they pointed out that transition was unaffected by any reduction in the free stream turbulence below 0.08%, a result that was qualitatively confirmed by Spangler et al (1968).

disturbances with a wide spectrum, only that part predicted by the linearised theory was amplified. Although the Tollmein-Schlichting waves can be three-dimensional since oscillation in the boundary layer may occur at all orientations, yet a theorem by Squire (1933) stated that, at incompressible speeds, a skew wave is always more stable than the corresponding two-dimensional Tollmien-Schlichting wave. (It is interesting that for supersonic speeds skew waves were observed to amplify more rapidly than streamwise waves, Morkovin, 1978).

As for the critical Reynolds number for the amplification of small disturbance, Schubauer et al (1956) generated artificial turbulent spots by spark discharge in the laminar boundary layer. The sparks were always strong enough to create turbulence locally at all Reynolds numbers. However, turbulence only propagated into the surrounding laminar flow when the Reynolds number exceeded the critical value predicted by the stability theory.

The second theory was put forward by G. I. Taylor (1936) which assumed that the finite disturbances in the free stream were the principle factor in causing transition. That is, transition is caused by momentary separation (or points of inflexion in the velocity profiles) in the region of adverse pressure gradient associated with the turbulent velocity fluctuations at sufficiently large values of the Karman-Pohlhausen parameter $\left(\frac{\delta^2}{\mu U} \cdot \frac{dP}{dx}\right)$. Using this assumption, Taylor was able to show that the critical Reynolds number of transition was a function of $\frac{u}{U}\left(\frac{X}{M}\right)^{1/5}$. Taylor found that his theory correlated with the transition on a sphere reasonably well. Also Schubauer (1938) successfully applied this theory to transition over elliptic cylinders.

Although some doubt was levelled against the theory by the fact that it failed to correlate transition over the flat plate in the experiment of Hall et al (1938) despite the fact that the theory was

basically for flat plates. Yet, it was held by some investigators, notably Dryden (1947), to account for transition at high free stream turbulence levels of 0.5% and over, especially as Schubauer et al (1940) reported that at free stream turbulence levels higher than 0.02%, the Tollmien-Schlichting waves were still there but were very difficult to detect due to the presence of irregular fluctuations and the short distance between the appearance of these oscillations and transition.

In fact, in an attempt to improve Taylor's correlation of the transition results, Fage et al (1941) suggested the use of the local parameter (θ/L_x) at transition instead of (X/M) in Taylor's parameter where X is the distance from the plate leading edge and M is the grid mesh size. But, to the best of my knowledge, the usefulness of this suggestion was not tried.

As the hot-wire technique developed, the accuracy of detecting the oscillations in the boundary layer increased until Bennett (1953) was able to observe a considerable amplification of that part of the spectrum predicted by the stability theory before transition developed beneath a free stream turbulence of intensity 0.42%.

Moreover, Klebanoff et al (1959) found no sign of intermittent separation before transition even at a free stream turbulence of 0.8%.

Also, Klebanoff et al (1959) and others observed that transition to turbulence generally occurred much later than the critical Reynolds number predicted by the stability theory. Schubauer et al (1955), Hama et al (1957), Dhawan et al (1958) and Klebanoff et al (1962) and many others observe that in the boundary layers at any given time, transition does not occur at the same (X) across the span, but rather has a three-dimensional and unsteady character. In fact, Charters (1943) found that behind a fixed local disturbance, tongues of turbulent flow appeared contaminating only the adjacent laminar flow at a near constant

angle and did not trigger transition across the span.

Added to this was the fact that, it had become known that from the point where the breakdown of the amplified disturbance started up to the point where the boundary layer was fully turbulent, there was a region where the non-linear processes dominated the flow development in a manner not predictable by the linearised theory.

These observations have led the supporters of each of the two theories to modify their stands. Hence, the stability theory was restricted to accounting for the initial stages of boundary layer transition while the question concerning its applicability in the case of high free stream turbulence levels was left unanswered.

On the other hand, nearly all the investigators (such as Wells (1967), Hall (1968), Spangler et al (1968) and Michel (1974) and others) correlated their transition results with the free stream turbulence intensity directly and did not use Taylor's parameter at all. While some other investigators reported more scatter when their transition results were correlated with Taylor's parameter rather than the free stream turbulence intensity directly (e.g. Hall et al (1972) and McKeough, 1976).

Recognition of the intermittent character of the breakdown of the laminar boundary layer directed the attention to the fundamental processes involved. The observations and theoretical work of Emmons (1951) and the experiments of Tani et al (1953), Mitchener (1954), Schubauer et al (1955), Hama et al (1957) and Dhawan et al (1958) and others showed that transition in a boundary layer is characterised by intermittent appearance of turbulent spots moving downstream with the fluid.

Until now, the mechanism of spot formation has not been completely clear. Nevertheless, the experimental observations and flow

visualisation of Webb et al (1956), Hama et al (1957), Schubauer (1957), Klebanoff et al (1959) and Klebanoff (1962) suggest that the amplification of the two-dimensional Tollmien-Schlichting waves becomes associated at some stage with the concentration of vorticity along discrete lines which subsequently distort into vortex loops in the boundary layer. The above investigators observed that, in shear flows, two-dimensional vortex lines tend to form strong three-dimensional vortex loops or what was termed by Chen et al (1971) as spanwise peak-valley development. These vortex loops themselves go through a process of distortion and extension finally resulting in the creation of spots of turbulence which take place nearly at the top of the vortex loop. Once created, these spots are swept along with the mean flow growing laterally as well as axially with laminar flow in their trail. The spots originate in a more or less random fashion, and at first, their growth is non-linear but further downstream they assume a nearly linear manner of growth until they merge and completely fill the flow.

All this can be considered reasonable as long as all the sources of disturbance mentioned earlier in this chapter are carefully isolated, for if they are not, the picture drawn in the above paragraph becomes increasingly less certain.

The earliest known major parameters that may affect the process of transition in a laminar boundary layer are the free stream turbulence, the pressure gradient, the leading edge shape and perhaps the surface roughness together with the relatively later known factor of acoustic waves.

Such factors draw attention to the new issue of the boundary layer receptivity which denotes the means by which a particular forced disturbance enters the boundary layer and the nature of its signature on it. We already know that if such a disturbance is small, it will

tend to excite the boundary layer natural modes (i.e. the Tollmien-Schlichting waves). But if it is large enough, it "can grow by forcing mechanisms to non-linear levels and lead directly to turbulent flow" (Reshotko, 1976). In other words, the problem in this case is not an eigenvalue problem.

As for the effects of free stream turbulence on the laminar boundary layer transition, we are faced with an interesting situation. Beneath a turbulent free stream, a "laminar boundary layer may be highly randomly agitated and yet retain laminar behaviour" (Schubauer (1957), Morkovin (1958) and Tani, 1969).

Both the dimensional analysis and the experiments have for long suggested the importance of two free stream turbulence parameters, namely, the intensity and the length scale. Here, the old question poses itself again: "Is the effect of the free stream turbulence on the transition of the laminar boundary layer local and, therefore, can be correlated by something like Taylor's parameter, or is its effect to interfere with the process of exciting the Tollmien-Schlichting waves and/or the process of forming the turbulent bursts, thus accelerating the two processes and shortening the regions of the laminar boundary layer and/or the transitional boundary layer?" And if it is the second effect, will it be a local effect or a continuous process of interfering with the development of the instability modes of the boundary layer?

The failure of Taylor's parameter to correlate the reported experimental results (quoted earlier on in this chapter) weakens the position of such a theory. While also Hall et al (1972) believe that local values are insufficient to correlate the conditions of the boundary layer to the likelihood of transition and some knowledge of the previous history of the flow must be included, e.g. the history of

θ, u/U or the pressure gradient.

In fact, the question of what is the right value of u/U to use in Taylor's parameter is quite an interesting one. Is it the value at the leading edge of the flat plate or that value just outside the boundary layer at transition or that value at transition but away from the boundary layer edge? The fact that the grid turbulence decays in the downstream direction makes the first two different, while the theoretical finding of Hunt and Graham (1978) (that just outside the boundary layer over the flat plate, the turbulence intensity is in fact less than its value further away from the wall) makes the third value different from the other two.

Also Bradshaw (1974), Tsuji et al (1975) and Thomas et al (1977) believe that the conditions in the inner layer of the turbulent boundary layer are independent of the free stream turbulence if the Reynolds number is high enough. The question now is, would the effect of the free stream turbulence develop from causing local separation at transition to that situation argued by the above investigators for the turbulent boundary layer?

On the other hand, Morkovin (1958) and Rogler et al (1975) believe that although the stability theory does not directly incorporate the properties of the free stream turbulence field, yet these properties are implicitly recognised since the Tollmien-Schlichting waves are sensitive to a wave number range that is usually within the range covered by the free stream turbulence field, and that (as hot-wire observations indicate that the free stream turbulence decays as it is convected into the growing laminar boundary layer and assimilated by it) the free stream turbulence will serve to initiate disturbance inside the laminar boundary layer which, depending on its amplitude and Reynolds number, will amplify or decay according to the stability

theory (or if its amplitude is large enough, the disturbance will grow by forcing mechanisms).

Moreover, they argue that once the disturbance is introduced inside the laminar boundary layer, the free stream turbulence field is presumed to have no further influences on the development of the boundary layer.

Rogler et al (1975) on the other hand, cautiously indicate that the stability theory need not serve as the only possible mechanism for disturbance growth or decay inside the laminar boundary layer, for the same mechanism by which the disturbance is introduced into the layer may remain to influence subsequent development. Indeed, Chen et al (1971) claim that the disturbance spectrum affects not only the location of transition but also the frequency of spot formation, i.e. the extent of the transition zone.

In fact, Morkovin (1978) made the role of the stability theory in the case of turbulent free stream less certain by pointing out that the attachment stream line at the leading edge is very sensitive to small changes in v/U which tend to slosh it around.

Evidence that the instability of the laminar boundary layer with free stream turbulence may be less straight-forward than just being confined to the excitement of the Tollmien-Schlichting waves is given by Wortmann (1969) who, while studying the instability of the Görtler longitudinal vortices, found that first, a second order instability developed causing the mean velocity profile to develop two inflexion points, and then further downstream, a three-dimensional form of instability superimposed on the previous two-dimensional one developed just prior to breakdown. In another paper, Wortmann (1977) showed that in a flat plate laminar boundary layer just before breakdown, two-dimensional finite amplitude Tollmien-Schlichting waves tend

to form three-dimensional structures containing longitudinal counter-rotating vorticity sheets which are inclined downstream as they overlap each other leading to breakdown into turbulence.

Moreover, Gaster et al (1975) during an experimental investigation of the propagation of a wave packet generated by a short duration acoustic pulse in a laminar boundary layer observed some oblique modes growing over the original packet.

These are all evidence indicating that the linearised stability theory may just not be comprehensive enough to account for all the instability processes that may take place in practice.

There is also another question that remains unanswered regarding any possible effects of the "inactive" motion (Townsend (1961) and Bradshaw, 1967a, 1967b) induced by the free stream turbulence and/or the turbulence in the outer region of the boundary layer on the process of transition.

In fact, what gives both the two traditional theories on transition some credit is that, while they both anticipate transition as resulting from the existence of a position in the laminar boundary layer with an inflexional velocity profile in either a local or intermittent fashion, the experiments of Dhawan et al (1958), Klebanoff et al (1959), Klebanoff et al (1962), Wortmann (1969), Chen et al (1971) and Nishioka et al (1975) indicate that the spots are produced from mean or instantaneous velocity profiles with points of inflexion. Indeed, Kim et al (1971) observe that even in the process of turbulence production in the innermost layer of the turbulent boundary layer, a form of oscillatory breakdown of momentarily inflexional velocity profile is the mechanism responsible for such turbulence production.

The role of the free stream turbulence length scale needs some clarification. For while the general behaviour of this parameter is

expected to be as predicted by Taylor's parameter (i.e. transition is more promoted by smaller scale turbulence), yet Green (1972) argues that if the length scale is an order of magnitude larger than the boundary layer thickness, then we should expect the boundary layer to respond to the free stream turbulence as a large scale unsteadiness rather than a source of turbulent energy.

In the case of a laminar boundary layer growing under a uniform pressure gradient, positive pressure gradient is known to promote transition through effecting an inflexional velocity profile. Hall (1968) made a comprehensive study of both the theoretical techniques and the available experimental data on the subject. Of interest is the criterion of detecting the position of transition for the case of free stream turbulence and uniform pressure gradient acting together developed by van Driest et al (1963). The method assumed that transition would occur when the maximum local vorticity Reynolds number (T_r) in the boundary layer reached a predefined value which was the same for all pressure gradients and free stream turbulence levels $\left[T_r = \left(\frac{y^2}{\nu} \cdot \frac{dU}{dy}\right)_{max}\right]$. Effects of the pressure gradient on (T_r) was found using Pohlhausen's boundary layer profiles. Effects of the free stream turbulence was found using Taylor's assumption that it induced instantaneous variations in the velocity gradients, i.e. pressure gradients $\left[\text{or } \lambda_\theta = \frac{\theta^2}{\nu} \cdot \frac{dU}{dx}\right]$. They derived an equation for T_r as a function of λ_θ and u/U with two undetermined constants that were obtained by curve fitting of the available experimental results of R_{θ_T} vs. u/U (for zero pressure gradient) where T refers to transition. Wells (1967) found that his experimental results agreed reasonably well with the theory at high free stream turbulence intensity (u/U). At low (u/U) however, conditions at the leading edge dominated, and the results taken on different plates for different leading edge shapes did not collapse on

the theoretical curve.

This takes us to the question of how critical the geometry of the leading edge is as far as the position of transition over the plate is concerned. The issue was first brought up by Hall et al (1938) who were the first to point out that the leading edge shape had an effect on transition with no turbulence in the free stream. But for a turbulent free stream, turbulence dominated, they argued. In fact, Sutera et al (1963) reasoned that the leading edge effect could cause intensification of the streamwise vorticity by vortex stretching due to the favourable pressure gradient near the leading edge.

Hence, around the leading edge we have two factors simultaneously affecting the laminar boundary layer development besides the disturbing effects of the free stream turbulence entrained by the boundary layer. One is the pressure gradient pattern around the leading edge and the other is the vortex stretching of the longitudinal vortices in the on-coming free stream turbulence. Nevertheless, the precise role of the leading edge geometry in determining transition is not yet clear. This fact induced Morkovin (1978) to call for more tests on leading edges with different thicknesses and geometry.

The importance of acoustics, on the other hand, although rather recently acknowledged as a factor that may affect transition, yet may prove to be the responsible factor for causing transition in some of the more baffling cases. Morkovin (in a private communication) has recently shown that an aerofoil with a laminar leading edge separation in an undisturbed free stream had completely attached flow when subjected to a 70 db acoustic wave directed at the separated layer.

In fact, the importance of acoustics as far as transition is concerned was realised first during supersonic flow tests. Laufer (1961) observed that transition was affected by the sound produced by the

turbulent boundary layer growing on the wind tunnel walls. This observation was confirmed by Wagner et al (1970), while Pate et al (1969) also supported this observation through an interesting experiment during which a continuous increase in the transition Reynolds number was detected with increasing tunnel size. Spangler et al (1968) believe that the acoustic standing waves in the tunnel also play an important role in determining transition.

However, the importance of the acoustic waves in low speed experiments, especially coupled with the strong and better documented effects of free stream turbulence and pressure gradient, is yet to be discovered through more experiments.

Transition experiments are very difficult to set up, mainly because they are sensitive to a large number of variables which are very often simultaneously present in any experiment in an unavoidable manner. This produces a large scatter in the results even when the results are collected on a single apparatus.

Analytical work does not fare any better, for due to the same complexity of the phenomenon, work has largely been confined to defining the criteria for the stability of the laminar boundary layer and the growth of disturbances in the boundary layer under particular flow conditions. Apart from the stability theory, Reshotko (1976) has categorised the theoretical work in this field under three main categories, namely:-

(i) That dealing with the response of the boundary layer to a moving sound wave notably the work of Gaster (1975) and Gaster et al (1975).

(ii) That studying the disturbance in the boundary layer introduced

by a low intensity array of single-wave-number vortices convected at the mean free stream speed notably the work of Criminale (1971) and Rogler et al (1975).

(iii) That studying the effect of surface roughness on transition.

Therefore, and despite the difficulty of performing the transition experiments, the present state of affairs is such that one must depend on the experiments to bridge the gap between our understanding and inability to come forward with a more sophisticated theoretical model on one hand and the complete understanding of the physical phenomenon on the other hand.

The low speed regime provides the best experimental condition for examining the mechanics of transition mainly because the hot-wire anemometer can be used more easily and also because the boundary layer is thicker than in the high speed regime.

In the following experiments, the following issues will be studied in some detail:-

(a) The effect of grid turbulence on the transition position, defined as the position of the start of the appearance of turbulent bursts. The study of Taylor's parameter as a possible criterion for the occurrence of transition.

(b) The effect of changing the plate thickness on transition through an attempt to separate its effects through changing the pressure gradient around the plate leading edge, and that through changing the free stream turbulence characteristics around the plate nose due to vortex stretching.

(c) The evolution of the average values of the mean and fluctuating velocity components and quantities within the laminar-transitional boundary layer region. Also here, an attempt will be made to follow the evolution of the different energy quantities that occur in the turbulent kinetic energy equation through the same range.

(d) Study of the bursting phenomena through inspection of different oscillograph records and plots, together with a spectral analysis of the signals in order to detect the frequency bands most amplified by the free stream turbulence.

In the present study, the free stream turbulence intensity is defined as, the ratio between the root mean square of the fluctuating component in the streamwise direction, and the mean speed in the same direction, i.e. $\frac{\sqrt{\overline{u^2}}}{U}$.

CHAPTER 2

MEASURING EQUIPMENT AND TECHNIQUES

2.1 Wind Tunnel

The wind tunnel that was used in the experiments is the Imperial College, Department of Aeronautics' 3 feet x 3 feet, low speed, closed circuit wind tunnel. A complete description of the wind tunnel, the driving fan, the driving motor and all their controls are given in the Departmental manual.

Here it is sufficient to say that the tunnel is driven by a 40 BHP thyristor controlled variable speed drive motor that gives a reliably steady fan speed up to about 700 rpm. At such a fan speed, the induced air speed in the test section is about 50 m/s. Beyond that fan speed, very often the fan speed and the input current to the fan motor start to fluctuate.

The wind tunnel test section is 15 feet long and contains 8 windows, 4 on each side. The roof of the test section is partly covered with two aluminium sheets re-enforced with aluminium alloy ribs of T cross section. The sheets are of total length of 5.33 feet and they form a part of the traverse gear bed. The rest of the roof is covered with moveable formica plated wooden slabs.

The turbulence producing grids can be slid in place at the beginning of the test section.

The turbulence level inside the empty tunnel test section in the speed range up to 30 m/s is about 0.15% at most (see Fig. 4.8a).

2.2 Traverse Gear

The roof of the wind tunnel test section is fitted with a three-directional traverse gear arrangement that can probe virtually any

point inside the volume contained by the test section.

In the present experiment, a unidirectional "slide rule" type traverse gear was used to traverse the probe across the BL in the y-direction over the plate. This traverse has a stroke length of 15 cm ($\sim$ 6 inches). This traverse is mounted on the bed of the original traverse, whereby providing motion in the other x and z directions.

It was necessary to mount the traverse gear onto the tunnel traverse bed and support it onto the surface of the flat plate in such a way that any relative vibration between the plate and the traverse should be absorbed.

To satisfy this requirement, the arrangement shown in Fig. 2.1, was designed by the author. It is composed of a stand for the traverse gear that is free to move vertically for a short distance relative to its supporting rod against a spring force. This rod is fitted with a perforated splitter plate to eliminate vortex shedding behind it. The supporting rod-splitter plate arrangement is screwed onto the tunnel traverse bed. When the tunnel traverse bed moves in the x or z directions, the traverse foot moves along with it sliding over the plate surface on a ball made of hard plastic. This spring-loaded motion of the traverse foot and supporting rod serves to keep the traverse foot always sliding on the flat plate surface and may absorb any possible relative vibrations.

Traversing the y-direction was powered by means of a Portescap P26 12 V DC electric motor (reported in Dean (1974), Fig. 2.4a). It incorporates a Sakae linear potentiometer type 20 LP 100 which can travel a distance of 10 cm with a resolution of 0.33 mm giving a voltage proportional to the distance travelled. The motor and the potentiometer were both controlled by a remote control box with a built-in voltage stabiliser and a zero adjustment screw for the

potentiometer. Various probes (pressure tubes, hot-wires, etc.) could be mounted on this traverse.

2.3 Model

In designing the flat plate used in the experiment, the following requirements were kept in mind:-

(i) Its length should be large enough to get a reasonably turbulent BL over the rear third of its surface at the approximate working speed of 30 m/s with nominally zero turbulence in the free stream.

(ii) It should have side plates and should not be jointed to the tunnel walls to avoid interaction between the tunnel wall BLs and the plate BL.

(iii) The working section of the plate should be metal for a better surface finish.

(iv) Since one of the objectives of this experiment was to study the effects of plate thickness on transition, it was decided that two plates of different thicknesses were to be used. A simple and economical way of combining the two was preferable.

(v) The plate suspension and supports inside the tunnel should be independent of the tunnel walls and directly connected to the test section supporting panel which is more massive and rests directly on the floor.

Hence, the plate shown in Fig. 2.2 was produced. Its ribs can be replaced by bigger ones for the thicker plate. The upper surface is a $\frac{1}{4}$" thick aluminium sheet while the lower surface is a $\frac{1}{4}$" thick wooden sheet.

One of the problems that was faced during the design of this model was to choose the nose section such that the static pressure on the plate surface would recover to the free stream value in a distance from the LE as short as possible with no region of positive pressure gradient over the plate surface, since transition is known to be promoted by positive pressure gradient (van Driest et al (1963), Hall (1968) and Michel, 1974). Therefore, the elliptic nose section was chosen as the most suitable for this purpose.

Preliminary investigations, however, showed that even for the elliptical nose section, the region of non-zero PG extended over most of the nose section length and also that there existed a region with positive pressure gradient as shown in Figs. 4.3 and 4.5.

Attempts to get rid of the positive pressure gradient region and decrease the extent of the non-zero pressure gradient region and/or nullify their effects on the transition will be discussed in Sections 3.9 and 5.3. In the course of such attempts, the following nose sections were used (see Fig. 2.4):-

1. An 8" long elliptic nose mounted on a 1.5" thick flat plate so that $X_n/t = 5.6$ (the slenderness ratio) where X_n and t are the minor and half the major axes of the ellipse respectively.

2. An 8" long elliptic nose mounted on the 4" thick flat plate so that $X_n/t = 2$.

3. A 3" long elliptic nose mounted on the 1.5" thick flat plate so that $X_n/t = 2$.

4. A shaped nose to give an effective elliptic LE section of $X_n/t = 6.3$.

5. An elongated nose for the 1.5" thick plate that, when put at an angle of 0.9^o to the flow, gives a pressure distribution that is nearly free from regions of positive PG (see Fig. 4.4).

Static pressure tappings were drilled along the upper surface of the plate and nose. Also, in order to check the alignment of the plate with the direction of the mean flow inside the tunnel, two static pressure holes were drilled 1.0 mm on both sides of the leading edge.

The trailing edge is pointed and is made of wood. The nose section and the trailing edge can be screwed onto the plate. When assembled, the nose and the plate surface together form a continuous surface smooth to the touch.

And knowing that the disturbance level inside the tunnel working section without a turbulence producing grid is roughly 0.1%, and inferring that the transition region extends over the range of:-

$$R_{e_x} = \frac{U_\infty x}{\nu}$$

$\simeq 3 \times 10^5 - 3 \times 10^6$ (Schlichting, 1968, pp. 458)

Hence for the speed of 30 m/s, the length of 220 cm (or roughly 86 inches which is the overall plate length including leading and trailing edge sections) is suitable to allow the BL to develop past the transition region for the case of a quiescent free stream.

The thickness of the wooden ribs screwed to both the upper and the lower surfaces determines the overall thickness of the plate. Using the same upper and lower surface sheets, the thin plate can be made into the thick one simply by changing the ribs and using thicker ones and vice versa.

The plate has two supporting beams that are screwed onto the aluminium sheet inner surface and clamped onto two side beams that run alongside the tunnel working section as shown schematically in Fig. 2.3. Those side beams are, in turn, bolted to the supporting panels of the tunnel working section. This system of supporting beams was so designed as to fulfill the following requirements:-

1. The plate is directly supported by the test section supporting panel and not the tunnel wall.

2. Freedom to tilt the plate at an angle up to ± 1.25 degrees in order to have some control over the pressure gradient on the plate surface.

3. Using the clamps to apply tension to the supporting beams in order to raise the natural frequency of the arrangement.

4. Positioning of the supporting beams relative to the plate and positioning of the plate supporting beams relative to side beams so that the system has the maximum natural frequency possible.

So, using the formula defining the natural frequency (ω_1) of a simply supported beam of length ℓ, stiffness E with a uniformly

distributed loading (w), namely:-

$$\omega_1 = \pi^2 \cdot \sqrt{\frac{EI}{w\ell^4}}$$

And that for concentrated loads, namely:-

$$\omega_1 = \sqrt{\frac{g\Sigma wY}{\Sigma wY^2}}$$

where g is the gravitational acceleration, I is the moment of inertia of the beam cross-section and Y is the beam deflection at the position of the load.

Using these formulae, the natural frequency of the side beam was found to be about 35 c/s while that of the supporting beam was found to be 50 c/s under the weight of the 50 Kg plate* which was made so heavy to decrease the amplitudes of vibration of the whole combination.

Fig. 2.3 shows the supporting beam end, the clamp and the side beam arrangement wherein, by turning the hexagonal end of the hollow cone, both ends of the supporting beam are pulled against the side beam, thus applying tension to the supporting beam.

This design made it possible to install the plate at virtually any position inside the test section. Also by turning the vertical bolts at the four clamps, the incidence of the plate can be adjusted

---

* Vibrating loads due to aerodynamic effects are thought negligible in this case, since these forces are unlikely to be correlated over any considerable distance in a nearly isotropic turbulence and they are of small value anyway at the speeds of the experiment.

within ± 1.25 degrees.

2.4 Velocity Measurements

2.4.1 Using the Pitot Tube

A standard $\frac{1}{8}$" outside diameter pitot static tube with holes for both static and total pressure measurements was always used to detect the air speed away from the plate in the no FST case (see Fig. 2.5). Also a total pressure tube (Fig. 2.5) was occasionally used to determine the BL velocity profiles. This tube had an external diameter of 1.0 mm and an internal diameter of 0.6 mm.

Except when a quicker response was needed, the tubes were connected to an AVA Betz manometer with accuracy better than 0.02% in the speed range of the experiment. When a quicker response was needed (usually at high speeds) the much faster inclined Airflow MK5 manometer provided a more convenient means of detecting the tube reading.

2.4.2 Using the Hot-Wire Anemometer

In most cases, hot-wire probes incorporating 5 μm and 7.5 μm Wallaston wires (made at the Imperial College Aeronautical Department) were used. For a full description of the method of making those wire probes, refer to Bradshaw (1976). The following wires were used in the experiment.

1. U-wire probe of overall length of 3 mm and approximately 1.0 mm sensitive wire length. It was used for measurements of longitudinal mean and fluctuating velocity components and for the detection of transition.

2. X-wire probe of wire projected length of about 1.0 mm and with a distance of 1.0 mm between the two wires. It was used to measure the following turbulent quantities: $\sqrt{\overline{u^2}}$ $\sqrt{\overline{v^2}}$, $\overline{uv}$, $\overline{u^2v}$, $\overline{uv^2}$, $\sqrt{\overline{w^2}}$, $\overline{u^2w}$, $\overline{u^3}$, $\overline{v^3}$. These quantities were either measured directly using real time analogue measurements (e.g. $\sqrt{\overline{u^2}}$, $\sqrt{\overline{v^2}}$ in some cases), or computed from digitised recorded output of the X-wire probe as in the case with most of the reported quantities.

3. Double U-wire probe that was formed of two parallel wires distance 0.35 mm apart, both having a sensitive length of 1.0 mm of a 5 μm tungsten wire. This wire was used to measure the gradients of the longitudinal fluctuating velocity component in the y and z directions $\left(\frac{\partial u}{\partial y} \text{ and } \frac{\partial u}{\partial z}\right)$. The gradient in the x-direction $\left(\frac{\partial u}{\partial x}\right)$ was determined by taking the time derivative of the signal from a single wire and assuming Taylor's hypothesis.

In conjunction with these probes, the DISA 55 D01 constant temperature anemometer and/or the DISA 55 M system with 55 M 20 temperature bridge were used along with the DISA 55 D35 RMS meter. It was decided not to use the DISA linearisers not only because it would drift considerably during the time of completing one traverse (2^+ hours) but also because it was not certain that it would give more accurate results.

Also, the DATRON model 1030 true RMS digital voltmeter was used to get the mean square of the fluctuating quantities. All the voltages were displayed digitally on SOLARTRON digital voltmeters.

The ROCKLAND model 452 dual HI/LO filter (that had a range of

0.01 Hz to 111 kHz and accuracy at cut-off frequency of ± 2% with 3 db attenuation at cut-off) was used as an AC and/or DC filter.

Some of the second order turbulent quantities like $\overline{uv}$ were sometimes determined electronically by feeding the output of an X-wire to an analogue module which contained two operational amplifiers and then to a multiplier. Full details can be found in Bradshaw (1976).

A FARNELL LFM2 sine/square oscillator was used in anemometer calibration and other purposes. A dual-beam TEKTRONIX (type 502) oscilloscope was used for visual display of the fluctuating signal.

The chart in Fig. 2.6 shows the arrangement for U-wire probe experimenting while the chart in Fig. 2.7 shows that arrangement for an X-wire. Arrangement for recording measurements of the double wire is identical to that of the X-wire.

The hot-wire probes were always calibrated in a turbulence-free flow against a pitot static tube giving static and total pressure in the vicinity of the probe. Fig. 2.9 shows a typical U-wire calibration curve plotted as V^2 vs. $U^{0.45}$. It was found that for the airspeed (U) and the wire output voltage (V), the characteristic relation:-

$$V^2 = A + BU^n$$

gave the best straight line fit to the calibration points when n was taken to be 0.45 (where $A = V_0^2$ at $U = 0$ and B is constant). But because the tunnel temperature increased with the tunnel running time (see Fig. 4.2) and also because of the drift of the hot-wire, the calibration of the wire changed with time so that it was found necessary to re-calibrate the wire every two to three hours. Fig. 2.9 shows the typical calibration curves for a single wire before and after running time of two hours.

As for the X-wire, it was calibrated against yaw using the arrangement plotted in Fig. 2.10. As in the figure, the X-wire was fixed to a rod across the tunnel working section through two holes in the tunnel walls. The rod could be turned around its axis from outside the tunnel, whereby yawing the wire with respect to the mean flow. The turning angle (α) was indicated to the nearest 0.1 degree on a scale attached to the tunnel wall.

If the two wires comprising the X-wire were identical and both soldered at 45°, then aligning the wire to the flow direction would give equal voltages across the two wires. But because the wires are usually not identical, their calibration curves look like those in Fig. 2.13.

In order to make this difference in the two wires' voltages insensitive to variations in the U-component along the wire axis, the wire was set parallel to the flow direction and the tunnel was run at nearly half the expected working speed during the experiment (because all the measurements were to be made within the BL). Then the tunnel speed was varied within ± 10% of its value while the anemometers decade resistances were simultaneously adjusted to give as little variation as possible in the voltage difference between the two wires. This process amounts to equalising the slopes of the two calibration curves in Fig. 2.13 locally at the working speed.

Having done this, the wire was turned at different angles (α) to the horizontal so that a vertical velocity component (U sin α) was effected. Plotting the wire incidence versus the difference between the two wires' voltages (which was proportional to U sin α) should produce a very nearly straight line (as in Fig. 2.11) which should pass through the origin if the two wires were identical.

It is also shown in Fig. 2.11 that, beside the wire drift with

running time, the calibration of the wire changes with the mean air speed. Such change is typically shown in Fig. 2.12. Also, Fig. 2.13 shows a typical wire drift after two hours running time. Again, the practice was to calibrate the wire every two hours running, or before the start and at the finish of the experiment, should this time be shorter than two hours. Every time a curve similar to the one in Fig. 2.12 was produced. In the analysis of the data by the computer, and for measurements through a BL, the computer program incorporated a second order interpolation routine using Newton's divided difference method to get values of the angle of inclination of the wire yaw calibration line to the horizontal for different air speeds similar to those in Fig. 2.11.

The X-wire was also calibrated in a parallel flow against a pitot tube. The slopes of its calibration curves were needed in the computer analysis of the recorded X-wire output and in setting the PHI module "DISA test" (sum-and-difference) unit used in determining the values of u, v, $\overline{uv}$ electronically (see Fig. 2.8). This "DISA test" unit contains operational amplifiers which accept the output of the two wires of the X-wire simultaneously, and with its controls set according to the constants occurring in each individual wire characteristic equation, its output will represent the instantaneous values of u and v. The process is described in Bradshaw (1975).

2.5 Pressure Measurements

2.5.1 Static Pressure Measurements

Static pressure measurements along the plate surface were made using either the static tubes (connected to the Betz manometer or the MK5 Airflow manometer) or by the static pressure tappings drilled flush

with the plate surface along the mid-section of the plate.

The first type was either an L-shape pitot static tube with holes around its circumference or a disc static probe (see Fig. 2.5) which was made of a hypodermic tube bent as shown in the figure, ending with a brass circular disc of diameter 6.4 mm (0.25 in) and thickness of 0.9 mm. The disc had two holes, one on each side, of diameter 0.38 mm. This type of probe is insensitive to yaw within $\pm 3^{o}$ in the plane normal to the disc plane (Bryer and Pankhurst, 1971). The calibration of this tube involves finding the constant γ in the expression:-

$$\gamma = \frac{P - P_{\Delta}}{\frac{1}{2}\rho U^2}$$

where P is the true static pressure, P_{Δ} is the static pressure as measured by the disc probe and $\frac{1}{2}\rho U^2$ is the dynamic pressure at the calibration point. The calibration employed in the present work was reported (for the probe used in the present experiment) by Chandrsuda (1975) in Fig. 3.2 of his Ph.D. thesis.

On the other hand, the static pressure tappings on the plate surface were made by inserting 1.0 mm hypodermic tubes flush with the plate surface and glued in position using Araldite. The number of the tappings is 22, mostly concentrated near the LE in the region of non-zero pressure gradient. They, nevertheless, covered a distance of 75% of the plate length. Their positions (in inches) are tabulated on the next page.

No.	1	2	3	4	5	6	7	8
X	$-\frac{1}{16}$	$+\frac{1}{16}$	1	2	3	4	5	6
No.	9	10	11	12	13	14	15	16
X	7	$7\frac{26}{32}$	$8\frac{25}{32}$	$9\frac{24}{32}$	11	13	18	22
No.	17	18	19	20	21	22		
X	28	34	40	46	52	60		

2.5.2 Total Pressure Measurements

Two types of probes were used for this purpose:-

(i) The standard pitot static tube was used for measurements in the free stream.

(ii) A plane ended L-shape pitot tube made of 1.0 mm hypodermic tube. This tube was used for measurements in the BL.

These tubes are shown in Fig. 2.5. The readings of the static pressure tappings were measured on a TEM multi-tube manometer from which an idea of the static pressure distribution over the plate surface was readily obtained.

2.6 Skin Friction Measurements

Three methods of determining the skin friction coefficient (C_f)

along the plate surface were used:-

1. The first one was used for the TBL using the logarithmic law of the mean velocity profile. This method was employed in the computer program discussed in Section 3.4.

2. Another method for which measurements of the skin friction were obtained was by means of a Preston tube of diameter 0.9 mm (similar to the total pressure tube reported in Fig. 2.5). As for method (1), the accuracy of the present method decreased as the LBL was approached. Yet its inclusion in the graphs gives an idea about the trend of the C_f change in the longitudinal direction. The calibration reported by Patel (1965) was used in determining the skin friction coefficient (C_f) in the present work. In the TBL range, this method also served as a check on the accuracy of method (1). They were found to agree to within 5%.

3. The third method was used for the cases where the mean velocity profiles were also available as a check to the values obtained by the above two methods. This method made use of the relation that $C_f = 2 \frac{d\theta}{dx}$ (where θ is the momentum thickness). The disagreement was found to be a little worse than 5%.

2.7 Free Stream Turbulence Generation

Five different bi-planer grids were used to generate turbulence in the test section. They were all composed of rectangular rods. The dimensions of the grids used are tabulated on the next page.

No.	Mesh in.	Bar Size	
		Width in.	Depth in.
1	1.5	$\frac{3}{8}$	$\frac{3}{8}$
2	3.0	$\frac{1}{2}$	$\frac{1}{2}$
3	4.0	$\frac{1}{2}$	$\frac{1}{2}$
4	6.0	$1\frac{1}{4}$	$\frac{1}{2}$
5	9.0	$1\frac{1}{2}$	$\frac{1}{2}$

The grids generated a homogeneous turbulence after about 10 - 15 mesh lengths depending on the mean speed of the flow. The differences between the three fluctuating components of turbulence were within 5% in the RMS (see Section 4.4).

The turbulence generated by these grids had an intensity that varied between 1.7% to 5.5% of the mean flow velocity. Such variations were a function of the grid dimensions, the mean flow velocity (or the grid $R = U_\infty M/\nu$) and the distance from the grid (see Figs. 4.6 and 4.8b).

Upon comparison of the present results reported in Figs. 4.6 and 4.8b with Fig. 8 in Baines et al (1951), we find that within the range of X/M common to both experiments, there was complete agreement.

2.8 Detection of Place of Transition

Two techniques of defining and detecting the place of the onset of turbulence in the BL over the flat plate were employed in the present work.

1. The first one involved detecting the place of the start of amplification of small disturbances inside the BL. The equipment used was one U-wire probe, an anemometer, an AC filter, a digital voltmeter and one TEKTRONIX 549 storage type oscilloscope. A technique was developed to look for the first amplified small disturbances at about 0.2 δ, i.e. roughly at the estimated position of the critical layer. The method depended heavily on personal judgement and visual observation of the U-wire signal on the oscilloscope screen. And although the method might look tedious, yet the time spent in detecting the position of transition was cut down very sharply by experience as time went by. The following plots were needed to be handy during the experiment:-

   (a) A plot of the calibration curve of the wire used plotted as V vs. U.

   (b) An arbitrary plot showing a linear relationship between the scanning speed of the hot-wire output by the oscilloscope beam and the mean speed of the flow. This made it simple to interpolate roughly by the eye at any intermediate speeds during the experiment. The terminal values on the velocity axis should cover the range expected during the experiment and those on the scanning speed axis should be such that the observer can always comfortably watch the signal.

Both plots are schematically reported in Fig. 2.14. The process

is explained fully in the chart in Fig. 2.15. Usually two or three streamwise movements of the wire are sufficient to decide upon the position of the start of appearance of amplified disturbances. One of the bases of the method is the postulate that the pattern of the generated bursts of amplified disturbances is not a function of the absolute value of the local convection speed. Otherwise for the same grid and the same plate but different mean velocity, the frequency of the observed appearance of amplified disturbances (within a short distance at the start of transition) would not correlate with the local mean speed (which would be somewhat different from the local convection velocity). Another of the bases of this method is the postulate that the nature of the process of producing turbulent bursts is not a function of the nature of free stream turbulence. Because if it was not so, then results for the same plate and the same R number but for different grids would not be correlated. There is some strong experimental evidence (Morkovin (1958), Emmons (1951) and Schubauer et al, 1948) in favour of these two postulates.

2. The second method involved detecting the place of minimum skin friction, i.e. the position where the mean velocity profile would start to show signs of departure from Blasius profile. The equipment used consisted of a preston tube similar to the one reported in Fig. 2.5, and a Betz manometer. The whole region of the laminar-transitional BL was traversed in the streamwise direction with the tube adjacent to the wall. The reading of the tube was taken every 4.0 cm. Then

a plot similar to the one reported in Fig. 2.16 would be produced. The position of transition would be taken to be where the gradient of the tube reading in the x-direction was zero. And because only a qualitative assessment of the tube reading was needed to determine the position of transition, no calibration of the tube was applied. And since the skin friction is a monotonically increasing function of the tube reading, hence the plot in Fig. 2.16 is against arbitrary units.

The first method had a clear advantage over the second at high FST levels. Since transition had to be pushed off the pressure gradient zone, i.e. X had a minimum that was, nevertheless, a considerable distance from the LE, transition often occurred at relatively low speeds, sometimes even less than 5 m/s for large FST intensities (0.05^{+}). In such cases, not only the reading of the tube throughout the whole transition range would be very low, but also changes in the reading would be very slow. So that to traverse the length of the laminar-transitional BL zone and take a reading every 4.0 cm and decide upon the position of transition would take three times as long as it would take to arrive at transition using the first method. Also as the concave part of the plot in Fig. 2.16 becomes flatter, error in deciding upon the position of zero gradient becomes greater.

Therefore, the first method was used exclusively during the experiment. The second method was only used as a check on the accuracy of the first method and as a measure of the amount of scatter. Fig. 5.1 shows some results obtained by the two methods. As expected, the first method detected earlier transition while the

degree of scatter remained roughly the same.

2.9 Analogue Signal Recording and Digitization

2.9.1 Analogue Signal Recording

For most of the fluctuating quantities, the output of the hot-wire was recorded on a one inch analogue magnetic tape using an Ampex FR1300 analogue tape recorder so that the data (after digitization) could be analysed by the computer. The tape recorder had 14 channels and 6 speeds (from $1\frac{7}{8}$ in/sec up to 60 in/sec).

The peak-to-peak amplitude of the input signal to the tape recorder had to be within ± 1.0 volt. But because near the wall, at most stations studied, the amplitude of the unamplified signal sometimes exceeded ± 0.8 volt, and in order to avoid distortion of the recorded signal, no amplification was applied to the signal throughout the experiment. This resulted in poor signal to noise ratio in some cases where the signal itself was weak. This ratio was estimated to be 20 : 1 at worst. A correction of this error was employed in the analysis program which amounted to subtracting the $(\text{RMS meter reading at zero. air speed})^2$ from all the reported measurements.

During recording, the input signal and the recorded one were always displayed simultaneously on a dual oscilloscope as a check. For the purpose of calibrating the gain of the recorder, a Farnel sine-wave generator was always used to record a signal of known amplitude and frequency at the beginning of each recorded traverse and recheck them again when playing the signal back for digitization or other purposes.

The recording speed of the tape recorder was determined by the following factors:-

1. Availability of space on the analogue tape used.

2. Length of record required, which depends on the nature of the experiment. For the present experiment, this was controlled by the expected time needed to produce converged averages during the computation of the turbulent quantities which tended to be larger for records taken in the transitional BL than for those in the LBL or in the TBL. And since this time was not known beforehand, and subject to factor (1) above, a length of 3 minutes was usually recorded at every point.

3. The frequency band of the signal.

4. The need to play the signal back at different recorder speeds.

During the present experiment, most of the hot-wire signals were digitized and analysed by the computer (see Section 2.4).

2.9.2 Analogue Signal Digitization

To render the analogue data suitable for analysis using the computer, the signal has to be evaluated at discrete points. To do this, the Imperial College, Aeronautics Department digital data logging system, described fully by Weir et al (1974), was used. Detailed description and operating instructions are also given in Bradshaw (1975).

During the spectral analysis, and in order to avoid aliasing, two actions were taken, namely:-

1. Filtering the input signal above the maximum frequency of interest.

2. Sampling the remaining signal at (at least) double the maximum frequency above which the signal was filtered off.

Filtering was done using either KEMO dual variable filter (type VBF/1 which had a range of 1 Hz to 100 kHz) or the ROCKLAND HI/LO dual filter (model 452 with a range of 0.01 Hz to 111 kHz). The sampling frequency of the signal, i.e. the rate of transfer from the A/D converter to the core of the minicomputer was set by a crystal clock.

The system could handle up to 12 channels carrying analogue voltage signals (of amplitude ± 1.0 volt peak-to-peak) and convert them into 10 bit binary numbers. The binary numbers were then recorded in pure binary form on 7 track half inch digital magnetic tape (of total length of 6 minutes real time approximately) in "black IBM" format compatible with the Imperial College and University of London CDC computers.

In determining the sampling frequency of a particular signal, the following were taken into account:-

(a) Samples should not be too close to each other to avoid unnecessary computation.

(b) The sampling frequency should be (at least) two times the highest frequency in the signal in order to avoid aliasing.

(c) As the digital tape ran at a constant speed regardless of the sampling rate, the sampling rate should not be too low so

that the error due to low ratio of signal to blank bits on the digital tape would be reduced.

(d) The frequency range of the signals in question.

(e) The convergence properties of the signal in question.

(f) The real time scale of the signal of interest.

During the present analysis, the effective sampling rates used for the different purposes are reported in the table below.

Wire	Purpose	Sampling rate/ Channel per sec
U-wire	Signal plotting	5,000
	Spectral analysis	5,000
	Intermittency determination	5,000
X-wire	Averaging of turbulent quantities	20,000
Double wire	Turbulent derivatives	20,000

These rates were decided upon by inspection of the frequency contents of the signal in question and trying different sampling rates and comparing the results obtained for each sampling rate. These rates were found by practice to present more than 95% of the signals' required properties. For example, for the purpose of plotting the physical signals, 5,000 samples/sec. did not only show the details of all the fluctuating signals in the transitional BL, but it also left

much room for plot magnification along the time axis without distorting the plot's general appearance to the naked eye.

Also since aliasing affected only the information in the time domain, the process of determining the conventional averages of the turbulent quantities was not affected by it.

2.10 Sound Pressure Level Measurements Using Electronic Apparatus

The sound pressure level was detected by the B & K $\frac{1}{4}$ in. condenser microphone cartridge (type 4136) together with the associated B & K cathode follower (type 2615). The frequency response at the condenser microphone was flat with no variation in the frequency range 20 c/s to 10,000 c/s, and with a maximum variation ± 1 db in the frequency range 10,000 c/s to 40,000 c/s.

The narrow band frequency spectra were obtained from the output of the condenser microphone using the B & K audio frequency spectrometer (type 2112) consisting of a series of 1/3 octave band pass filters giving the part of the signal with frequency that occurred within the band width of each filter.

2.11 Alignment of Plate with Flow Direction

This was accomplished with the aid of thin cotton tufts taped over the nose section and around the LE using a fine adhesive tape. The tufts had a free length of about 2.0 cm. Also, the static pressure distribution was simultaneously observed especially those readings of pressure by the two tappings on each side of the LE. The incidence of the plate was adjusted so as to give:-

1. Equal readings for the above-mentioned two tappings.

2. All tufts on both sides of the LE along the plate span bent in the downstream direction, thus indicating no flow separation.

Also a single tuft fixed at the tip of a thin rod was found very useful in checking the flow conditions at the TE at any doubtful point.

CHAPTER 3

DATA PROCESSING TECHNIQUES AND THE UNDERLYING THEORETICAL BASIS

3.1 Determination of the Mean (Longitudinal) and the Fluctuating Turbulent Quantities

3.1.1 From the Output of a U-Wire

The mean velocity was found using the hot-wire characteristic equation, namely:-

$$V^2 = A + BU^n$$

where V is the wire reading in volts, U is the speed in m/s, A is the wire reading at zero speed (i.e. V_0^2) and B and n are constants. Or we may write:-

$$U = \left(\frac{V^2 - V_0^2}{B}\right)^{1/n}$$

As discussed in Section 2.4.2, n was taken to equal 0.45. The constants V_0 and B were determined from a plot of the wire calibration curve as:-

V^2 vs. $U^{0.45}$

using the least squares method to fit a straight line through the points of the calibration curve and V_0 was taken to be the intercept of the curve with the voltage axis.

The longitudinal fluctuating velocity component, on the other hand, was found from the relation that would follow from differentiating the wire characteristic equation, i.e:-

$$\frac{u}{U_{local}} = \frac{2V\ dV}{n(V^2 - V_0^2)}$$

where dV is the root mean square of the fluctuating component in the longitudinal direction (in volts).

3.1.2 From the Output of an X-Wire

The recorded output of an X-wire was analysed using the Imperial College Aeronautics Department standard program, DIG2U. This program is explained fully in Weir et al (1974).

The credibility of the results obtained by analysing the digitized data by the computer was checked at some stations by comparing the computed values of $\sqrt{\overline{u^2}}$, $\sqrt{\overline{v^2}}$ and $\overline{uv}$ with the equivalent values obtained by analogue means from the output of the X-wire probe, see Section 2.4. The results obtained agreed reasonably well with those found by digital processing.

The data analysis program could, in short, be divided into two main parts. The first part consisted of the subroutines that would convert the multiplexed data on the digital magnetic tape into standard computer words in proper storage locations, or in other words data retrieval subroutines. The second part contained the analysis subroutines.

The program accepted the simultaneously recorded outputs of each of the two wires constituting the X-wire together with their respective constants. Then the conventional averages of two components (u, w or u, v depending on the position of the wire relative to the wall) of the fluctuating velocity and their higher moments would be found as running averages. Each time the program would add the answers obtained from the current patch of data to that from the previous ones.

The quantities computed by the programs are U, V, $\sqrt{\overline{u^2}}$, $\sqrt{\overline{v^2}}$, $\overline{u^2}$, $\overline{v^2}$, $\overline{uv}$, $\overline{u^3}$, $\overline{v^3}$, $\overline{u^2v}$, $\overline{v^2u}$, $\overline{u^4}$, $\overline{v^4}$, skewness of u, skewness of v, flatness of u, flatness of v and where u, v (or w) are the parallel and normal components to the wire axis respectively. The values of u, v were found from the X-wire output which was proportional to u + v, u - v, whence all the other quantities would follow directly, while the skewness and flatness of the velocity components were found as:-

$$\text{skewness} = \frac{\overline{u^3}}{(\overline{u^2})^{3/2}}$$

$$\text{flatness} = \frac{\overline{u^4}}{(\overline{u^2})^2}$$

The process of averaging out the quantities computed would continue until the convergence criteria, namely:-

$d\overline{u^2}$, $d\overline{v^2}$ < 2% of current $\overline{u^2}$, $\overline{v^2}$

was satisfied, then the process would halt.

3.1.3 From the Output of a Double-Wire

The instantaneous derivatives of the fluctuating velocity in the x-direction, i.e.:-

$$\overline{\left(\frac{\partial u}{\partial y}\right)^2}, \overline{\left(\frac{\partial u}{\partial z}\right)^2}$$

were obtained by averaging the difference between the instantaneous readings of the two wires constituting the double wire over a sufficiently long time. Ideally, the separation between the two wires

should be less than the length scale of the eddies responsible for the energy dissipation. This can be estimated for the homogeneous turbulence (as in Batchelor, 1953) as follows. For homogeneous turbulence, we have:-

$$\eta = \left(\frac{\nu^3}{\varepsilon}\right)^{1/4}$$

$$\varepsilon = -\frac{3}{2}\frac{du^2}{dt}$$

$$\frac{du^2}{dt} = -A\frac{u^3}{\ell}$$

i.e:- η = length scale of smallest eddies

$$= \left(\frac{\nu^3}{\frac{3}{2}A\frac{u^3}{\ell}}\right)^{1/4} \qquad A \simeq 1.1$$

where ν is the kinematic viscosity, ε is the energy dissipation and ℓ is the length scale of the large eddies.

If we assume that the eddies responsible for the dissipation do not have a preferred direction and that ℓ equals the size of the flow, i.e. the BL thickness, hence for the smallest BL in the present experiment, i.e. at X = 20 cm where δ = 2.32 mm and assuming that $u^3 = (0.01)^3$, we get:-

$$\eta \simeq 0.3 \text{ mm}$$

But because the wire was manufactured by the author, it was only possible to make the gap between the two wires equal to 0.35 mm since

the practical problems of soldering two wires at such a small distance from each other proved formidable.

It was thought that free convection would not cause any appreciable error to the readings of the two wires, being only that small distance apart, since the gap was still 70 times bigger than the wire size (5 μm). Also, any resulting effect on the velocity derivatives would be minimised by the fact that the two wires would simultaneously affect each other in the same way (such an effect, if existing, would tend to make every wire indicate a slower flow than the reality). Also, in the presence of a moving fluid the effect of free convection would be very small compared with that of the forced convection.

Also, if there was a cross flow at the wire position, one wire might lie in the wake of the other and large error might result. However, this situation was very unlikely since in the flat plate's 2D − BL flow, the U component was always much larger than all the other velocity components. In any case, the two signals from the two wires were always displayed simultaneously on the oscilloscope screen and there identicality was always obvious.

3.2. Determination of Profiles of the Mean Velocity Component Normal to the Plate (V)

Assuming that the flow over the plate is 2D and steady, the mass flow conservation equation can be written as:-

$$\frac{\partial U}{\partial x} + \frac{\partial V}{\partial y} = 0$$

or:-

$$V(y) = -\int_0^y \frac{\partial U(y)}{\partial x}\, dy$$

This integral was evaluated using the measured mean velocity profiles U(y) according to the following procedure:-

1. Evaluating all the U profiles at the same distances from the wall by interpolation using Newton's divided difference method.

2. Smoothing the resulting profiles in the x-direction using the smoothing routine described in Section 3.10.

3. Evaluating the differential in the x-direction using the parabolic technique described in Section 3.3.

4. Integrating the resulting profiles of the first derivative of the mean speed in the y-direction using a step-by-step method that employed Simpson's rule.

The value of V at the edge of the BL gave an estimate of the entrainment velocity of the free stream by the BL.

3.3 Computation of the Different Terms in the Turbulent Energy Equation

The 2D steady turbulent energy equation can be written as*:-

---

* Here, the derivatives in the x-direction are included since within the transitional region, the development of nearly all the turbulent quantities are expected to be quite high (yet still much smaller than that in the y-direction) as turbulence is setting into the LBL.

$$U \frac{\partial}{\partial x} \overline{q^2} + \dot{V} \frac{\partial}{\partial y} \overline{q^2} = - \overline{u^2} \frac{\partial U}{\partial x} - \overline{v^2} \frac{\partial V}{\partial y} - \overline{uv} \left(\frac{\partial U}{\partial y} + \frac{\partial V}{\partial x} \right)$$

$$- \frac{1}{2} \left(\frac{\partial \overline{u^3}}{\partial x} + \frac{\partial \overline{v^3}}{\partial y} + \frac{\partial \overline{u^2 v}}{\partial y} + \frac{\partial \overline{v^2 u}}{\partial x} + \frac{\partial \overline{w^2 u}}{\partial x} + \frac{\partial \overline{w^2 v}}{\partial y} \right) - \frac{1}{\rho} \left(\frac{\partial \overline{p' u}}{\partial x} + \frac{\partial \overline{p' v}}{\partial y} \right) +$$

$$+ \nu \left(\overline{u \nabla^2 u} + \overline{v \nabla^2 v} + \overline{w \nabla^2 w} \right)$$

where $q^2 = \frac{1}{2} (\overline{u^2} + \overline{v^2} + \overline{w^2})$. The following terms were not measured in the experiment at all:-

- The pressure term, i.e. $- \frac{1}{\rho} \left(\frac{\partial \overline{p' u}}{\partial x} + \frac{\partial \overline{p' v}}{\partial y} \right)$.
- The last term in the expression of diffusion, i.e. $\frac{\partial \overline{w^2 v}}{\partial y}$.

And the remaining terms were computed in the following forms:-

1. The advection terms of turbulent energy, i.e.
   $U \frac{\partial}{\partial x} \overline{q^2} + V \frac{\partial}{\partial y} \overline{q^2}$

2. The production terms, i.e.
   $- \overline{u^2} \frac{\partial U}{\partial x} - \overline{v^2} \frac{\partial V}{\partial y} - \overline{uv} \left(\frac{\partial U}{\partial y} + \frac{\partial V}{\partial x} \right)$

3. The terms expressing turbulent diffusion of turbulent energy
   $- \frac{1}{2} \left(\frac{\partial \overline{u^3}}{\partial x} + \frac{\partial \overline{v^3}}{\partial y} + \frac{\partial \overline{u^2 v}}{\partial y} + \frac{\partial \overline{v^2 u}}{\partial x} + \frac{\partial \overline{w^2 u}}{\partial x} \right)$

4. The viscous dissipation of turbulent energy
   $\nu (\overline{u \nabla^2 u} + \overline{v \nabla^2 v} + \overline{w \nabla^2 w}) =$

$$= \nu\left[\frac{1}{2}\overline{\nabla^2 u^2} - \overline{(\nabla u)^2} + \frac{1}{2}\overline{\nabla^2 v^2} - \overline{(\nabla v)^2} + \frac{1}{2}\overline{\nabla^2 w^2} - \overline{(\nabla w)^2}\right]$$

$$= \nu(\overline{\nabla^2 q^2} - \overline{(\nabla u)^2} - \overline{(\nabla v)^2} - \overline{(\nabla w)^2})$$

where $\nabla = \frac{\partial}{\partial x}, \frac{\partial}{\partial y}, \frac{\partial}{\partial z}$. In fact, as will be discussed in item (j) below, not all the terms in the above expression for the dissipation were measured and instead, the relations for the isotropic turbulence were used to express the non-measured terms in terms of the measured ones. The following procedure was followed to compute the different terms in the equation:-

(a) The outputs from a U-wire, an X-wire and a double wire were analysed by the computer (as detailed in Section 3.1) and the following quantities were averaged out:-

$$U,\ V,\ \sqrt{\overline{u^2}},\ \sqrt{\overline{v^2}},\ \sqrt{\overline{w^2}},\ \overline{uv},\ \overline{q^2},\ \overline{u^2 v},\ \overline{v^2 u},\ \overline{uw^2},\ \overline{u^3},\ \overline{v^3},$$

$$\left(\overline{\frac{\partial u}{\partial x}}\right)^2, \left(\overline{\frac{\partial u}{\partial y}}\right)^2, \left(\overline{\frac{\partial u}{\partial z}}\right)^2$$

(b) All the quantities were then normalized by the mean free stream velocity (U_∞).

(c) The distances from the points at which measurements were taken to the wall were then corrected using the technique described in Section 3.5.

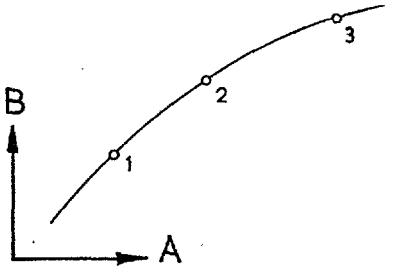
(d) The different BL integral parameters were then evaluated using the technique detailed in Section 3.4.

(e) The routine described briefly in Section 3.11 was then used

for smoothing of all the input profiles of different turbulent quantities.

(f) All the input profiles were then re-evaluated at some common heights from the wall so that data from a U-wire and data from an X-wire (or a double wire) might be added together. For this purpose, a direct linear interpolation technique using two points was used to get the new profiles.

(g) Then the required first and second derivatives (see Section 3.3) were determined for all the profiles using a three point parabolic differentiation formula, namely:-



$$\left.\frac{DB}{DA}\right|_2 = \left[(B2 - B1) \cdot \frac{(A3 - A2)}{(A2 - A1)} + (B3 - B2) \cdot \frac{(A2 - A1)}{(A3 - A2)}\right] / (A3 - A1)$$

(h) Then the first derivative of the mean velocity in the x-direction was integrated in the y-direction using Simpson's rule (see Section 3.2) in order to evaluate the mean velocity (V) normal to the wall.

(i) Different terms in the energy equation mentioned above were then computed and normalised using the mean free stream speed (U_∞) and the BL thickness (δ).

(j) The viscous dissipation terms which had not been measured (i.e. ∇v and ∇w) were then evaluated using the isotropic turbulence relations as:- and Klebanoff's (1954) experimental results

$$\overline{\left(\frac{\partial v}{\partial x}\right)^2} \simeq 0.6\overline{\left(\frac{\partial u}{\partial x}\right)^2}$$

$$\overline{\left(\frac{\partial v}{\partial y}\right)^2} \simeq 0.5\overline{\left(\frac{\partial u}{\partial y}\right)^2}$$

$$\overline{\left(\frac{\partial v}{\partial z}\right)^2} \simeq \overline{\left(\frac{\partial u}{\partial z}\right)^2}$$

$$\overline{\left(\frac{\partial w}{\partial x}\right)^2} \simeq 0.9\overline{\left(\frac{\partial u}{\partial x}\right)^2}$$

$$\overline{\left(\frac{\partial w}{\partial y}\right)^2} \simeq \overline{\left(\frac{\partial u}{\partial y}\right)^2}$$

$$\overline{\left(\frac{\partial w}{\partial z}\right)^2} \simeq 0.5\overline{\left(\frac{\partial u}{\partial z}\right)^2}$$

For more details, see Klebanoff (1954), Batchelor (1953), Townsend (1976) and Hinze (1975).

(k) Finally, the terms representing the pressure diffusion together with any errors resulting from inaccuracy of the above estimates were then estimated by algebraically subtracting the terms representing the production, the velocity diffusion and the viscous dissipation from the terms representing the advection of the turbulent KE (i.e. by balancing the terms in the energy equation).

3.4 Determination of the BL Parameters

The BL thickness δ was defined in this work as the distance from the surface of the plate at which the local mean velocity U was 0.995 of the external velocity U_∞. This thickness was computed by interpolating the value of 0.995 on the normalised mean velocity profile using a second order Newton's divided difference formula.

In computing the rest of the BL parameters, namely, δ^*, θ, H, C_f and the log law constants, the following definitions were adopted:-

Displacement thickness $$\delta^* = \int_0^\delta \left(1 - \frac{U}{U_\infty}\right) dy$$

Momentum thickness $$\theta = \int_0^\delta \frac{U}{U_\infty}\left(1 - \frac{U}{U_\infty}\right) dy$$

Shape factor $$H = \frac{\delta^*}{\theta}$$

The relevant routines were taken from the Imperial College Aeronautics Department standard program VELPROF explained fully in Brederode (1973). Here it is sufficient to mention that, the check whether the BL was turbulent or not, i.e. whether there was a log law region (where the condition of the local equilibrium would be satisfied) or not, was made by looking for the points in the measured profile satisfying the condition:-

$$1250.0 < \frac{yU_\infty}{\nu} < 0.2\,\frac{\delta U_\infty}{\nu}$$

These points would lie in the log law region, namely:-

$$\frac{U}{U_\tau} = \frac{1}{K}\left(\ln \frac{Uy}{\nu} + C\right)$$

where K and C are constants.

Strictly speaking, this condition was found experimentally to be valid in the TBL in a smooth free stream. But since no experimental (or otherwise) evidence was reported in the literature (or in the present work) to the effect that the inner layer equilibrium was affected by the FST, this condition was used in the present work.

Then a least squares fit of a straight line in the log law region gave the constants in the Clauser chart co-ordinates, i.e. the constants A and B in the expression:-

$$\frac{U}{U_\tau} = A + B \ln \frac{U_\tau y}{\nu}$$

and writing the log law as:-

$$\frac{U}{U_\tau} = \frac{1}{K}\sqrt{\frac{C_f}{2}}\left(\ln \frac{U_\tau y}{\nu}\sqrt{\frac{C_f}{2}} + C\right)$$

the wall friction coefficient C_f could be determined.

3.5 Determination of the Position of the First Measuring Station Relative to the Wall

In making traverses with some probe inside a BL, the question of locating the first measuring point relative to the surface always presents a problem, especially where the whole layer of interest is so small that any slight error in determining the position of the wall constitutes a considerable percentage of the thickness of the relevant

layer. And as the usual optical or electrical methods that can be used in this respect depend to some extent on personal judgement (e.g. stopping the traverse gear when the electric contact between the probe and the wall is signalled), they were not used in the present work. Instead, a method that depends mainly on the properties of the flow in the viscous region of the BL was adopted.

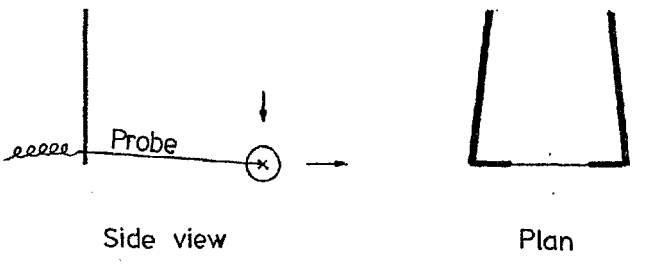
The underlying idea is that the mean velocity very near the wall is a linear function of the distance from the wall or very nearly, so, i.e.:-

$$\frac{U}{U_\infty} \propto \frac{U_\infty y}{\nu}$$

Hence, if we have a few points very near the wall so that they lie inside this region, then by extrapolating a straight line fit through these points to the point of zero velocity, the distance from the first measuring point to the point where the mean velocity vanishes can be determined.

The following steps were followed in the process:-

1. In the experiment of measuring the mean velocity using a single wire, the wire used was made such that the tungsten wire was soldered right on the tips of the prongs as in the sketch below.



Side view Plan

2. The wire should be mounted on the traverse gear such that its axis would make an angle with the horizontal as in the sketch.

3. With the help of a magnifying lens, the probe was traversed as near to the wall as was possible.

4. After taking the first reading at the position nearest to the wall, the wire was then traversed outwards and a few readings were taken in as short a distance as was mechanically possible by the traverse gear used.

5. In the analysis routine, a least squares fit was then employed to pass a straight line through the first four points in the array nearest to the wall.

6. By extrapolating this line to intersect with the velocity axis on the velocity profile plot, the required correction distance could be determined (see Fig. 3.1).

7. During the present work, the limits set on this correction distance D_c were:-

$$0.0 \text{ mm} < D_c < 0.3 \text{ mm}$$

If these limits were satisfied, the correction would be added to all the points in the array.

After defining the true position of the measuring points of the U-wire, the resulting corrected mean velocity profile was used to

adjust the profiles measured at the same X-station using the X-wire. This was done by conforming the mean velocity profiles at the same station measured by both wires. The process involved interpolating the values of U/U_∞ = 0.5, 0.7 and 0.9 on both curves. The average difference between their respective y/δ's (as determined from both profiles) was taken to be the required correction. In other words, the correction in this case was the distance the U-profile, measured with an X-wire, should move to coincide with that measured with a U-wire. Such a correction was then added to the distances of all the points from the wall.

A possible source of error in this method is the possibility that the heat losses from the wire by free convection may become appreciable very near the wall (due to the higher thermal conductivity of the metal wall and the slower fluid). This error may result in an overestimated air speed near the wall. Applying the correction proposed by Wells (1962) to the expected worst case, i.e. the first 3 points nearest to the wall in the thinnest laminar profile in the experiment, errors in the measured speeds were estimated at 44% for the first point, 12% for the second and 3% for the third which resulted in a 2% error in determining the value of δ at this station. This error was very much reduced as the BL got thicker.

3.6 Burst Intermittency Detection

In the course of analysing the U-wire recordings taken in the transitional BL, one of the purposes was to study the statistics of the turbulent bursts. In order to do this, a computer program was developed to compute the burst formation rate, the burst size and the burst intermittency averaged over the length of the record in question. The algorithm would follow the following procedure:-

1. Digitized signal representing fluctuating velocity in the x-direction would be converted into velocity units using the hot-wire calibration constants.

2. The signal would be squared, and the first and the second derivatives of the squared signal would then be computed using a linear difference technique, i.e. to get:-

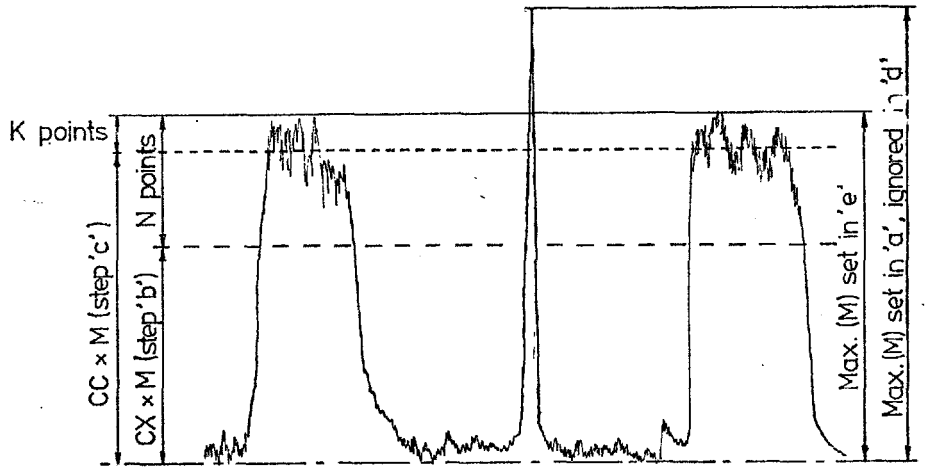
$$u^2, \frac{\partial u^2}{\partial t}, \frac{\partial^2 u^2}{\partial t^2}$$

3. In order to obtain a relative criteria of turbulence or burst occurrence, the program would:-

   (a) Find the absolute maximum in the whole record for each of u^2, $\frac{\partial u^2}{\partial t}$, $\frac{\partial^2 u^2}{\partial t^2}$.

   (b) Retain only the points in the records of u^2, $\frac{\partial u^2}{\partial t}$, $\frac{\partial^2 u^2}{\partial t^2}$ whose amplitude (A) would satisfy the condition:-

   $A \geq$ CX times the respective absolute maximum [CX (< 1) is an arbitrary constant (input)], i.e. the program would retain N points which would be less than the original total number of points in the whole array and would only operate on them.



(c) Find the number of points (K) in (N) (K < N) such that:-

Amplitude (A) ≥ CC times the respective maximum

(where CC is an arbitrary input constant less than unity).

(d) Declare these maxima to be adequate to define the burst throughout the signal record if:-

K ≥ CCC times N

[where CCC is an arbitrary constant less than unity (input)].

(e) If not, update the maximum in question such that:-

New maximum ≡ CC times old maximum

(where CC is defined in (c) above). Steps (c) - (e)

would be repeated until adequate maxima would be found.

(f) Define the criteria of the burst occurrence as:-

$$\frac{\partial u^2}{\partial t} \geq \text{FACB times } \frac{\partial u^2}{\partial t}\Big|_{max}$$

or:-

$$\frac{\partial^2 u^2}{\partial t^2} \geq \text{FACA times } \frac{\partial^2 u^2}{\partial t^2}\Big|_{max}$$

(where FACA and FACB are arbitrary input constants less than unity).

4. In order to eliminate all the dropouts in the intermittency plot, the whole plot would be scanned and dropouts of width (B) such that:-

$$B < \text{PERIOD}$$

would be ignored. Here PERIOD is an arbitrary input constant of dimension time.

During the present work, it was found through trial and error that the following values for the arbitrary constants gave satisfactory results:-

CX = 0.2

CC = 0.85

CCC = 0.1

FACA = 0.15

FACB = 0.15

PERIOD = 0.012 second

It should be pointed out, however, that as the criteria used in the present work were relative ones, in any run there should be at least one genuine burst of turbulent flow to set the criteria right, because if this program was tried on a laminar signal with no bursts of turbulent flow, the program would magnify the noise in the signal and would consider it as turbulence, thus giving wrong results. To overcome this situation, a minimum threshold should be imposed on the amplitude maxima below which the signal should be declared laminar. In the present work, it was not felt necessary to look for such a threshold since all the runs without exception contained genuine turbulent bursts in them.

It should also be said that a normal signal with a thin spike of a very high amplitude relative to the rest of the signal would not fool the routine as it would certainly contain very few points so that the process in step (d) will ignore it. Appendix I contains the listing of the routine used. For a review of the recent relevant work on the subject, see Bradshaw et al (1973).

3.7 The Power Spectral Analysis

The evaluation of the power spectral density of the turbulent signals was performed using the Imperial College Aeronautics Department standard computer program POWSPEC developed by Davis (see Davis, 1974).

The program employed a Fast Fourier Transform (FFT) method following the Cooley-Tukey procedure. For a signal y(t) such that:-

$$y(t) = y\left[\frac{n}{s}\right]$$

where s is the sampling rate, n = 1, 2 .... N and N is the number of points in the signal record. The power spectral density is defined as the Fourier transform:-

$$\int_0^T y(t)\, e^{-i2\pi ft}\, dt$$

or as the Fourier components:-

$$X_K = \sum_{n=0}^{N-1} y(n)\, e^{-i\frac{2\pi Kn}{N}}$$

defined at f = K/Nh, K = 0, 1, 2 ...., N - 1, where h = 1/s.

And while each of the Fourier components is expressed as a series of N terms according to the above formula, the FFT method is based upon decomposing N into its composite non-unity factors (multiple of 2 in the case of the Cooley-Tukey procedure) and proceeding on the smaller number of composite terms that add up (in an iterative procedure) to the right value of the Fourier component X_K. For a detailed discussion of the procedure, see Bendat et al (1971).

In the program, the record length considered was $1024 = 2^{10}$ points and the final results were taken as the averages over a total record length of 40,000 points. This represented an input signal of length 8 seconds real time sampled at 5,000 sample/second and filtered at 2,500 c/s to avoid aliasing. The bases on which the above sampling

rate was chosen is discussed in detail in Section 2.9.2, while in order to arrive at the optimum length of the record to be analysed, the analysis was performed on some records for different lengths of up to 80,000 points. But although the computation time was nearly doubled, yet the spectra obtained were only about 5% different on the average from those of length of 40,000 points. Therefore, this length of 40,000 points was used throughout the analysis. The program produced the spectra plotted as (spectral analysis vs. frequency). The results obtained are discussed in Chapter 7.

3.8 Estimation of the Convection Velocity for the Disturbances of Different Wave Number at Different Heights Inside a BL

The convection velocity (U_c) is the speed at which the pattern of turbulence is convected past a fixed observer, which is usually different from the local mean flow velocity and also different for different wave numbers (WN). In a BL, and in order to render the spectra at different y/δ's amenable to direct comparison one with the other, the effects of variations in the local (U_c) both with the WN and with y/δ (as seen by a fixed observer) must be removed. To discuss this issue, we first look at the question of determining the local (U_c) for the turbulent eddies of different sizes in a BL.

The first attempt to tackle this problem was made by Taylor through the assumption of a frozen turbulence pattern. This assumption amounted to assuming that:-

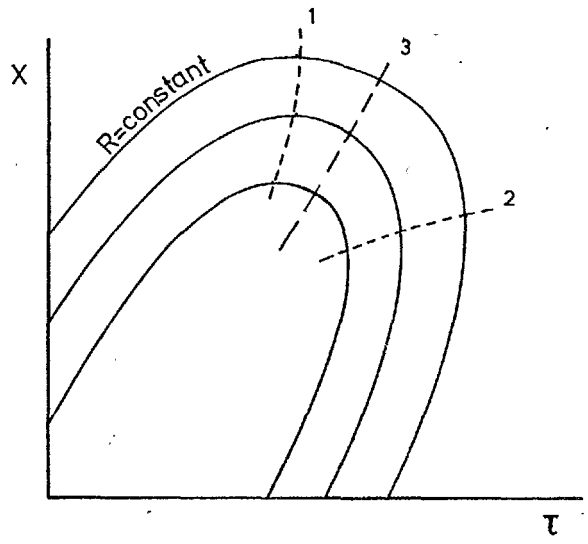
$$u(x + U\tau,\ t + \tau) \neq f(\tau)$$

where U, u are the mean and fluctuating longitudinal velocity components respectively at the point (x, t) and t, τ are time. In the case of

non-sheared grid turbulence, measurements confirmed Taylor's postulate that the local U_c was approximately equal to the local speed of the fluid. Yet, Lin (1952) showed that Taylor's hypothesis was valid only if the turbulence level was low, viscous forces were negligible and the mean shear was small. Obviously none of Lin's conditions would be observed in a BL.

The problem of defining the convection velocity for the disturbances travelling in a BL can be looked at from two angles. The first is the problem of defining an overall convection velocity at which the turbulence pattern as a whole travels which, according to all the investigators, is somewhat different from the local mean velocity. And the second is that of defining the convection velocity at which a disturbance with a particular wave number travels at a certain point inside the BL. The second is the one of interest in the present context.

As to the question of how to define a measurable U_c, Favre et al (1957, 1958) devised a technique based on the measured two point space-time correlation that defined U_c as:-



U_c = local slope of the tangent to curve 1 in the above figure along which $\left(\frac{\partial R}{\partial \tau} = 0\right)$, or;

U_c = local slope of the tangent to curve 2 in the above figure along which $\frac{\partial R}{\partial x} = 0$, i.e.

$U_c = \frac{\partial x}{\partial \tau}$ along 1 or 2

where $R(x, \tau)$ is the two point space-time correlation for the separation x and time delay τ.

On the other hand, Willmarth et al (1962) introduced the slightly different definition of U_c as the speed of the frame of reference in which the decay of the correlation would be minimum, i.e.:-

$\frac{\partial x}{\partial \tau}$ at ∂R = minimum

or the slope of the tangent to curve 3 in the above figure.

Wills (1964), on the other hand, used the complete WN/phase velocity spectrum of the fluctuations in estimating the convection velocity, whereby providing a readily obvious distinction between the dominant U_c at a particular wave number, and an overall U_c for the whole motion.

The convection velocity of the pressure producing eddies are better documented (see Blake (1970), Bull (1967), Willmarth et al (1962, 1965, 1967, 1970), Wills (1970) and Corcos, 1963).

As for the velocity fluctuations, investigators like Favre et al (1967) and Favre (1965) reported estimates of U_c in a BL, whereas Wills (1964) studied U_c in the outer region of a jet discharging in

still air. The following values are taken from Wills' results:-

Frequency	Convection Velocity
Whole Pattern	U_c (overall)
200 c/s	0.95 U_c
2,000 c/s	1.05 U_c

i.e. variations of about 10% (0.95 - 1.05) in the overall U_c were experienced as the frequency increased from 200 c/s to 2,000 c/s (which would not be considered as a low frequency relative to the frequency range of interest in the present experiment). Nevertheless, it could be argued that Wills' results should be carefully applied to the outer region of a wall layer only, as they were obtained for the outer region of a jet, because the highly turbulent, highly sheared flow near the wall might render his results inapplicable.

On the other hand, Favre and co-workers argued that the fluctuations inside the BL were one of two categories, namely:-

1. Small scale fluctuations (high WN) for which:-

$$U_{c_1} \sim U_{local}$$

throughout the whole BL width.

2. Large scale fluctuations (low WN) which would tend to travel at more or less the average mean speed across the BL, i.e.

for a fully developed TBL (say):-

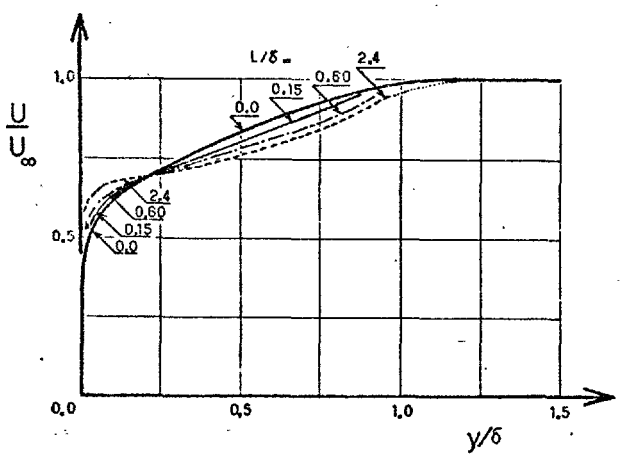
$$U_{c_2} > U_{local} \text{ at } y/\delta < 0.24$$

$$\simeq U_{local} \text{ at } y/\delta \simeq 0.24$$

$$< U_{local} \text{ at } y/\delta > 0.24$$

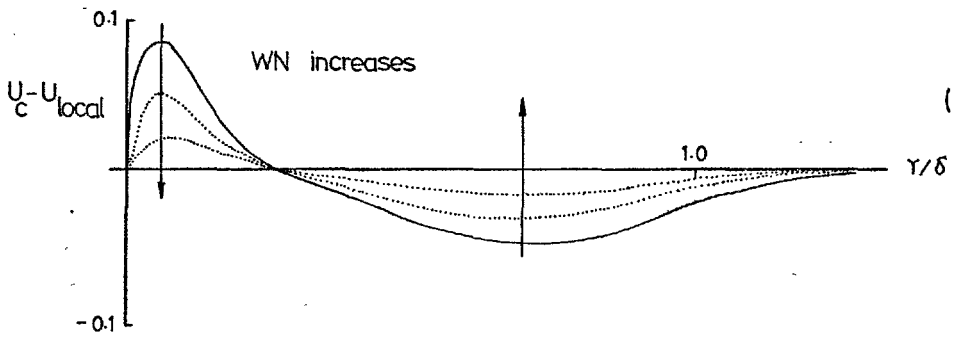
where $y = 0.24\ \delta$ is where the local mean speed equals the average speed across the layer. This is plausible since the smaller eddies are less distorted by the large scale motion and the mean shear than larger eddies and, therefore, smaller eddies are expected to behave more according to Taylor's hypothesis.

Favre et al (1967) reported the plot sketched below for the TBL:-



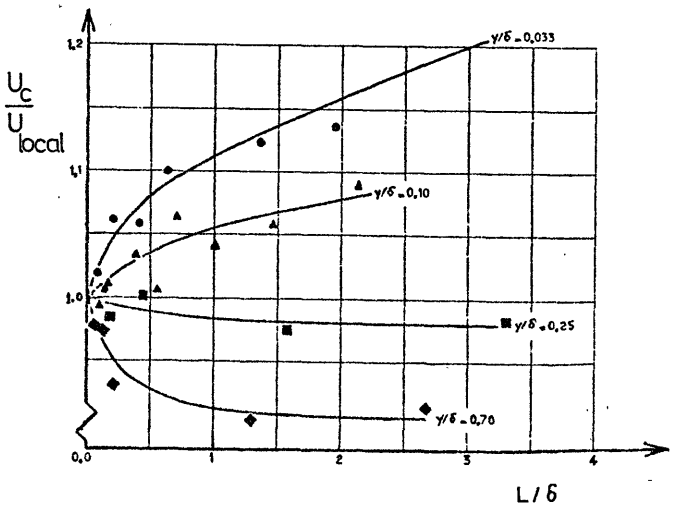
(curve A)

from which the plot sketched below could be produced.



(curve B)

They also reported that the experimental variations in convection velocity, for different WN for different heights in a TBL, might be represented as sketched in the figure below:-



(curve C)

Here, it should be pointed out that curve C could be considered as another way of presenting the data in curve B. For plotting U_c vs. y/δ with the WN as a parameter would produce curve B, while plotting U_c vs. the WN with y/δ as a parameter would produce the curve C.

In order to render spectra at different y/δ comparable, they must be plotted as a function of the WN defined using the local convection velocity $U_c(\omega)$. The following approximate procedure was followed in order to define $U_c(\omega)$ (L is the wave length):-

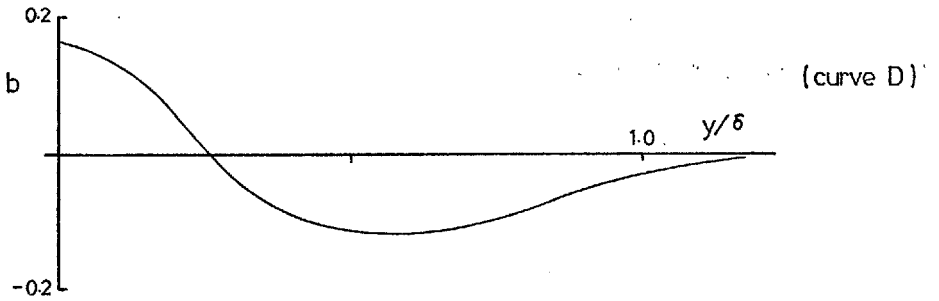
(i) Referring to curve C, it was assumed that:-

(a) At every y/δ, the U_c curve would asymptote to a certain value as L/δ increased (i.e. ω decreased). And that those limiting values could be inferred from the plot at every y/δ reported.

(b) Those curves could be approximated by ellipses so

that at, say $L/\delta = 4$, every curve would complete one quarter of an ellipse, i.e. the intersection of each curve with the line $L/\delta \simeq 4$ to the point where $U_c/U_{local} = 1.0$ would give half the minor axis (b) of that ellipse.

(ii) Hence, the following curve for the turbulent BL could be plotted as equivalent to curve C.



(iii) As fluctuations with high WNs would move at nearly the local mean velocity and those with low WNs would move at nearly the average mean velocity of the flow across the BL, it could be shown that the point at which the curve D would cross the horizontal axis would be the point where:-

$U_{local} \simeq U_{average\ across\ layer}$

(iv) It was also postulated that the limiting values for U_c/U_{local} at the BL edge and near the wall would be nearly the same for both laminar and turbulent BLs for low WN fluctuations.

(v) Hence an approximate curve similar to curve D could be obtained for any BL mean velocity profile, provided that it would cross the axis where the average velocity across

this particular layer would be equal to the mean velocity.

In other words, the following steps should be followed in order to determine the values of $U_c(\omega)$ at any point inside the BL:-

1. From the mean velocity profile, find the point where $U_{local} = U_{average}$ and using the terminal values reported by Favre et al (1967), sketch a curve similar to curve D.

2. For every y/δ, get the length of half the minor axis (b) of the relevant ellipse from curve D.

3. Take $L \simeq \frac{U_{local}}{f}$ as a first guess.

4. If $L/\delta > 4$, put $L/\delta = 4$.

5. $a = 1 - \frac{L/\delta}{4}$.

6. $$\frac{U_c(\omega)}{U_{local}} = 1 + \frac{b}{|b|}\sqrt{b^2(1 - a^2)}$$

Ideally, steps 3 - 5 should be iterated using the newly calculated $U_c(\omega)$ in step 3 instead of U_{local} and so on until convergence. Yet to within the accuracy of the method, one iteration should be sufficient.

A computer routine was developed to perform this correction procedure. The spectra corrected using these methods are presented in Chapter 7.

3.9 Static Pressure Distribution Around the Nose-Plate Combination Using the Potential Flow Theory

In order to find the shape of the nose-plate combination that would give the best approximation to a monotonically decreasing static pressure (i.e. negative pressure gradient) all the way over the nose-plate surface (for reasons that were discussed in detail in Section 2.3), the static pressure distribution was calculated over a large number of nose section shapes (fitted onto the flat plate) using the potential flow theory. The method used in the calculation was the surface source method due to Hess and Smith (1967).

In the method, the flow around the given body is approximated by an initially unknown distribution of sources (or vortices) in the shape of straight line segments. In other words, the surface of the given body is divided into straight line segments meeting at nodes (to be specified as input). The solution for velocity and pressure on the body is obtained by imposing the appropriate boundary conditions normal to the surface. Such a boundary condition for a solid surface like our case is that the velocity (V) normal to the surface is zero ($V = 0$). This leads to an integral equation for the unknown source density distribution (or the source strength per unit length of surface). This equation is then solved (in the computer program used) in a finite difference form. After obtaining the source density distribution, it is then easy to solve for the tangential velocity distribution and hence, from Bernoulli's equation, the pressure distribution around the body.

The method was developed to handle bodies of arbitrary shapes at arbitrary angles of attack provided that separation occurred only at a single (trailing) edge. The results obtained are discussed in Section 4.3.

3.10 Determination of the Longitudinal Integral Length Scale of Turbulence (L_x)

Considering the integral time scale of turbulence as being defined as:-

$$T = \frac{1}{u^2} \int_0^\infty R(\tau)\, d\tau$$

where $R(\tau)$ is the auto-correlation of the signal for a time delay (τ). And assuming the validity of Taylor's hypothesis that, for short distances in the absence of strong pressure gradient and viscous forces:-

$$U \int_0^\infty R(\tau)\, d\tau = \int_0^\infty R(x)\, dx$$

Therefore, if T is the characteristic time scale, hence:-

$$L_x = \int_0^\infty R(x)\, dx$$

$$= UT$$

= Characteristic length scale of the energy containing eddies in the x-direction

$$= \frac{U}{u^2} \int_0^\infty R(\tau)\, d\tau \qquad (a)$$

And as:-

F(n) = Power spectral density at frequency n

$$= 4 \int_0^\infty R(\tau) \cos(2\pi n\tau)\, d\tau$$

or:-

$$F(0) = 4 \int_0^\infty R(\tau)\, d\tau$$

Hence:-

$$L_x = \frac{1}{4} \frac{U}{u^2} F(0) \qquad (b)$$

Therefore, there are two possible methods of determining the length scale of turbulence using either formula (a) or that of (b).

It is worth noting that both methods have some degree of uncertainty since the power spectrum (the correlation curve) has to be extrapolated* (integrated) to the origin (to infinity) to get the value of F(0) (T) (see Fig. 3.2). Such uncertainty is not helped by the fact that when the signal is recorded, the DC filter used is not ideal, something that may cause distortion of the signal at low frequencies.

Yet while method (b) was tedious since it involved spectral analysis, there was a practical advantage for method (a) since the HP correlator model 3721A was available during the experiment. This correlator gave directly a plot of the auto-correlation vs. time on its screen which could easily be plotted on paper using an x-y plotter. In any case the two methods were used in determining the length scale

---

* The spectrum plot is extrapolated (to get the value of F(0)) using Corrsin (1951) conclusion that the spectrum of homogeneous turbulence is flat at low frequencies. This, however, is not precisely accurate in the case of filtered grid turbulence signal like the present case. Yet, such uncertainty is expected to be within the accuracy of measuring the turbulence integral length scale.

of turbulence and wherever there was a large discrepancy between results obtained by them, the one obtained by method (a) was adopted.

The charts in Figs. 3.3 and 3.4 show the experimental arrangement of measuring the integral length scale of turbulence using the two methods respectively.

3.11 Data Smoothing

Because the experimental data might contain some odd values at some unexpected regions, and in order to avoid undue waviness in the computed first and second derivatives, the input data profiles were smoothed before performing the process of differentiation.

The smoothing routine used was a standard routine at the Imperial College Aeronautical Department that was developed at the NPL. The routine could handle an array containing at least 3 values not necessarily equally spaced. If the number of terms in the array was large enough, the routine would take every 6 values and would fit a polynomial of the third degree through them using the least squares method. It would then compute the standard deviation from the new curve for all the points and would assign its value to all the points which would be considered wild, i.e. which would deviate from the new curve with more than the standard deviation. The routine would also fix the first and the last points in the input array.

The program was found to be very suitable for smoothing the BL type profiles. The resulting smoothed profiles have continuous first and second derivatives. The routine was also tested by using it to smooth curves which contained waviness in them. It was found that the routine preserved all the features of the original profile in a remarkable way provided that the particular feature was defined with at least three points.

CHAPTER 4

GENERAL PROPERTIES OF THE FLOW FIELD IN THE EXPERIMENT

4.1 The Sound Pressure Level Inside the Tunnel

It is known that aerodynamic noise in general can, if its level is high enough, promote transition. Therefore, it seemed important that the sound level inside the tunnel as well as outside it should be checked in order to avoid any highly excited mode of the duct or any noise from the fan that might affect the results of the experiment.

It was also reported by Gardner (1975) that, the fluctuating lift generated by the FST flowing over a flat plate with a sharp TE, can cause some acoustic modes to resonate inside the tunnel duct. Hence, this experiment was also meant to check that the presence of the (thin) flat plate inside the tunnel had no unfavourable effect on the sound pressure field of the tunnel.

For this purpose, the narrow band sound pressure level $S_{pp}(\omega)$ was measured using a condenser microphone and an electronic spectrum analyser in the following two cases:-

1. Inside the wind tunnel with the microphone inserted through the tunnel wall so that its diaphram was flush with the tunnel inner surface.

2. Outside the wind tunnel with the microphone taped to the tunnel side wall. In this case, the microphone was placed near the tunnel breathing gap (at about 10 cm). The aim was to be able to distinguish between the pressure fluctuations

due to turbulence and those due to acoustic noise.

The measurements were obtained for four different tunnel fan speeds, i.e. at mean flow speeds (U_∞) of 15, 26, 39 and 44 m/s. The turbulence was introduced into the flow by means of the grid of 1.5 in. mesh size (see Section 2.7). The output of the spectrum analyser $S_{pp}(\omega)$ was normalised by the free stream speed (U_∞), the free stream turbulent kinetic energy ($\overline{q_\infty^2}$) at the position of the microphone, and the condenser microphone diameter (d). Fig. 4.1 shows the plotted results as:-

$$\frac{S_{pp}(\omega) \cdot U_\infty}{q^2 \cdot d} \text{ vs. } \frac{\omega \cdot d}{U_\infty}$$

where (ω) is the frequency in Hz ($\omega = 2\pi f$). It is seen from the plot that:-

1. The value of the spectrum outside the tunnel was always less than 1% of the corresponding value inside the tunnel at the same frequency. This clearly indicated that the major source of the sound pressure inside the tunnel was the pressure fluctuations coming from the growing BL on the tunnel walls from the FST, from the duct modes, if any, and from the fan blade passing frequency and the like.

2. Changes in the flow speeds showed some effect on spectra outside the tunnel at low frequencies due to the increased noise of the compressor that drove the tunnel which was fixed onto the floor of the room. Nevertheless, this had very

little or no effect on the pressure spectra inside the tunnel.

3. None of the resonant frequencies which were reported by Gardener (1975) were present in the tunnel.

4. There was no appreciable concentration of power at any of the ducts modes detected previously by the author (Abdel-Kereem, 1975).

5. Since the BL over the microphone position for the spectra taken inside the tunnel was laminar, there was not any appreciable power in the energy containing frequency range of BL type turbulence. This was demonstrated by the steep fall in energy in the mid-section of the plot.

4.2 Temperature Drift Inside the Tunnel Due to Prolonged Tunnel Operation

The following table was composed for the grids that were used in the present experiment (dimensions are in inches).

No.	Grid dimensions	Area blockage ratio	Total length of wetted edge of grid rods	Air speed at 600 rpm
1	1.5 x 3/8 x 3/8	0.422	2592	23.0
2	3.0 x 0.5 x 0.5	0.281	1440	29.0
3	4.0 x 0.5 x 0.5	0.210	1134	32.5
4	6.0 x 1.25 x 0.5	0.317	684	25.3
5	9.0 x 1.5 x 0.5	0.234	480	28.4

It is seen from the table that the air speed downstream of a particular grid for a constant tunnel fan speed was very nearly inversely proportional to the grid area blockage ratio (Area blockage ratio ≡ Projection area of the grid/total area of the tunnel cross section).

It is also seen that the 1.5 in. grid was the one offering the highest resistance to the air flow. And since this particular grid was the one most used in the present experiment, and that the tunnel was a closed circuit type, special care was taken to ensure that the temperature rise inside the tunnel did not cause errors such as a decrease in the tunnel speed due to a decrease in the air density, a change in R due to changes in U and ν or inaccurate hot-wire measurements due to the wire drift.

Therefore, an experiment was carried out to assess the rise in the static temperature (^{o}C) inside the tunnel as a result of prolonged tunnel operation with and without the 1.5 in grid. For convenience and ease of performing the experiment, the air temperature was measured at two fan speeds, namely, 500 rpm and 250 rpm, and the result is shown in Fig. 4.2. From the figure, we notice the following:-

1. The increase in temperature due to the introduction of the grid was about 5% of the atmospheric temperature (^{o}C) at the fan speed of 500 rpm, while the increase was only 3% or less at the speed of 250 rpm.

2. The rate of temperature increase with time increased as the fan speed increased.

3. The fluid temperature inside the tunnel asymptoted to a constant value that was directly proportional to the fan rpm.

And hence, because the static temperature inside the tunnel increased at a high rate at the start of the tunnel operation, it was, therefore, thought adequate to leave the tunnel running for at least two hours before taking any measurements. In this way, a steady state working temperature was ensured inside the tunnel. Unfortunately, this did not completely get rid of the hot-wire drift due to operating at a changing fluid temperature. Nevertheless, such an effect was minimised by calibrating the wire used about once every two running hours.

4.3 Static Pressure Distribution Over the Plate

The static pressure distribution along the plate surface mid-section was investigated experimentally using the static pressure tappings drilled along the plate surface (see Section 2.5).

Figs. 4.3a and 4.3b show the measured static pressure over the thin and the thick plates respectively at zero incidence for the case of no grid and that of the 3.0" grid inserted in the tunnel. The plots are characterised by:-

(a) A very steep negative pressure gradient just after the LE which was less for the thick plate.

(b) A region of positive pressure gradient following the negative pressure gradient region that extended over the rest of the nose section. And while it was not as steep as the negative pressure gradient region, it showed the same tendency of getting milder as the plate thickened.

(c) No significant change in the pressure distribution is brought about by the FST of intensity 0.03.

It was observed that the pressure gradient decreased in general with increasing plate thickness. It was also seen that as the nose section got longer, the gradient of the pressure decreased*. That is, $\partial P/\partial x$ scales to $1/L$ where L is the length of the nose section.

Since it is known (Hall (1968) and Hall et al, 1972) that transition is promoted by positive pressure gradient, it was necessary to find the shape of the nose section (other than an ellipse) and the incidence of the plate that would give the least positive pressure gradient over the nose (see Section 2.3).

For this purpose, the programed potential flow calculation due to Hess and Smith (1967) was employed to calculate the static pressure distribution over the nose-plate arrangement. After performing the calculation for more than 20 different shapes, a nose geometry was arrived at through trial and error. This shape was nearly an ellipse but was elongated near the junction to the flat surface whereby the nose surface was allowed to joint the flat plate surface more gradually (nose No. 5 in Fig. 2.4). The results of the calculations are plotted in Fig. 4.4.

Placing the plate at incidence was also studied and the results for such calculations for the incidences of -0.5^{o} and -1.0^{o} are also presented in Fig. 4.4. It is clearly demonstrated that using the elongated nose section while placing the plate at an angle of -1.0^{o} to the horizontal practically completely eliminated the positive part of the pressure gradient.

An experiment to measure the static pressure distribution over

---

* This is true until a certain limit where curvature of leading edge is so large that pressure overshoots and a region of positive pressure gradient results.

the plate with this new nose (No. 5 in Fig. 2.4) fitted was carried out. The results obtained (plotted in Fig. 4.5) show excellent agreement with the calculated ones.

4.4 The Nature of the Flow Behind the Turbulence Producing Grids

Measurements were made behind the grids used in the experiment in order to assess the degree of homogeneity of the turbulence generated by them in the spanwise direction as well as its development in the streamwise direction. Fig. 4.6 shows that for the three grids (M = 1.5", 3.0" and 6.0") the streamwise component of the turbulent KE (plotted as $U_\infty^2/\overline{u^2}$ vs. X/M where M is the grid mesh size) decays at a very nearly constant rate. It also shows that for slower mean flow, the turbulence requires a larger distance to settle down to a more or less homogeneous isotropic turbulence (i.e. following the decay rate of the homogeneous isotropic turbulence in the initial period - see Batchelor (1953) and Baines et al (1951) for more details). Therefore, the experiments have to be performed either at a reasonably high mean flow speed or at a distance from the grid large enough to allow the FST to settle. Based on this fact, the relation:-

$$\frac{U^2}{u^2} \propto \frac{1}{C_D}\left[\frac{X}{M} - \frac{X_o}{M}\right]$$

(where C_D is the drag coefficient of the grid and X_o is the settling distance behind the grid to where the turbulence is homogeneous) accounts for the observed decay of the grid turbulence.

As for the mean flow over the plate, its development along the plate surface at zero incidence is plotted in Fig. 4.7. The observed increase in U along the plate was due to the growing BL over

its surface and was about 6% across the plate length for the 3.0" grid and a little more for the other grids (6.0" and 9.0").

No attempts were made to improve this mean velocity distribution over the plate first because most of the transition measurements were made in the first quarter of the plate length where the decrease in the mean flow was only about 2% of its value at the LE and secondly because the job of changing the tunnel roof configuration to effect a constant mean flow along the plate was proved to be very difficult practically because:-

(a) The large number of movements of the plate up and down the tunnel test section.

(b) The presence of the traverse gear over the measuring station.

(c) Fear of disturbing transition by any unaccounted for changes in the pressure distribution along the plate that may result thereby.

The intensity of the turbulence component in the streamwise direction, on the other hand, decreases monotonically in the x-direction as seen in Figs 4.8a and 4.8b. As for the intensity of turbulence in the case of no grid in the tunnel, the process of determining it was very difficult due to the small signal to noise ratio. But as seen in Fig. 4.8a, and despite the effort that was made to filter all the noise and retain only the signal of interest, there was no sign of any particular trend of change in the intensity along the plate and it remained nearly constant throughout.

While this detected change in the intensity of turbulence in

the free stream might pose a problem in deciding on the intensity that would correlate with the occurrence of transition for different grids and R 's, yet the argument put forward in Chapters 5, 6 and 7 (that the FST is vital inasmuch as it provides turbulence to the BL while it is very thin over a relatively very short distance well before transition occurs) might avoid this problem.

No measurements of the intensity of the three fluctuating components were made far away from the plate. Nevertheless, those ones taken at about 6 cm from the plate and reported in Fig. 4.8b could give a fairly accurate idea about the FST over the plate. From the figure, the u and w-components were only slightly different while apparently the v-component was still affected by the wall blockage at the height of 6 cm. Anyway, within the expected experimental inaccuracy, this plot showed that the grid turbulence generated behaved closely like the homogeneous isotropic turbulence.

The non-uniformity of the flow through the largest grid used in the experiment (9.0" grid), on the other hand, posed some threat to the credibility of the homogeneity assumption for the turbulence produced by this grid. And a question arose as to whether transition would still occur at the same streamwise distance throughout the plate span or not.

In order to clarify this issue, measurements were made of the components $\sqrt{u^2}$ and U outside the BL around transition at a distance of about 12M downstream of the M = 9.0" grid. The results are reported in Figs. 4.9a and 4.9b as three-dimensional plots of:-

$$\left(x \, , \, \frac{U - U_{ref}}{U_{ref}} \, , \, z \right)$$

and:-

$$\left(x \, , \; \frac{\frac{\sqrt{\overline{u^2}}}{U} - \frac{\sqrt{\overline{u^2}}}{U}\Big|_{ref}}{\frac{\sqrt{\overline{u^2}}}{U}\Big|_{ref}} \, , \; z \right)$$

respectively. The subscript ref refers to a reference value with which all values were compared.

Also the first derivative of the u-component was measured inside the BL in the same region at a constant height from the wall of about 1.0 mm. This result is also presented in the form of a three-dimensional plot of:-

$$\left(x \, , \; \frac{\sqrt{\overline{\left(\frac{\partial u}{\partial x}\right)^2}}}{\sqrt{\overline{\left(\frac{\partial u}{\partial x}\right)^2}}} \, , \; z \right)$$

in Fig. 4.9c. The relative positions of the grid bars are also marked on the figures.

Inspecting Fig. 4.9a, we see no definite pattern or wake at this distance behind the grid bars on the mean velocity which had a maximum deviation from the average of about 0.7%. On the other hand, there was a trace of a wake in the form of zones of high intensity that were localised behind the grid vertical bars in Fig. 4.9b which amounted to about 8% deviation from the average value. In spite of such a large non-uniformity in the FST, Fig. 4.9c fails to show any sign of such non-uniformity thus providing yet another argument in favour of the postulate discussed in Chapters 5 - 7 that the FST is decisive to the process of transition only inasmuch as it disturbs the newly growing LBL while it is still very thin. Anyway, this leaves unanswered the question of the transition uniformity across the

span. Nevertheless, it is shown in Section 5.2.3 that across the span, a variation of 7% in R_{x_T} is not unlikely in the general case of large FST intensities of 2% and over.

4.5 The Longitudinal Integral Scale of Grid Produced Turbulence

The integral length scale of grid turbulence (L_x) has always been a source of uncertainty, not only due to the pitfalls in measuring it, but also due to the nature of its definition that makes it a function of nearly all the parameters of the flow field behind the turbulence producing grids.

From the analysis of Batchelor (1953) and Townsend (1976), it may be shown that:-

$$\frac{L_x}{M} \simeq \frac{U}{u} \cdot F\left[R \quad , \frac{X - X_o}{M} \text{ , grid geometry}\right]$$

Therefore, the job of including L_x in the analysis had to be tackled very carefully. L_x inside the test section was determined experimentally using the technique discussed in detail in Section 3.10. Typical results are shown in Figs. 4.10 - 4.11. The data are plotted as:-

$$\frac{L_x}{M} \text{ vs. } \frac{X}{M} \quad \text{and} \quad \frac{L_x}{b} \text{ vs. } \frac{X}{b}$$

where M and b are the grid mesh size and the grid bar width respectively. The amount of scatter is more or less the same in the two plots which makes it difficult to say which of the two grid dimensions correlated the results better. Nevertheless, the mesh size M was used in the analysis to come wherever a representative length scale of the grid was

needed. The plot in Fig. 4.12 shows clearly the variation of the longitudinal scale of turbulence (L_x) with the turbulence level (U/u) (in effect, this plot shows the well-known fact that downstream of the grid, u/U decreases while L_x increases).

4.6 The Changes in the Characteristics of the Mean and the Fluctuating Velocity Profiles in the LBL Due to Changes in the Plate Thickness

As discussed in Section 2.3, two plates of different thicknesses were made available for use in order to study the effect of changes in the plate thickness on the transition. While the thin plate was the one chosen to perform the extensive measurements of all the flow properties over its surface, it was thought adequate to carry out some measurements for the mean and the fluctuating velocities inside the LBL over the thick plate and compare them with similar measurements over the thin plate within the same region at the same R .

For this purpose, measurements of U, $\sqrt{\overline{u^2}}$, $\sqrt{\overline{v^2}}$, $\sqrt{\overline{w^2}}$ over the thick plate (at X = 15 cm and 20 cm) and over the thin plate (at X = 20 cm) were made downstream of the pressure gradient region over the nose. Fig. 4.13 shows the normalised mean velocity profile at all the stations for both plates together with the Blasius profile for the LBL in the quiescent stream. The figure shows a very good collapse on the Blasius profile for all the cases. One can, therefore, say that the development of the LBL over the two plates at least within the same range of R and before the onset of amplified disturbances are very nearly identical and they follow the Blasius profile very closely. This was true since the measurements were taken where the pressure gradient was zero, although the rate at which the profiles developed was affected by the history of the pressure gradient as will be discussed in Section 6.3.

In spite of this observed similarity of the mean flow profiles. the profiles for the fluctuating velocity components were not identical. Fig. 4.14 emphasises that there were more turbulent activities in the layer over the thick plate than that over the thin one. As a matter of fact, Fig. 4.14 shows that the turbulence intensity at station X = 20 cm over the thick plate was about twice as much as that over the thin plate at the same position and R_{θ}. This would clearly indicate that an earlier transition should be expected over the thick plate at the same R_{θ} and FST level. This subject will be investigated in detail in Chapter 5.

Plotting the same turbulent quantities of Fig. 4.14 until well outside the BL as in Fig. 4.15, we notice that the differences in the intensities of u, v and w did not only become larger in the case of the thick plate, but they also persisted over a larger distance in the y-direction. This was possibly attributable to the higher rate of production in the x and z directions at an early position where the BL was neither thick enough (so that the effect of the wall blockage would be minimised) nor turbulent enough (i.e. more turbulent mixing) for the v component to follow closer.

An interesting thing to notice is the slight drop in the value of all the profiles of Fig. 4.15 just outside the BL. This matter is discussed in detail in the following section.

4.7 Homogeneous Turbulent Flow Past a Flat Plate

It is known that homogeneous turbulent flow past a rigid flat plate undergoes certain changes near the surface of the plate (irrespective of the BL) due to the blocking action of the plate. It is also known that the v-component suffers the largest blockage effect which affects turbulence within a distance:-

$Y = F.L$

where L is the length scale of the turbulence, and F is constant.

In the present work, it was necessary to study the development of the grid turbulence as it was convected past the plate so that a better choice of the FST intensity to correlate with transition could be made.

Hunt and Graham (1978) theoretically investigated the problem for an idealised model. They assumed a high R inviscid flow with low intensity turbulence flowing over a flat plate that was long enough to ignore any effects on the solution of the conditions at the LE and the TE. Using a disturbance potential, they calculated all the components of the turbulent energy in the vicinity of the plate as a function of (y/L).

As discussed in Section 4.6 and reported in Figs. 4.13 - 4.15, measurements were taken over the thin plate for the mean speed of 6 m/s at three positions (X = 15, 20 and 25 cm) with a FST level of 0.018. The same measurements were also made over the thick plate at the same speed and X-stations, for the same FST level.

These results are plotted in Figs. 4.16 - 4.20 as:-

$$\frac{\overline{v^2}}{v_\infty^2}, \frac{\overline{q^2}}{q_\infty^2}, \frac{\overline{u^2}}{u_\infty^2}, \frac{\overline{v^2}}{v_\infty^2}, \frac{\overline{w^2}}{w_\infty^2}$$

respectively, all versus y/L_x where ∞ denotes values well away from the wall.

Fig. 4.16 which represents $\overline{v^2}/\overline{v_\infty^2}$ vs. y/L_x demonstrates a reasonable agreement between the theory and the experiment in the whole region covered by the experiment except within the BL region. It

is also interesting to note that as R_x increased, deviation from the theory just outside the BL increased. This indicates that the theory was more accurate in the region where the BL was thinner which is plausible since the theory was originally for potential flow.

The figure also highlights the possibility that the turbulence inside and that outside the BL are of different nature. This question will be discussed in Chapters 6 and 7 in greater detail. Here, it is sufficient to notice that the profile appears to be composed of the superimposition of two fields; that due to the free stream and that due to the BL. The latter seems to develop downstream independent of the former or at least in a way that is not correlated by the free stream integral length scale.

Fig. 4.17 shows a plot of $\overline{q^2}/q_\infty^2$ vs. y/L_x. Again, a good agreement with the theory is observed. The deviation from the theory can partly be attributed to the possible inadequacy of the length scale of turbulence (L_x) in correlating the curves of $\overline{q^2}/q_\infty^2$. Also, the expected failure of the theory near the wall due to the BL is seen clearly from the curve.

Figs. 4.18 - 4.20 show that right out to the BL edge and beyond, the $\overline{v^2}/v_\infty^2$ component was the one most attenuated and that although none of the components show any appreciable change in the downstream direction (i.e. in the direction of increasing R_x) outside the BL, yet inside the BL they change considerably in this direction especially very near the wall due to the production of turbulent energy there.

It is also interesting to note that $\overline{v^2}/v_\infty^2$ inside the BL had the highest rate of development in the x-direction. This could be due to the increased turbulent mixing in the outer region of the BL which would tend to homogenise the turbulence in that region. This can also

be seen from Fig. 4.15 where upon comparison between the turbulent profiles at the two stations X = 15 cm and X = 20 cm one can see a closing of the gap between the v-components on one hand and the u, w components on the other hand outside the BL. In fact, this development is more than can be attributed to the BL growth in the downstream direction only, and it may also be due to some loosening of the plate blockage as the flow develops downstream.

In any case, one is left with the conclusion that the v-component is the component developing at the highest rate through the x-distance covered by this experiment (i.e. in the thin LBL range) both inside the BL and outside it.

Here it is worth noting that, as reported in Fig. 5 in Hunt and Graham (1978), the measurements of $\overline{v^2}$ component made by Thomas et al (1977) over the moving surface show very nearly the same agreement with the theory as the present results (excluding, of course, the BL region).

And although Figs. 4.16, 4.18 and 4.19 show only fair agreement between the theoretical and the measured profiles of u and v especially just outside the BL, yet there is a striking agreement in Fig. 4.20 for the w-component nearly everywhere except in the wall region (notice the double crossing of the theoretical and experimental curves of the value of 1.0 at the approximate y-positions of 0.5 L_x and 2 L_x). Such an agreement suggests that the discrepancy in the profiles of $\overline{u^2}$ indicates a development of the longitudinal component in the direction normal to the surface. This development is possibly caused by diffusion of the turbulent energy towards the wall which results in a decrease in that component of the turbulent energy just outside the BL. This view is supported by the interesting observation that away from the BL, the $\overline{u^2}$-profile crosses the value of 1.0 at $y \simeq 2\ L_x$ in

Fig. 4.18, just as the $\overline{w^2}$-profile does in Fig. 4.20.

In conclusion we say that this theory describes fairly well the behaviour of turbulence outside the LBL while it is still thin. It loses accuracy near the wall and increasingly so as the BL develops in the downstream direction.

We may also conclude that the value of the FST intensity well away from the wall where there is no trace of the effect of wall blockage is the value that represents the particular grid turbulence best. On the other hand, the intensity just outside the BL, being so different from the intensity away from the BL, is thought to be a more suitable choice to use in Taylor's parameter (see Chapter 5).

CHAPTER 5

PARAMETERS AFFECTING TRANSITION OF A LAMINAR BOUNDARY LAYER OVER A FLAT PLATE

5.1 Introduction

In the present work, the experiments discussed in Chapter 6 and Chapter 7 are devoted to acquiring a better insight into the physical processes involved in the phenomenon of transition.

On the other hand, this chapter is concerned with discussing the experiments that were devoted to studying the possible parameter that may correlate the position of transition.

It is now generally agreed that as far as transition of incompressible low speed fluid inside a BL is concerned, two characteristic qualities of the FST are of a dominant importance. These are the intensity* and the integral length scale of the FST.

The present chapter is, therefore, divided into two main sections, namely:-

(i) The effect of FST on transition which in turn is subdivided as follows:-

(a) The effect of the FST intensity $\left(\frac{\sqrt{\overline{u^2}}}{U}\right)_\infty$.

(b) The effect of the FST integral length scale L_x.

---

* As discussed in Chapter 1, the FST intensity is taken to be $\left(\frac{\sqrt{\overline{u^2}}}{U}\right)_\infty$ in the present work.

Then a possible way of correlating these two factors with the occurrence of transition (e.g. through Taylor's (1936) parameter) is discussed.

(ii) The effect of changes in the flat plate thickness on transition. Such changes may be looked upon from two different angles:-

(a) As far as the FST is concerned, a change in the plate thickness will induce changes in the mean strain rates around the plate LE which, in turn, will cause changes in $\frac{\sqrt{\overline{u^2}}}{U}$ and L_x in the region close to the plate surface.

(b) As far as the BL over the curved part of the nose section is concerned, such changes in the plate thickness also have the effect of exposing the BL over the nose section to different static pressure distributions.

In the work presented below, the two view points are discussed.

5.2 Effect of Free Stream Turbulence on Transition

5.2.1 Effect of the Free Stream Turbulence Intensity $\left(\frac{\sqrt{\overline{u^2}}}{U}\right)$

The position of the start of amplification of small disturbances or the start of appearance of high frequency bursts in the LBL (see Fig. 7.1) was detected over the surface of the thin (1.5" thick) plate using the method described in Section 2.8. The experiment was carried out for

the 5 grids tabulated in Section 2.7. For each grid, (except the 9" grid) two positions of the plate were studied, one with the plate LE at about 12M from the grid and the other with the plate as far downstream of the grid as was possibly allowed by the test section length. For each of these two positions, transition was detected at three tunnel speeds. The results are plotted in Figs. 5.1 and 5.2 as:-

$$\left.\frac{\sqrt{\overline{u^2}}}{U_\infty}\right|_T \quad \text{vs.} \quad R_{X_T} = \left(\frac{U_\infty X}{\nu}\right)_T$$

$$\left.\frac{\sqrt{\overline{u^2}}}{U_\infty}\right|_T \quad \text{vs.} \quad R_{\theta_T} = \left(\frac{U_\infty \theta}{\nu}\right)_T$$

respectively, where T denotes values at the transition position.

Although nearly all the workers who have reported on the subject calculated the momentum thickness θ_T from the LBL relations, yet in the present work, θ_T was always measured (i.e. calculated from the measured mean velocity profiles at transition). This is because, as discussed in Section 6.2.3, the FST induced some variations in the values of the BL integral parameters.

Also shown in Fig. 5.1 are some estimates of the position of transition obtained using a surface tube as described in Section 2.8 for the purpose of comparison with those obtained using the hot-wire technique (see Section 2.8). But because the tube indicates where changes in the mean velocity profiles take place, the results tend to give slightly higher estimates of R_{X_T} as in the figure. The comparison serves also to show that the estimates of R_{X_T} obtained using the hot-wire technique are trustworthy.

The figures show that the turbulence intensity $\sqrt{\overline{u^2}}/U_\infty$ represents

a major parameter in deciding upon the place of transition. The observed scatter in the plot can be due to:-

(i) The fact that (as discussed below) $\frac{\sqrt{\overline{u^2}}}{U}$ may not be sufficient to correlate the occurrence of transition with the FST.

(ii) The previously discussed (Section 2.8) uncertainty in detecting the precise position of transition and calculating θ_T.

Fig. 5.2 represents purely local values at transition, but the improved collapse obtained in Fig. 5.1 shows that such local values are not sufficient to correlate transition and somehow, the history of the development of the LBL beneath the turbulent stream needs to be included.

It remains to say that the curves shown in both figures represent a fit to the experimental points and they will be used during the discussion to follow as representing these two sets of points.

5.2.2 Effect of the Integral Scale L_x

Fig. 5.3 shows the dependence of R_{θ_T} on (L_x/t) where (t) is the plate thickness which is constant for this set of points.

Also shown in the figure is a line formed by the triangular symbols. This line is obtained by plotting the values of $\frac{\sqrt{\overline{u^2}}}{U}$ belonging to each curve in the figure at R_{θ_T} of the intersection of the lines L_x/t = constant and the respective curve. The process is repeated for L_x/t = 0.5 and 0.6. We observe the following:-

(i) The interesting linearity of the curve of transition at constant L_x suggests that it is changes in L_x that cause the

observed scatter of the data in Fig. 5.2 and possibly cause the relation between $\frac{\sqrt{\overline{u^2}}}{U}$ and R_{θ_T} to deviate from linearity.

(ii) It is shown that at constant $\frac{\sqrt{\overline{u^2}}}{U}$:-

$$R_{\theta_T} \propto L_x/t$$

i.e. the LBL is less sensitive to large scale turbulence. This is a plausible result since the BL will tend to see large scale turbulence as unsteadiness in the free stream while at the same $\frac{\sqrt{\overline{u^2}}}{U}$, a larger L_x will tend to cause less disturbance to the BL. It may also be said that the intensity of the pressure fluctuations associated with grid turbulence increases as L_x is decreased at constant $\frac{\sqrt{\overline{u^2}}}{U}$.

Figs. 5.4 and 5.5 show the ratio θ/L_x at transition as a function of R_{x_T} and R_{θ_T} respectively with $\frac{\sqrt{\overline{u^2}}}{U}$ as a parameter. The two curves show that in general, at the same $\frac{\sqrt{\overline{u^2}}}{U}$, transition is more sensitive to smaller values of L_x/θ (which is expected to be true until a certain limit - which was not investigated in the present experiment - since at very small L_x/θ, the linear instability processes become more evident). This result is in line with the observation of Fig. 5.3. Also, Figs. 5.4 and 5.5 show that R_{x_T} is in general less sensitive to changes in θ/L_x at smaller values of $\frac{\sqrt{\overline{u^2}}}{U}$.

5.2.3 Transition Parameter

In the previous two sections, the dependence of the transition Reynolds numbers (R_{x_T} and R_{θ_T}) on $\frac{\sqrt{\overline{u^2}}}{U}$ and θ/L_x was studied. It was

concluded that:-

$$R_T = F\left[\frac{\sqrt{\overline{u^2}}}{U}, \frac{\theta}{L_x}\right]$$

Hence, it is reasonable to expect that any parameter correlating the transition with the FST should have, besides $\frac{\sqrt{\overline{u^2}}}{U}$, a representative length of the BL in the numerator and another representative length of the FST in the denominator.

Taylor (1936) deduced such a parameter as:-

$$\frac{\sqrt{\overline{u^2}}}{U}\left(\frac{X}{M}\right)^{1/5} = f(R_X)$$

where X is the distance over the plate until transition and M is the grid mesh size.

In Appendix II, this parameter is modified using the homogeneous turbulence relations based on more recent experimental data so that it becomes:-

$$\frac{\sqrt{\overline{u^2}}}{U}\left(\frac{X}{M}\right)^{1/6} = f(R_X)$$

Fig. 5.6 shows the data points presented in Fig. 5.1 plotted as:-

$$\frac{\sqrt{\overline{u^2}}}{U}\left(\frac{X}{M}\right)^{1/6} \text{ vs. } R_{X_T}$$

Upon comparison between Figs. 5.6 and 5.1, we see that presenting the parameter as such did not improve the collapse of the data. In fact, the scatter is greater in general in Fig. 5.6, and, therefore, Taylor's

parameter as such does not correlate the present transition data. Hislop (1940) and Hall et al (1938) found the same result where the scatter in their plots eventually increased when they were plotted using Taylor's parameter. Most of the later workers did not bother to pursue the issue any further and they simply correlated their results with $\frac{\sqrt{\overline{u^2}}}{U}$ only.

Nevertheless, from the discussion of the last two sections, it is felt that if Taylor's parameter is expressed in terms of local quantities that may express the changing development of the LBL beneath the FST, a better collapse of the transition data may be obtained. For representing transition using the grid dimensions and the distance until transition implies assumptions about the nature of the FST at transition and the way the LBL develops until transition that may not be strictly true (see Appendix II and Section 6.2.3).

From Figs. 6.23b and c, it is not unreasonable to replace X with θ in the modified Taylor's parameter, whereas from the analysis in Section 4.5, it can be assumed that very roughly:-

$$L_x \propto M$$

This assumption is also supported by the present experimental observations.

Hence another way of presenting the modified Taylor's parameter which is also in agreement with the observations discussed in Sections 5.2.1 and 5.2.2 may be written as:-

$$\frac{\sqrt{\overline{u^2}}}{U}\left(\frac{\theta}{L_x}\right)^{1/6} \simeq f(R_x)$$

at transition. Plotting the same results of Figs. 5.1 and 5.6 against

this new parameter, we get the plot of Fig. 5.7. It is clear that the scatter is reduced in this case. When plotting the same set of points as:-

$$\frac{\sqrt{\overline{u^2}}}{U}\left(\frac{\theta}{L_x}\right)^{1/6} \quad \text{vs.} \quad R_{\theta_T}$$

i.e. correlating transition on a purely local basis, we see from Fig. 5.8 that the collapse is not as good as in Fig. 5.7 using R_{x_T}. This can partly be due to the possible uncertainty in measuring θ at transition. Or it may be that the length over which the LBL grows beneath the turbulent stream until transition must somehow be represented in the correlation. The argument in Chapter 7 may lend support to this. Nevertheless, the scatter in Fig. 5.8 is still much less than that in Figs. 5.1 or 5.6 (notice the change in the scale of the ordinate).

We conclude that the occurrence of transition of the LBL over a flat plate beneath a FST is reasonably correlated with the flow parameters based on local estimates of such quantities as follows:-

$$\frac{\sqrt{\overline{u^2}}}{U}\left(\frac{\theta}{L_x}\right)^{1/6} \simeq f(R_{x_T})$$

at transition.

In fact this conclusion gives more weight to the argument put forward in detail in Chapters 6 and 7 that the FST affects the LBL stability while the layer is still very thin. For in this case, the increased turbulence entrained by the layer will cause it to develop in a way different from that in a smooth flow and will cause θ to be different at transition. This change in θ is gradual rather than local

as seen from Fig. 6.33. Hence the use of θ/L_x rather than X/M in the parameter, although being local parameters, yet allowed for the observation that the development of the LBL beneath the FST was different or, in other words, was an expression of the history of the LBL.

5.3 Effect of Change in the Plate Thickness on Transition

As discussed in Section 5.1, and because the characteristics of two regions take part in determining the position of transition, i.e. the LBL before transition and the FST outside that BL, we will look at the effect of changing the plate thickness on the characteristics of these two regions separately as related to transition.

5.3.1 Effect of Changes in the Free Stream Turbulence Characteristics Induced by Changes in the Plate Thickness on Transition

It is known (Bearman (1972) and Hunt, 1973) that turbulence approaching a bluff body undergoes certain changes in intensity near the LE depending on its (length scale (L_x)/body thickness (t)) ratio. These effects may be summarised as follows:-

(i) If $(L_x/t) \gg 1$, u will attenuate along the mean stagnation streamline and, in general, the normal component will attenuate everywhere, while away from the stagnation streamline, the turbulent eddies and vortices will simply be skewed around the body by the action of $\partial U/\partial y$. Also, $\partial U/\partial x$ will be significant only in a small region near the LE and as L_x/t increases, turbulence around the LE will suffer less intensification by vortex stretching through the action of $\partial U/\partial x$.

(ii) If $L_x/t \ll 1$, u along the plate surface will amplify because of vortex stretching by the mean strain rate $\partial U/\partial x$.

(iii) If $L_x/t = O(1)$, combined effects of (i) and (ii) will occur.

It follows that the streamwise vortex lines will be intensified by vortex stretching while those normal to the plate will be skewed first, thus creating a component in the streamwise direction which, in turn, will be stretched by the mean strain rate $\partial U/\partial x$.

Sutera et al (1963) argue that due to this process of vortex stretching and skewing, turbulence near the BL in the nose region will have larger intensity than that further away from the plate. It is also useful to note that this region near the BL is expected to be a region of strong anisotropy of the turbulence, an observation which complicates the issue even further since transition may be sensitive to a particular velocity component more than to others.

From the above discussion, we conclude that:-

(i) Such activities in the nose region will depend to a large extent on the mean rate of strain in the streamwise direction that causes the vortex stretching, i.e. $\partial U/\partial x$ which, in turn, is a strong function of the plate thickness (see Fig. 4.14).

(ii) The amount of intensification of the turbulence in the nose region will depend on the scale of the oncoming turbulence.

Therefore, an obvious parameter to investigate is:-

L_x/t

where t is the plate thickness.

Fig. 5.9 shows the result of detecting the position of transition over two plates (1.5" thick and 4.0" thick) both fitted with an elliptic nose of length 8.0" (No. 1 and No. 2 in Fig. 2.4). The results are plotted as:-

$\frac{L_x}{t}$ vs. R_{x_T}

with $\frac{\sqrt{\overline{u^2}}}{U}$ as a parameter.

The following remarks may be made about the figure:-

(i) As argued above transition is more delayed as L_x/t increases at the same $\frac{\sqrt{\overline{u^2}}}{U}$ (see Section 5.2.2).

(ii) As $\frac{\sqrt{\overline{u^2}}}{U}$ increases, the changes in the ratio L_x/t becomes less critical, for then the effect of $\frac{\sqrt{\overline{u^2}}}{U}$ dominates transition.

(iii) The effect of L_x/t is small on the whole.

Attention is drawn here to the fact that the data in Fig. 5.9 is affected by the difference in the pressure gradient over the two plates, a subject that will be dealt with in detail in the following section. But since this was the case throughout the experiment that produced the data shown in Fig. 5.9, it can be taken to show the trend as L_x/t changes.

5.3.2 Effect of Changes in the Plate Thickness on Transition as Reflected Through the Induced Changes in the Pressure Distribution Over the Nose Section

From plots of static pressure distribution over the thin and

thick plate surfaces (fitted with elliptic nose sections both of length 8.0"), Figs. 4.3a and b, we see that the main features of the static pressure distribution over the two plates are:-

1. A region near the LE with positive $\partial U/\partial x$ (i.e. negative static pressure gradient). That gradient is higher for the thinner the plate.

2. Another region that follows that mentioned above where $\partial U/\partial x$ is negative (i.e. positive $\partial P/\partial x$). This region is there because the pressure in (1) overshoots to a value higher than the free stream value so that such a region of positive $\partial P/\partial x$ evolves to take the value of P back to the equilibrium state. Again the gradient in this region is higher for the thin plate.

3. A region of nearly zero $\partial P/\partial x$ that extends over the rest of the plate.

Therefore, it is expected that the pressure distribution will be similar if the slenderness ratio of the nose section (elliptic nose thickness t/nose length X_n) is constant. Or in other words:-

$$C_p = f\left(\frac{X}{X_n} \ , \ \frac{X_n}{t}\right)$$

In fact, the effect of having a different pressure gradient around the LE is clearly represented in Figs. 5.10a - e where the transition was detected on the two plates 1 and 2 (in Fig. 2.4) for an

arbitrary x-distance from the LE. The dashed curves in the figures represent the results for the thin plate No. 1 (reported in Section 5.2, Figs. 5.1, 5.2, 5.6 and 5.8).

The following observations may be made on the figures:-

(i) The data obtained in the two cases form two distinct groups. The more stable (as far as transition at the same $\frac{\sqrt{\overline{u^2}}}{U}$ or $\frac{\sqrt{\overline{u^2}}}{U}\left(\frac{\theta}{L}\right)^{1/6}$ is concerned) is the thinner plate (No. 1).

(ii) The value of R_{x_T} at a certain $\frac{\sqrt{\overline{u^2}}}{U}$ on the thin plate (with a higher X_n/t) is very nearly a constant multiple (~ 1.9) of the value of R_{x_T} for the other plate at the same $\frac{\sqrt{\overline{u^2}}}{U}$.

(iii) The same observations made in Section 5.2.3 on the use of local parameters in correlating transition are, in general, valid, i.e. the use of $\frac{\sqrt{\overline{u^2}}}{U}(\theta/L_x)^{1/6}$ rather than $\frac{\sqrt{\overline{u^2}}}{U}$ only (or $\frac{\sqrt{\overline{u^2}}}{U}(X/M)^{1/5}$ as in the original Taylor's parameter) improved the data fit, although in this case, the scatter is generally more than that obtained for the thin plate for reasons which will be discussed later in this section.

(iv) Despite the improvement in the scatter obtained when plotting the results against $\frac{\sqrt{\overline{u^2}}}{U}(\theta/L_x)^{1/6}$ (Fig. 6.10d), this process has no effect on collapsing the results of the two plates onto a single curve. The reason for this could be that the changes in the pressure distribution interfered somehow with the growth of the LBL and changed its stability characteristics.

The larger scatter observed in the thick plate results may be

due to the fact that as X_T was arbitrary and $\partial P/\partial x$ did not completely vanish where transition was detected because transition occurred earlier than in the thin plate case for all values of $\frac{\sqrt{\overline{u^2}}}{U}$, the LBL was exposed to a pressure gradient for varying distances . This argument was proved to be true as a better collapse was obtained for the thin plate when transition was detected at the same X from the LE (the result of this experiment is reported in Fig. 5.11).

In fact, this argument was brought home through an experiment during which the transition was made to occur at the distances X_2 and X_3 over the plates with noses 2 and 3 respectively (which have the same X_n/t ratio) such that:-

$$X_{T_3} = X_{T_2} \frac{X_{n_3}}{X_{n_2}}$$

i.e. the LBL was exposed to a similar pressure gradient when plotted as C_p vs. X/X_n. Fig. 5.12 shows that in this case the data of the two plates were at last made to collapse on a single curve, though with a large scatter. Plotting this result against $\frac{\sqrt{\overline{u^2}}}{U} (\theta/L_x)^{1/6}$ did in fact improve the collapse which indicates that the scatter was due to differences in θ/L_x, for not only did the values of L_x vary over a wide range, but this was also the case with θ since the ratio of the absolute X_T distances was $X_{T_3}/X_{T_2} = X_{n_3}/X_{n_2} \simeq 2.66$ in this case. This result nearly resolved the issue of having two separate curves for the two plates with different thicknesses.

Also the constant ratio of R_{x_T}'s for both plates at all values of $\frac{\sqrt{\overline{u^2}}}{U}$ and L_x (mentioned in (i) and (ii) above) indicates that the separate curves obtained for the two plates were caused by geometrical differences between the two plates, or in other words, due to differences

in the pressure distribution over them.

In fact, the different pressure gradient near the nose could have been the reason for the scatter in the reported results measured on different surfaces when they were plotted together, because in Fig. 5.13 for the nose No. 4 (as also in Fig. 5.10), the LBL became more stable when the negative pressure gradient at the LE was made effectively steeper than the case of the noses 1 and 2*.

As for the other investigators, although they report transition as taking place in a region of zero pressure gradient on a flat surface, yet the LBL in each case is exposed to a different pressure history around the LE, a history that is still remembered and can have a severe effect on the transition position. Fig. 5.14 shows the results for the cases tabulated on the following page.

We notice from the figure that as the slenderness of the nose section increases (i.e. negative $\partial P/\partial x$ gets steeper near the LE), the LBL becomes more stable and R_{x_T} increases at the same $\frac{\sqrt{\overline{u^2}}}{U}$. The reason why Fig. 5.14 does not show more results reported by other workers is that many of them never gave a detailed description of the nose section fitted to their plate from which the slenderness could be inferred.

From the above discussion, we may conclude the following:-

(i) The pressure gradient around the nose of a flat plate has a

---

* For the case of Fig. 5.11, the increased BL stability could have partly been caused by the fact that the destabilizing positive pressure gradient part over the nose acted, for a shorter distance, on a thinner BL that was more capable of sustaining it.

Symbol	Report	Surface	Nose
○	Present (Fig. 5.10a)	Flat plate	Elliptic, 4" thick, 8" long
△	Present (Fig. 5.1)	Flat plate	Elliptic, 1.5" thick, 8" long
□	Present (Fig. 5.13)	Flat plate	Elliptic (shaped), $\frac{10"}{16}$ thick, 4" long
◇	Schubauer et al (1948)	Flat plate	Pointed (2 circular arcs), 4" long
•	Wells (1967)	Channel floor	-

large effect on determining the position of transition, i.e. on the stability of the LBL.

(ii) Generally, as the slenderness of the nose X_n/t increases (negative $\partial P/\partial x$ increases), the LBL becomes more stable and the position of transition moves backwards on the plate.

(iii) Data measured for different nose shapes (i.e. different pressure gradient near the LE) cannot, in general, be correlated together (see Fig. 5.14).

(iv) Fixing the position of transition (i.e. causing the LBL to experience the same pressure history) collapses the otherwise scattered data on a single curve (see Fig. 5.12 & ρρ 23).

For the pressure distribution around the LE to have such an effect on the position of transition, we refer to the papers by van Driest et al (1963), Hall (1968), Hall et al (1972) and Michel (1974) which report theories and experiments on the effect of uniform pressure gradients throughout the flow range upon the beginning of transition. Two of their plots are reproduced in Figs. 5.15 and 5.16. From those plots, we see that:-

$$\left.\frac{\partial R_{\theta_T}}{\partial U_x}\right|_{\text{positive } U_x} > \left.\frac{\partial R_{\theta_T}}{\partial U_x}\right|_{\text{negative } U_x} \qquad (1)$$

and:-

$$R_{\theta_T}\Big|_{\text{positive } U_x} > R_{\theta_T}\Big|_{\text{negative } U_x} \tag{2}$$

and:-

$$\frac{\partial R_{\theta_T}}{\partial U_x}\Big|_{\text{low } u/U} > \frac{\partial R_{\theta_T}}{\partial U_x}\Big|_{\text{high } u/U} \tag{3}$$

where $U_x = \partial U/\partial x$ and T refers to transition.

Van Driest et al (1963) derive an expression for the dependence of R_{θ_T} on the Pohlhausen parameter:-

$$\Lambda = -\frac{\delta^2}{\mu U}\frac{\partial P}{\partial x}$$

$$\propto \frac{\partial U}{\partial x}$$

based on the concept of the vorticity Reynolds number as:-

$$\frac{A}{R_{\theta_T}} = 1 - B\Lambda + CR_{\theta_T}$$

where A, B and C are constants, so that:-

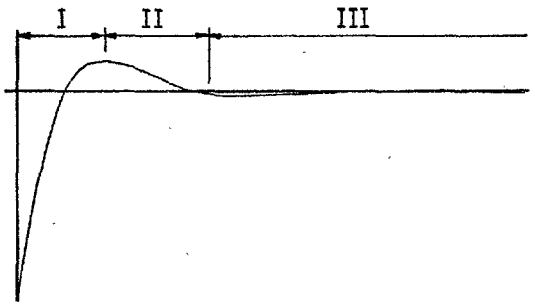
$$\frac{\partial R_{\theta_T}}{\partial \Lambda} = \frac{BR_{\theta_T}}{1 - B\Lambda + CR_{\theta_T}}$$

or:-

$$\left.\frac{\partial R_{\theta_T}}{\partial \Lambda}\right|_{\text{positive } \Lambda} > \left.\frac{\partial R_{\theta_T}}{\partial \Lambda}\right|_{\text{negative } \Lambda}$$

which is the same result observed by the experiments above.

Reviewing the present data in view of the relations 1 - 3, we see that as the general shape of the pressure profile over the plate (see Fig. 4.3) can be sketched as below:-



The plot can be divided into three main regions, namely:-

I A region of nearly constant positive U_x (i.e. negative $\partial P/\partial x$).

II A region of nearly constant negative U_x (i.e. positive $\partial P/\partial x$).

III A region of nearly zero U_x (i.e. zero $\partial P/\partial x$).

From the relations 1 - 3 above, we see that:-

1. R_{θ_T} (or R_{x_T}) is higher (i.e. more stable LBL) for the steeper pressure gradient in region I.

2. The effect of the pressure gradient in region I on R_{θ_T} is larger than that of II on R_{θ_T} (i.e. positive pressure gradient

stabilises the LBL more than a negative pressure gradient of the same magnitude destabilises it (see Fig. 5.15)).

3. Decrease in $\frac{\sqrt{\overline{u^2}}}{U}$ (as in the case of decaying grid turbulence in the x-direction) over region I stabilises the LBL by a larger degree than the same changes in $\frac{\sqrt{\overline{u^2}}}{U}$ destabilises the LBL if it occurs over region II (see Fig. 5.16).

Hence, the observed effect of the shape of the nose may be justified.

With all this in mind, an experiment was launched to see the effect of eliminating the positive part of the pressure distribution on the position of transition. The plate used in this experiment was fitted with the nose No. 5 shown in Fig. 2.4 (of thickness 1.5"). This nose was arrived at using the design technique described in Section 3.9. This gave a pressure distribution over the plate surface similar to that reported in Sections 4.3 and 4.4c when placed at an incidence of -1.0^{o}. We notice that although the region of positive pressure gradient nearly disappeared, yet the negative $\partial P/\partial x$ near the LE did also decrease and became similar to the region of negative pressure gradient over the 4" thick plate (see Fig. 4.3b), i.e. the negative pressure gradient became milder and extended over a larger x-distance. Since (as discussed earlier on in this section) the changes in the negative pressure gradient are more critical to the LBL instability and transition than changes in the positive pressure gradient, we expect that the destabilising effects resulting from the decrease in negative pressure gradient will dominate the stabilising effects resulting from eliminating the positive pressure gradient region.

The results of the experiment as plotted in Fig. 5.17 confirm

this. This figure shows:-

$$\frac{\sqrt{\overline{u^2}}}{U} \text{ and } \frac{\sqrt{\overline{u^2}}}{U}\left(\frac{\theta}{L_x}\right)^{1/6} \text{ vs. } R_{x_T}$$

measured over the 1.5" thick plate fitted with the nose No. 5. The figure also shows two curve fits representing the data reported in Figs. 5.1 and 5.10a for the 1.5" and 4" thick plates respectively. The points are nearer to the 4" thick plate results although they are measured over the 1.5" thick plate. Therefore, the effect of the positive pressure gradient near the LE of the plate on transition can only be inferred from the results of the experiments with uniform positive pressure gradient over the whole plate as was done earlier on in this section.

To conclude this section, it is thought too early to say conclusively whether the changes in the plate thickness affected R_{x_T} through changes in the FST or through changes in the stability of the LBL. Yet the results presented in Fig. 5.14 do show that even at the rather low values of FST intensities reported in the plot, the curves for different nose shapes preserved their separation distance which tends to give more weight to the effect of thickness on the LBL instability through the mechanism of changing the LBL profile. In any case, the issue needs further experimental investigation.

CHAPTER 6

LAMINAR-TRANSITIONAL BOUNDARY LAYER BENEATH A TURBULENT FREE STREAM

6.1 Introduction

The characteristics of the laminar-transitional BL along the thin plate (fitted with an elliptic nose section of length 8 inches) were studied experimentally. The convenience of having a sizeable laminar region off the nose section (i.e. off the region of pressure gradient as discussed in Chapter 5) dictated the use of the thin plate in this experiment. The measurements reported in this chapter were made to fulfill two major objectives:-

(i) To assess the effects of the FST intensity and length scale on the fluctuating quantities inside the BL. In this experiment, measurements are quite brief and cover only profiles for the U and u components. In this case, all the velocity measurements were made using a single hot-wire and all the data processing was performed electronically, whereas surface shear stress over the plate was probed using a Preston tube.

(ii) To study in detail the effects of a moderately high turbulence level of about 1.85% (generated by the smallest grid available of M = 1.5") on the development of the BL over the thin plate. This experiment involved the measurements (throughout the laminar-transitional BL) of profiles for:-

$$U,\ V,\ \sqrt{\overline{u^2}},\ \sqrt{\overline{v^2}},\ \sqrt{\overline{w^2}},\ \overline{uv},\ \overline{u^2v},\ \overline{v^2u},\ \overline{u^2w},\ \overline{uw^2},\ \overline{q^2}$$

together with the turbulent velocity derivatives in different directions. In this respect a U-wire, an X-wire and the double wire (described in detail in Section 2.4) were used to measure the required quantities. Then the different terms in the turbulent energy equation were computed and a balance of the turbulent energy was obtained at some stations. In this case, the data were processed digitally using the Imperial College CDC 6400 computer.

The results of both experiments are discussed in what follows.

6.2 The Laminar-Transitional BL Beneath a FST of Different Intensities and Length Scales

6.2.1 The Wall Friction Measurements

A Preston tube was traversed along the surface of the thin flat plate. Theoretically, if the tube lies in the viscous sublayer (or the wall layer) of the BL, then its reading gives a measure of the wall friction which can be determined from the tube reading using the Preston tube calibration curve as reported by Head et al (1962) or Patel (1965) say. The following table gives the free stream speeds for which the

Case	Speed m/s		
	1	2	3
No grid	20	-	-
1.5" grid	20	14.5	6.3
3.0" grid	20	14.5	6.3
6.0" grid	20	14.5	6.3

results are reported for different grids. Because the tube travels along the laminar-transitional BL so that the calibration curve used may be rendered inaccurate, the results are meant only to show the relative order of magnitude. Therefore, Fig. 6.1 shows the coefficient of skin friction C_f defined as:-

$$C_f = \frac{P - P_{st}}{\frac{1}{2}\rho U_\infty^2}$$

where P is the tube reading and P_{st} is the reference static pressure, plotted against arbitrary units. The following remarks can be made:-

1. All the curves regardless of free stream speed and turbulence level are basically similar.

2. The region of steep decrease in C_f that characterises the laminar region, and that region from where the gradient of C_f in the x-direction is zero until where the curve levels out again which characterises the beginning of the transition region, both regions clearly shrink in extent as the FST level and/or the mean speed of the free stream increases.

3. In general, the skin friction at any position over the plate surface is an increasing function of the R number.

Using some previously reported experimental results, Green (1972) proposed a linear relationship between the relative increase in the skin friction coefficient ΔC_f beneath a TBL and the FST intensity for constant R_θ as follows:-

$$\frac{\Delta C_f}{C_{f_o}} = 4.8 \frac{\sqrt{\overline{u^2}}}{U_\infty}$$

where C_{f_o} is the coefficient for the quiescent free stream. When applying this principle to the values in the present results taken in the turbulent region of the BL, the curve in Fig. 6.2 is obtained representing:-

$$\frac{\Delta C_f}{C_{f_o}} \text{ vs. } \frac{\sqrt{\overline{u^2}}}{U_\infty}$$

From this figure, we see that Green's principle of linear relationship between ΔC_f and $\frac{\sqrt{\overline{u^2}}}{U_\infty}$ seems to hold although the exact relation that correlates the present results becomes:-

$$\frac{\Delta C_f}{C_{f_o}} = \left[3.7 \frac{\sqrt{\overline{u^2}}}{U_\infty} - 0.045 \right] R_x \times 10^{-5}$$

This relation is valid along the turbulent region of the BL beneath a FST level up to 0.06.

6.2.2 The Mean Velocity Profiles

Traverses were made of the BL along the thin plate fitted with nose No. 1 in Fig. 2.4 at some stations covering the laminar-transitional-turbulent regions of the BL for all the cases mentioned in the table of Section 6.2.1. With the available data, the profiles presented in Figs. 6.3 - 6.7 are chosen to represent the phenomena. They represent the mean velocity profiles' development in the x-direction for the following values of the FST intensity $\frac{\sqrt{\overline{u^2}}}{U_\infty}$:-

Grid \ Speed	6.3 m/s	20 m/s
	$\sqrt{\overline{u^2}}/U_\infty$ %	
No grid	-	0.1
1.5" grid	2.2	2
6.0" grid	5.9	5.4

Although a more thorough study of the development of the U-profiles beneath a turbulent free stream will be given in Section 6.3.2 for the case of the 1.5" grid at U_∞ = 8.5 m/s, it is possible to make the following remarks on the profiles reported:-

(i) As reported by all the investigators (and reviewed by Morkovin, 1958), the effect of increasing the FST level seems to shorten the distance over which the layer evolves from the laminar state to the turbulent state. The same is also true with increasing the R .

It is noticed from the figures that the velocity profile measured for the no grid case at station 175 cm at a free stream speed of 20 m/s is nearly identically reproduced at the same station with the 1.5" grid but at U_∞ = 6.3 m/s only, while it is nearly reproduced by the 6.0" grid at the speed of 20 m/s at only 45 cm from the LE of the plate.

(ii) Some irregularities are observed in the profiles taken within the supposedly laminar (yet highly agitated) region. Such irregularities are repeated too often with the same definite

trend to be simply dismissed as inaccuracy on the part of the measuring equipment, although such inaccuracy is not unlikely in such a highly agitated thin layer.

In fact, Dhawan et al (1958) (during a study of the non-linear stage of BL instability), Klebanoff et al (1959) and Klebanoff et al (1962) (while investigating the instability of the ribbon generated waves in the non-linear range), Wortmann (1969) (in a study of the instability of the Görtler vortices) and Nishioka et al (1975) (during a study of the instability of a plane Poiseuille flow) all reported mean velocity profiles within the transitional BL with the same peculiar waviness. They all take it to be a characteristic of the transitional BL in their respective cases.

Returning to the present profiles, this waviness seems to exist for some profiles, e.g. the ones taken at X = 45 cm in Fig. 6.3, at X = 15 cm in Fig. 6.4, at X = 14 cm in Fig. 6.6 and that at X = 50 cm in Fig. 6.7.

(iii) The beginning of transition is so distinctively represented by a near abrupt increase in the mean speed near the wall.

This observed similarity between natural transition and transition in the presence of the FST as far as the U-profiles are concerned indicates that, the transition process from the beginning of the non-linear region until the BL becomes turbulent may follow some kind of a universal process regardless of the mean flow conditions which serve only to either speed up or delay the process.

Having mentioned the observed irregularities in item (ii)

above, it is interesting to see how the profiles reported in Figs. 6.3 - 6.7 differ from the Blasius profile for LBL at zero FST. Figs. 6.8 - 6.10 show such differences for the profiles reported in Figs. 6.5 - 6.7. From these figures, we notice:-

1. Within the agitated LBL, the maximum deviation from the Blasius always occurred between 0.25 δ - 0.3 δ for all the FST levels. This position of the highest activity then moved slowly to finish with its centre at about 0.1 δ or less further downstream, again for all the cases reported in the figures.

   Bradshaw (1974) argues that for the TBL in a turbulent free stream, the FST first affects the outer layer while the law of the wall and the inner layer energy balance remain effectively independent of the FST, just as they are independent of the outer layer. This argument is plausible and the present results lend support to it in the TBL region. As for the developing laminar-transitional BL such a principle is still open to question, although the present results tend to suggest that a similar principle may be valid. The subject will be taken up again later in this chapter.

2. The comparison between the first profile and the second profile in both figures of 6.8 and 6.10 suggests a rather locally steep pattern or regions of high velocity gradient that may be due to a localised tendency to develop a point of inflexion. Although the second profile in both curves may indicate that such a process is well under way, yet for the first profile in Fig. 6.8 and the second in Fig. 6.10 to have regions of positive and negative signs indicates that

such a point of inflexion is developed after some oscillations of the mean profiles around the value given by the Blasius solution. Further discussion of this point will be given in Section 6.3.3.

Figs. 6.11 - 6.13 show the mean velocity profiles for the cases of no grid and the 1.5" grid at U_∞ = 20 m/s plotted on a Clauser chart, i.e.:-

$$\frac{U}{U_\infty} \text{ vs. } \frac{yU_\infty}{\nu}$$

The plots show the following:-

(a) The wake component decreases if either the FST intensity increases or the R_x for transition decreases. This can clearly be seen upon comparing profiles at X = 175 cm in Figs. 6.11 and 6.12 and profiles at X = 76 cm in Figs. 6.12 and 6.13. Such a decrease signifies a slower merging of the BL flow into the external flow over a larger distance.

(b) Fig. 6.12 shows the difference in shape between the profiles measured in the laminar, the transitional and the TBL. It looks as if, since there is a universal inner layer for the turbulent BL where the log plot remains nearly unchanged while the wake component gets modified (profiles at X = 142, 165 and 175 cm in Fig. 6.12), there may also be a layer of this sort in the transitional BL. This is observed on profiles at X = 46, 53, 76 and 107 cm of Fig. 6.12 where the inner part of the profiles seem to change very little, while

there is quite a noticeable change in the outer part. It is also worth noticing that the change in the inner part of the profile at X = 107 cm to that at X = 142 cm seems quite steep. The same is also noticed at higher R_x in Fig. 6.13, though less clearly due to faster development of the BL. This observation can be taken as an indication of the existence of some kind of a universal process of development of the BL in the non-linear region leading to the fully TBL.

6.2.3 BL Parameters

(a) The BL Thickness (δ)

The BL thickness is defined as the distance from the wall at which the local speed U is 0.995 of the free stream value U_∞. It was calculated from the measured profiles for all the cases of the table in Section 6.2.1 and plotted in Figs. 6.14 and 6.15 as:-

$$\delta \text{ (mm) vs. } R_x = \frac{U_\infty x}{\nu}$$

where x is the distance to the leading edge. The curve for the no grid case is in complete agreement with the theoretical relations:-

$$\delta = 5 \sqrt{\frac{\nu x}{U}}$$

for the LBL and:-

$$\delta = 0.37\, x_o\, R_{x_o}^{-1/5}$$

for the TBL taking x_o to be the distance to the virtual origin of the TBL. It is also demonstrated in the figures that δ is a decreasing function of R_x due to the diminishing effects of viscosity while it is an increasing function of the FST intensity due to the higher spreading rate of turbulence (or in other words, due to the increased entrainment caused by the higher turbulence intensity in the outer layer) and the larger scales of turbulence involved.

When values of δ are plotted against X (cm) as in Fig. 6.16, we see that the effects of the FST seems to dominate the BL growth and we get approximately a single curve (with some scatter) for all the grids. This is so at least within the first half of the flat plate, no matter what sort of a BL (LBL, transitional BL or TBL) there is (to within the usual accuracy of determining the BL thickness).

The slope of this approximate curve in the x-direction increases with increasing $\left(\frac{\sqrt{\overline{u^2}}}{U}\right)_\infty$. This result is in agreement with the data reported by Charnay et al (1971).

(b) The BL Shape Factor (H)

The shape factor H defined as:-

$$H = \frac{\delta_1}{\theta}$$

where δ_1 and θ are the displacement and momentum thicknesses respectively, is computed for all the test cases in the table of Section 6.2.1 using the technique described in Section 3.4. The results are plotted in Fig. 6.17 against $R_\delta = U_\infty \delta/\nu$ on a log scale. For convenience, a curve fit is passed through every set of data points in the figure and then these curves only are plotted together in Fig. 6.18. From these two plots, we see that H asymptotes to the value of 1.4 at a rate that is a

weak function of R_δ. The curves suggest that there is a limit on the value of $\frac{\sqrt{\overline{u^2}}}{U_\infty}$ beyond which any increase in $\frac{\sqrt{\overline{u^2}}}{U_\infty}$ does not affect the H curves when plotted against R_δ. Yet one may say that H is a decreasing function of $\frac{\sqrt{\overline{u^2}}}{U_\infty}$, i.e.:-

$$H = F\left(\frac{U}{\sqrt{\overline{u^2}}}\right)$$

That, of course, is attributed to the increased mean shear in the inner layer on the one hand and the decreased wake component on the other.

The only comprehensive work on the subject that came to my knowledge is that due to Green (1972) for the TBL. In the present work, there are not enough measured stations in the fully TBL to do any serious comparison with his proposed numerical formula.

(c) The Wall Shear Stress Coefficient (C_f)

Values of C_f were computed from the profiles that were in the turbulent region according to the method and criteria discussed in Section 3.4. Fig. 6.19 shows the coefficient plotted as:-

C_f vs. R_x

Plotted this way, the results are not correlated for different R_x and $\frac{\sqrt{\overline{u^2}}}{U_\infty}$, whereas when the same values are plotted in Fig. 6.20 as:-

C_f vs. R_δ

where δ is the BL thickness, they seem to collapse on a single curve (though with some scatter) for all the values of $\left(\frac{\sqrt{\overline{u^2}}}{U}\right)_\infty$. This curve

is notably distinct from the one for a BL beneath a quiescent free stream. This seems to support the argument that the inner layer is effectively independent of the FST characteristics especially at high values of R_δ which amounts to confirming the argument of Bradshaw (1974) (see Section 6.2.2).

And since on the last figure 6.20 there is a distinct gap between the points with and without turbulence in the free stream, Bradshaw's argument seems to be valid only beyond a certain limit on $\left(\frac{\sqrt{u^2}}{U}\right)_\infty$, i.e.:-

$$C_f = f\left[\left.\frac{\sqrt{u^2}}{U}\right|_\infty\right) \qquad 0 < \left.\frac{\sqrt{u^2}}{U}\right|_\infty < A$$

No attempts were made to determined the value of A.

6.2.4 The Stream-Wise Turbulent Velocity Profiles

Measurements of the u-component fluctuations were made for the same stations as the mean velocity $\frac{U}{U_\infty}$. Figs. 6.21 to 6.25 show the resulting profiles. The following remarks can be made:-

1. In the BL near $y = \delta$, turbulence is strongly affected by the FST. Although turbulence in the outer region is generally higher than that outside the BL, it asymptotes to the free stream value over a distance that is a function of the ratio:-

$$\frac{\delta}{L_x}$$

where L_x is the length scale of turbulence. This can be seen in Fig. 4.18 and Section 4.7 where Hunt and Graham's (1978)

theory is compared with some of the present results.

2. The outer layer of the transitional BL seems to develop a wider plateau in the region $y/\delta = 0.1 \sim 0.5$ in the case of turbulent free stream than in the case of quiescent stream. This plateau width seems to be some function of the grid R ($U_\infty M/\nu$ or $U_\infty X_G/\nu$ where X_G is the distance from the grid). This plateau suggests that the generated turbulence bursts in the transitional BL travel across a larger part of the BL in the case of FST, which may be attributed to the higher diffusivity of the surrounding flow.

3. It is also noticed that upon comparing profiles for the same free stream speeds U_∞, we see that the inner region turbulence seems to asymptote to a universal profile for all values of $\left(\frac{\sqrt{\overline{u^2}}}{U}\right)_\infty$. (Compare the last two profiles in each figure). Charnay et al (1971) made similar observations in a similar situation.

4. The observed high peaks near the wall in the case of quiescent free stream suggest that turbulence in the inner layer is of a finer scale when the FST intensity is lower. This may be so because earlier transition caused by higher FST intensity caused the BL to become turbulent before the vortex stretching and skewing extended the newly generated BL turbulence to finer scales. The low dissipation terms reported in Section 6.3.8 support this argument.

5. In the no grid case, the BL disturbances (turbulence) extended

far beyond the mean flow BL in the y-direction. It took about 5 δ for the flow near the LBL (and about 1.0 δ for the flow over the TBL) to get rid of such wall disturbances (turbulence). On the other hand, only about 0.5 δ in the case of the LBL (and less for the TBL) was needed by the wall disturbances (turbulence) to merge in the turbulent free stream*. This is due to the ability of the turbulence to entrain the non-turbulent flow and diffuse in the turbulent one.

6. The highest turbulence intensity in the LBL is centred round about 0.25 δ, but then it moves to about 0.1 δ. Recalling that this coincides with the region of maximum deviation from Blasius profile (see Section 6.2.2 and Figs. 6.8 - 6.10), this may be viewed (on the average) as a result of that extra strain rate generating turbulence (the position of this extra strain rate does not necessarily coincide with the point of maximum rate of strain). Further discussion of this subject will be given in Sections 6.3.3 and 6.3.4.

6.3 Development of the Laminar-Turbulent BL Beneath a Turbulent Free Stream of a Nearly Constant Intensity

Measurements of all mean and fluctuating quantities inside the BL beneath a turbulent free stream produced by the 1.5" grid at U_∞ = 8.5 m/s in the range from where the BL is still laminar until near

---

* Merging here is considered complete where the BL turbulence coincides with the value of the free stream turbulence as given by Hunt and Graham's (1978) theory, and confirmed by experiments (see Section 4.7).

the end of the transition region were made at the following 19 streamwise stations:-

X = 20, 24, 28, 32, 36, 40, 44, 48, 52, 56, 60, 64, 68, 72, 96, 100, 104, 108, 112 cm

Traverses were made every 4 cm in order to improve the accuracy of obtaining the streamwise derivatives.

Out of these 19 stations, only 7 were chosen to be presented herein, namely:-

X = 20, 32, 44, 56, 68, 96, 108 cm

The first two lie in the highly agitated LBL, while the rest represent different stages of the transitional BL. In what follows, different results will be presented and discussed.

6.3.1 The Mean Velocity Distribution in the Working Section Over the Plate

Fig. 6.26 shows the variations of the mean speed at mid-distance between the plate surface and the tunnel roof. It is seen from the figure that the maximum variation is about ± 2% around the average. Such a variation is quite acceptable within the expected accuracy of the present experiment.

6.3.2 The Distribution of Wall Shear Stress Over the Plate

The plate surface was traversed around transition in two directions by means of a Preston tube. Then, the distribution of the wall friction coefficient (C_f) was determined using the technique

described in Section 3.4. The experiment was carried out for two cases, with no grid inside the tunnel at U_∞ = 30 m/s and with the 1.5" grid placed in the tunnel at U_∞ = 15 m/s. The extent of the tube traverses covered the distance of 100 cm in the streamwise direction and about 50 cm in the spanwise direction around the transition region. Then by means of a standard routine in the Imperial College computer library, the carpet graphs in Figs. 6.27 and 6.28 were produced.

In Fig. 6.27, there are some span-wise variations in the value of C_f. These variations were most likely due to irregularities in the plate surface. In Fig. 6.28, apparently the effects of the FST on the BL instability and transition dominated over any likely effects of the surface irregularities observed in Fig. 6.27. Also the uniformity of the C_f distribution in the mid-section of the plate surface (where most of the measurements were taken) indicates that the assumption of the 2D mean flow in the LBL (and in the transitional BL also but may be to a lesser extent as will be seen in Section 6.3.3) is not unreasonable.

6.3.3 The Mean Velocity Profiles Throughout the BL

The longitudinal mean velocity profiles (U/U_∞ vs. y/δ) which were measured using a single U-wire probe, are presented in Fig. 6.29. Using those profiles and the continuity equation, the normal velocity (V) was calculated by integration (see Section 3.2). The resulting profiles are plotted in Fig. 6.30 as (V/U_∞ vs. y/δ). It was also thought instructive to assess the deviation of each profile from that given by Blasius solution for the LBL. This is plotted for all the profiles in Fig. 6.31. Inspection of these curves reveals that:-

1. At the beginning of the range studied, we see from Fig. 6.31

that Blasius profile closely describes the velocity distribution, i.e.:-

$$\frac{U}{U_\infty} = f(y/\delta)$$

and within this range, $\partial U/\partial x$ is negative and V is positive throughout.

2. Along a stream line or roughly at any constant distance from the wall within the LBL (true also for the fully developed TBL), the flow can only get retarded by the wall, i.e.

$$\frac{\partial U}{\partial x} = \text{negative}$$

due to the action of viscosity in the case of LBL. This is supported by the positive V in Fig. 6.30.

3. If:-

$$\frac{\partial U}{\partial x} = 0 \qquad (\text{i.e. } V = 0)$$

and if the BL is also growing, then the U-profile will deviate from the theoretical Blasius profile. In this case, retardation due to the mean strain rate (wall shear) balances the increase in speed due to the mixing of the newly generated turbulence. Hence, the deviation shown in Fig. 6.30 together with the zone of zero V in Fig. 6.30 (for the third station)

are justified.

4. Such a preliminary negative mean strain rate in the streamwise direction ($\partial U/\partial x$) will induce the U-profile to develop a point of inflexion (see the first three profiles in Fig. 6.29).

5. The waviness of the U-profiles shown in Figs. 6.29 and 6.31 indicates that such points of inflexion may be created locally due to some sort of a 3D instability pattern that may develop possibly with some resemblance to the reported 3D instabilities by (see Section 6.2.2) Dhawan et al (1958), Klebanoff et al (1959), Klebanoff et al (1962), Wortmann (1969) and Nishioka et al (1975).

6. As a result of the role of the newly generated turbulence mixing and diffusion in relaxing the mean strain rate created by the wall retardation and confining it to a thinner layer near the wall, the local V will become negative within the growing BL and the profile will depart from the Blasius profile and the flow inside the BL will eventually accelerate.

7. For 2D thin shear layer with FST, the x-component turbulent energy transport equation is:-

$$\frac{D}{Dt}\left(\frac{1}{2}\overline{u^2}\right) = -\overline{uv}\frac{\partial U}{\partial y} - \text{Diffusion} - \text{Dissipation}$$

In a LBL, the diffusion and the dissipation of the turbulent energy are negligibly small. Initially, therefore, and in the presence of such a high $\partial U/\partial y$, any disturbance will

activate the generation term in the last equation, i.e. $\left(-\overline{uv}\,\frac{\partial U}{\partial y}\right)$. This will momentarily create a small region of high local x-component fluctuation which, in turn, will partly be diffused into the other two directions through the action of the pressure term (according to the continuity of the turbulence $\frac{\partial u}{\partial x} + \frac{\partial v}{\partial y} + \frac{\partial w}{\partial z} = 0$). And from the shear stress transport equation, namely:-

$$\frac{D}{Dt}\left(-\overline{uv}\right) = \overline{v^2}\,\frac{\partial U}{\partial y} - \text{Diffusion} - \text{Dissipation}$$

more shear stress will be produced.

In fact, amid such a high mean rate of strain $\partial U/\partial y$, a disturbance in any direction may ultimately lead to the same result according to the above-mentioned equations (i.e. a breakdown of the flow in the critically stable mean flow profile). Then the newly generated turbulence will entrain the surrounding sheared flow and mix it, thus relaxing the mean rate of strain locally. Since the whole layer is sheared throughout and due to the increased local speed (as $\partial U/\partial y$ is relaxed), this localised turbulent zone will be swept away. This argument can be taken as another way of looking at the process of the formation of Emmons' spots.

The accumulation of such turbulence inside the BL and their effect on $\partial U/\partial y$ may eventually lead to the observed accelerated flow in the downstream direction at constant (y) (i.e. negative V, or a fuller BL U-profiles in the transition region).

Fig. 6.32 shows the Clauser plot for the smoothed U-profiles $\left(\frac{U}{U_\infty} \text{ vs. } \frac{yU_\infty}{\nu}\right)$ evaluated at some common points. Only every other profile is represented in the figure, i.e. at the following X stations:-

X = 20, 28, 36, 44, 52, 60, 68, 96, 104, 112 cm

The plot shows, in a much clearer way what has already been observed in Figs. 6.8 - 6.11 (see Section 6.2.2), i.e.:-

(i) The gradual disappearance of the wake component as the BL developed downstream.

(ii) The formation of the log law region.

(iii) The near universality of the inner layer in the LBL; or, in other words, for the LBL:-

$$\frac{U}{U_\infty} = f\left(\frac{yU_\infty}{\nu}\right)$$

But the observation that the profiles collapse onto a single curve for the LBL and onto another one for the non-linear region of the transitional BL is not clear here.

Looking at the development of the BL thicknesses δ and θ in Figs. 6.33a and b, we see that the development in the BL thickness δ within the laminar range is of a higher rate than in the smooth flow. The preliminary bigger thickness in the case of quiescent flow may be due to the high shear in the LBL which is partly diffused by the

action of the FST thus resulting in an initial decrease in δ and θ. Further downstream as more fluid is entrained into the layer, the layer grows at a higher rate in the case of FST. Hence the observed increases in δ and θ result.

6.3.4 Development of the Profiles of the Turbulent Velocity Components Along the Plate

From measurements obtained using the U-wire probe and the X-wire probe, profiles were obtained for the three turbulent components in the three orthogonal directions x, y and z. Out of the 19 stations at which measurements were taken, those at only four stations are reported in Figs. 6.34a - d. These figures show the profiles for:-

$$\frac{\sqrt{\overline{u^2}}}{U_\infty}, \frac{\sqrt{\overline{v^2}}}{U_\infty} \text{ and } \frac{\sqrt{\overline{w^2}}}{U_\infty} \quad \text{vs. } y/\delta$$

for the stations:-

X = 32, 44, 68 and 108 cm

where X = 32 cm lies in the laminar region, X = 44 cm lies at the beginning of transition, while X = 68 and 108 cm lie in the transitional region of the BL. From the figure, it is noticed that:-

1. As observed before (Section 4.7), the v-component is the one most attenuated.

2. The $\sqrt{\overline{u^2}}$ and $\sqrt{\overline{w^2}}$ profiles assume the peaky shape near the wall rather suddenly at a station within the transitional BL.

3. The profiles indicate that the x-direction is the definite preferred direction for the turbulence inside the BL particularly in the LBL and the early transitional BL. This is due to the mean strain rates in the x and y directions.

4. The position of the highest activity in the BL starts by being around $y/\delta = 0.35$ and then moves to the previously reported position (Section 6.2.2) of $y/\delta \simeq 0.25 - 0.3$ at transition. Then it moves to $y/\delta \leq 0.1$ as the BL develops downstream. It is interesting to notice that those different y/δ's represent a nearly constant height from the wall of about 1.0 mm (the possible inaccuracy in determining the position of the wire and finding $\delta_{0.995}$ was unlikely to be much higher than 5%). This does not seem to agree with the height of van Driest et al (1963) critical layer of ($0.6\ \delta$) which was experimentally supported by Klebanoff et al (1959) and Kovasznay et al (1962) as being where the turbulent bursts first appear inside the BL without FST. It seems that either the position where the turbulent bursts make their appearance is less than $y/\delta = 0.6$ in the case of the FST, or that the origin of the bursts is different altogether. Further discussion of the subject will be given in Chapter 7.

5. Although the profiles taken in the TBL are similar to those reported by Klebanoff (1954) in the inner half of the BL, yet the present profiles do not collapse on one curve near the BL edge. This is probably because of the different wake components which will result in the observed discrepancy between the turbulent components, and also the fact that the

FST components are not equally blocked by the wall (see Section 4.7). Also the fact that in Klebanoff's experiment, R_δ was at least three times higher than R_δ in the present experiment may act to make turbulence in the outer part of the BL less affected by the wall.

6.3.5 The Development of the Turbulent Kinetic Energy ($\overline{q^2}$) Inside the BL Along the Plate Surface

After evaluating the profiles of the three fluctuating velocity components at some common points, their squared values were added to give the value of the turbulent kinetic energy ($\overline{q^2}$) as:-

$$\overline{q^2} = \frac{1}{2}\left(\overline{u^2} + \overline{v^2} + \overline{w^2}\right)$$

Fig. 6.35 shows the smoothed resulting profiles of ($\overline{q^2}$) through the laminar-transitional BL.

It remains to say that because the BL was not fully turbulent within the range studied, it was possible to take a few measurements near the wall using a U-wire and the lower wire of an X-wire and two points v_i and w_i were added to each of the v and w profiles very near the wall such that:-

$$v_i \simeq \sqrt{v_{x_i}^2 - 2u_i^2} \qquad (i = 1, 2)$$
$$w_i \simeq u_i$$

where v_{x_i} is the velocity measured by the lower wire of the X-wire and u_i is that measured by the U-wire. Then a parabolic fit was used to join the last point on the original X-wire profiles v and w with the origin going through these two new points v_i and w_i (i = 1, 2).

The figure shows the following:-

(i) Just after the mean velocity profile assumes a jump in the shape factor H (after station X = 44), the $\overline{q^2}$ profiles exhibit a sharp increase near the wall. Again such a high rate of production of $\overline{q^2}$ in the inner layer of the BL (see also Section 6.2.4) and the relatively low turbulence in the outer layer and the free stream, makes the chances that the transition process and/or the BL parameters at transition are correlated by local values of the FST very slim. This view is held by Bradshaw (1974) to be true for the TBL. I argue that it is also true everywhere except while the BL is still laminar and very thin, i.e. near the LE of the plate.

(ii) It is also noticed that the point with the highest value of $\overline{q^2}$ inside the LBL has an almost constant absolute height of about 0.9 mm, while this height in the later stages of the transitional BL becomes about 0.5 mm. This may mean that as far as the value of the turbulent energy near the wall is concerned, the wall blockage plays a dominant role.

6.3.6 Development of the Reynolds Stress ($\overline{uv}$) Profiles Through the Laminar-Transitional Layer

Fig. 6.36 shows the shear stress ($\overline{uv}$) profiles throughout the range studied in the present work. The figure does not fail to show that the LBL starts off by being almost free of turbulent shear. As discussed earlier in Section 6.3.4, and due to the strongly preferred streamwise direction, the beginning of transition is characterised by a sharp increase in the value of ($\overline{uv}$). Within the transitional layer,

therefore, $\overline{uv}$ in the inner layer of the BL assumes a higher value than that in the TBL.

It is also interesting to note that the value of $\overline{uv}$ at the edge of the BL has always a non-zero value at $y = \delta$ and it stays non-zero for some distance outside the BL. Similar results were reported by Huffman et al (1972). Bradshaw (1974) argues that such unexpected behaviour of the $\overline{uv}$ profiles near $y/\delta = 1.0$ in a turbulent free stream can be due to one (or both) of the following two reasons:-

(i) An increase in the entrainment velocity (V_E) due to the diffusivity of the turbulence, since near the edge of the TBL with no FST:-

$$\overline{uv} \simeq \rho(U_\infty - U)\, V_E$$

where U is the local mean velocity which can vary slightly in a turbulent stream.

(ii) A balance of $\partial\overline{uv}/\partial y$ with $\partial\overline{u^2}/\partial x$ (and/or $\partial P/\partial x$) where for grid turbulence $\partial\overline{u^2}/\partial x$ is non-zero, while for the flow over a flat plate in a wind tunnel, $\partial P/\partial x$ can be non-zero.

When plotting the computed results of $\overline{uv}/\overline{q^2}$, Fig. 6.37 is produced. In the figure, we clearly notice a peculiar hump just outside the BL. It is argued that such a hump in the profile of $\overline{uv}/\overline{q^2}$ is expected for the following reasons:-

(i) As argued above, the $\overline{uv}$ profiles have unexpectedly high values outside the BL. These non-zero values then slowly vanish in

the y-direction.

(ii) It is reported in Section 4.7 and shown in Fig. 4.17 that both the present experiment and the theory due to Hunt and Graham (1978) show a region just outside the BL where the value of $\overline{q^2}$ is actually less than the value well away from the BL and also less than its value inside the BL.

Taking these two factors into account, the observed hump in $\overline{uv}/\overline{q^2}$ profiles follows immediately. This development in fact shows that the $\overline{uv}/\overline{q^2}$ parameter is unlikely to be a very useful one in the study of transition.

Durbin (1978) also theoretically anticipated an increase in $\overline{uv}$, although his analysis produces an infinite value of $\overline{uv}$ at the edge of the BL because in his analysis, $\partial^2U/\partial y^2$ has an infinite value at $y = \delta$.

6.3.8 The Triple Products of the Turbulent Velocity Components in the Laminar-Transitional Layer

Figs. 6.38a - d shows some profiles for the triple products of $\overline{u^3}$ and $\overline{v^3}$ at the stations X = 32, 44, 68 and 108 cm, while Figs. 6.39a - d shows the triple products $\overline{u^2v}$, $\overline{u^2w}$ and $\overline{v^2u}$ at the same X stations.

In Fig. 6.38 (notice that the profiles of $\overline{u^3}$ are scaled down relative to those of $\overline{v^3}$) again the high activity near the wall around transition and the steep drop of the value of $\overline{u^3}$ and $\overline{v^3}$ in the outer part of the BL all tend to support the idea that the FST may only have a slight effect on the turbulence inside the BL at transition. The peaky shape of the $\overline{v^3}$ profiles is rather surprising, although it may signify, with its sharp gradient near the wall, a high diffusion of the $\overline{v^3}$ component of energy towards the wall (see Section 6.3.9). Similar

diffusion towards the wall can be seen from the $\overline{u^3}$ profiles. The hump in the $\overline{u^3}$ profiles and the non-zero values of $\overline{u^3}$ and $\overline{u^2v}$ at $y = \delta$ at transition indicate diffusion of $\overline{u^2}$ toward the free stream. This is not only compatible with the fact that the BL grows in thickness, but it also shows that even at the early stages of transition, turbulence diffuses from the BL towards the free stream and not vice versa. This observation lends support to the idea that the FST decisively affects the turbulence inside the BL only very early while the laminar layer is still very thin.

Fig. 6.39 on the other hand shows the cross products of the turbulent velocity components $\overline{u^2v}$, $\overline{u^2w}$, $\overline{v^2u}$. The interesting change of sign of the $\overline{u^2w}$ profiles indicates a change in the direction of the diffusion of u^2 by the action of w across the BL. The position of this change in sign moves progressively towards the wall as the LBL develops downstream until it disappears near the end of the transition region and the $\overline{u^2w}$ profile assumes a uniform sign across the layer.

Wortmann (1977) looked at a flat plate BL transition excited by the vibrating ribbon technique and suggested that, after the breakdown of the Tollmien-Schlichting instability modes, there exists a 3D structure composed of the basic flow and a longitudinal counter-rotating and overlapping sheets of vorticity that are inclined downstream. This present result seems to suggest the existence of a similar structure in a flat plate BL beneath a turbulent free stream.

The figure also confirms the observation that the turbulent transport of turbulent energy outside the BL is nowhere comparable to that inside the BL even at the earliest station reported, i.e. at X = 32 cm where the BL was still laminar.

6.3.8 The Evolution of the Turbulent Energy Within the Laminar-Transitional BL

This attempt to measure the development of the different terms in the turbulent energy equation within the laminar-transitional BL beneath a turbulent free stream is certainly one of the first attempts in this field. But despite the great care taken while performing the experiments or while computing the different terms in the equation from the hot-wire output, nothing really very much can be said about the interpretation of the turbulence bursting using such statistical averages taken at the highly intermittent flow in question. Nevertheless, the results give indications as to what the trend of things is and they may also serve to show the relative order of magnitudes of these quantities in this highly unknown flow.

The quantities are reported at four different stations as before, i.e. at X = 32 cm where the BL is still laminar but highly agitated, at X = 44 cm where transition has just started, and at X = 68 and 108 cm where transition is well developed. For the sake of clarity, and to make the direct comparison of the profiles of any particular quantity along the region studied easy, the profiles representing each quantity in the energy equation are plotted separately. Fig. 6.40 shows the profiles for advection of $\overline{q^2}$ computed as:-

$$U \frac{\partial \overline{q^2}}{\partial x} + V \frac{\partial \overline{q^2}}{\partial y}$$

Fig. 6.41 shows the profiles for the production terms computed as:-

$$- \overline{u^2} \frac{\partial U}{\partial x} - v^2 \frac{\partial V}{\partial y} - \overline{uv} \left(\frac{\partial U}{\partial y} + \frac{\partial V}{\partial x} \right)$$

Fig. 6.42 shows the profiles for the velocity diffusion terms computed as:-

$$-\frac{1}{2}\left[\frac{\partial\overline{u^3}}{\partial x}+\frac{\partial\overline{v^3}}{\partial y}+\frac{\partial\overline{u^2v}}{\partial y}+\frac{\partial\overline{v^2u}}{\partial x}+\frac{\partial\overline{w^2u}}{\partial x}\right]$$

Fig. 6.43 shows the profiles for the viscous dissipation terms computed as:-

$$\nu\left[\overline{\nabla^2q^2}-\overline{(\nabla u)^2}-\overline{(\nabla v)^2}-\overline{(\nabla w)^2}\right]$$

where $\nabla = \frac{\partial}{\partial x}, \frac{\partial}{\partial y}, \frac{\partial}{\partial z}$.

Here, the derivatives in the x-direction are included because during the onset of turbulence in the transitional BL, their values are much higher than those in the TBL.

Fig. 6.44 shows the profiles representing the balance of the measured terms (in Figs. 6.40 - 6.43) which includes the pressure diffusion terms and any errors in determining the other terms, notably the dissipation terms. The measuring techniques and the computer analysis used in determining these terms are discussed in detail in Sections 2.4 and 3.3 respectively. Finally, Fig. 6.45 shows the different terms for the station X = 68 grouped together, thus showing the balance of the turbulent energy near the end of the first third of the transition region. The following remarks can be made about the figures:-

(i) Station X = 44 cm where the transition takes place (i.e. beginning of the appearance of the turbulent bursts) seems to witness a sharp increase in the turbulent activity.

(ii) At station 32 and 44 advection is positive across the whole layer as expected since $\partial\overline{q^2}/\partial x$ is large and positive over the whole layer (see Fig. 6.35) especially at station 44, while $\partial\overline{q^2}/\partial y$ is very high (because the BL is very thin) and positive over most of the layer except perhaps near the edge of the BL where $\overline{q^2}$ asymptotes to the free stream value.

(iii) At stations 68 and 108 in the transitional BL, the advection profiles reverse sign in the inner part of the layer where both $\partial\overline{q^2}/\partial x$ and $\partial\overline{q^2}/\partial y$ reverse sign, because $\overline{q^2}$ does not only peak near the wall, but also decreases in the x-direction after reaching a maximum near the beginning of transition. This trend of change indicates that further downstream, where $\partial\overline{q^2}/\partial x$ becomes negligibly small with reference to $\partial\overline{q^2}/\partial y$, the profile will be of a negative sign (i.e. representing a net loss of energy) across the whole layer similar to that reported for the TBL by Klebanoff (1954) except perhaps very near the wall in the viscous sublayer. It is interesting to note that the advection profiles reported by Townsend (1976) for the self-preserving TBL behave in a very similar manner to the present ones, although the former is of a much higher value.

(iv) Advection has a relatively high value at the BL edge due to the rapid growth of the layer and the entrainment by the BL of the otherwise low intensity turbulent flow of the free stream (i.e. $\partial\overline{q^2}/\partial x \neq 0$) which is highest near transition. Also the blockage effect of the flat plate will give non-zero values for $\partial\overline{q^2}/\partial y$ near $y = \delta$ (see Section 4.7).

(v) For the production profiles, as the laminar-transitional BL develops (stations 32, 44), the production seems to reach a maximum over nearly the whole width of the layer except perhaps near the BL edge where it exhibits a decrease that can be attributed to a flattening of the velocity profile due to the effect of the newly generated turbulence (and the FST) diffusivity, or in other words, due to the gradual disappearance of the wake component of the mean velocity profile (see Fig. 6.32).

(vi) As the layer develops, the process of generating turbulence seems to be more and more concentrated in a thin region near the wall. While the production decreases over most of the flow width, it assumes an expected sharper peak near the wall that gets thinner as the layer develops downstream. In the last station (X = 108 cm) nearly 70% of turbulence is produced in the region $0 < y/\delta < 0.05$.

(vii) Looking at the term representing the viscous dissipation of the turbulent energy in Fig. 6.44 (notice the magnified profiles of the first three stations), we may make the following remarks:-

(a) Over most of the layer at the stations 32 and 44, the production of the turbulent energy is almost 10 times the turbulent energy that is dissipated by viscosity. It can be said in support of such a low dissipation that, for turbulence to set-in and the BL to develop to the turbulent state, dissipation has to lag behind

the production in the early stages of transition. Also as discussed in Chapter 7, the newly generated turbulence is of a relatively large scale and, therefore, it is plausible that only further downstream (after the process of vortex stretching and skewing is given a chance to increase the local turbulent velocity gradient to such a level that they become vulnerable to dissipation by the viscous forces) that the dissipation becomes of the same order as the production.

On the other hand, such difference may have partly been caused by the fact that the techniques used in the measurements of the dissipation terms and the validity of the assumptions of local isotropy of the eddies responsible for the dissipation are both open to question. Since a gap of 0.35 mm between the two wires used to get the velocity gradient in the y and z directions may prove to be too large. While the application of the local similarity concept is strongly conditioned by the local similarity of the eddies responsible for the dissipation. That is, it is dependent on the dissipation derivatives obeying the isotropic relations:-

$$\overline{\left(\frac{\partial u}{\partial x}\right)^2} = 2\overline{\left(\frac{\partial v}{\partial y}\right)^2} = \overline{\left(\frac{\partial w}{\partial x}\right)^2} \quad \ldots\ldots$$

And while this condition may be reasonably satisfied in the outer part of the BL, it becomes increasingly inaccurate as the wall is approached. For the TBL, Klebanoff (1954) reported an order of magnitude difference

between values of the ratios of $\partial u/\partial y$ and $\partial u/\partial z$ to $\partial u/\partial x$ (estimated from the isotropic relations) and the measured value which is also observed during the present experiment. Nevertheless, such uncertainty is not likely to produce such an effect on the measured values of the production and the dissipation.

(b) The view expressed in the beginning of item (a) above is supported by the fact that in Fig. 6.44 for the stations 68 and 108, the dissipation increases to such a level that a region of a near local equilibrium (y/δ = 0.1 - 0.2) emerges at the station 108 where the production very nearly balances the dissipation.

(c) Klebanoff (1954) reported that for the TBL, and in order to balance the equation, the dissipation must assume a larger value than the production within a thin region near the wall (i.e. a flow of energy towards the wall). Although such a region was not detected in the present experiment, yet in Fig. 6.44 the way the profiles develop in the x-direction tends to show that this may become the case further downstream.

(viii) As for the turbulent diffusion by the turbulence in Fig. 6.42, the profiles seem to be divided into two regions:-

(1) A region near the wall ($y/\delta < 0.15$) where there is a net loss of energy by diffusion. This loss reaches a maximum near station 68 and then exhibits a decrease until

station 108 as in the figure.

(2) A region that covers the rest of the flow width where the velocity diffusion represents a net gain that also reaches a maximum at stations 44 and 68 and then decreases downstream at station 108 to one-third of its value at station 44.

(ix) Looking at Fig. 6.44 which represents the balance term of the above-mentioned terms, we also notice that the profile taken at X = 44 cm (where transition nearly starts) represents an absolute maximum over most of the BL width it covers. This balance term tends to decrease again as the BL evolves until station 108.

Besides the possible inaccuracy in determining the dissipation term which may have masked the true behaviour of the pressure diffusion term in the outer layer, the large value of the pressure dissipation near the wall provides the necessary requirement for the turbulent energy to flow towards the wall (see Townsend (1951, 1976) and Klebanoff, 1954). While this result should be viewed with caution because of the sources of error mentioned above, one must also consider that as discussed in Chapter 7, the nature of the newly generated turbulent bursts amid the otherwise highly agitated laminar flow indicates that the pressure diffusion will have a larger effect on the balance of the turbulent energy.

(x) The turbulent diffusion terms at station 108 behave similarly to the reported diffusion profiles by Townsend (1951) for a

fully developed TBL except that the present ones give a value to the pressure diffusion nearly double that reported by Townsend. Also the present profiles exhibit a net loss in the outer region of the BL rather than a net gain as reported by Townsend. These differences may have been caused by either the intermittent nature of the flow inside the transitional BL or by the improved measuring techniques since the date of Townsend's paper (1951) or both.

From the above discussion (and the profiles in Figs. 6.40 - 6.45) we see that the turbulence inside the BL seems to develop independently of the turbulence outside the BL even at the first station reported (X = 32 cm) where the BL is still laminar. This seems to give more support to the postulate that the FST affects the laminar-transitional BL behaviour appreciably only where the BL is still laminar and very thin, after which there seems to be a mutual independence of the turbulence and the turbulent activities in each region.

CHAPTER 7

MECHANICS OF TRANSITION

7.1 Introduction

In what follows, an attempt to understand the phenomenon of transition will be made through a comparative study of different oscillogram records and power spectra, recorded at different heights and stages of BL development beneath a FST of varying intensity.

A word of caution must be said concerning comparison of signals or spectra of records taken at (x, y) positions with different values of $\frac{\sqrt{\overline{u^2}}}{U_\infty}$, since such comparison can only be qualitative. A quantitative study could possibly be made using records taken at the same relative position with reference to the extent (in two directions) of the BL region in question (i.e. the transition region streamwise length and the BL thickness, say). The fast development of the laminar-transitional BL in the streamwise and normal directions makes such comparisons inaccurate, to say the least.

In this chapter, a laminar burst, refers to a single spike of a short duration similar to the ones in trace No. 1 in Fig. 7.1b.

7.2 Hot-Wire Oscillogram Records Throughout the Laminar-Transitional Boundary Layer

Before proceeding to discuss the physical processes associated with the phenomenon of transition, it is thought useful to present some pictures of what the fluctuating velocity component in the x-direction looks like, when the measuring wire is placed at different points throughout the laminar-transitional BL.

Figs. 7.1a - e show such a signal plotted as a function of the time (T) for different heights y from the wall. In this case, the FST

is produced by the 1.5" grid $\left(\frac{\sqrt{\overline{u^2}}}{U} \simeq 0.02\right)$. Here, Fig. 7.1a is taken within the still LBL while the other four figures represent different stages of the transitional BL development. Also Figs. 7.2a - b show the same for the case of the FST produced by the 3.0" grid $\left(\frac{\sqrt{\overline{u^2}}}{U} \simeq 0.027\right)$.

It is worth mentioning that the plots in Fig. 7.1 are not suitable for direct quantitative comparison since each curve in the plots is normalised by its maximum*. On the other hand, the plots in Fig. 7.2 are scaled relative to a common maximum for each figure.

While postponing the discussion of the relative amplitudes and energy at different frequencies to the sections dealing with power spectra, the following remarks can be made about the figures:-

1. In Fig. 7.1a, although no high frequency bursts are detected, yet there are zones of high $\partial u/\partial t$ (or $\partial u/\partial x$) which may be going to develop into a burst further downstream (see Section 7.3). The accumulation of such (laminar bursts) in space may explain the observed oscillations of the mean velocity profiles around the value given by Blasius (see Sections 6.2.2 and 6.3.3).

2. From the three traces nearest to the wall in Fig. 7.1b, we see that it may be likely that a burst of high frequency fluctuations at a certain height (and instant of time) may only be a laminar spike at another height (or at another instant of time) nearer to the wall.

---

* It had to be so since the plots were by-products of the program that computed the burst statistics which required a large computer core. Therefore, each plot had to be processed separately.

This may indicate that if the idea put forward by Kim et al (1971) (that the viscous sublayer is the source of turbulent bursts) is true, then it seems from the plots that such a sublayer instability starts by causing tongues of laminar flow to errupt away from the wall (see Section 7.3). Such a laminar tongue is continuously disturbed by whatever disturbances are present, causing it to flare-up away from the wall until a certain distance where it breaks down into high frequency fluctuations. In this context, one recalls the concept of vorticity Reynolds number put forward by van Driest et al (1963) as a possible criterion for the distance from the wall at which such breakdown takes place. Their argument can be posed as saying that the breakdown takes place when the ratio of the inertial forces to the viscous forces reaches a certain limit.

3. In Fig. 7.1b (at X = 56 cm), zones of high strain rates (that are not turbulent) are observed near the wall which cannot be dissipated by laminar viscosity in that region. It is known that for length scales greater than Kolmogoroff's length scale (i.e. away from the viscous turbulent energy sink) and/or away from solid boundaries (i.e. away from the viscous laminar energy sink), a strain rate can only be broken up into strain rates (i.e. from bigger eddies into smaller eddies).

From an analysis of the dynamics of decay of the homogeneous turbulence, it is demonstrated by Batchelor (1953, pp. 83-84) that the rate of change of the energy associated with a certain

wave number is a function of all the other wave number pairs whose sum equals the wave number in question. That is, points in the wave number space can be regarded as connected to each other through inertia forces. Hence, once energy exists at a certain wave number, it is transferred to higher wave numbers through inertia forces (without changing the total amount of energy associated with any directional component of the energy).

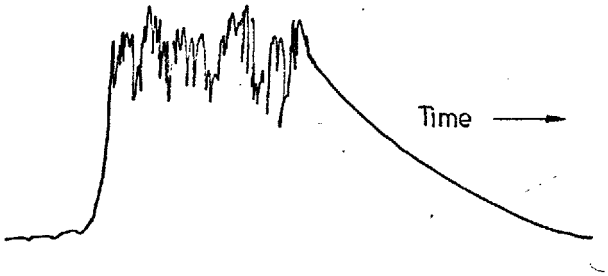
Hence, as soon as a laminar instability (a laminar burst) occurs inside the disturbed LBL, it starts to dissipate itself by viscosity (via inertia forces after a process that is usually termed, vortex stretching). The natural outcome of this process is turbulence of scales smaller than that of the original laminar burst localised in the form of a spot (or a turbulent burst).

It is also plausible to expect that such a process will be possible when this laminar burst is sufficiently remote from the wall or in other words when the ratio of the local inertia forces to the local laminar viscous forces reaches a certain value. This brings us back to the concept of vorticity Reynolds number (R_v) put forward by van Driest et al (1963). And although they reported that such breakdown occurs when R_v reaches a maximum at a distance inside the BL for which they quote the value of $y/\delta = 0.6$, here it is argued that from the experimental observations of Fig. 7.4 (see next section) and the results discussed in Sections 6.2.4 and 6.3.4, such breakdown may occur when R_v reaches a certain value that may not necessarily be the maximum within the layer. This condition

seems to be satisfied at $y/\delta = 0.25 - 0.3$.

4. It looks as if the fluid inside such a laminar tongue moves at a nearly constant speed, which may plausibly be a function of the laminar shear at the point of breakdown and the nature of the disturbances that caused it. Such a speed, though higher than the local speed near the wall, is still lower than that of the flow in the outer region of the BL. This can clearly be seen upon making a comparison between the bursts at different heights shown in the same figure.

5. As observed by Schubauer et al (1956), the line of demarcation between the ambient flow and the leading edge of the burst (for the traces near the wall) is sharp, while after the passage of the turbulent bursts, the flow recovers its speed after a relatively short interval which Schubauer et al called the recovery trail.



As seen in the sketch above, such trails are caused by the fact that as fluid inside the burst moves faster than the fluid near the wall, it leaves a wake of relatively faster moving fluid behind it. This argument is supported by the disappearance of such trails in the records taken in the outer region of the BL where the fluid inside the burst is

slower than the surrounding fluid. A further explanation of this will be given in Section 7.3.

6. The last record in each figure (nearest to the free stream) shows the relative magnitude of the FST. Even at station X = 56 cm just after where the bursts make their first appearance, the FST seems to be relatively too weak to cause anything like a local separation at transition. This subject will be returned to during the discussion of power spectra.

7. It is also interesting to observe that the sharp and thin spikes of turbulent flow occur only near the outer edge of the BL and never near the wall. It seems that such small regions of high rate of strain ($\partial u/\partial x$) are only possible within a flow of a certain Reynolds number, i.e. within a turbulent flow where the laminar viscous forces are not large enough to prevent it.

Figs. 7.2a - b also show records taken within the LBL and the transitional BL. Here each figure is scaled relative to a common maximum (notice the change in the time scale). Besides the previously discussed observations, it can be seen from comparing Fig. 7.2b with Fig. 7.1c that the rate of production of the turbulent bursts is increased considerably although R_x is nearly halved.

While keeping in mind the weakness of the turbulence outside the BL relative to that inside it near transition (as seen from Fig. 7.2b), we conclude that the increase in the bursting activities due to the increase in $\frac{\sqrt{\overline{u^2}}}{U}$ is not likely to come about through local effects of the FST at transition. This subject will be discussed further in

Sections 7.4 and 7.5.

7.3 Statistical Study of Burst Formation Within a BL

Records taken at different positions were studied using the program of Section 3.6 which detects the turbulent bursts and then computes the following quantities:-

(i) The rate of burst formation.

(ii) The average width of bursts.

(iii) The bursting intermittency defined as the ratio of duration of the burst to the total time.

All the computed quantities were averaged over the total length of the record (here, 10.0 seconds were found adequate to give true statistical averages). Samples of the program output are shown in Figs. 7.3a - c. The figures show the physical signal as well as the intermittency function (γ) which is set to 1.0 when the particular zone is declared turbulent by the program and to zero otherwise. Upon compiling the results of such analysis (for different stations within the transitional BL) together, the plots in Figs. 7.4, 7.5 and 7.6 can be produced. The figures show:-

- The rate of formation of bursts vs y
- The average width of burst vs y
- The burst intermittency vs y

respectively, evaluated at the following X-stations:-

X = 56, 68, 96, 104 and 112 cm

From inspection of Figs. 7.3 - 7.6, the following picture may emerge:-

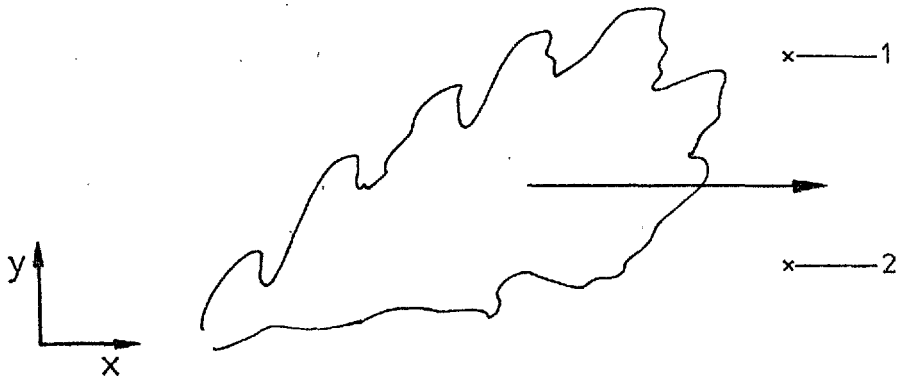
(i) Once the bursts start to show in the BL, they first increase in both width and rate of formation. This is understandable since turbulent spots grow in size by entraining laminar flow around them from all directions. Also the process of erruptions of the laminar tongues near the wall discussed in the previous section (Section 7.2) may serve to trigger more erruptions through the disturbances they create to the near flow profile.

(ii) As bursts are swept downstream, they merge together forming bigger regions of turbulent flow until they eventually fill the flow. Although they initially increase in number as well as in size, yet further downstream, the combined effect of the decrease in the rate of burst formation (due to the stabilising effects of the newly generated turbulence on the BL profile manifested in a fuller profile downstream of transition as in Fig. 6.29) and also due to the process of merging, the number of the observed bursts starts to drop.

(iii) As seen in Figs. 7.4 - 7.6, at the same X-station, there is a little change in γ, the rate of burst formation and the burst width over most of the outer region of the BL which suggests that each formed burst sweeps the whole BL.

(iv) Recalling the irregular shape of a burst (or a turbulent eddy

boundary) as seen from the sketch below (see Bradshaw et al (1973) and Reshotko, 1976):-



the observed decrease in both γ and the average burst width coupled with an increase in the burst formation rate near the outer region of the BL can be plausibly justified since they will depend on the position of the measuring device relative to the oncoming burst as seen from the sketch.

The present picture of the mechanism of formation of turbulent spots can thus be viewed as a combination of Kim et al (1971) type of viscous sublayer activity leading to Emmons' (1951) spots when van Driest et al (1963) vorticity Reynolds number reaches a certain limit that is found to occur at $y/\delta \simeq 0.25 - 0.3$ in the present work.

Also the general picture of transition reported by Schubauer et al (1956) is confirmed. That is, transition is composed of two stages:-

(i) Initial breakdown of laminar flow due to growth of disturbance (occurrence and growth of bursts).

(ii) Growth of turbulent bursts into the surrounding laminar region

until merging.

As for the low wave number fluctuations initially present in the LBL, they increase to a certain limit, and once the turbulent bursts start to form, they dissipate such low wave number fluctuations gradually, then completely near the end of the transition region through vortex stretching (see Figs. 7.1d - e and discussion of Sections 7.4 and 7.5).

7.4 Development of Energy at Different Wave Numbers Within the Laminar-Transitional BL Beneath a Turbulent Free Stream of Varying Intensity

During this experiment, the output of a U-wire was analysed using the technique outlined in Section 3.7 and different spectra were produced. The results presented in this section are mainly presented in the form of plots of (spectral density x frequency) versus frequency. Such a method of presentation, although it did not have much quantitative importance, is still very useful as a qualitative measure of the amount of energy at different frequency bands. It also serves to highlight the significance of any peaks that may be found in the spectrum.

It is thought informative to report spectra taken at a position just before the start of amplification of small disturbances for the case of no grid in the wind tunnel (i.e. at $\frac{\sqrt{\overline{u^2}}}{U} \simeq 0.09\%$). Fig. 7.7 shows a multiplot of the physical signal and the spectrum plotted once as the (spectral density) and once as the (spectral density x frequency) both versus the frequency in Hz. From the figure, we see that a narrow band of frequencies is excited with a concentration of power at a frequency that lies comfortably within the predicted unstable range by Tollmien-Schlichting theory for this particular layer (such an unstable frequency band is indicated by the hatched region in the figure). The

figure also indicates that most of the power is concentrated at the excited band.

Figs. 7.8a - c and 7.9 a - c report spectra within the laminar, transitional and turbulent regions for both the 1.5" grid and the 3.0" grid respectively. They are plotted as:-

(Spectral density x frequency) vs. frequency (Hz)

Those spectra are reported for three different heights (y) from the wall in each case as indicated on the figures. Since only a qualitative comparison is intended at this stage, it was not felt necessary to correct the plots by accounting for the effects of variations in the local convection speeds (a subject that will be dealt with in detail in Section 7.5). Upon inspecting the figures, the following remarks may be made:-

1. Apart from the peak observed at the frequency of 100 Hz (twice the mains frequency) which is pronounced only when the signal is weak and which was probably caused by the tape recorder used in recording the analogue data, and unlike the case of no grid discussed above (Fig. 7.7), there are no other observed peaks or excited narrow bands of frequencies with an appreciable amount of power at or just before transition. And although this is not where this particular issue will be discussed, yet it can be said that this may be taken as an indication of either an indistinguishably wide band of frequencies around the band predicted by the stability theory (since disturbances of all wave numbers exist in the FST outside the BL along the surface) or a different mechanism

altogether controlling the process of transition beneath a turbulent free stream. Further observations discussed in the next section (Section 7.5) tend to give support to the first possibility.

2. Further upstream (Figs. 7.8a and 7.9a) spectra taken near the wall and those taken at $y/\delta = 1.0$ become of comparable magnitude and it becomes more reasonable for the FST to affect (locally) the stability of the BL.

3. In general, transition is characterised by an increase in power at all frequencies but mainly at low frequencies, whereas, within the turbulent region, spectra are characterised by an increase in the power at high frequencies coupled with a decrease in power at low frequencies (near the end of the transition region) as seen upon comparing Figs. 7.8a - b with Figs. 7.8b - c for the 1.5" grid and Figs. 7.9a - b with Figs. 7.9b - c for the 3.0" grid.

4. The demarcation between the amount of energy at the low frequencies (originating from the amplified disturbances in the LBL) and energy at high frequencies (brought about through turbulent bursting) as seen in Figs. 7.8a and 7.9a, indicates that although the process of energy transfer along the wave number axis starts off by being gradual (see Figs. 7.8b and 7.9b), yet later in the transitional region and due to the combined effect of the turbulent energy production near the wall and the turbulence intensification at high wave numbers by vortex stretching, energy starts to be transferred

to the high frequencies, as seen in Figs. 7.8c and 7.9c, causing this observed change of slope of the spectra.

Fig. 7.10 shows how that energy at low frequencies inside the transitional BL disappears as the transitional BL develops. Such a development is further illustrated in Figs. 7.11a - b, which show spectra taken at the constant height of y = 1.35 mm in the laminar, transitional and turbulent regions respectively for the 1.5" grid, and plotted together as:-

(Spectral density) vs. frequency

and in Figs. 7.12a - b, which show the same for the 3.0" grid.

Again, it is asserted that the comparison between the reported spectra can only be qualitative, since the exact position of the measuring point inside the BL strongly affects the absolute value of the spectral power which changes at a high rate as the BL develops in the x and y directions.

7.5 Development of the Energy at Different Wave Numbers Within the Laminar-Transitional BL Beneath a Turbulent Free Stream of Nearly Constant Intensity

A detailed study of spectra of the U-wire output at different positions within the laminar-transitional BL were obtained using the technique outlined in Section 3.7 for the situation with the following particulars:-

1. The 1.5" grid producing turbulence of intensity $\left(\frac{\sqrt{\overline{u^2}}}{U}\right)$ of roughly 0.0185.

2. Uniform air speed (U_∞) of 8.5 m/s.

3. The 1.5" thick flat plate with the 8" long elliptic nose section (No. 1 in Fig. 2.4).

In order to render the frequency spectra at different heights from the wall and different distances from the plate LE amenable to direct comparison in terms of wave length, two types of corrections for the differences in conection speeds were adopted, namely:-

(i) The first one assumes a frozen pattern of turbulence moving at the local mean speed. In this case, spectra need only be plotted against:-

$$\left(\text{frequency} \times \frac{U}{U_{local}}\right)$$

rather than against frequency. This correction in fact accounts for most of the discrepancy between different spectra.

(ii) The second correction is the one discussed in detail in Section 3.8, which involves computing the convection speeds (U_c) for different wave numbers. This correction is shown to be most effective at high wave numbers although the improvement relative to the first correction amounts to only about 7% (at most) of the power at any particular wave number.

The results of this study are presented in Figs. 7.13a - d and as:-

(Spectral density) vs. $\left[\text{frequency} \times \frac{U_\infty}{U_{local}}\right]$

with y as a parameter (y = 0.6, 0.85, 2.2 and 9.0 mm) for the stream-wise stations:-

X = 20, 44, 56 and 96 cm

respectively, and in Figs. 7.14a - d and as:-

$$\frac{F(\omega) \cdot f}{\overline{u_\infty^2}} \text{ vs. } \frac{\omega M}{U_c}$$

with y as a parameter (y = 0.6, 0.85, 1.2, 2.2, 9.0 and 17.0 mm), where $F(\omega)$ is the spectral density, f is the frequency in Hz, ω is $2\pi f$, $\overline{u_\infty^2}$ is the mean square velocity fluctuations, M is the grid mesh size and U_c is the calculated wave number convection speed. In this figure, the range of frequencies covered by the plot is:-

f = 0.5 → 2500 Hz

And, therefore, the range covered by the plots in Figs. 7.13a - c extends roughly to about where the peak occurs in Figs. 7.14a - d.

Figs. 7.14a - d also represent spectra at the following stream-wise stations:-

X = 20, 32, 44 and 56 cm

respectively.

On the other hand, Figs. 7.15a - c represent plots of:-

$$\text{(Spectral density) vs. } \left[\text{frequency} \times \frac{U_\infty}{U_{local}}\right]$$

with X as a parameter (X = 20, 44, 56 and 96 cm) for the following values of the distance y from the wall:-

y = 0.6, 0.85, 2.2 and 9.0 cm

Inspection of the different graphs reveals the following (recalling that transition took place at nearly X = 44 cm):-

(a) As indicated in Fig. 7.13a, the unstable range of frequencies predicted by Tollmien-Schlichting theory did not particularly contain much energy. And although there is a trace of a peak there, yet this cannot be taken as a conclusive proof that the linear stability described by the theory is the dominant process that leads to transition of the LBL beneath the FST.

(b) From Figs. 7.13a, 7.13b and 7.14a, 7.14b we see that, at low frequencies, the differences in power between the spectra near the wall and those taken in the outer region of the BL get much larger as the LBL develops. While that part of energy at high frequencies, although it starts by being damped (by viscous forces), yet further downstream, within the LBL it increases again until it becomes comparable with that in the free stream.

Those energised low frequency disturbances mentioned at the

beginning of this item will act to disturb the LBL during its early stages.

(c) As seen from Figs. 7.13c - d and 7.14c - d, as transition develops, energy at all wave numbers increase markedly (with a higher rate of increase at high wave numbers than at low wave numbers).

(d) From Figs. 7.13b and 7.14b, we clearly see that the local values at transition based on the integral parameters of the FST (i.e. dominated by energy containing eddies of the FST) cannot really offer a genuine parameter to predict the occurrence of transition, because the FST is likely to have enough power to affect the flow inside the BL only while the BL is still very thin. For it seems from the figures that there is a class distinction between turbulence in the two regions at transition.

(e) From Figs. 7.15a - c, there seems to be some power at the first and third duct modes computed as:-

$$D_n = \frac{nc}{b}$$

where c is the sound speed, b is the duct width and n = 1, 2, 3 ..... These odd modes are shown by Abdel-Kereem (1974) to be excited by the passage of homogeneous turbulence in the rectangular duct of the wind tunnel. From plots for stations near the wall, the BL spectra seem to contain power mainly at low frequencies and at some selected bands of high frequencies (notably at the above-mentioned duct modes which highlights the importance of isolating such modes in the study of transition).

As the BL develops downstream, there seems to be less and less energy acquired at low frequencies with an increasing power at high frequencies until eventually the hump in the spectra at X = 96 cm at low frequencies disappears altogether when the BL becomes fully turbulent (see Figs. 7.1a - e).

Finally, it is thought interesting to present spectra at a constant height well away from the BL along the streamwise direction. Fig. 7.16 shows such spectra at the following streamwise stations:-

X = 20, 32, 44, 56, 68, 96, 104 and 112 cm

respectively.

It is interesting to see that, with a BL of a thickness of

about 5 mm, the violent activities inside the layer at transition still make themselves felt at a distance 6 times the BL thickness.

In this context, the inactive motion discussed by Townsend (1961) and Bradshaw (1967a, b) together with the diffusivity of the turbulent flow in the free stream, offer themselves as possible explanations for the increased power at all frequencies at such a height above the BL.

The observed peak at 50 Hz was due to the mains and it is so much pronounced due to the low signal to noise ratio, since no amplification was applied to the signal of interest in this experiment.

CHAPTER 8

CONCLUDING REMARKS

In concluding the discussion of the results of the present experiment, the following remarks and suggestions may be made:-

1. In general terms, it is suggested that the argument put forward by Hall et al (1972) (that the local values at transition are not sufficient to correlate the likelihood of transition and an account of the past history of some flow parameters, notably u/U, the pressure gradient and θ must be taken into account) may be a valid argument. This is so despite the experimentally supported argument that local parameters at transition do, in fact, correlate the transition results better than the parameters based on non-local values (e.g. the grid mesh size and the distance from the plate leading edge). Because the inclusion of θ in the transition parameter, although it is a local parameter, implies a statement about the development of the laminar layer beneath the free stream turbulence. This suggestion is based on the following observations:-

   (a) Spectral analysis of the turbulent signals within the laminar-transitional range tends to suggest that, because the magnitude of the turbulent energy in the transitional boundary layer is many times that of the free stream turbulence, local values at transition based on the integral parameters of the free stream turbulence (i.e. dominated by the energy containing

eddies) cannot offer a genuine parameter to predict the occurrence of transition.

(b) While neither u/U alone nor Taylor's parameter $\frac{u}{U}\left(\frac{X}{M}\right)^{1/5}$ correlated with the likelihood of transition, a better collapse of the data was obtained using the modified Taylor's parameter of the form $\frac{u}{U}\left(\frac{\theta}{L_x}\right)^{1/6}$.

(c) The pressure gradient around the leading edge proved to have an important effect on transition since the data measured over the same plate with different nose shapes could not be correlated together.

2. At the same u/U, transition is promoted by smaller scale turbulence (i.e. smaller L/t and L/θ where t is the plate thickness and L is the turbulence length scale) although such changes are less critical as u/U increases.

3. More experiments are needed in order to assert with certainty whether the changes in the plate thickness affect the Reynolds number of transition through affecting changes in the free stream turbulence (by the increased vortex stretching around the nose section) or through changes in the laminar boundary layer instability (i.e. through the pressure gradient near the nose). In fact, two distinct curves were obtained for transition over the two plates with different thicknesses which were tested. Nevertheless, the present results do show that even at the low values of the free stream turbulence intensities covered by the experiment, the data for different

plate thicknesses still collapsed on two separate curves. This tends to give more weight to the effect of the pressure gradient on the boundary layer instability through the mean velocity profile.

4. It is shown that as the turbulence level in the free stream increases, the extent of the transition region decreases. Indeed, there is evidence that the laminar boundary layer integral parameters δ, θ and H may be some function of the free stream turbulence intensity. This may indicate that the use of the calculated values of θ (from the laminar boundary layer relations in smooth flow) rather than the measured ones at transition with free stream turbulence in correlating the flow parameters with the likelihood of transition may lead to errors.

5. The reported results tend to show that prior to transition, the boundary layer mean velocity profiles develop a wavy shape which was detected for all the values of the free stream turbulence intensities covered by the experiment, with some evidence that a local point of inflexion in the mean velocity profile may develop (possibly due to some unknown three-dimensional instability) after some oscillations around the value given by Blasius solution. Indeed, the oscillograph plots together with the power spectra throughout the range studied, while perhaps showing that flow reversal is unlikely by the action of the free stream turbulence, may indicate that the high activity at the low wave numbers inside the layer may induce the boundary layer profile to oscillate.

6. It is also observed that after the breakdown, the mean velocity profiles may suggest a universal process for the transitional boundary layer development until the end of transition (including the gradual disappearance of the wake component) in the case of free stream turbulence.

7. Although the turbulent velocity profiles within the transitional boundary layer show a strong dependence on the value of the free stream turbulence (the observed discrepancy between the turbulent velocity components near $y = \delta$ may be due to the unequal wall blockage effect on the three components), yet the triple product terms tend to show that the diffusion of the turbulent kinetic energy is towards the free stream and not vice versa. Indeed, the way the turbulent energy develops in the inner part of the boundary layer seems to be independent of the free stream turbulence. On the whole, the spectra and the magnitudes of turbulence in the boundary layer and in the free stream are of comparable magnitudes only early in the laminar region while the boundary layer is still very thin.

8. Inside the boundary layer, the turbulent kinetic energy seems to reach the highest level within the transition region just after breakdown (just after the U-profile assumes a sharp increase near the wall). It is observed that there, the turbulent production is nearly 10 times the value of the viscous dissipation, while the pressure diffusion reaches a maximum there. This is probably due to the large size of the newly generated turbulence (i.e. bigger than the dissipation length scale) which is being generated in an intermittent fashion.

9. No noticeable concentration of energy at the range predicted by the linearised theory (despite a trace of a peak there which could not be considered as a conclusive proof that the mechanism described by the theory dominated the process of instability in this case). Eventually, transition was characterised by an increase in power at all frequencies which developed further downstream near the end of the transition region to a situation with less power at the low frequencies and more power at the high frequencies.

10. The theory put forward by Kim et al (1971) (that the viscous sublayer - or the wall layer - is the source of turbulent bursts in the turbulent boundary layer) may be valid here as well, since it was noticed that, in the highly agitated laminar boundary layer prior to the formation of the bursts, a sort of a tongue of locally high $\partial u/\partial t$ (or $\partial u/\partial x$, i.e. a laminar burst) may errupt away from the wall as a manifestation of perturbations to the state of critical equilibrium of the laminar viscous forces and the inertial forces inside the layer. Such tongues are continuously disturbed by whatever disturbances are present in the layer as they flare up away from the wall, until a certain distance (possibly van Driest et al (1963) critical distance where the vorticity Reynolds number reaches a critical value which is thought here to be $0.25\ \delta$ - $0.3\ \delta$, where the turbulent activities are the highest within the transitional layer) where it breaks down into high frequency fluctuations.

11. The picture of the transition process may be viewed as follows:-

(a) Entrainment of turbulence by the very thin laminar boundary layer near the plate leading edge and the disturbing effect of the nearby turbulence on the boundary layer.

(b) The growth of the low wave number disturbance inside the boundary layer (by forcing mechanisms or otherwise).

(c) The appearance of laminar bursts inside the boundary layer (see Fig. 7.1b) possibly according to Kim et al (1971) theory.

(d) The breakdown of such laminar bursts into Emmons' (1951) type turbulent bursts when the van Driest et al (1963) vorticity Reynolds number reaches a certain limit (that is found to occur at 0.25 δ - 0.3 δ).

(e) The growth of such turbulent bursts into the surrounding laminar flow, diffusing in their way the low wave number fluctuations into high wave number fluctuations.

(f) The merging of such turbulent bursts until they cover the whole boundary layer by the end of the transition region.

Finally, it is thought useful that the future work should look into the following issues:-

(i) A survey of the free stream turbulence around the leading edge

of a plate with different thicknesses to assess the change in its characteristics in that region, and the way the laminar boundary layer responds to such changes.

(ii) To follow the development of the free stream turbulence as it is entrained by the growing laminar layer, possibly through following the development of a heated layer of fluid (by means of a heated wire).

(iii) Developing an analytical approach (possibly similar to that of van Driest et al, 1963) that may predict transition, taking the pressure distribution around the nose section into account.

(iv) A visual study of transition on flat plates with turbulent free streams using the hydrogen bubbles technique to establish the truth about such instability modes and the U-profile's waviness inside the transitional layer.

APPENDIX I

COMPUTER ROUTINE FOR THE BURST INTERMITTENCY DETECTION

Glossary

CX Fraction of total number of points to be operated on.

CC Fraction of maximum amplitude above which there should be CCC . N points.

CCC Fraction of total number of points (N) whose amplitude is such that:-

Amplitude $\geq$ CC . Maximum Amplitude

NS Total number of points in record.

N Number of points in NS whose amplitude is more than CX times the relevant absolute maximum.

AMX Array containing absolute maxima of signal.

CRITB Final criterion of burst for $\partial u^2/\partial t$.

CRITC Final criterion for $\partial^2 u^2/\partial t^2$.

U 2D array containing u, $\partial u^2/\partial t$, $\partial^2 u^2/\partial t^2$ respectively.

PERIOD Input value of time interval below which dropouts are ignored.

GAM Intermittency factor.

KB Total number of burst in record of length (TIME).

TIME Total record length.

BRST Average burst width over record of length (TIME).

GAMAV Average intermittency factor over whole run.

TIMET Total duration of run.

LBURST Total number of bursts in whole run.

WIDTHAV Overall average burst with over the whole run.

A list of the program follows on the next page.

```
      SUBROUTINE SIGNAL
      COMMON/A/U(4,5000),AV(3),IHZ,NEX,IS,FACB,FACC,PRIOD,AMXX(3),AMX(3)
      DT1=(1.0/FLOAT(IHZ))*FLOAT(NEX)
      DO 1 I=1,NS
      UUU=U(1,I)**2
      IF(I.EQ.1) U0=UUU
      U(2,I)=UUU-U0
      IF(I.EQ.1) U00=U(2,I)
      U(3,I)=U(2,I)-U00
      U0=UUU
    1 U00=U(2,I)
      DO 2 I=1,3
      AV(I)=0.0
      DO 2 II=1,NS
    2 AV(I)=AV(I)+U(I,II)/FLOAT(NS)
      DO 3 I=1,3
      AMX(I)=0.0
      DO 3 II=1,NS
      U(I,II)=U(I,II)-AV(I)
    3 IF(ABS(U(I,II)).GT.AMX(I)) AMX(I)=ABS(U(I,II))
      DO 4 I=1,3
    4 AMXX(I)=AMX(I)
      RETURN
      END


      SUBROUTINE CRITRIA
      COMMON/A/U(4,5000),AV(3),IHZ,NEX,IS,FACB,FACC,PRIOD,AMXX(3),AMX(3)
      COMMON/C/CRITA,CRITB,CRITC
      CX=0.1
      CCC=0.2
      CC=0.85
      I=1
    1 I=I+1
      N=0
      IF(I.GT.3) GO TO 5
      DO 2 J=1,NS
      IF(ABS(U(I,J)).LT.CX*AMX(I)) GO TO 2
      N=N+1
      U(4,N)=ABS(U(I,J))
    2 CONTINUE
    3 K=0
      C=CC*AMX(I)
      DO 4 J=1,N
    4 IF(U(4,J).GT.C) K=K+1
      IF(FLOAT(K).GT.CCC*FLOAT(N)) GO TO 1
      AMX(I)=CC*AMX(I)
      GO TO 3
    5 CRITA=FACB*AMX(1)
      CRITB=FACB*AMX(2)
      CRITC=FACC*AMX(3)
      RETURN
      END
```

```
      SUBROUTINE GAMA
      COMMON/A/U(4,5000),AV(3),IHZ,NEX,IS,FACB,FACC,PRIOD,AMXX(3),AMX(3)
      COMMON/B/GAMAV,LBRST,TIMET,WIDTHAV,NCALLS
      COMMON/C/CRITA,CRITB,CRITC
      LOGICAL F
      CALL SIGNAL
C**** BURST
      CALL CRITRIA
      DO 1 I=1,NS
      F(I)=.F.
      U(4,I)=0.0
      IF(U(2,I).GT.CRITB.OR.U(3,I).GT.CRITC) U(4,I)=1.0
    1 IF(1.0-U(4,I).LT.0.5) F(I)=.T.
      KEND=0
      I=0
    2 I=I+1
      IF(I.EQ.NS) GO TO 7
      IF(F(I).AND..NOT.F(I+1)) GO TO 3
      GO TO 2
    3 K1=I+1
    4 I=I+1
      IF(I.EQ.NS) GO TO 7
      IF(.NOT.F(I).AND.F(I+1)) GO TO 5
      GO TO 4
    5 K2=I
      IF(KEND.EQ.2) GO TO 14
      C=1.0
      IF(KEND.GT.0) C=0.4
      IF((FLOAT(K2-K1)*DT1).GT.C*PRIOD) GO TO 2
      DO 6 K=K1,K2
      F(K)=.T.
      U(4,K)=1.0
    6 IF(KEND.GT.0) U(4,K)=0.0
      GO TO 2
    7 IF(KEND.EQ.2) GO TO 16
      IF(KEND.GT.0) GO TO 10
      KEND=1
      DO 9 I=1,NS
      IF(F(I)) GO TO 8
      F(I)=.T.
      GO TO 9
    8 F(I)=.F.
    9 CONTINUE
      I=0
      GO TO 2
C**** INTERMITANCY
   10 K=0
      DO 11 I=1,NS
   11 IF(.NOT.F(I)) K=K+1
      GAM=FLOAT(K)/FLOAT(NS)
      PRINT 12,GAM
   12 FORMAT (//10X,*GAMA  = *,F6.4)
      TIME=FLOAT(NS)*DT1
   13 FORMAT (10X,*NO. OF BURSTS  = *,I2//10X,*RECORD LENGTH  = *,F4.2,*
     +  SEC.*)
C**** AVERAGE BURST WIDTH
      KB=0
      KC=-1
      I=0
      KEND=2
      GO TO 2
   14 KB=KB+1
      ID(KB)=FLOAT(K2-K1)
      IF(KC) 2,17,18
   16 IF(F(NS)) GO TO 17
      K2=NS
      KC=0
      GO TO 14
   17 IF(F(1)) GO TO 18
      KC=1
      K1=1
      I=0
      GO TO 4
   18 IF(KB.EQ.0) GO TO 20
      BRST=0.0
      DO 19 I=1,KB
   19 BRST=BRST+FLOAT(ID(I))*DT1/FLOAT(KB)
   20 PRINT 21,BRST
   21 FORMAT (10X,*AVERAGE BURST WIDTH  = *,F6.4,*  SEC.*)
      PRINT 13,KB,TIME
      GAMAV=GAMAV+GAM/FLOAT(NCALLS)
      LBRST=LBRST+KB
      TIMET=TIMET+TIME
      WIDTHAV=WIDTHAV+BRST/FLOAT(NCALLS)
      RETURN
      END
```

APPENDIX II

INVESTIGATION OF THE EFFECT OF INTENSITY AND LENGTH SCALE OF THE FREE STREAM TURBULENCE ON THE LAMINAR BL OVER A FLAT PLATE

This problem was first studied by Taylor (1936) both theoretically and experimentally. He assumed that the disturbing effect of turbulence on the LBL is mainly due to the pressure gradients which accompany variations in pressure within turbulent flow. For high Reynolds numbers of turbulence, those pressure gradients depend on the dissipation length λ which was found from the experiments to be given by:-

$$\frac{\lambda}{M} = A \sqrt{\frac{\nu}{Mu}}$$

where M is the mesh size of the grid that produces the turbulence, u is the RMS longitudinal velocity fluctuations, ν is the kinematic viscosity and A is a constant. Such mean square pressure fluctuations $\overline{\left(\frac{\partial P}{\partial x}\right)^2}$ inside the turbulent flow can also be written for homogeneous isotropic turbulence as:-

$$\sqrt{\overline{\left(\frac{\partial P}{\partial x}\right)^2}} = \sqrt{2}\ \rho\ \frac{u^2}{\lambda_\eta}$$

where λ_η is the length determined in diffusion experiments and ρ is the air density.

Using a similar approach to the one used in the Karman-Pohlhausen theory of the BL, Taylor determined the fluctuating pressure gradient parameter Λ' to be given by:-

$$\Lambda' = \frac{-\ 34\ X \cdot \left(\frac{\partial P'}{\partial x}\right)}{\rho U^2}$$

where U is the mean velocity, X is the distance from the LE and the superscript (′) implies RMS. Taylor then concluded that transition takes place when:-

$$R_{X_T} = F\left[\frac{\sqrt{u^2}}{U}\left(\frac{X}{M}\right)^{1/5}\right]$$

is satisfied. Here T refers to transition.

Batchelor in a foot-note to Taylor's paper (Batchelor, 1960) suggested that, based on more recent experimental results for the homogeneous isotropic turbulence, the dissipation length parameter λ as quoted by Taylor needs some modification since λ was found to depend on the distance from the grid also. Following this approach, we may write that for grid turbulence (Batchelor, 1953):-

$$\frac{U^2}{u^2} = \frac{a}{M}\ (X - X_0)$$

and also:-

$$\lambda^2 = \frac{b\nu}{U}\ (X - X_0)$$

where X_0 is the distance from the grid after which the turbulence is assumed to have settled to a homogeneous state (i.e. the origin of turbulence) and (a and b) are constants. Eliminating $(X - X_0)$ to get:-

$$\lambda^2 = \frac{B\nu}{U} \cdot \frac{U^2}{u^2} \cdot M$$

i.e.:-

$$\frac{\lambda}{M} = B \left(\frac{UM}{\nu}\right)^{1/2} \left(\frac{\nu}{uM}\right)$$

where B is constant. Following Taylor's analysis, the equation for $\sqrt{\overline{\frac{\partial P^2}{\partial x}}}$ then becomes:-

$$\sqrt{\overline{\frac{\partial P^2}{\partial x}}} = \frac{C}{M} \rho u^2 \frac{uM}{\nu} \left(\frac{\nu}{MU}\right)^{1/2}$$

where C is constant. So that using Taylor's derived relation:-

$$\frac{X}{\rho U^2} \cdot \frac{\partial P}{\partial x} = f \left(\frac{XU}{\nu}\right)$$

we get:-

$$f_1 \left(\frac{UX}{\nu}\right) = \frac{X}{\rho U^2} \cdot \frac{\rho u^2}{M} \cdot \frac{uM}{\nu} \left(\frac{\nu}{MU}\right)^{1/2} = \left(\frac{u}{U}\right)^2 \frac{uX}{\nu} \left(\frac{\nu}{MU}\right)^{1/2}$$

or:-

$$f_2 \left(\frac{UX}{\nu}\right) = \left(\frac{u}{U}\right)^3 \left(\frac{X}{M}\right)^{1/2}$$

This may be written as:-

$$f_3 \left(\frac{UX}{\nu}\right) = \frac{u}{U} \left(\frac{X}{M}\right)^{1/6}$$

which is the equivalent parameter to Taylor's original one of power 1/5.

That is, the power of the length ratio in the present expression is less than in Taylor's original expression which indicates that the length scale of turbulence has, in general, a very slightly weaker effect on transition than originally thought by Taylor.

REFERENCES

ABDEL-KAREEM, M. S. E. (1974)
"Pressure fluctuations on walls of a duct containing a turbulent flow".
M.Sc. Rep., University of London, IC Aero. Dept.

ANTONIA, R. A. and BRADSHAW, P. (1971)
"Conditional sampling of turbulent shear flow".
IC Aero. Rep., 71-04.

BAINES, W. D. and PETERSON, E. G. (1951)
"An investigation of flow through screens".
Trans. ASME, Vol. 73, pp. 467.

BATCHELOR, G. K. (1953)
"The theory of homogeneous turbulence".
Cambridge University Press.

BATCHELOR, G. K. (Ed.) (1960)
Taylor scientific papers, Vol. 2, Paper 27, pp. 288.
Cambridge University Press.

BATCHELOR, G. K. (1967)
"An introduction to fluid dynamics".
Cambridge University Press, (Reprint 1974).

BATCHELOR, G. K. and PROUDMAN, I. (1954)
"The effect of rapid distortion of a fluid in turbulent motion".
Quart. J. Mech. and App. Maths., Vol. VII, pp. 83.

BATCHELOR, G. K. and TOWNSEND, A. A. (1948)
"Decay of isotropic turbulence in the initial period".
Proc. Roy. Soc. A., Vol. 193, pp. 539.

BEARMAN, P. W. (1972)
"Some measurements of the distortion of turbulence approaching two-dimensional bluff body".
JFM, Vol. 53, pp. 451.

BENDAT, J. S. and PIERSOL, A. G. (1971)
"Random data: Analysis and measurement procedures".
Wiley Interscience.

BENNETT, H. W. (1953)
Rep. Kimberly-Clark Corp., Neenah, Wis.

BENNEY, D. J. (1961)
"A non-linear theory for oscillations in a parallel flow".
JFM, Vol. 10, pp. 209-236.

BENNEY, D. J. (1964)
"Finite amplitude effects in an unstable laminar boundary layer".
Phys. Fluids, Vol. 7, pp. 319-326.

BENNEY, D. J. and LIN, C. C. (1960)
"On the secondary motion induced by oscillations in a shear flow".
Phys. Fluids, Vol. 3, pp. 656-657.

BLAKE, W. K. (1970)
"Turbulent boundary layer wall-pressure fluctuations on smooth and rough walls".
JFM, Vol. 44, pp. 637.

BRADSHAW, P. (1965)
"The effect of wind-tunnel screens on nominally two-dimensional boundary layers".
JFM, Vol. 22, pp. 679-687.

BRADSHAW, P. (1967a)
"Irrotational fluctuations near a turbulent boundary layer".
JFM, Vol. 27, pp. 209-230.

BRADSHAW, P. (1967b)
"Inactive motion and pressure fluctuations in turbulent boundary layers".
JFM, Vol. 30, pp. 241.

BRADSHAW, P. (1970)
"Experimental fluid mechanics".
Pergamon Press.

BRADSHAW, P. (1971)
"An introduction to turbulence and its measurements".
Pergamon Press.

BRADSHAW, P. (1972)
"An introduction to conditional sampling in turbulent flow".
IC Aero. Rep. 72.18.

BRADSHAW, P. (1974a)
"Effect of free stream turbulence on turbulent shear layers".
IC Aero. Report 74-10.

BRADSHAW, P. (1974b)
"Prediction of turbulent shear layers in turbomachines".
Paper presented at the International Symposium on Fluid Mechanics and Acoustics of Turbomachines, 1970.
NASA SP-304 proceedings.

BRADSHAW, P. (1975)
"The Imperial College Aero. Dept. digital mag-tape data logging system".
IC Aero. TN 72-101 (revised).

BRADSHAW, P. (1976)
"Aerodynamic equipment instrumentation manual, Part 2".
IC Aero. TN 76-101.

BRADSHAW, P. and FERRISS, D. H. (1965)
"The response of a retarded equilibrium turbulent boundary layer to the sudden removal of the pressure gradient".
NPL Aero. Rep. 1145.

BRADSHAW, P. and MURLIS, J. (1973)
"On the measurements of intermittency in turbulent flow".
IC Aero. TN 73-108.

BRANDT, A. (1971)
"Digital analysis of turbulent flows".
IC Aero. Rep. 71-27.

BRASLOW, A. L. (1966)
"A review of the factors affecting boundary layer transition".
NASA TN D-3384.

BREDERODE, V. (1973)
"Velprof - a boundary layer data analysis program".
IC Aero. TN 73-107.

BRYER, D. W. and PANKHURST, R. C. (1971)
"Pressure probe methods for determining wind speed and flow direction".
Her Majesty's Stationary Office, London.

BULL, M. K. (1967)
"Wall-pressure fluctuations associated with subsonic turbulent boundary layer flow".
JFM, Vol. 28, pp. 719-754.

CEBECI, T. (1971)
"Wall curvature and transition effects in turbulent boundary layers".
AIAA, Vol. 9, pp. 1868.

CEBECI, T. and BRADSHAW, P. (1977)
"Momentum transfer in boundary layers".
Hemisphere Publishing Corporation & McGraw Hill Co.

CEBECI, T. and KELLER, H. B. (1971)
"On the computation of unsteady turbulent boundary layers".
Inter. Union Theo. & App. Mech., IUTAM Symposium, Vol. 1, pp. 1072.

CHANDRSUDA, C. (1975)
"A reattaching turbulent shear layer in incompressible flow".
Ph.D. Thesis, Imperial College, University of London.

CHARNAY, G., COMTE-BELLOT, G. and MATTIEU, J. (1971)
"Development of a turbulent boundary layer on a flat plate in an external turbulent flow".
AGARD CP No. 93, Paper No. 27.

CHARTERS, A. C. (1943)
"Transition between laminar and turbulent flow by transverse contamination".
NACA TN, 891.

CHEN, K. K. and THYSON, N. A. (1971)
"Extension of Emmons' spot theory to flows on blunt bodies".
AIAA J., Vol. 9, No. 5, pp. 821.

COLLIS, D. C. and WILLIAMS, M. J. (1959)
"Two-dimensional convection from heated wires at low Reynolds numbers".
JFM, Vol. 6, pp. 357-384.

COMTE-BELLOT, G. (1966)
"The use of a contraction to improve the isotropy of grid generated turbulence".
JFM, Vol. 25, pp. 657.

COMTE-BELLOT, G. (1976)
"Hot-wire anemometry".
Ann. Rev. Fluid Mech., Vol. 8, pp. 209.

CORCOS, G. M. (1963)
"Resolution of pressure in turbulence".
J. Acoustic Soc. Am., Vol. 35, pp. 192.

CORRSIN, S. (1951)
"The decay of isotrpic temperature fluctuations in isotropic turbulence".
J. Aero. Sci., Vol. 18, pp. 417.

CORRSIN, S. (1951)
"On the spectrum of isotropic temperature fluctuations in an isotropic turbulence".
J. App. Phys., Vol. 22, pp. 469.

CORRSIN, S. and UBEROI, M. S. (1950)
"Spectra and diffusion in a round turbulent jet".
NACA TN 2124.

CRIMINALE, W. O. (Jr.) (1971)
"On structure of the laminar boundary layer in the presence of a fluctuating free stream".
IUTAM Symposium, Vol. 1, pp. 940.

DAVIS, M. E. (1974)
"Spectral analysis programs, POWSPEC and COPHASE".
IC Aero. TN 74-103.

DEAN, R. B. (1974)
"An investigation of shear layer interaction in ducts and diffusers".
Ph.D. Thesis, IC Aero. Dept., University of London.

DESPARD, R. A. and MILLER, J. A. (1971)
"Separation in oscillating laminar boundary layer flows".
JFM, Vol. 47, pp. 21-31.

DHAWAN, S. and NARASIMHA, R. (1958)
"Some properties of boundary layer flow during the transition from laminar to turbulent motion".
JFM, Vol. 3, pp. 418-436.

DONALDSON, C. D. (1969)
"A computer study of an analytical model of boundary layer transition".
AIAA J, Vo. 7, No. 2, pp. 271.

DRYDEN, H. L. (1947)
"Some recent contributions to the study of transition and turbulent boundary layers".
NACA TN No. 1168.

DURBAN, P. A. (1979)
"Rapid distortion theory of turbulent flows".
Ph.D. Thesis, Cambridge University.

DUTTON, R. A. (1957)
"The accuracy of measurement of turbulent skin friction by means of surface Preston tubes and the distribution of the skin friction on a flat plate".
ARC, R & M, No. 3058.

ELDER, J. W. (1960)
"An experimental investigation of turbulent spots and breakdown to turbulence".
JFM, Vol. 9, pp. 235.

EMMONS, H. W. (1951)
"The laminar-turbulent transition in a boundary layer, Part 1".
J. Aero. Sci., Vol. 18, No. 7, pp. 490.

EVANS, B. J. (1970)
"A preliminary report into the effects of free stream turbulence on blade performance in a compressor cascade".
Cambridge University, Dept. of Mech. Eng. Report.

EVANS, R. L. (1973)
"Free stream turbulence effects on the turbulent boundary layer".
Cambridge University, Eng. Dept. CUED/A turbo TR 41.

EVANS, R. L. and HORLOCK, J. H. (1973)
"Calculations of the development of the turbulent boundary layer with a turbulent free stream".
Cambridge University, Eng. Dept. CUED/A turbo TR 53.

FAGE, A. and PRESTON, J. H. (1941)
"On the transition from laminar to turbulent flow in the boundary layer".
Proc. R. Soc., A. Vol. 178, pp. 201.

FALKNER, V. M. (1943)
"The resistance of a smooth flat plate with a turbulent boundary layer".
A/C Engineering, pp. 65, March.

FAVRE, A. J. (1965)
"Review on space-time correlations in turbulent fluids".
J. App. Mech., Vol. 32E, pp. 241.

FAVRE, A. J., GAVIGLIO, J. and DUMAS, R. (1957)
"Space-time double correlations and spectra in a turbulent boundary layer".
JFM, Vol. 3, pp. 313.

FAVRE, A. J., GAVIGLIO, J. and DUMAS, R. (1958)
"Further space-time corrections of velocity in a turbulent boundary layer".
JFM, Vol. 3, pp. 344.

FAVRE, A. J., GAVIGLIO, J. and DUMAS, R. (1967)
"Structure of velocity-space-time correlation in a boundary layer".
Phys. Fluids Suppl., Vol. 10, Part II, S138.

FFOWES-WILLIAMS, J. E., ROSENBLAT, S. and STUART, J. T. (1969)
"Transition from laminar to turbulent flow".
JFM, Vol. 39, pp. 547.

FIEDLER, H. and HEAD, M. R. (1966)
"Intermittency measurements in a turbulent boundary layer".
JFM, Vol. 25, pp. 719.

FRENKIEL, F. N. and ITHACA, N. Y. (1948)
"The decay of isotropic turbulence".
J. Appl. Mech., Vol. 15, pp. 311.

FREYMUTH, P. (1966)
"On transition in a separated laminar boundary layer".
JFM, Vol. 25, pp. 683.

GARDNER, C. M. (1975)
"Excitation of acoustic resonance on a streamlined plate in a duct containing turbulent flow".
M.Sc. Report, IC Aero. Dept.

GASTER, A. (1975)
"A theoretical model of a wave packet in a boundary layer on a flat plate".
Proc. Roy. Soc. London, A, Vol. 347, pp. 271-289.

GASTER, M. and GRANT, I. (1975)
"An experimental investigation of the formation and development of a wave packet in a laminar boundary layer".
Proc. Roy. Soc. London, A, Vol. 347, pp. 253-269.

GIBBINGS, J. G. (1959)
"On boundary layer transition wires".
ARC CP No. 462.

GRAHAM, J. M. R. (1969)
"The development of the turbulent boundary layer behind a transition strip".
ARC, 31 492 FM 4090.

GRAHAM, J. M. R. (1975)
"Turbulent flow past a long flat plate".
IC aero. TN 75-101.

GRAHAM, J. M. R. (1976)
"Turbulent flow past a porous plate".
JFM, Vol. 73, pp. 565.

GRANT, H. L. and NISBET, I. C. T. (1957)
"The inhomogeniety of grid turbulence".
JFM, Vol. 2, pp. 263.

GREEN, J. E. (1972)
"Influence of free stream turbulence on a turbulent boundary layer as it relates to wind tunnel testing at subsonic speeds".
ARE TR 72201.

HALL, D. J. (1968)
"Boundary layer transition".
Ph.D. Thesis, University of Liverpool.

HALL, D. J. and GIBBINGS (1972)
"Influence of free-stream turbulence and pressure gradient upon boundary layer transition".
J. of Mech. Eng. Sc., Vol. 14, No. 2, pp. 134.

HALL, A. A. and HISLOP, G. S. (1938)
"Experiments on the transition of the laminar boundary layer on a flat plate".
ARC R & M, No. 1843.

HAMA, F. R., LONG, J. D. and HEGARTY, J. C. (1957)
"On transition from laminar to turbulent flow".
J. App. Phy., Vol. 28, pp. 388.

HAMA, F. R. and NUTANT, J. (1963)
"Detailed flow field observations in the transition process in a thick boundary layer".
Proc. Heat Trans. Fluid. Mech. Inst., Vol. 77.

HEAD, M. R. and BRADSHAW, P. (1971)
"Zero and negative entrainment in turbulent shear flow".
JFM, Vol. 46, pp. 385-394.

HEAD, M. R. and RECHENBERG, I. (1962)
"The Preston tube as a means of measuring skin friction".
JFM, Vol. 14, pp. 1.

HESS, J. L. and SMITH, A. M. O. (1967)
"Calculation of potential flow about arbitrary bodies".
Prog. Aero. Sci., Vol. 8, pp. 1.

HINZE, J. O. (1975)
"Turbulence".
McGraw Hill.

HISLOP, G. S. (1940)
"The transition of a laminar boundary layer in a wind tunnel".
Ph.D. Thesis, Cambridge.

HOFFMANN, G. D. (1972)
"A note on von Karman's constant in low Reynolds number turbulent flow".
JFM, Vol. 53, pp. 45.

HOFFMAN, G. D., ZIMMERMAN, D. R. and BENNETT, W. A. (1972)
"The effect of free stream turbulence level on turbulent boundary layer behaviour".
Agardograph, No. 164, Paper No. I5.

HUNT, J. C. R. (1973)
"A theory of turbulent flow round two-dimensional bluff bodies".
JFM, Vol. 61, pp. 625.

HUNT, J. C. R. and GRAHAM, J. M. R. (1978)
"Free stream turbulence near plane boundaries".
JFM, Nol. 84, pp. 209-235.

ISHIGAKI, H. (1971)
"Skin friction and surface temperature of an isolated flat plate fixed in a fluctuating stream".
JFM, Vol. 46, pp. 165.

KIM, H. T., KLINE, S. J. and REYNOLDS, W. C. (1971)
"The production of turbulence near a smooth wall in a turbulent boundary layer".
JFM, Vol. 50, pp. 133.

KLEBANOFF, P. S. (1954)
"Characteristics of turbulence in a boundary layer with zero pressure gradient".
NACA TN 3178.

KLEBANOFF, P. S. and DIEHL, Z. W. (1952)
"Some features of artificially thickened fully developed turbulent boundary layers with zero pressure gradient".
NACA Report No. 1110.

KLEBANOFF, P. S. and TIDSTROM, K. D. (1959)
"Evolution of amplified waves leading to transition in a boundary layer with zero pressure gradient".
NASA TN D-195.

KLEBANOFF, P. S., TIDSTOM, K. D. and SARGENT, L. M. (1962)
"The three-dimensional nature of boundary layer instability".
JFM, Vol. 12, pp. 1-34.

KOVASZNAY, L. S. G., KOMODA, H. and VASUDEVA, B. R. (1962)
"Detailed flow field in transition".
Proceedings of the 1962 Heat Transfer & Fluid Mech. Inst.
(Stanford University Press, Stanford, Calif.), pp. 1-26.

LAUFER, J. (1955)
"The structure of turbulence in fully developed pipe flow".
NACA Rep. No. 1174.

LIN, C. C. (1953)
"On Taylor's hypothesis and the acceleration terms in the Navier-Stokes' equations".
Q. App. Math., Vol. 10, No. 4, pp. 295.

MAHGOUB, H. E. (1978)
"Calculation of the interaction between a complex turbulent shear layer and an external inviscid stream".
Ph.D. Thesis, University of London, IC Aero. Dept.

MICHEL, R. (1974)
"Effect of flow turbulence and noise on aerodynamic phenomena and wind tunnel results".
AGARD R-615.

MITCHENER, M. (1954)
"Propagation of turbulence from an instantaneous point disturbance".
J. Aero. Sc., Vol. 21, pp. 350.

MORKOVIN, M. V. (1958)
"Transition from laminar to turbulent shear flow - A review of some recent advances in its understanding".
Trans. ASME, Vol. 80, pp. 1121.

MORKOVIN, M. V. (1978)
"Technical evaluation report of the fluid dynamics panel symposium on laminar-turbulent transition".
AGARD AR-122.

MORKOVIN, M. V. (1978)
"Instability and transition to turbulence and predictability".
AGARD AG-236.

MORKOVIN, M. V., LOEHRKE, R. L. and FEJER, A. A. (1971)
"On the response of LBL to periodic changes in free-stream speed".
International Union of Theoretical and Applied Mechanics, IUTAM Symposium, Vol. 1. pp. 60.

McDONALD, H. and KRESKOVSKY, J. P. (1974)
"Effects of free stream turbulence on the turbulent boundary layer".
Int. J. Heat & Mass Transfer, Vol. 17, pp. 705.

McKEOUGH, P. (1976)
"Effects of turbulence on aerofoils at high incidence".
Ph.D. Thesis, IC Aero. Dept., University of London.

NISHIOKA, M., IIDA, S. and ICHIKAWA, Y. (1975)
"An experimental investigation of the instability of plane Poiseuille flow".
JFM, Vol. 72, pp. 731-751.

PATE, S. R. and SCHUELER, C. J. (1969)
"Radiated aerodynamic noise effects on boundary layer transition in supersonic and hypersonic wind tunnels".
AIAA Journal, Vol. 7, No. 3, pp. 450.

PATEL, V. C. (1965)
"Calibration of the Preston tube and limitation on its use in pressure gradient".
JFM, Vol. 23, pp. 185.

PATEL, V. C. (1969)
"The effect of curvature on the turbulent boundary layer".
ARC R & M, No. 3599.

PATEL, V. C. and HEAD, M. R. (1969)
"Some observations on skin friction and velocity profiles in fully developed pipe and channel flow".
JFM, Vol. 38, pp. 181.

PERKINS, H. J. (1970)
"The formation of streamwise vorticity in turbulent flow".
JFM, Vol. 44, pp. 721.

PHILLIPS, O. M. (1957)
"On the generation of waves by turbulent wind".
JFM, Vol. 2, pp. 417-445.

PICHAL, M. (1968)
"Reynolds shear stress in the turbulent boundary layer in a highly turbulent stream".
Strojnicky Casopis, Vol. 19, pp. 180.

PRESTON, J. H. (1954)
"The determination of turbulent skin friction by means of pitot tubes".
J. Roy. Aero. Soc., Vol. 58, pp. 109.

RESHOTKO, E. (1976)
"Boundary layer stability and transition".
Annual Review of Fluid Mechanics, Vol. 8, pp. 311-350.

ROBERTSON, J. M. and HOLT, C. F. (1972)
"Stream turbulence effects on the turbulent boundary layer".
Proc. ASCE, J. Hyd. Div., Vol. 98, pp. 1095.

ROGLER, H. L. and RESHOTKO, E. (1975)
"Disturbances in a boundary layer introduced by a low intensity array of vortices".
SIAM J. App. Math., Vol. 28, No. 2.

SANDBORN, V. A. (1960)
"Measurements of intermittency of turbulent motion in a boundary layer".
JFM, Vol. 6, pp. 445.

SCHLICHTING, H. (1968)
"Boundary layer theory".
McGraw Hill.

SCHUBAUER, G. B. (1938)
"The effect of turbulence on transition of the boundary layer of an elliptic cylinder".
Proc. 5th Int. Cong. App. Mech., (John Wesley & Son, Chichester).

SCHUBAUER, G. B. (1956)
"Contribution on the mechanics of boundary layer transition".
NACA R 1289.

SCHUBAUER, G. B. (1957)
"Mechanism of transition of subsonic speeds".
Boundary Layer Research Symposium, Fresburg (Ed. H. Görtler), Berlin Springer Verlag, pp. 85.

SCHUBAUER, G. B. and SKRAMSTAD, H. K. (1948)
"Laminar boundary layer oscillation and transition on a flat plate".
NACA Rep. No. 909.

SMITH, D. W. and WALKER, J. H. (1959)
"Skin friction measurements in incompressible flow".
NASA TR R-26.

SPANGLER, J. G. and WELLS, C. S. (Jr.) (1968)
"Effects of free stream turbulence on boundary layer transition".
AIAA J, Vol. 6, No. 3, pp. 543-545.

SQUIRE, H. B. (1933)
"On the stability for three-dimensional disturbances of viscous fluids flow between parallel walls".
Proc. Roy. Soc. London, A, Vol, 142, pp. 621-628.

STAINBACK, P. C. (1971)
"Hypersonic boundary layer transition in the presence of wind tunnel noise".
AIAA J, Vol. 9, No. 12, pp. 2475-2476.

SUTERA, S. P., MAEDER, P. F. and KESTIN, J. (1963)
"On the sensitivity of the heat transfer in the stagnation point boundary layer to free stream vorticity".
JFM, Vol. 16, pp. 497.

TANI, I. (1969)
"Boundary layer transition".
Ann. Rev. Fluid Mech., Vol. 1, pp. 169.

TANI, I. and HAMA, F. R. (1953)
"Some experiments on the effects of a single roughness element on boundary layer transition".
J. Aero. Sc., Vol. 20, pp. 289.

TAYLOR, G. I. (1936)
"Statistical theory of turbulence. Part V: Effects of turbulence on boundary layer. Theoretical discussion of relationship between scale of turbulence and critical resistance of spheres".
Proc. Roy. Soc. (London), A, Vol. 150, pp. 307.

THOMAS, N. H. and HANCOCK, P. E. (1977)
"Grid turbulence near a moving wall".
JFM, Vol. 82, pp. 481-496.

TOWNSEND, A. A. (1956)
"The structure of turbulent shear flow".
Cambridge University Press, (2nd Edition, 1976).

TSUJI, Y. and IIDA, S. (1975)
"Influences of free stream turbulence on mean velocities of turbulent boundary layer without pressure gradient".
Trans. Japan Soc. Aero. & Space Eng., Vol. 15, pp. 105-116.

Van DRIEST, E. R. and BLUMER (1963)
"BL transition: free stream turbulence and pressure gradient effects".
AIAA J, Vol. 1, No. 6, pp. 1303-1306.

WAGNER, R. D., MADDALON, D. V. and WEINSTEIN, L. M. (1970)
"Influence of measured free stream disturbances on hypersonic boundary layer transition".
AIAA J, Vol. 8, No. 9, pp. 1664.

WEBB, W. H. and HARRINGTON, R. P. (1956)
"Vortex structure in pipe flow".
J. Aero. Sc., Vol. 23.

WEIR, A. D. (1976)
"Program TUTVER: An aid to selecting intermittency criteria".
IC Aero. TN 76-103.

WEIR, A. D. and BRADSHAW, P. (1974)
"Apparatus and program for digital analysis of fluctuating quantities in turbulent flow".
IC Aero. Report 74-09.

WELLS, C. S. (1967)
"Effects of free-stream turbulence on boundary layer transition".
AIAA J, Vol. 5, No. 1. pp. 172-174.

WILCOX, D. C. (1975)
"Turbulence-model transition predictions".
AIAA J, Vol. 13, No. 2, pp. 241.

WILLMARTH, W. W. and ROOS, F. W. (1965)
"Resolution and structure of the wall pressure field beneath a turbulent boundary layer".
JFM, Vol. 22, pp. 81-94.

WILLMARTH, W. W. and TU, B. J. (1967)
"Structure of turbulence in the boundary layer near the wall".
Phys. Fluids Suppl., 10, Part II, S134.

WILLMARTH, W. W. and WOOLDRIDGE, C. S. (1962)
"Measurements of the fluctuating pressure at the wall beneath a thick turbulent boundary layer".
JFM, Vol. 14, pp. 187.

WILLMARTH, W. W. and YANG, C. S. (1970)
"Wall pressure fluctuation beneath turbulent boundary layers on a flat plate and a cylinder".
JFM, Vol. 41, pp. 47-80.

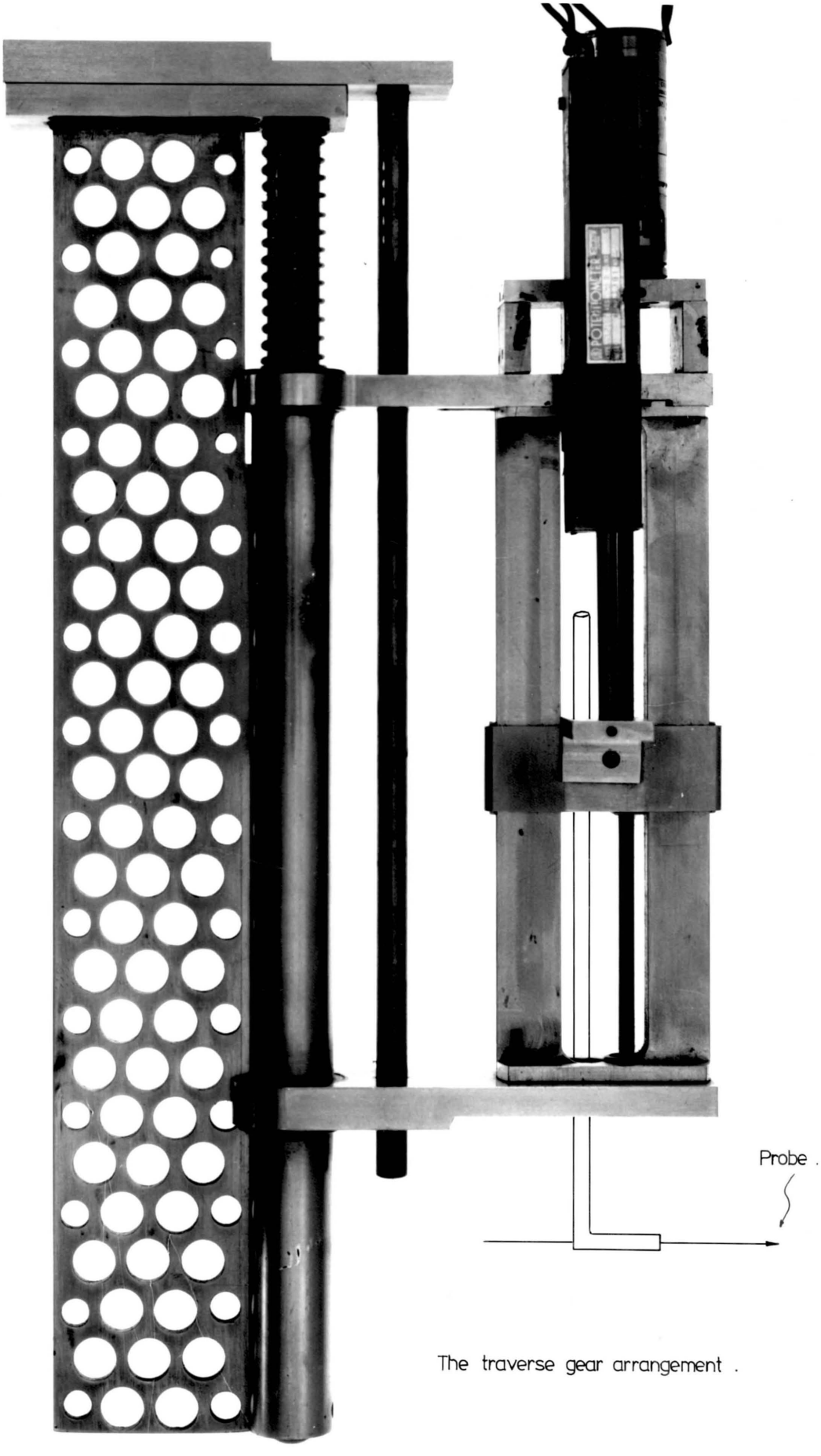
WILLS, J. A. B. (1962)
"The correction of hot-wire reading for proximity to a solid wall".
JFM, Vol. 12, pp. 388.

WILLS, J. A. B. (1964)
"On convection velocities in turbulent shear flows".
JFM, Vol. 20, pp. 417-432.

WILLS, J. A. B. (1970)
"Measurements of the wave number/phase velocity spectrum of wall pressure beneath a turbulent boundary layer".
JFM, Vol. 45, pp. 65-90.

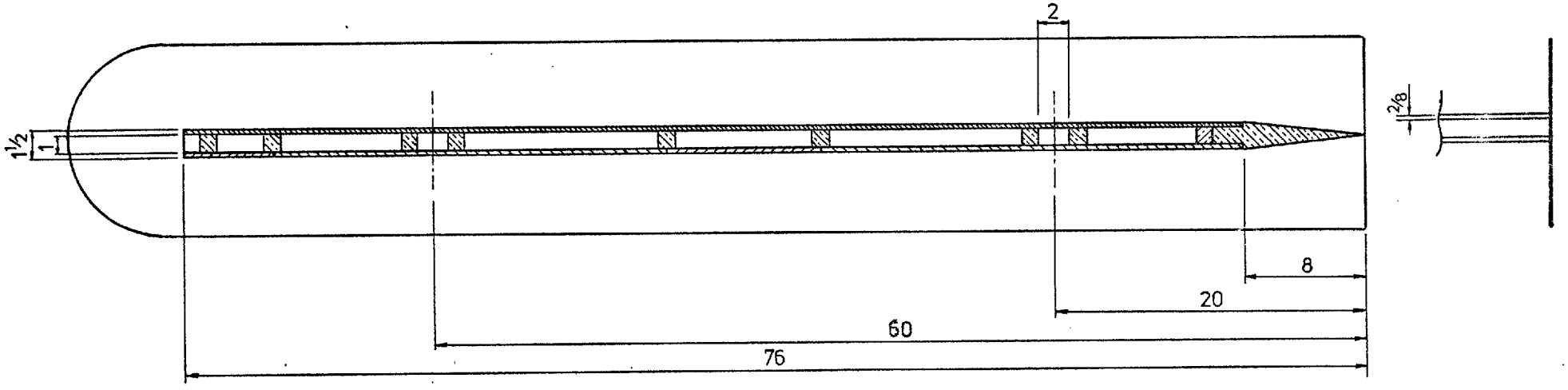
WORTMANN, F. X. (1969)
"Visualisation of transition".
JFM, Vol. 38, pp. 473-480.

WORTMANN, F. X. (1977)
"The incompressible fluid motion downstream of a two-dimensional Tollmein-Schlichting wave".
AGARD CP 224.



The traverse gear arrangement .

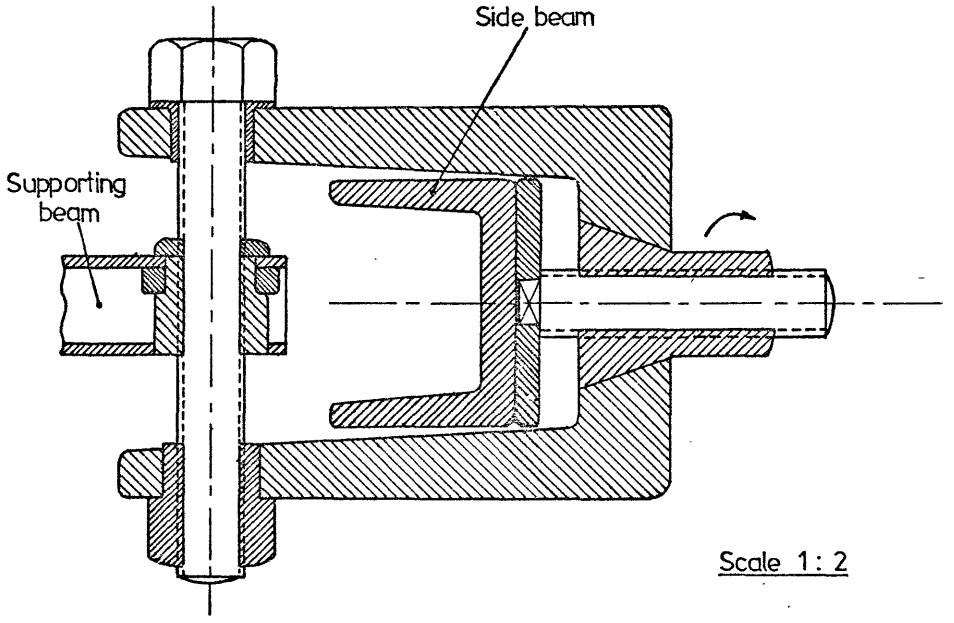
Fig. 2.1



Dimensions in inches.

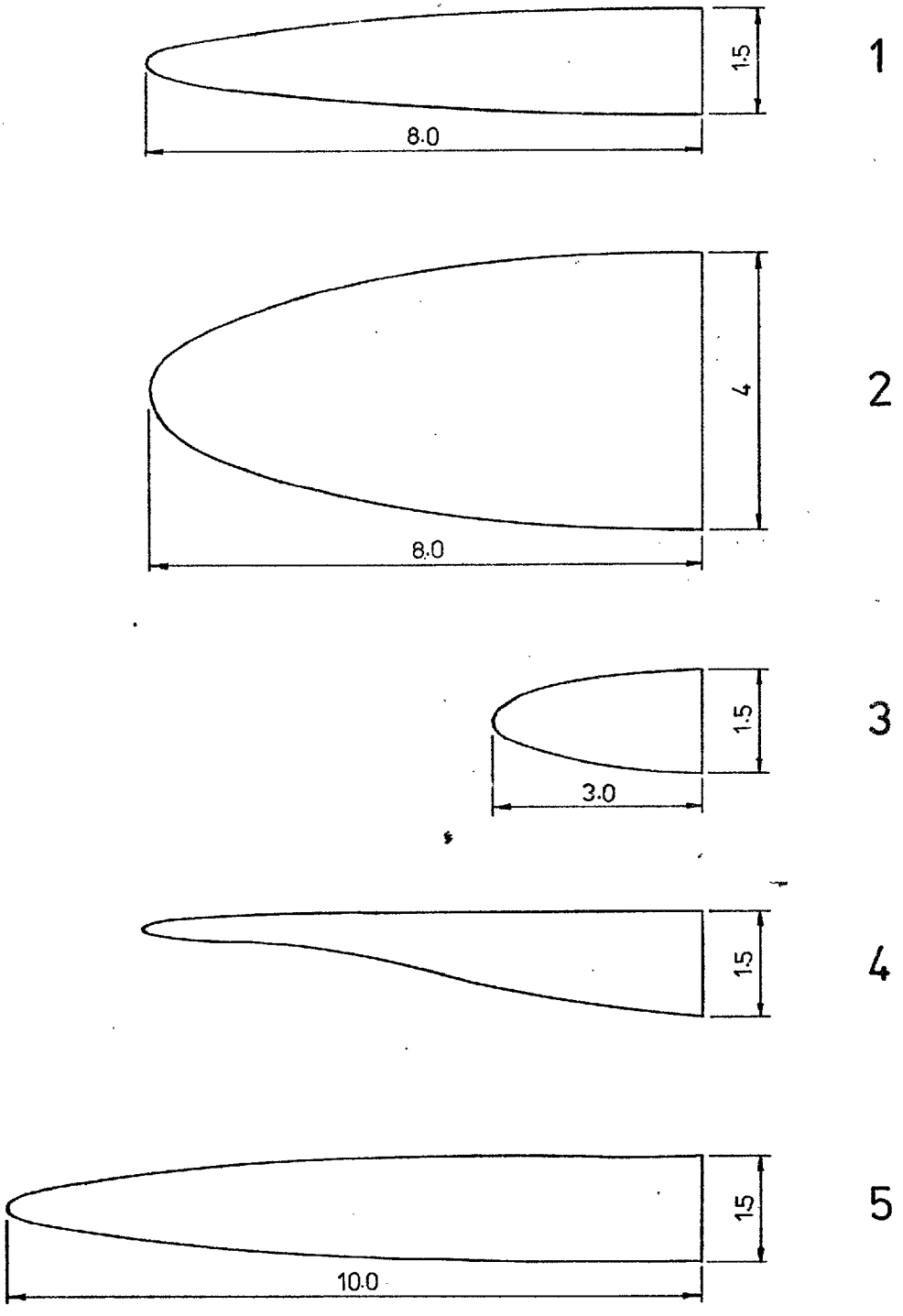
The flat plate

Fig. 2.2



The supporting beam-side beam clamp

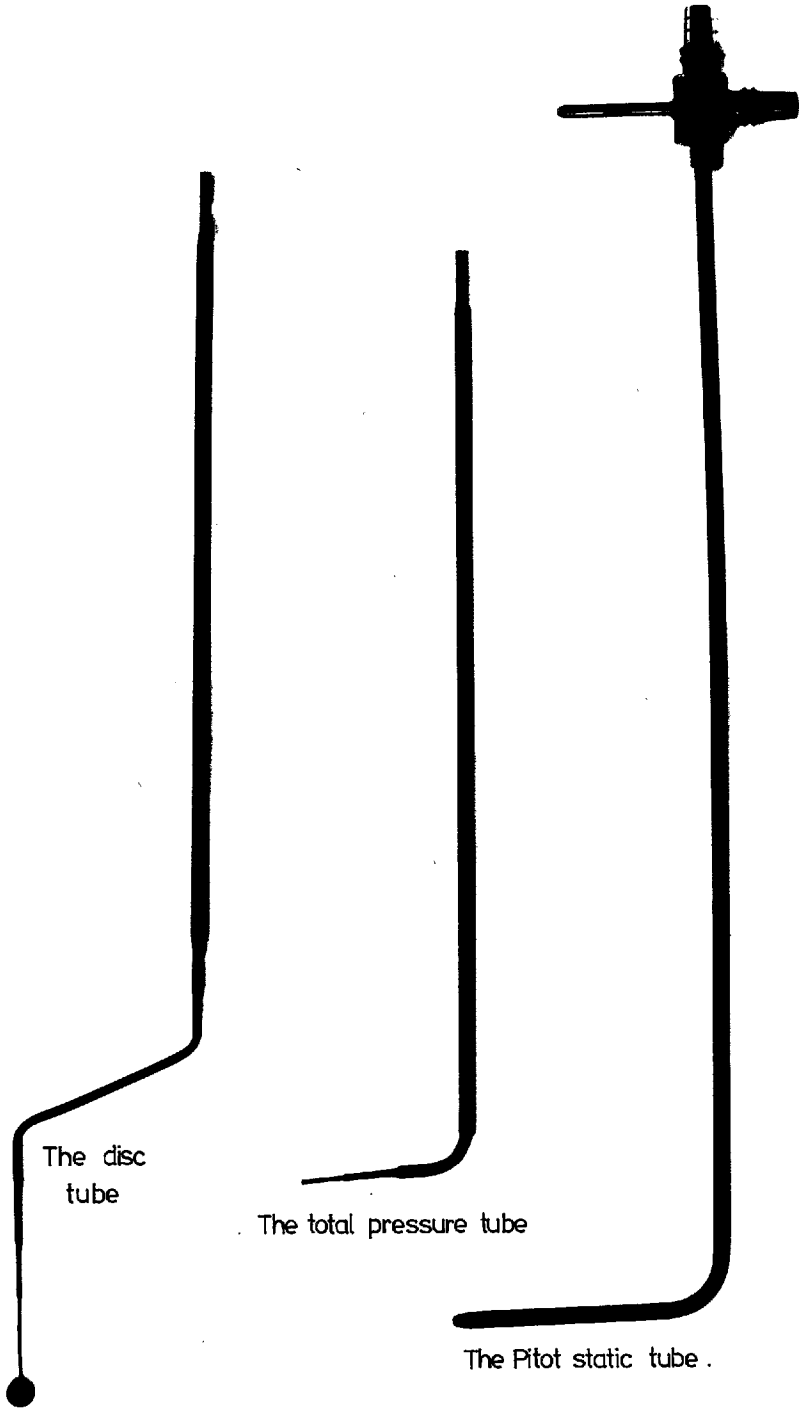
Fig. 2.3



Dimensions in inches .

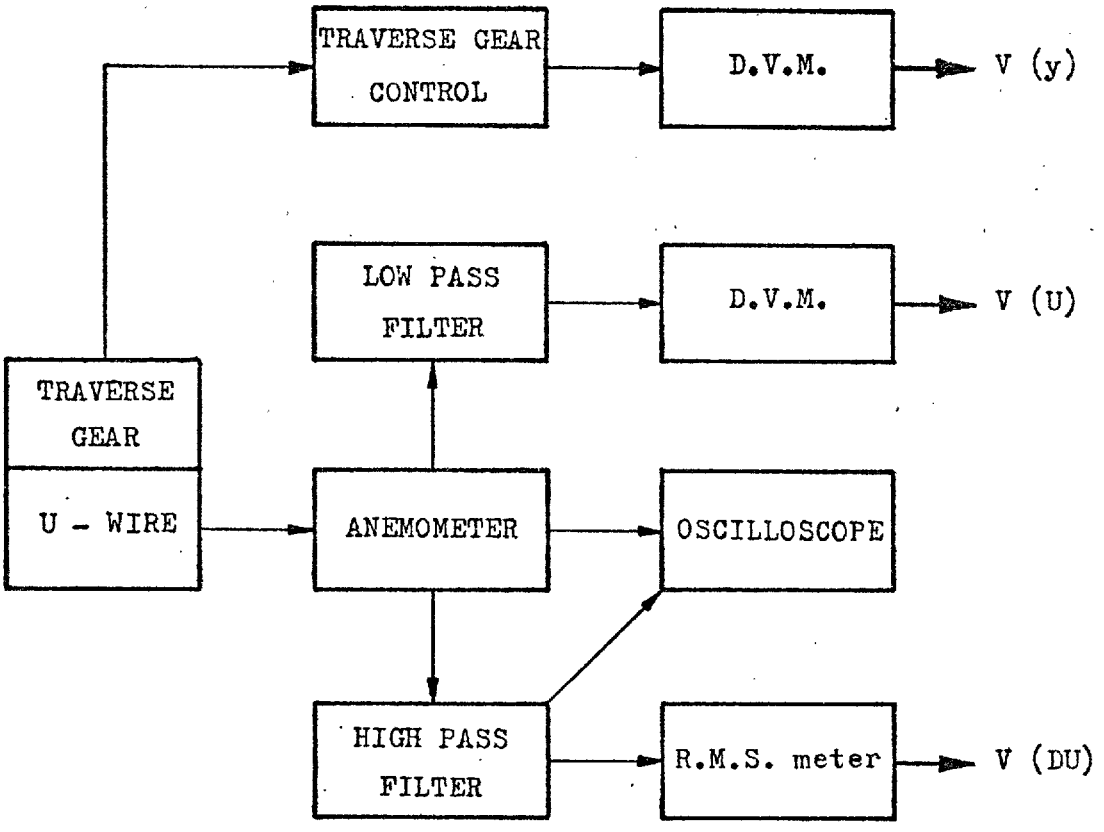
The nose sections used in the experiment

Fig. 2.4



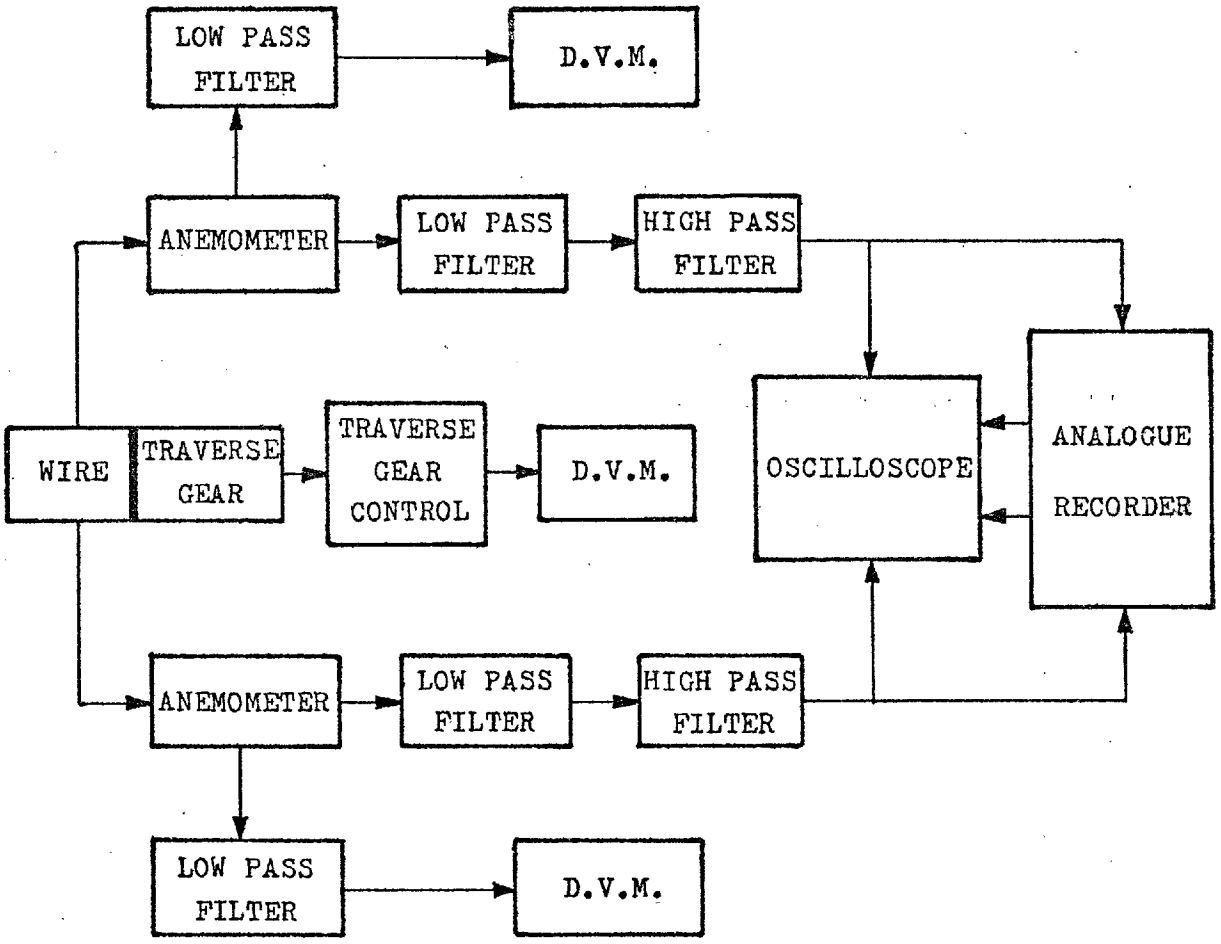
The pressure tubes .

Fig. 2.5



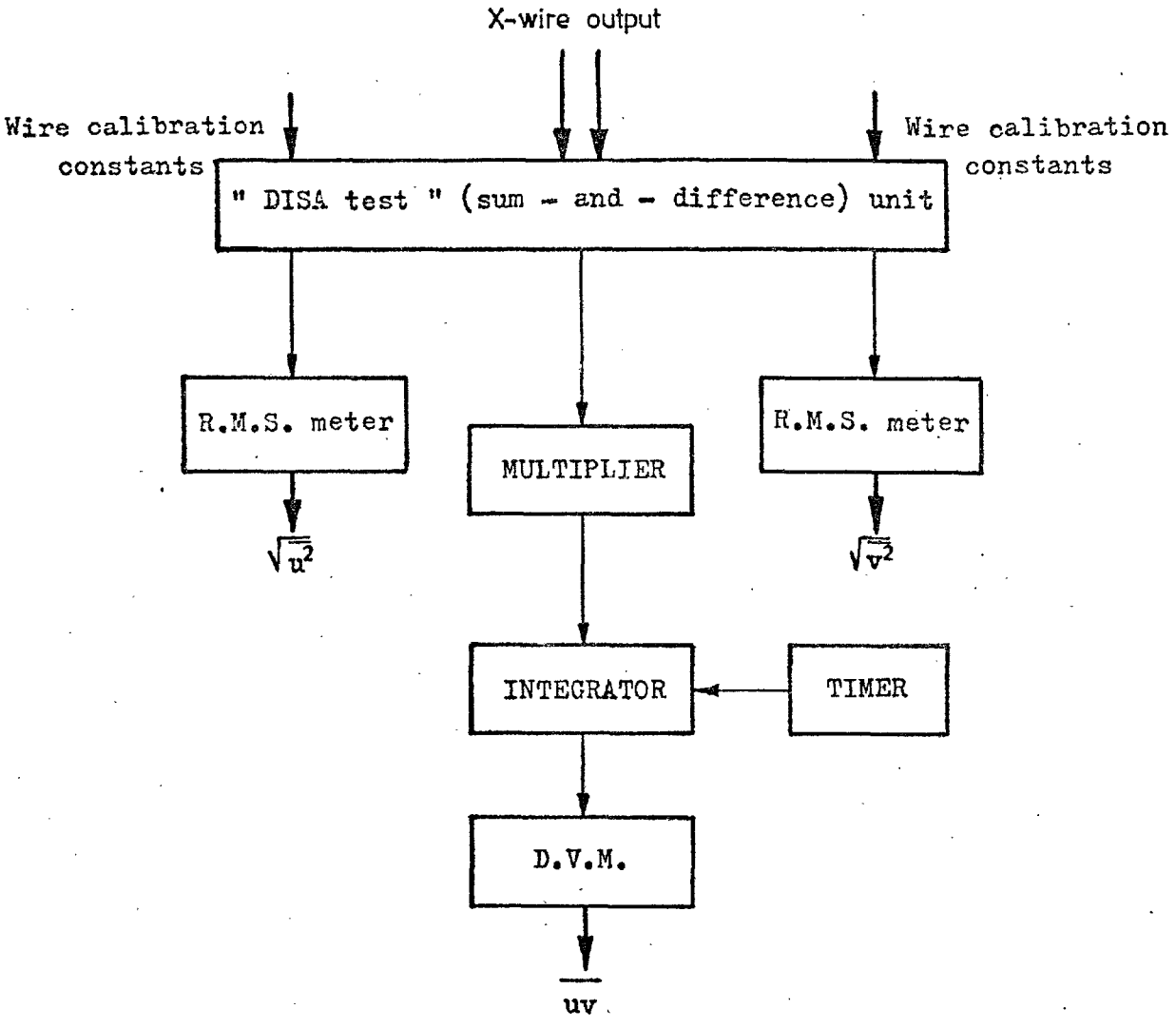
The arrangement for the U-wire measurements.

Fig. 2.6



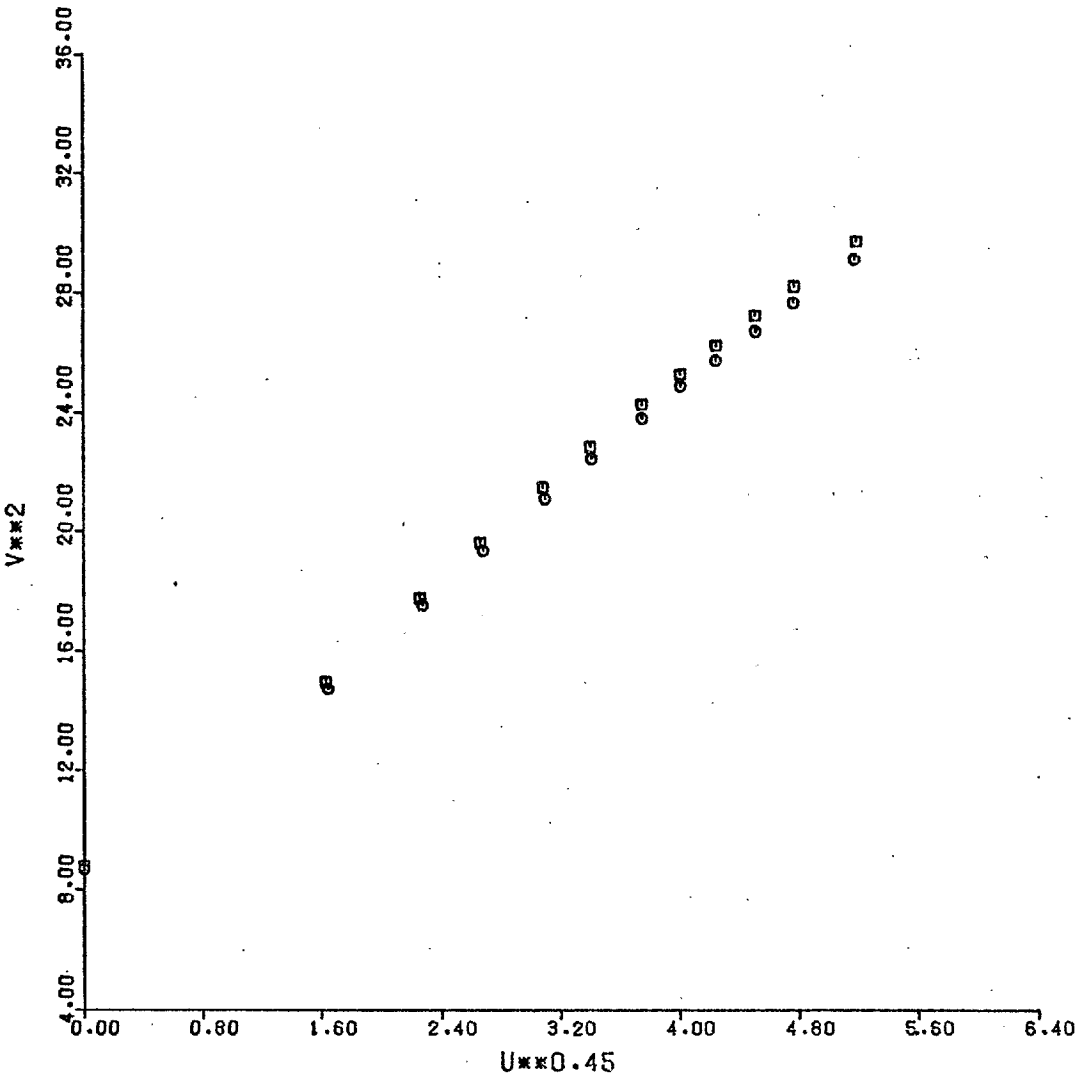
The arrangement for the X-wire measurements.
(and the double wire)

Fig. 2.7



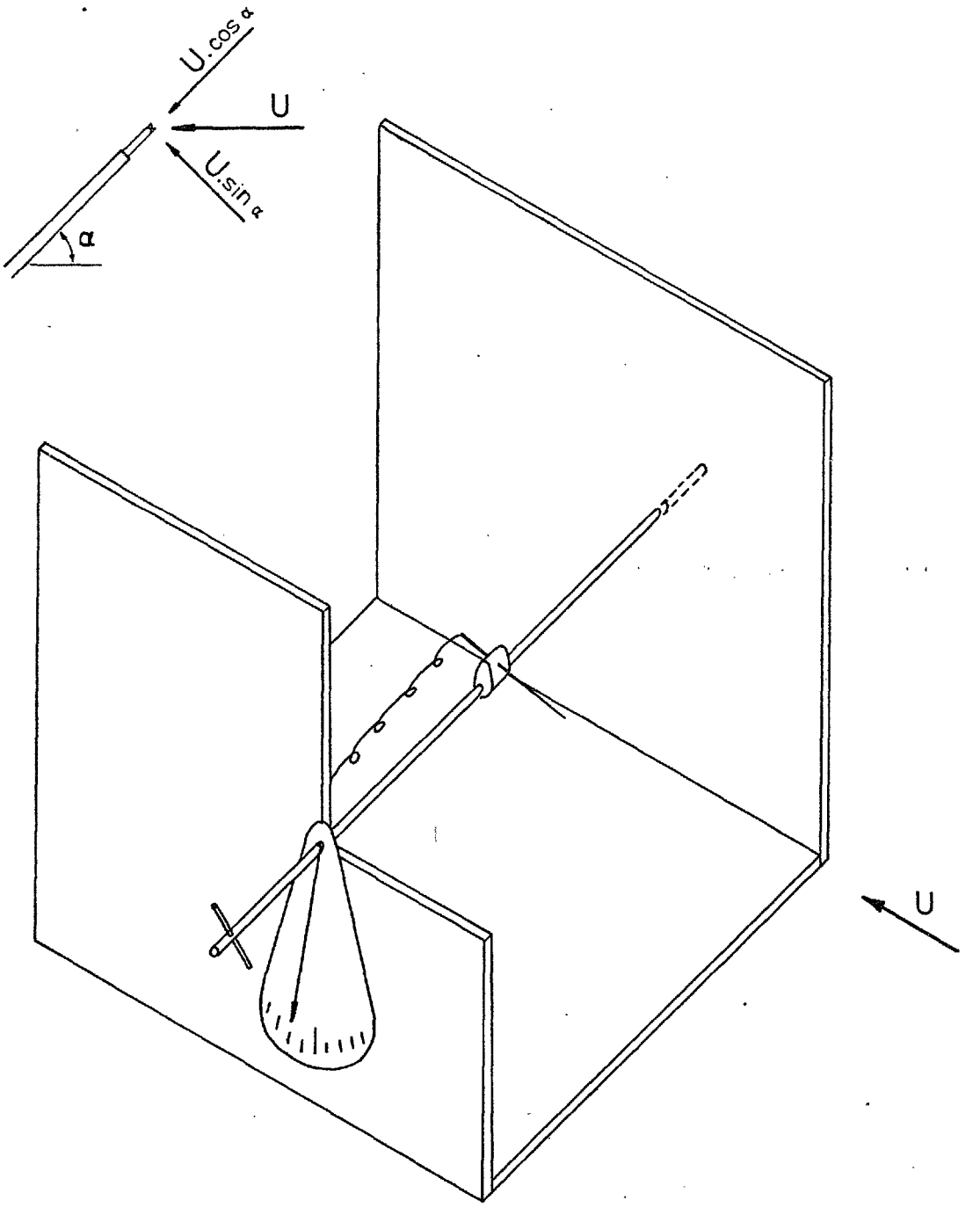
The arrangement for analysing the X-wire output electronically.

Fig. 2.8



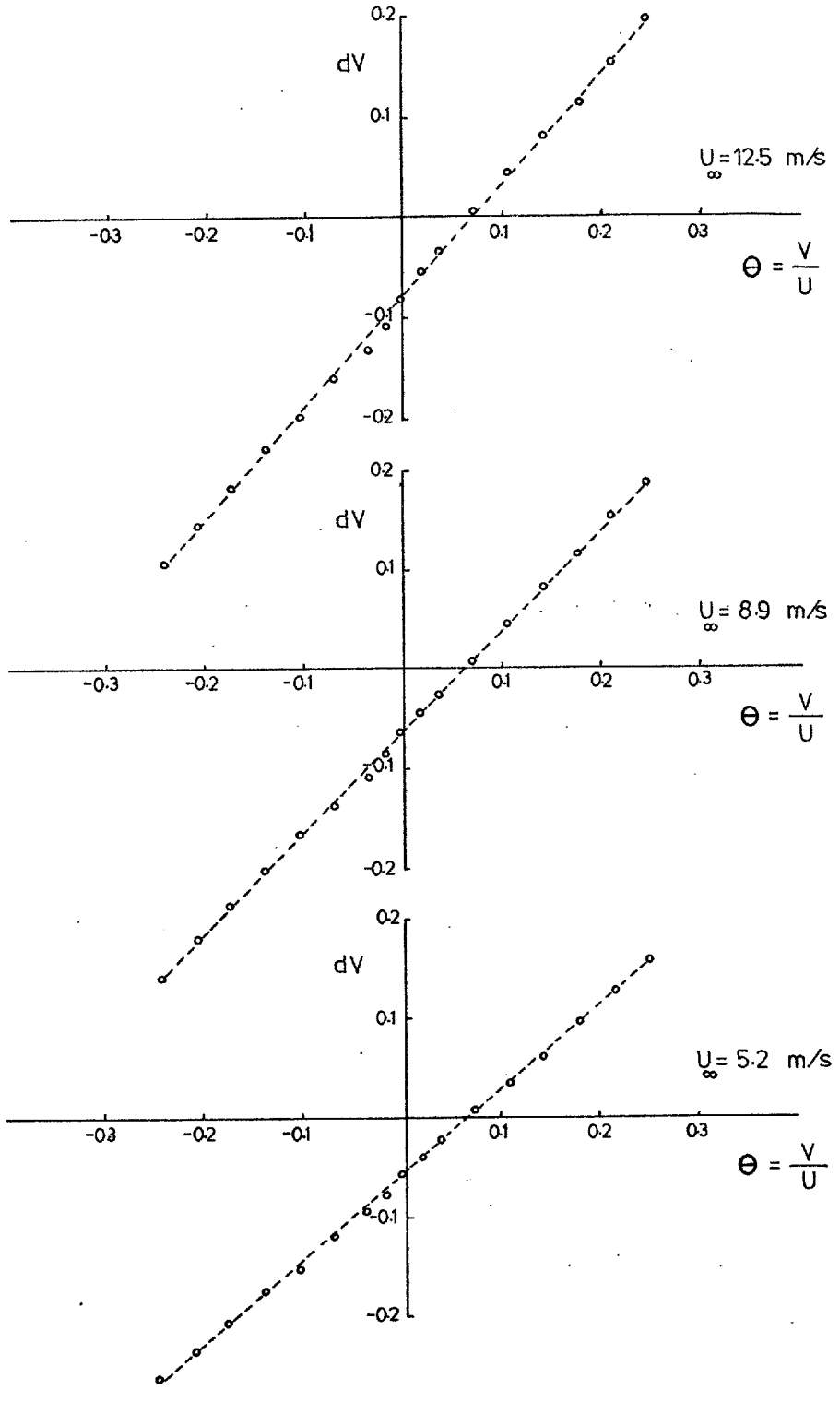
U-wire drift after two hours operation .

Fig. 2.9



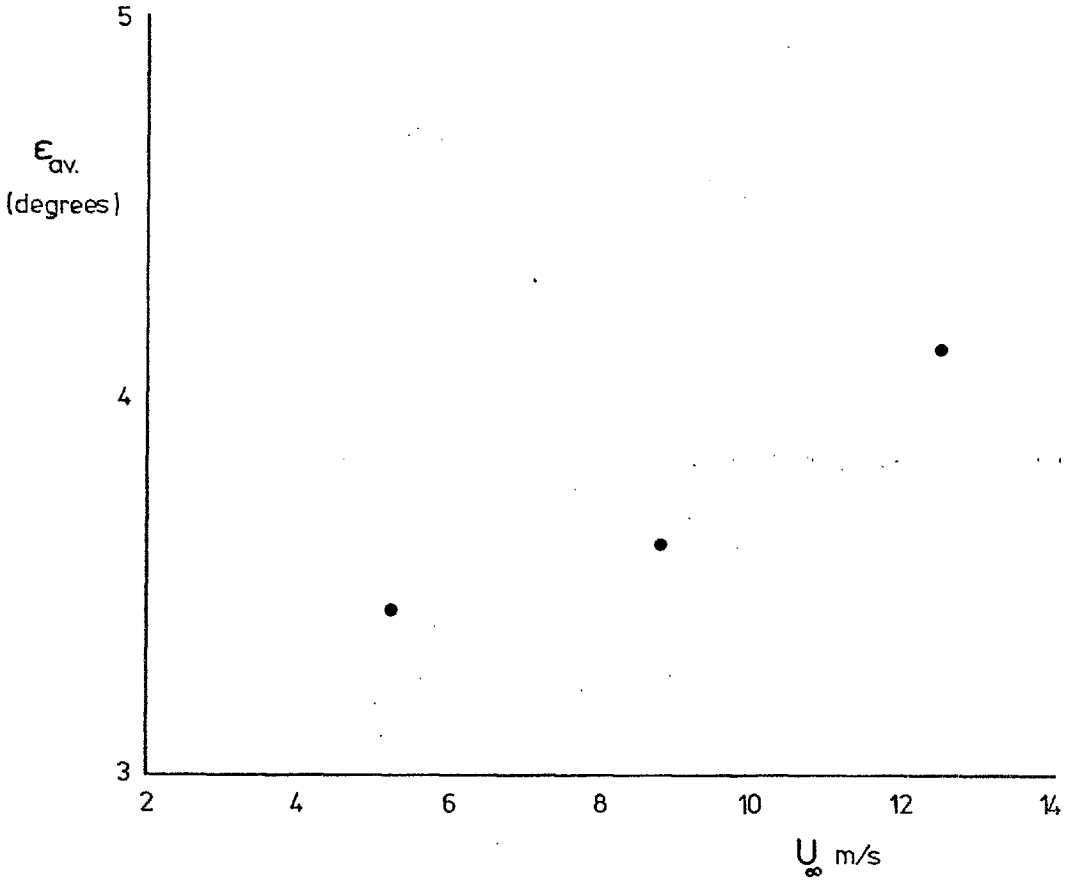
The arrangement for the X-wire yaw calibration

Fig. 2.10



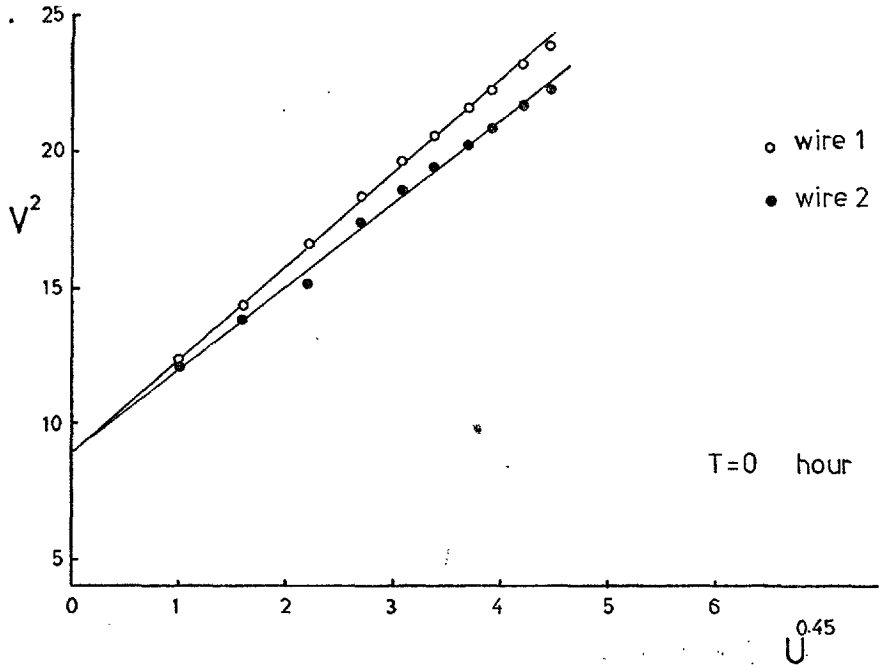
Typical X-wire yaw calibration curves.

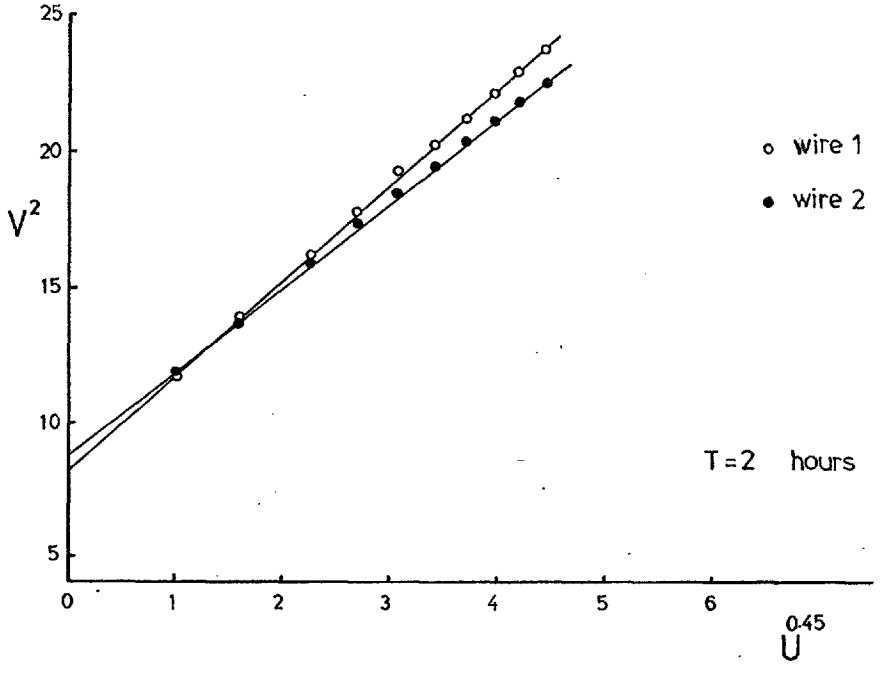
Fig. 2.11



Typical averages of yaw calibration line angles for different speeds.

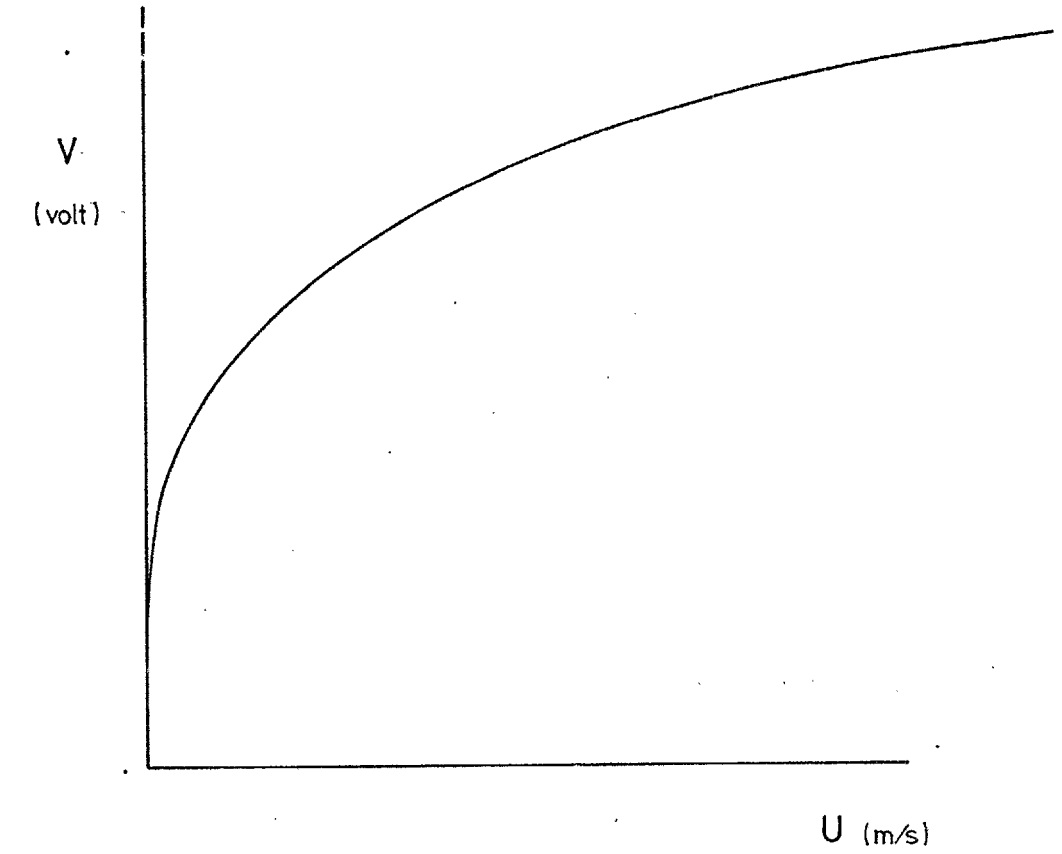
Fig. 2.12

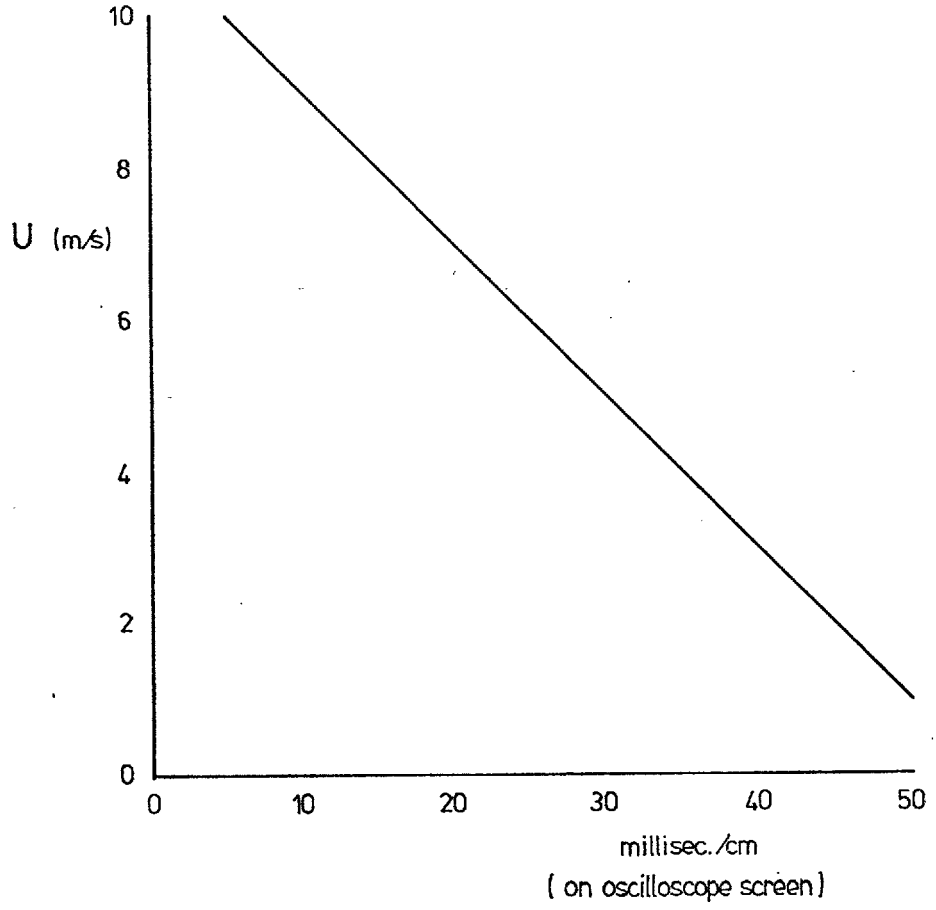




Typical X-wire drift after two hours operation.

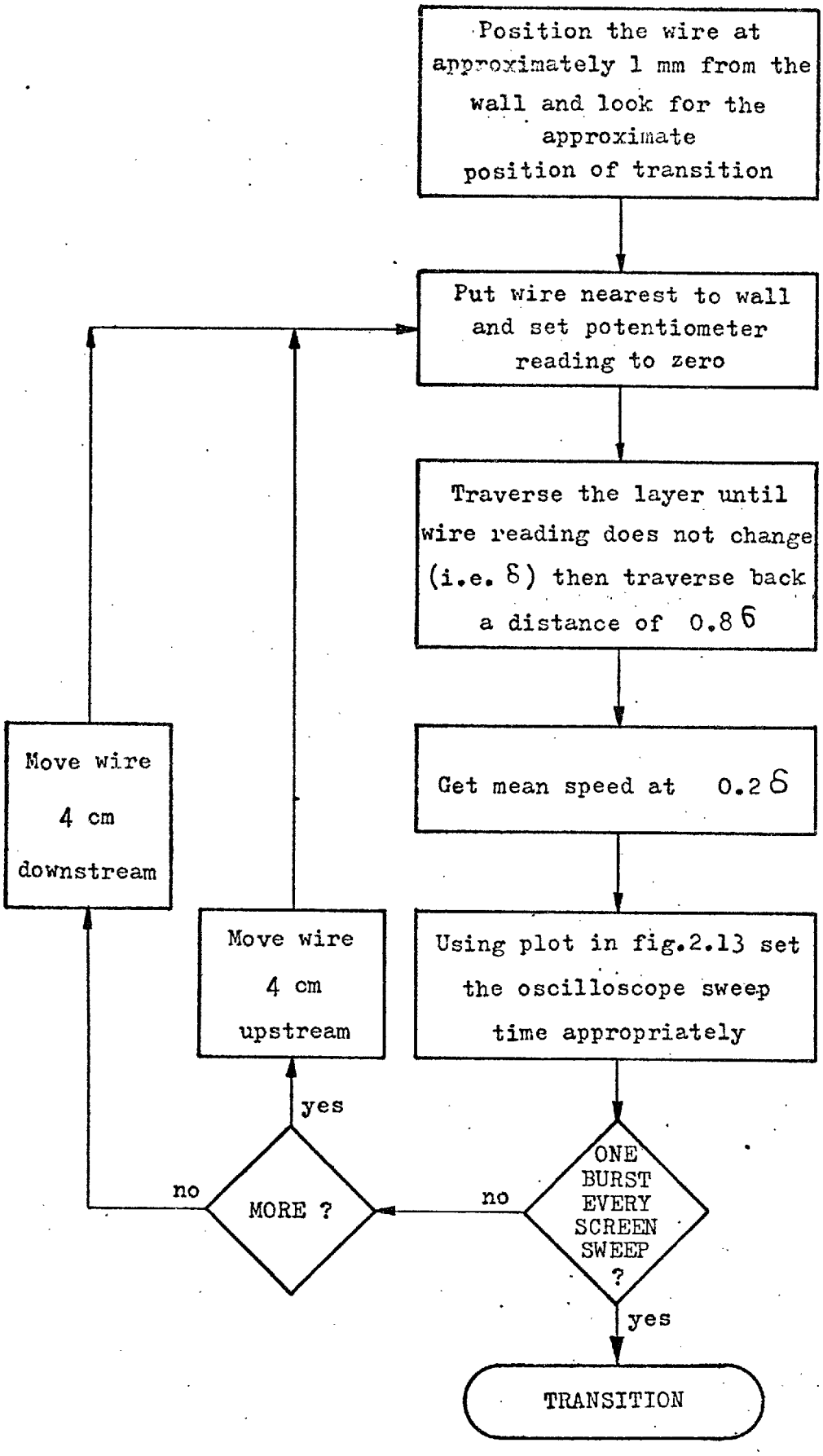
Fig. 2.13



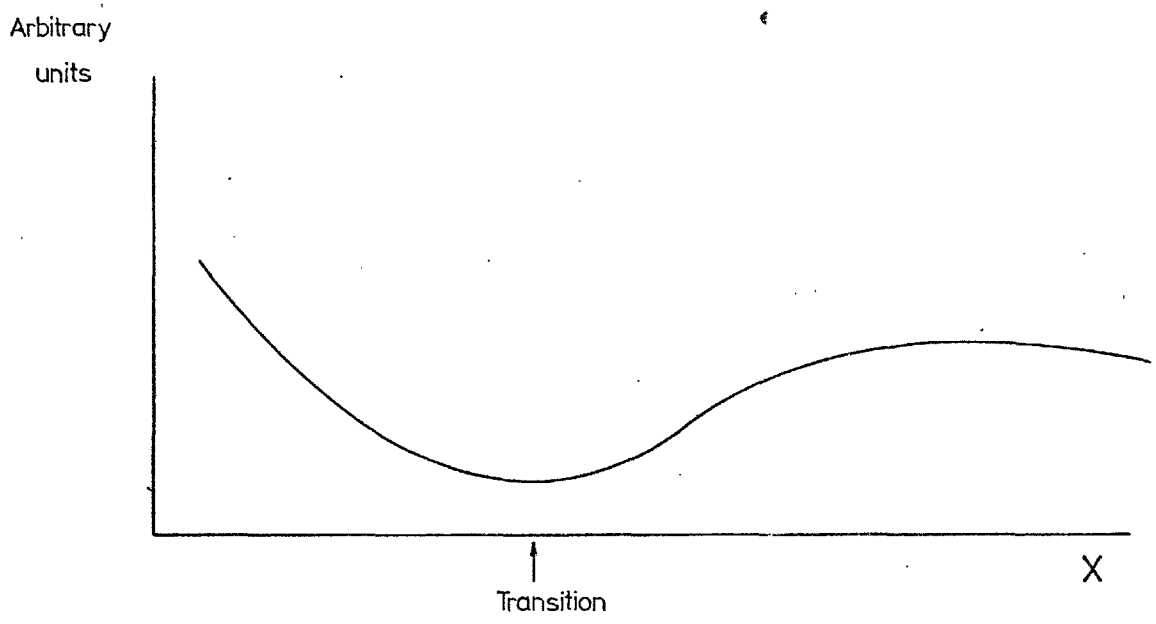


The approximate curves used in detecting transition .

Fig. 2.14

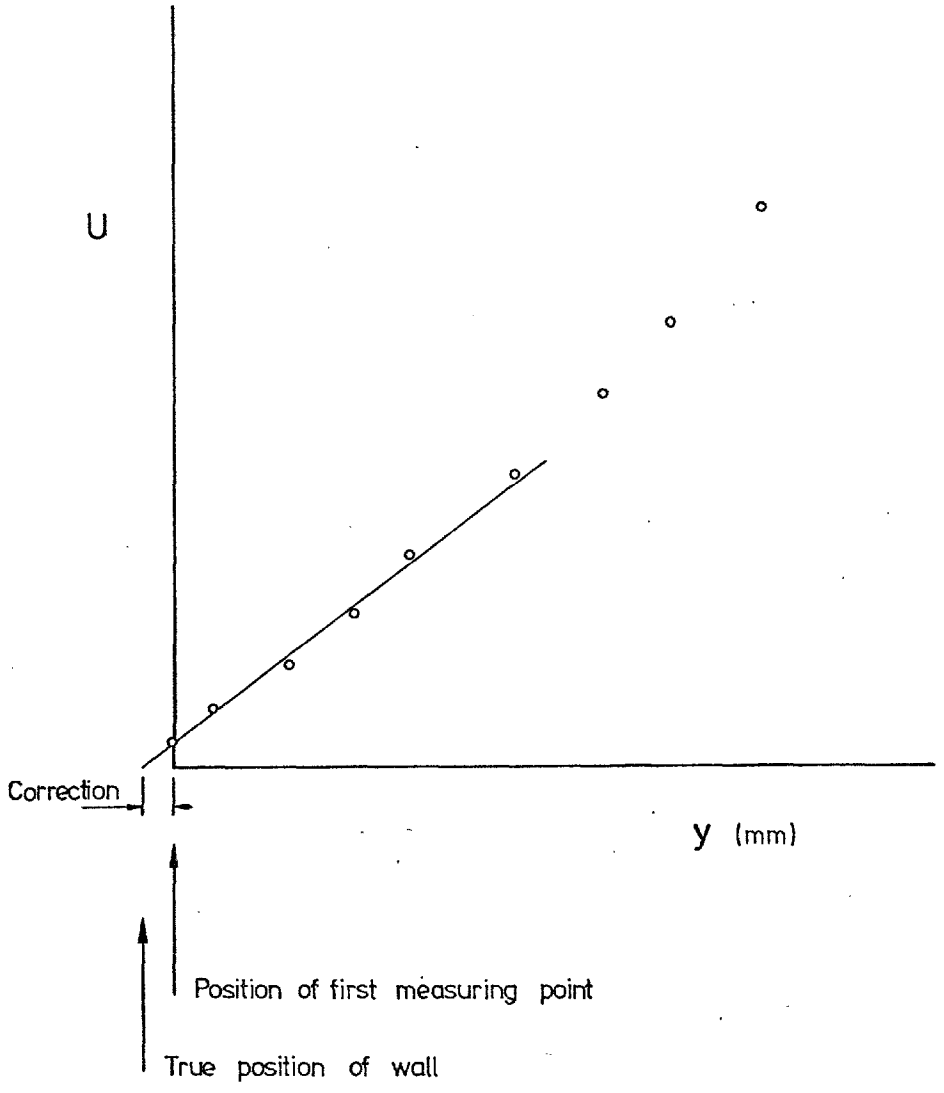


The procedure for detecting transition. Fig. 2.15



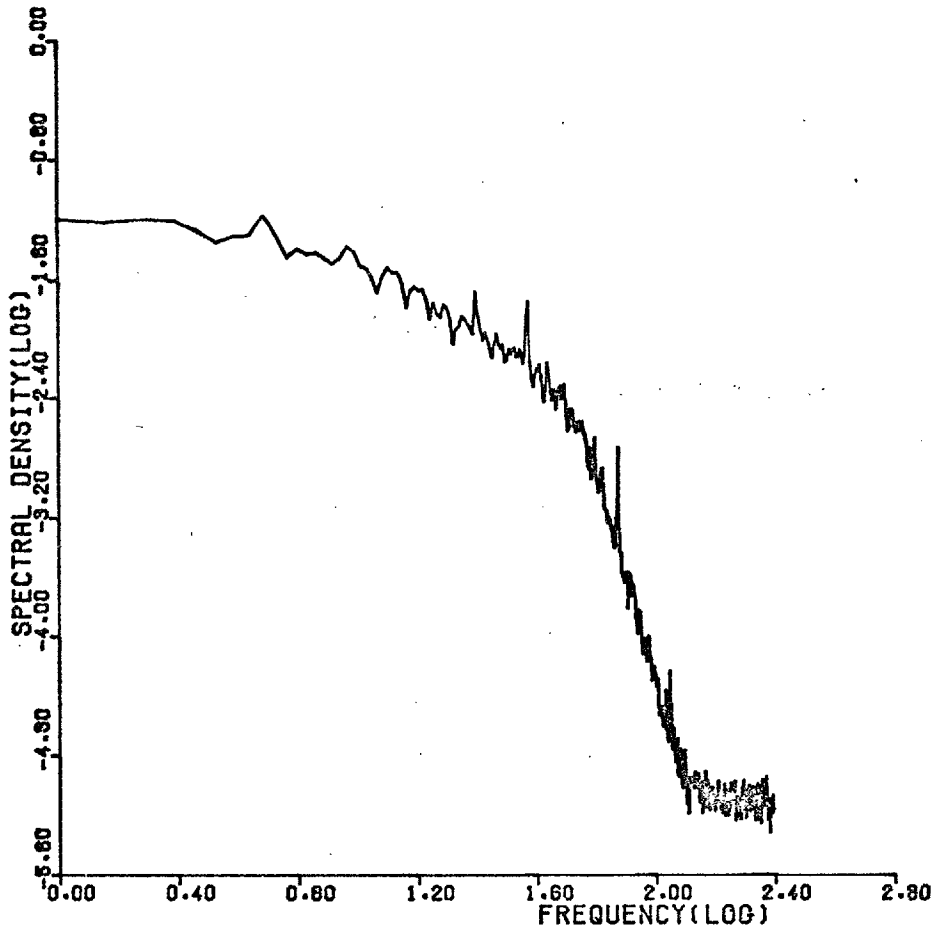
Readings of a pitot tube traversing
the laminar-transitional boundary layer.

Fig. 2.16



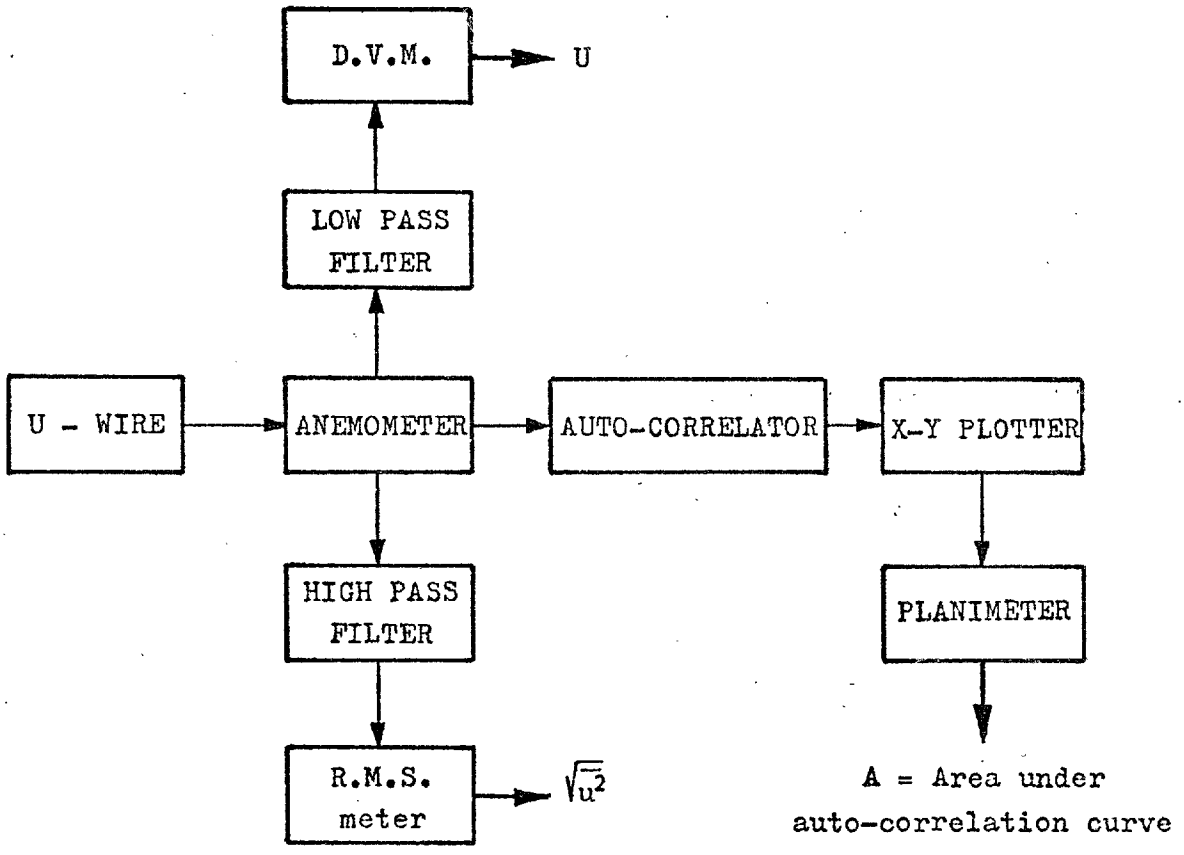
The U-wire height correction.

Fig. 3.1



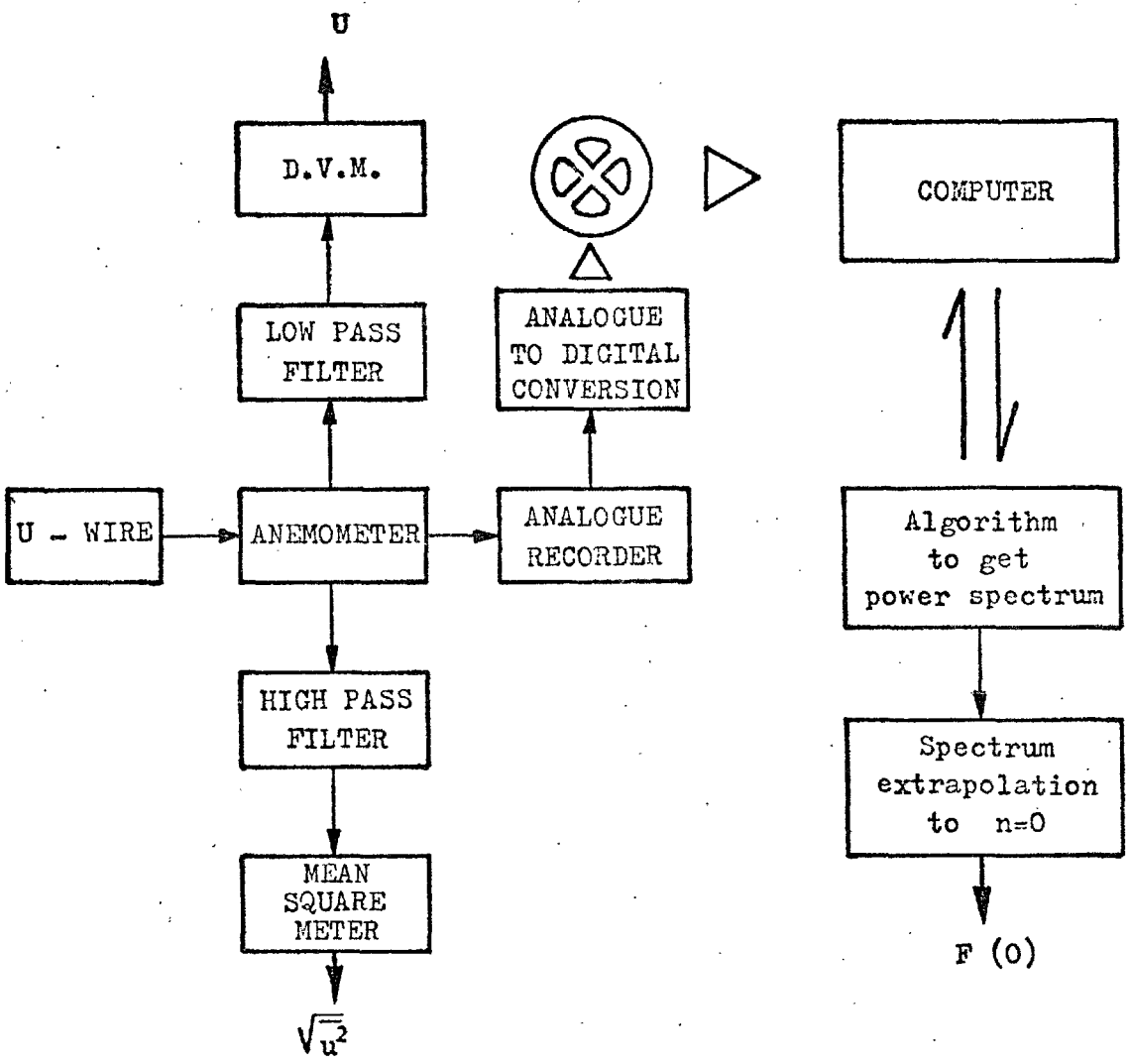
A typical example of determining L_x from F(0).

Fig. 3.2



The arrangement to determine L_x as $\frac{AU}{\overline{u^2}}$

Fig. 3.3



The arrangement to determine L_x as $\frac{F(0)}{4} \cdot \frac{U}{\overline{u^2}}$

Fig. 3.4

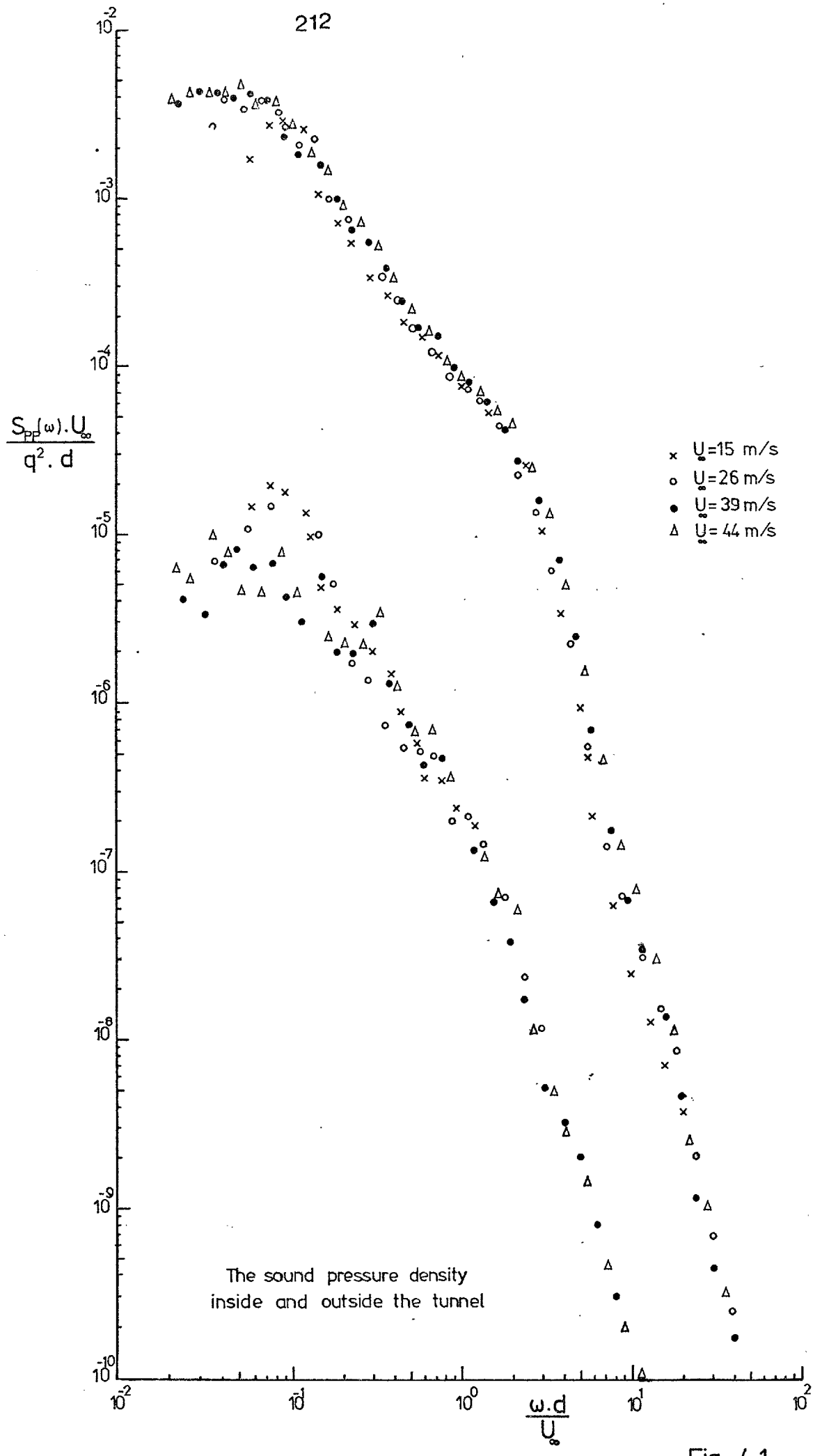

$\frac{S_{pp}(\omega).U_\infty}{q^2.d}$
10^{-2}
10^{-3}
10^{-4}
10^{-5}
10^{-6}
10^{-7}
10^{-8}
10^{-9}
10^{-10}
10^{-2}
10^{-1}
10^{0}
10^{1}
10^{2}
$\frac{\omega.d}{U_\infty}$
× U_∞=15 m/s
○ U_∞=26 m/s
● U_∞=39 m/s
△ U_∞=44 m/s
The sound pressure density
inside and outside the tunnel

Fig. 4.1

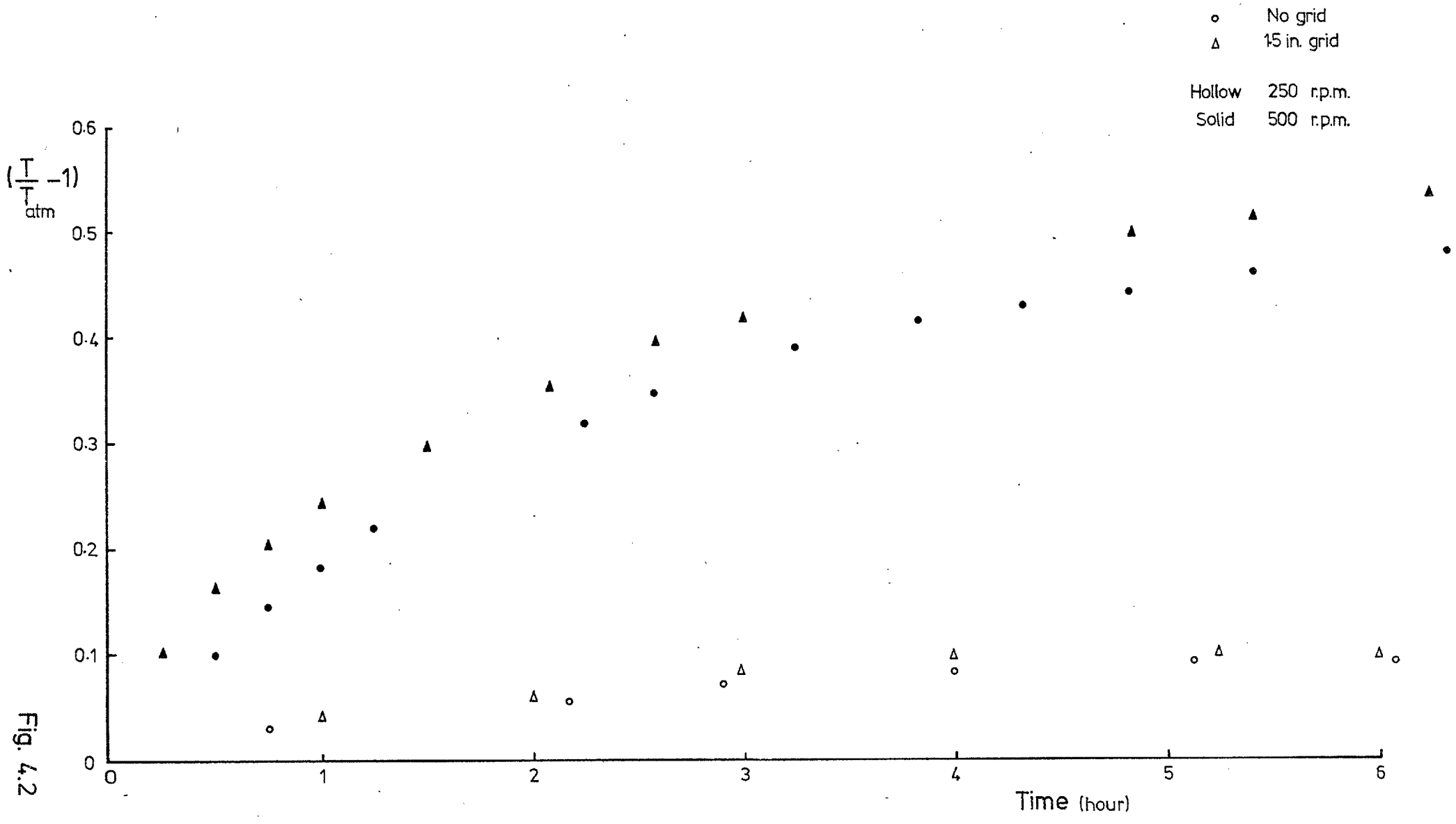
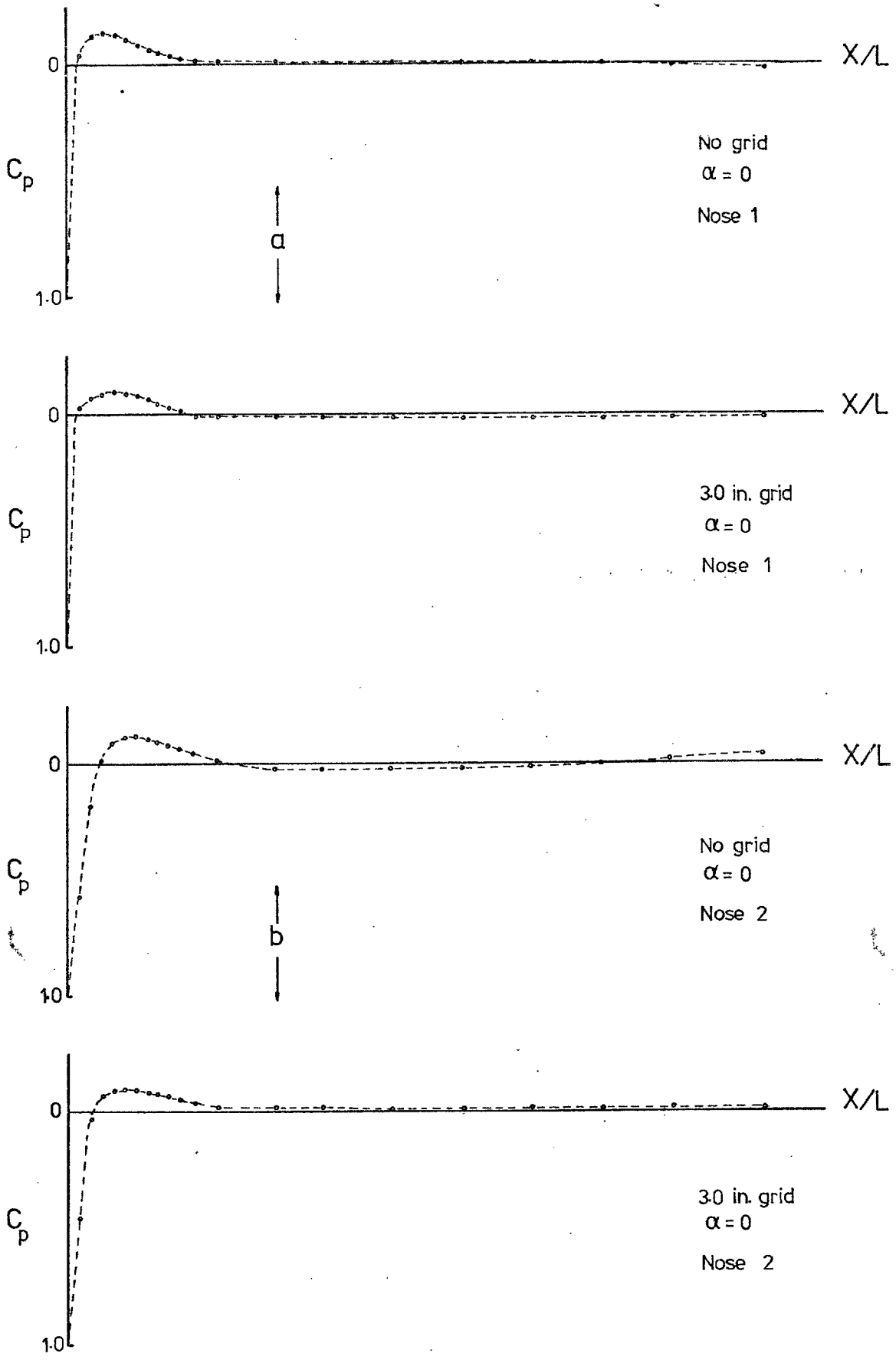


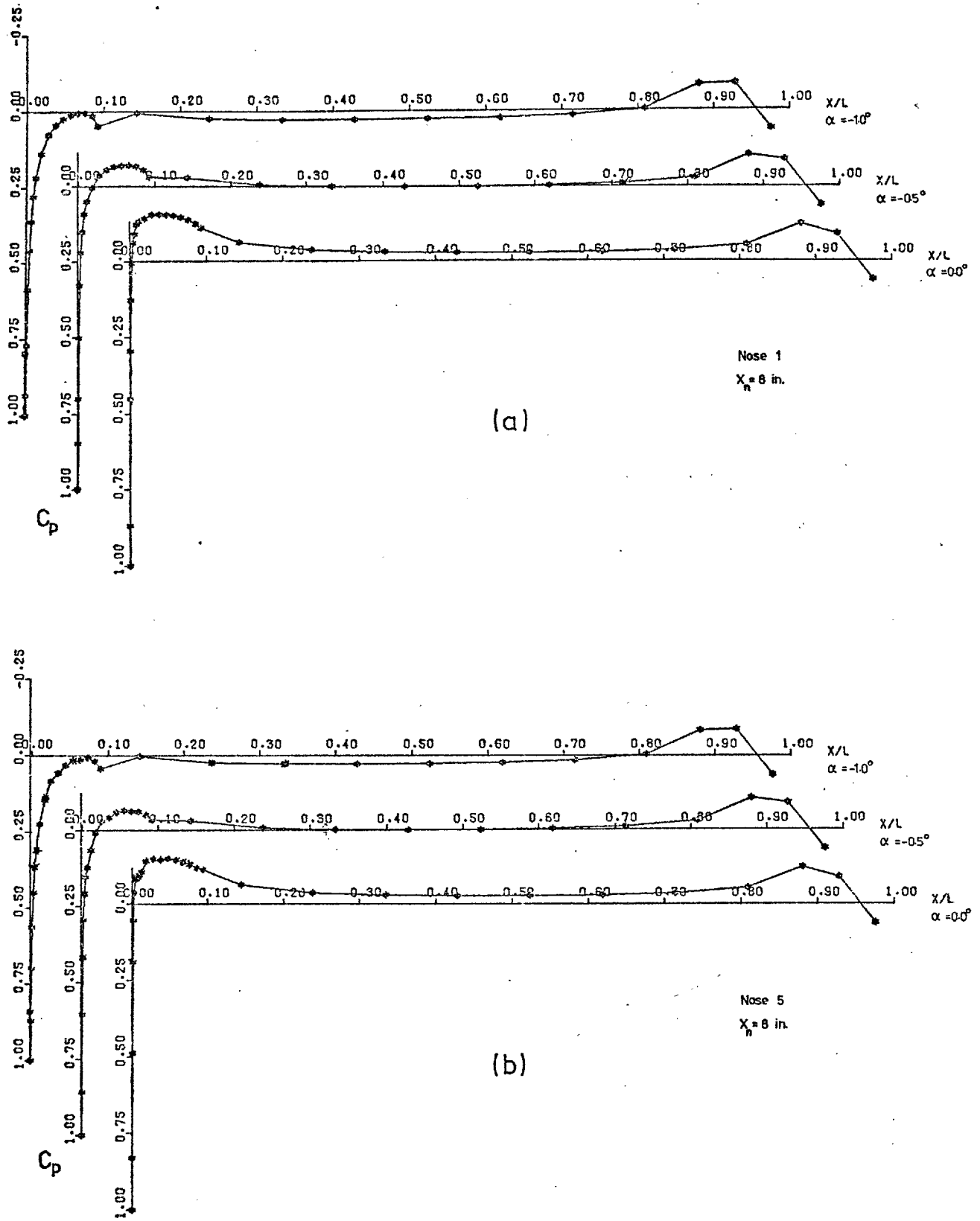
Fig. 4.2

The temperature rise inside the tunnel.



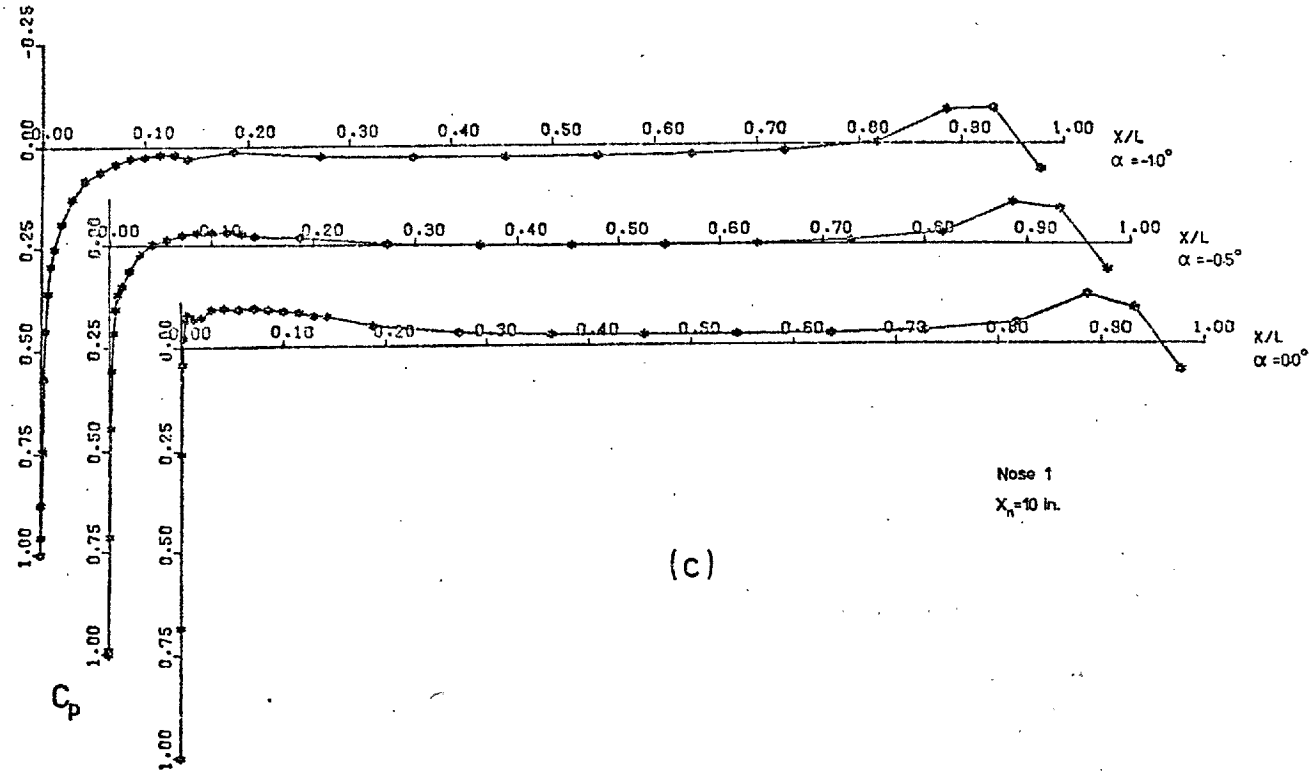
The measured C_p over the plate

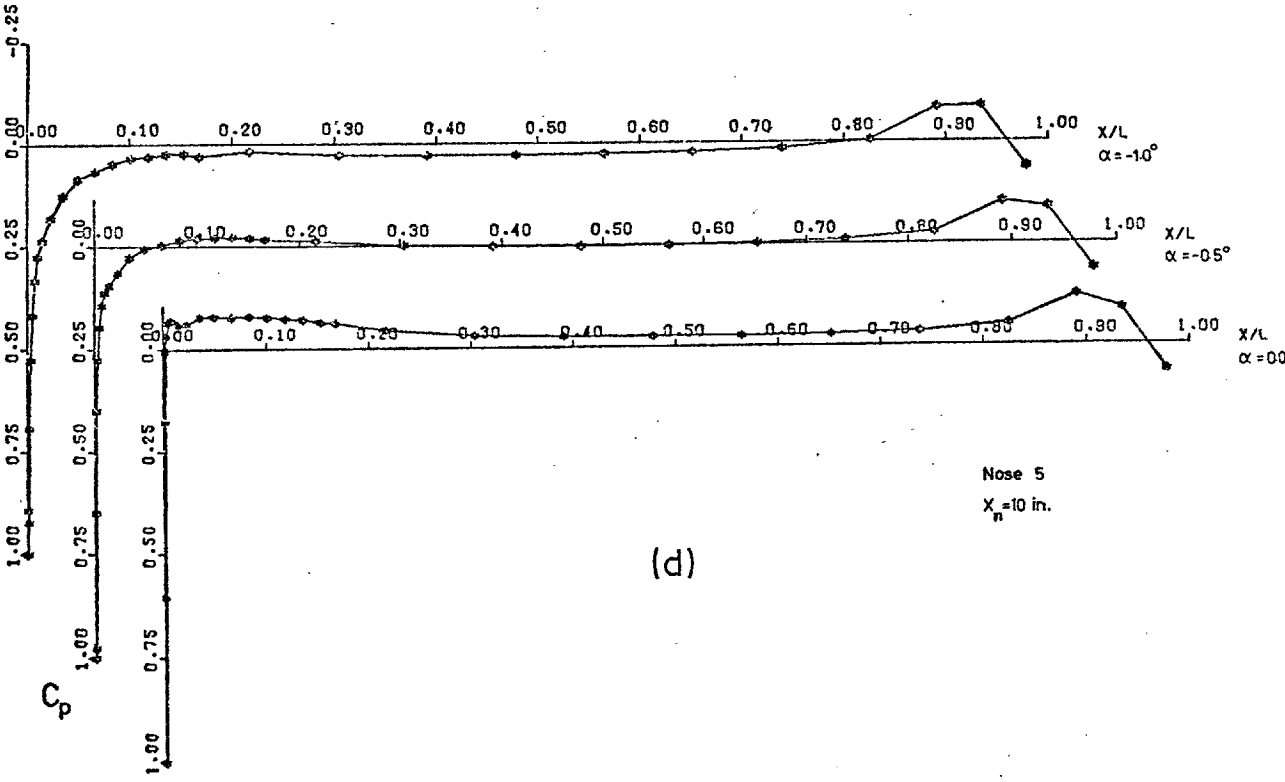
Fig. 4.3



The static pressure distribution over the nose-plate combination using the potential flow theory.

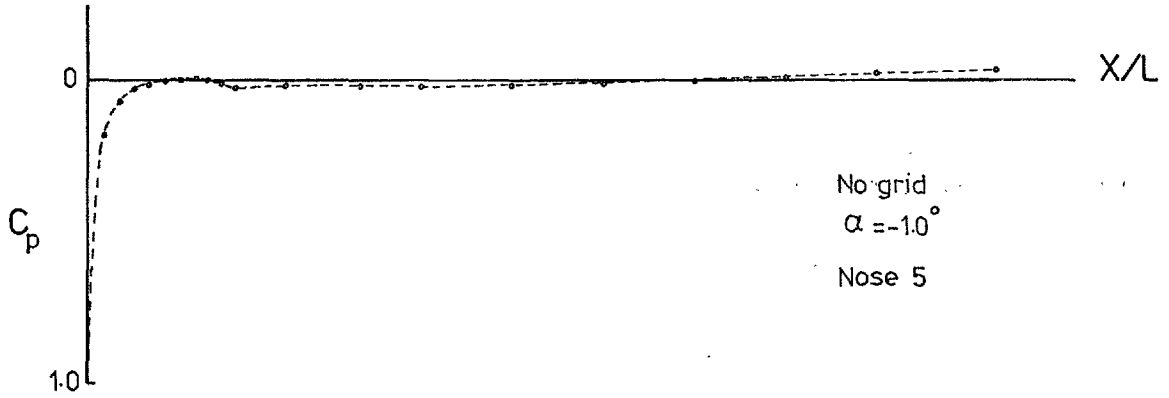
Fig. 4.4





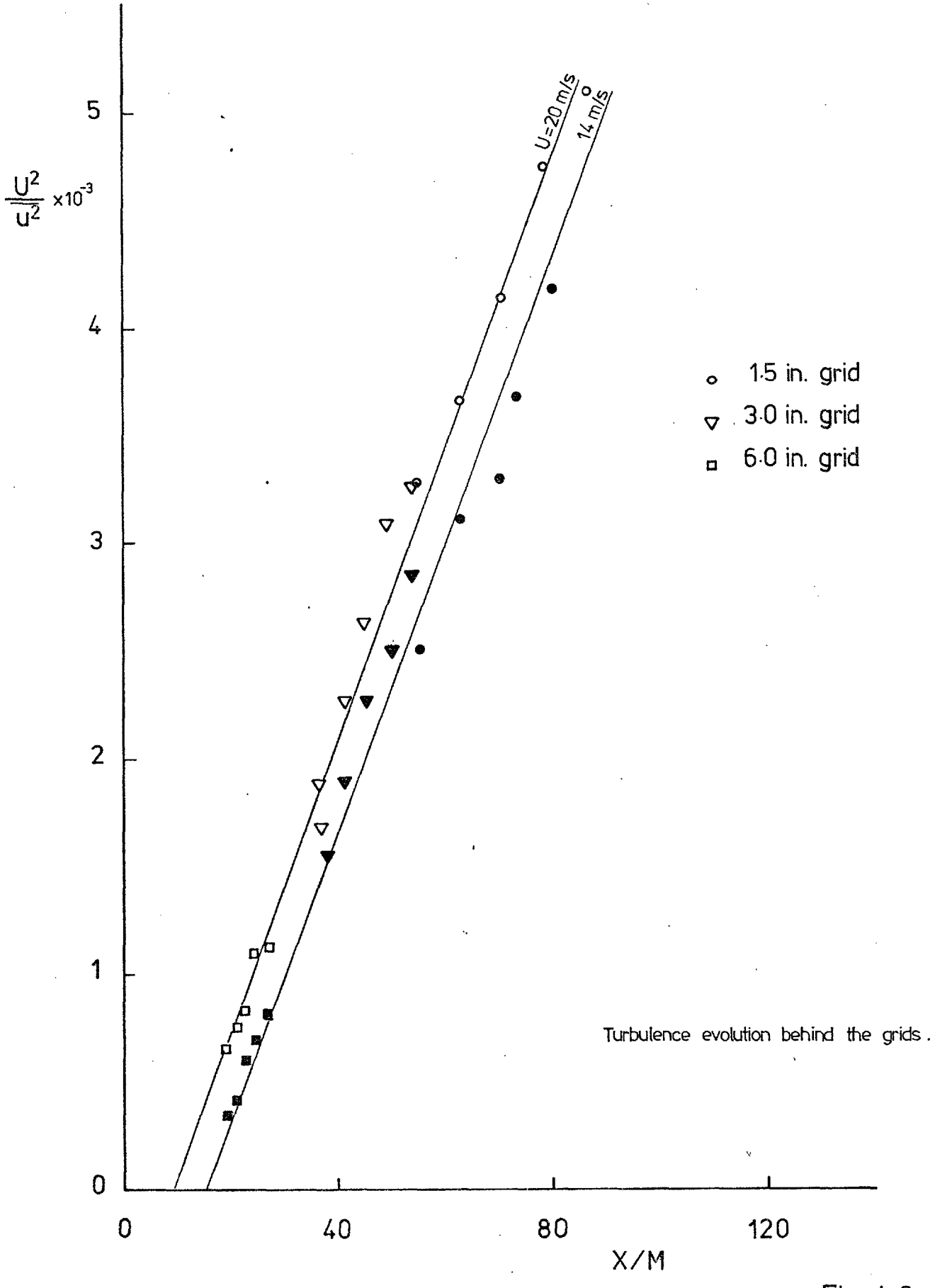
(continued)

Fig. 4.4



The measured C_p over the plate

Fig. 4.5



Turbulence evolution behind the grids.

Fig. 4.6

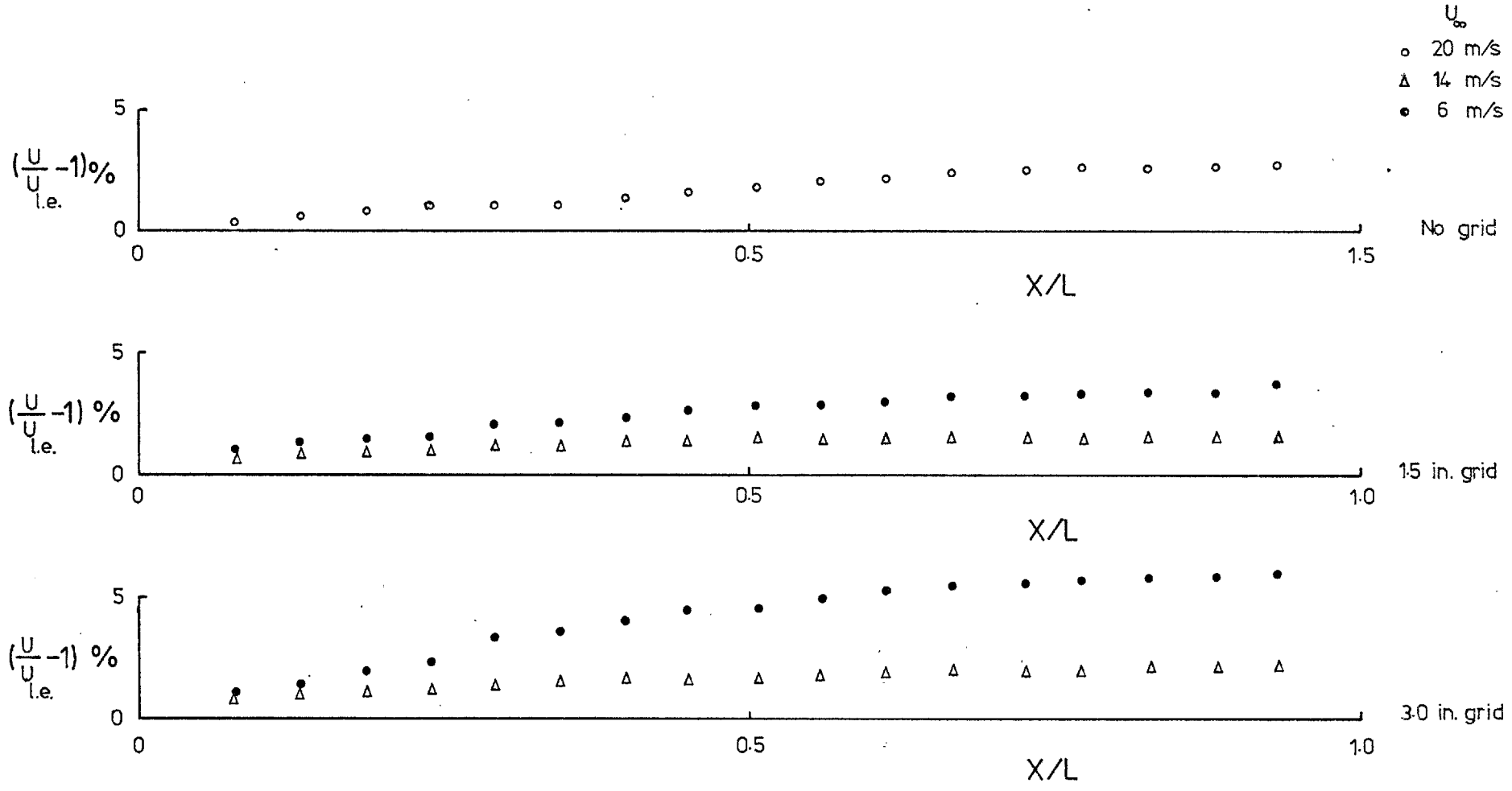
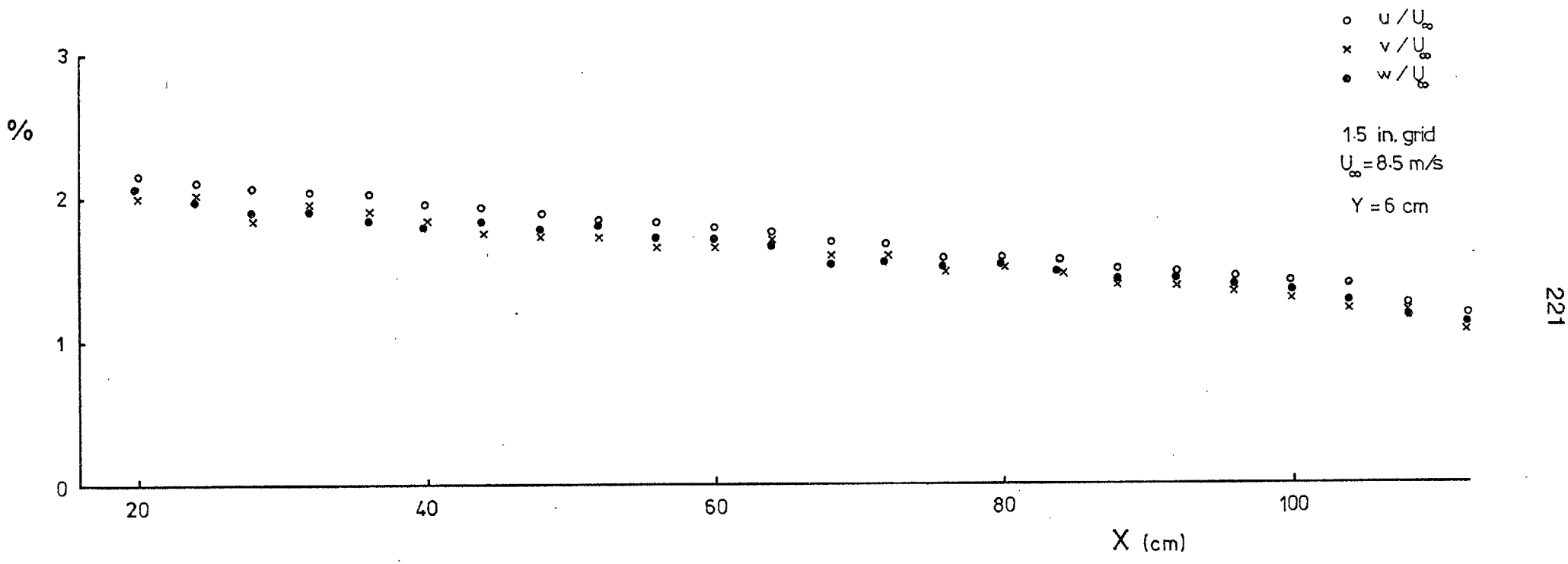


Fig. 4.7 The change in U_∞ along the plate.

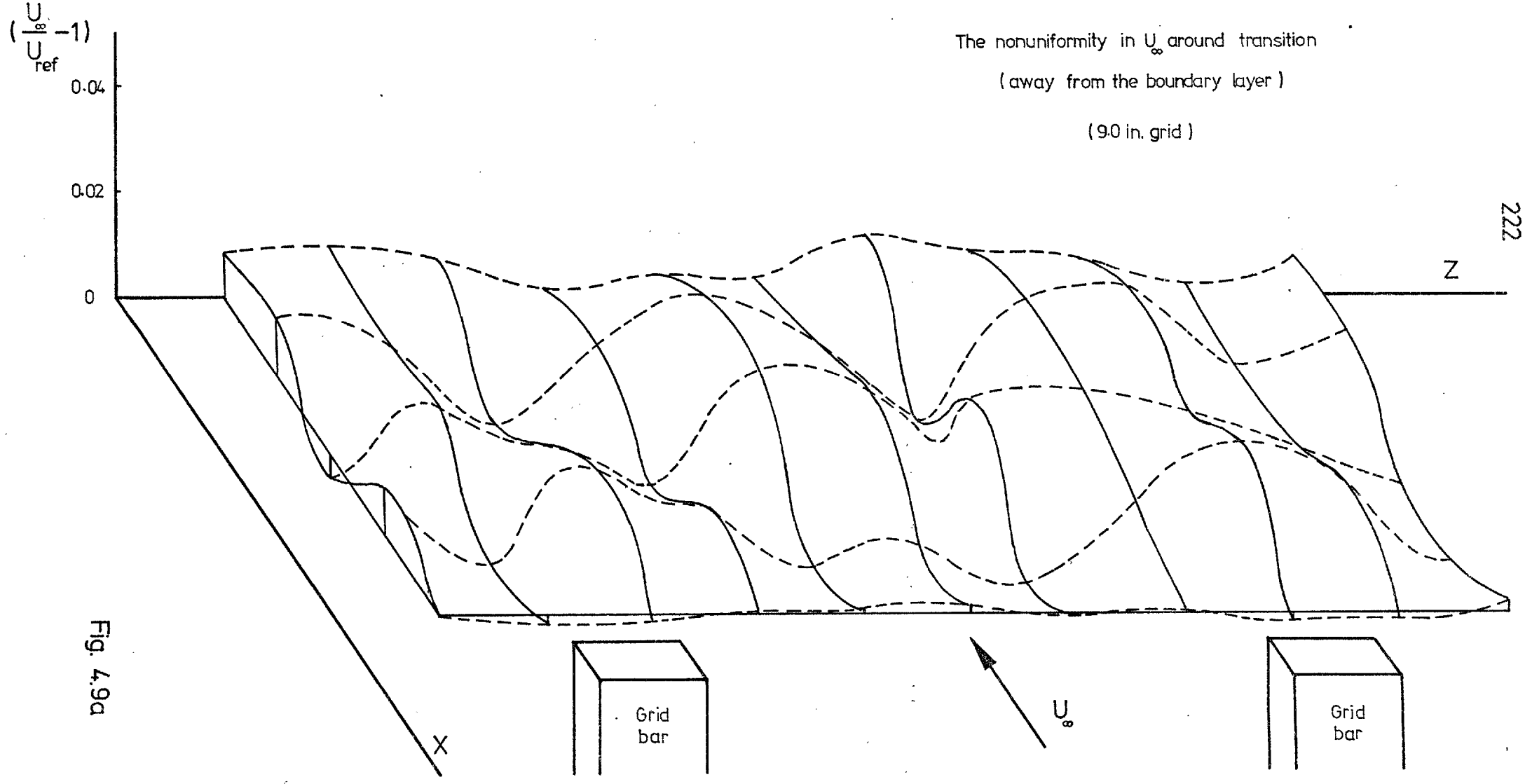
The change in $\frac{\sqrt{u^2}}{U}$ along the plate.

Fig. 4.8a



The turbulent velocity components along the plate.

Fig. 4.8b



The nonuniformity in U_∞ around transition

(away from the boundary layer)

(9.0 in. grid)

222

Fig. 4.9a

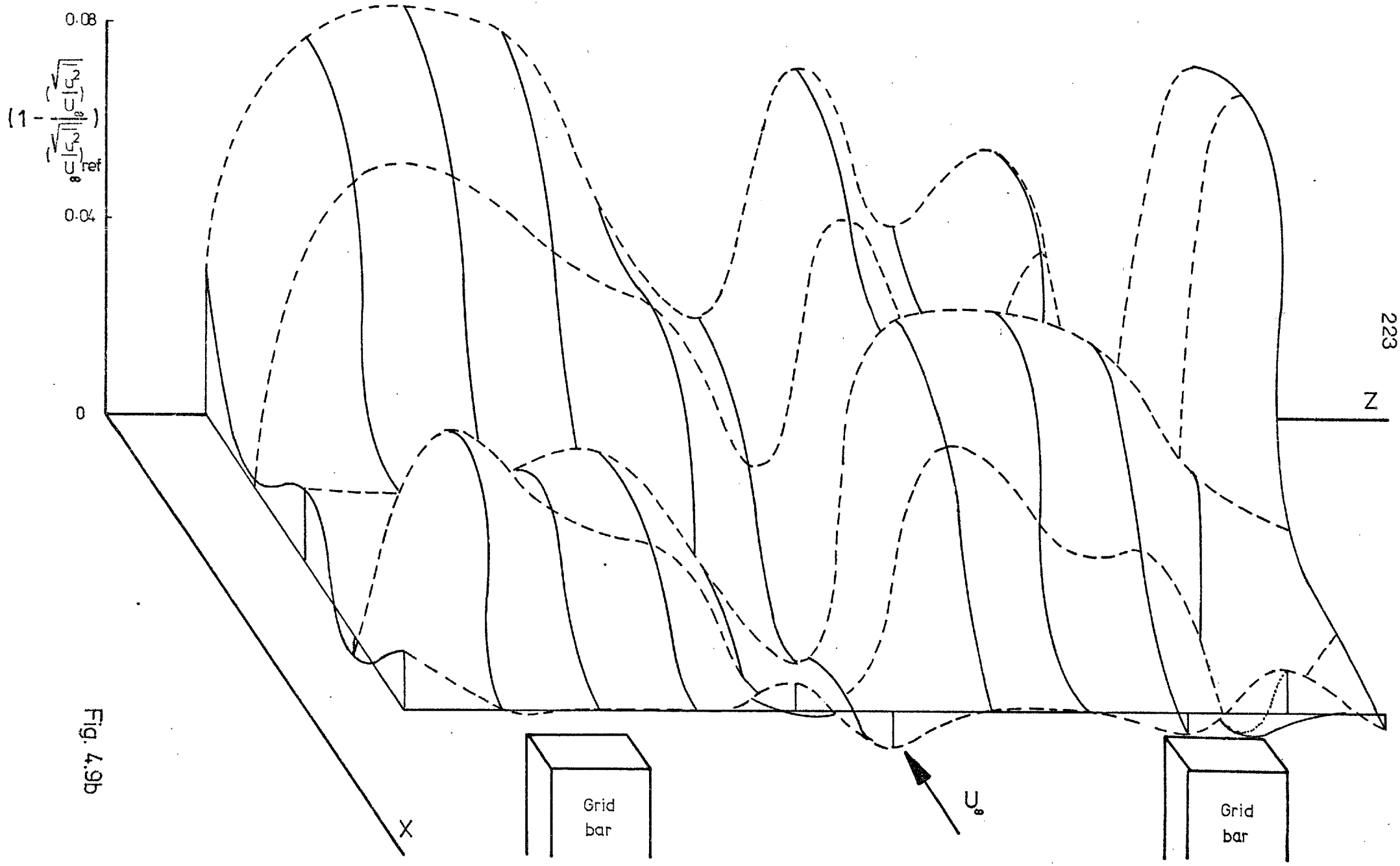


Fig. 4.9b

The nonunformity of turbulence around transition away from the boundary layer (9.0 in. grid).

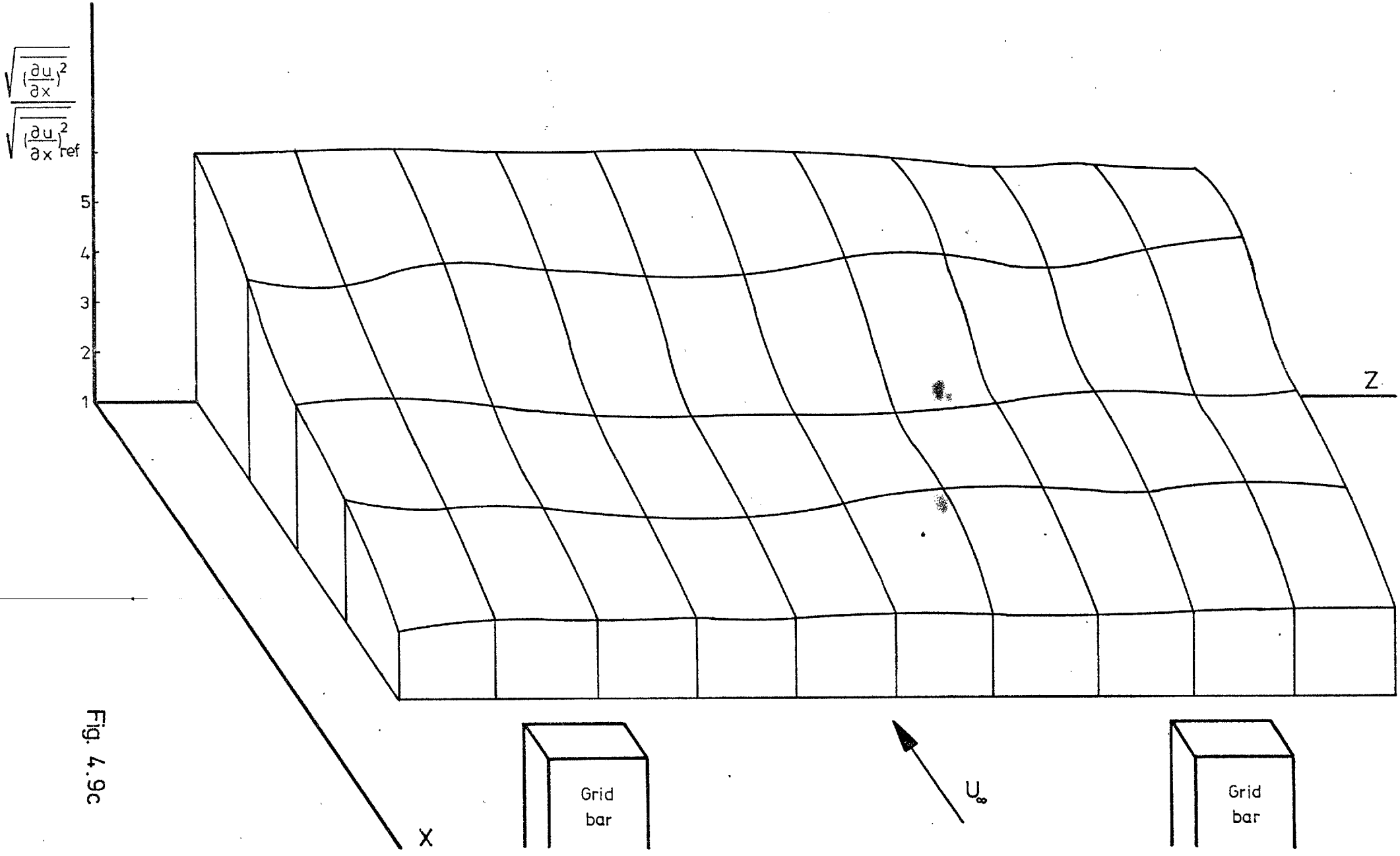
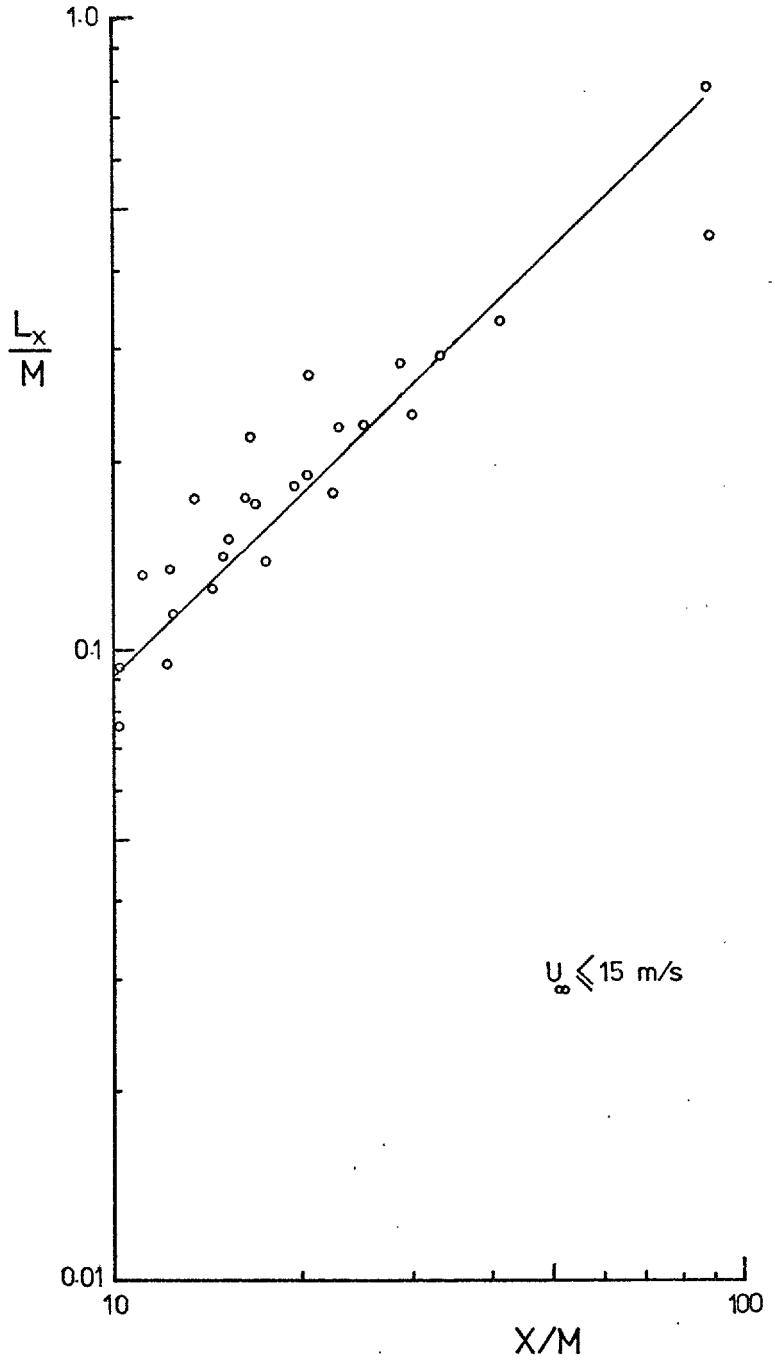


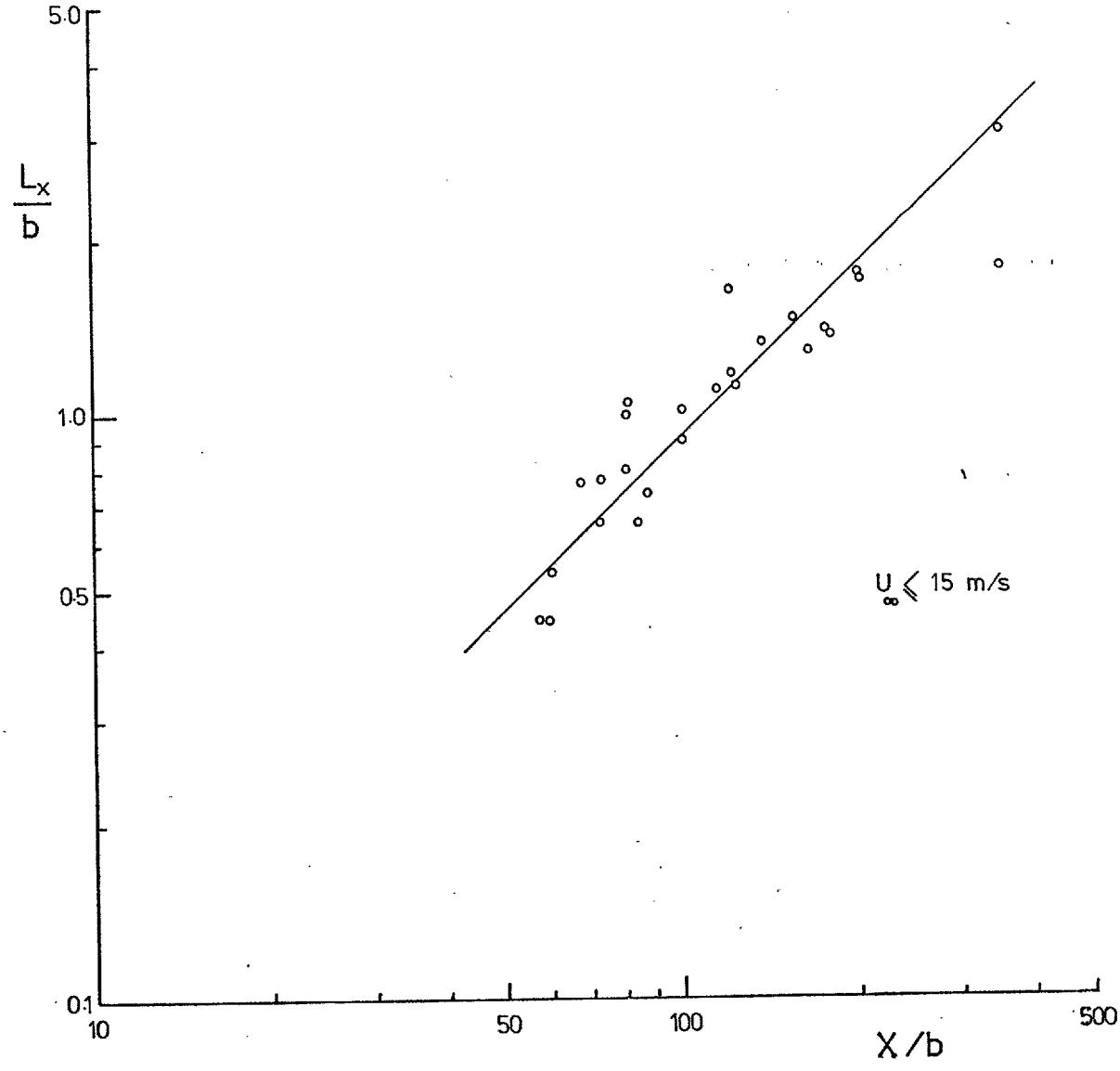
Fig. 4.9c

The nonuniformity of turbulence inside the boundary layer around transition . (9.0 in. grid).



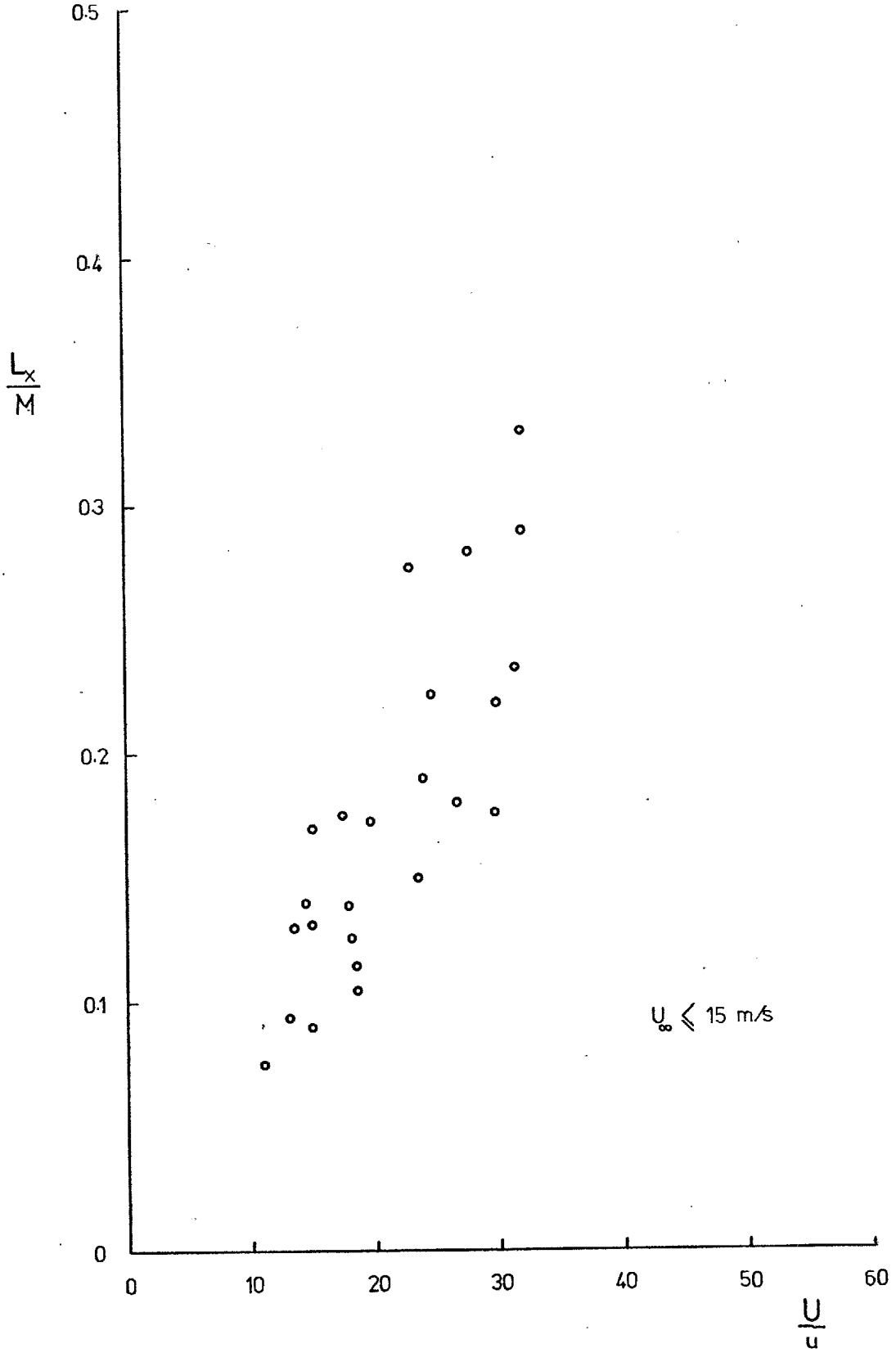
The turbulence length scale behind the grids.

Fig. 4.10



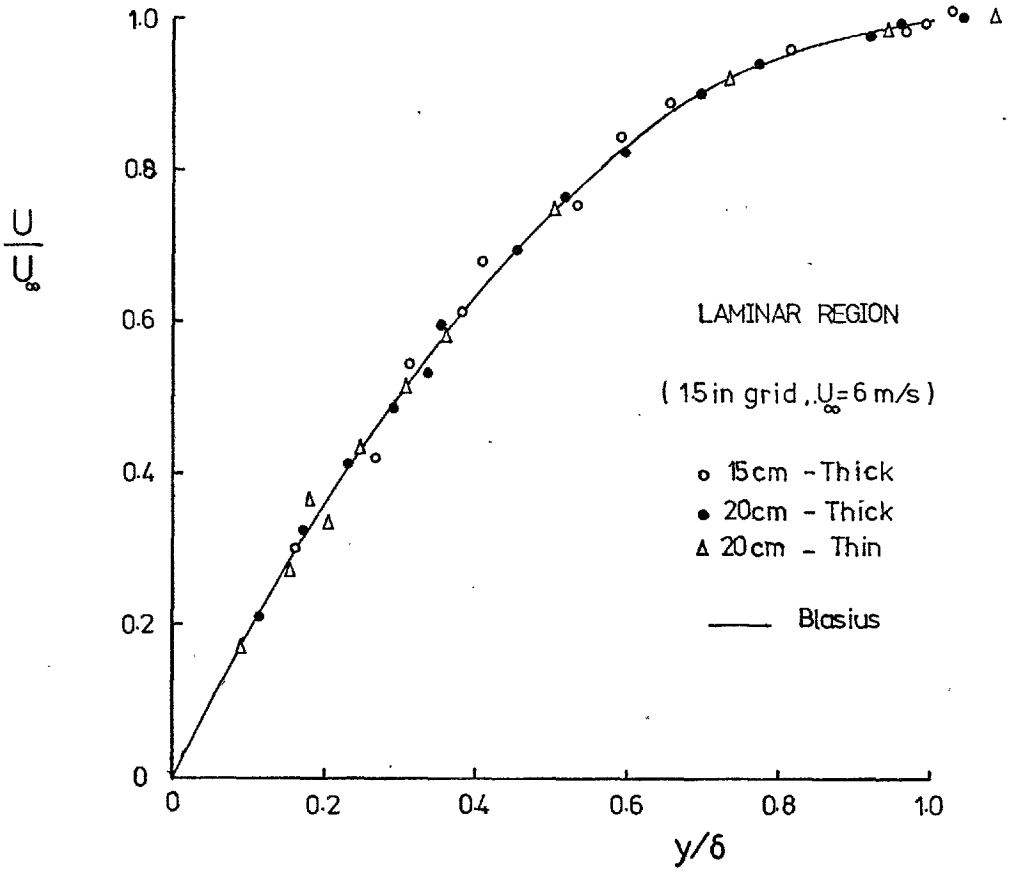
The turbulence length scale behind the grids.

Fig. 4.11



The turbulence length scale behind the grids .

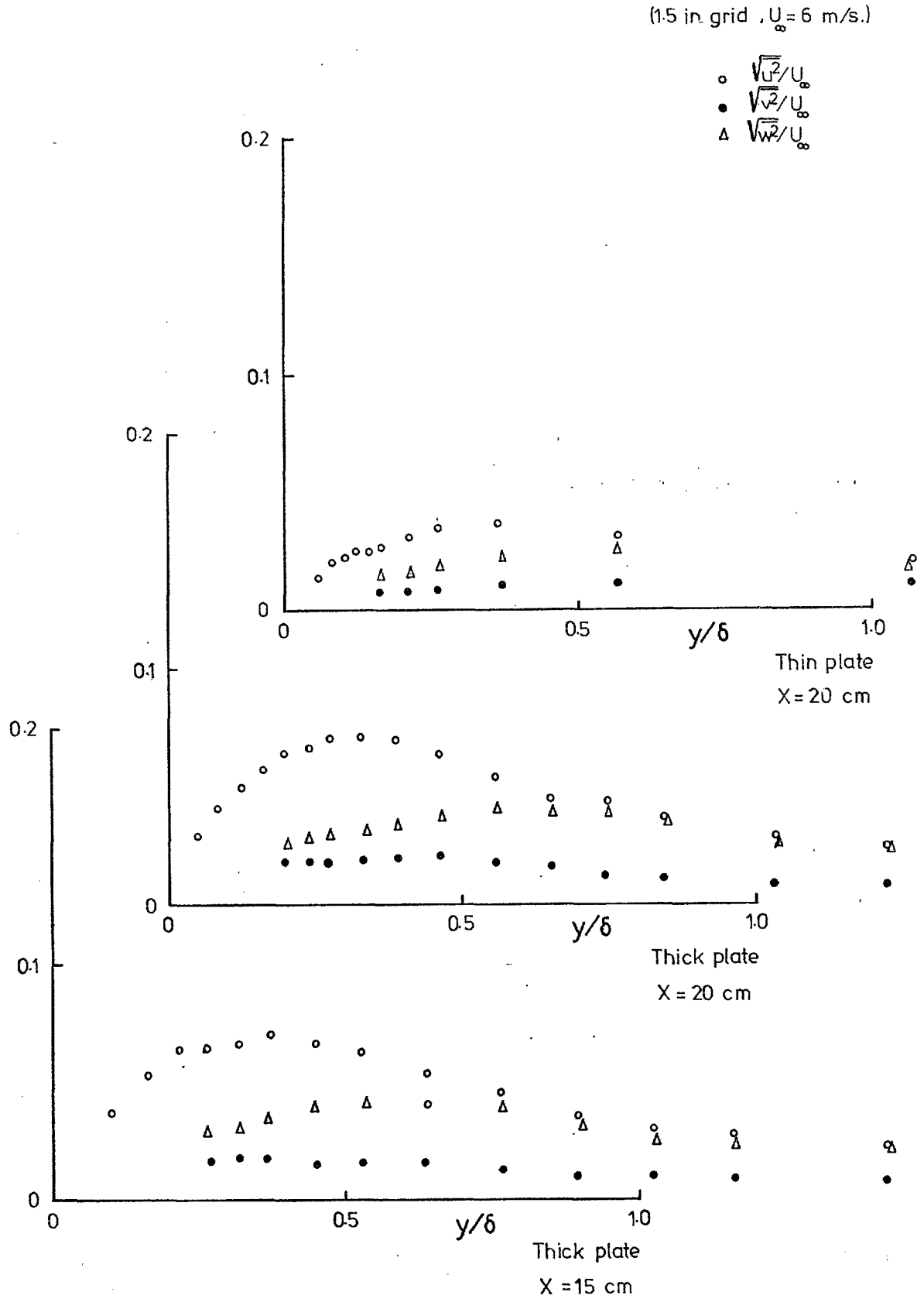
Fig. 4.12



U-profiles in the laminar region over the two plates.

(noses 1 & 2)

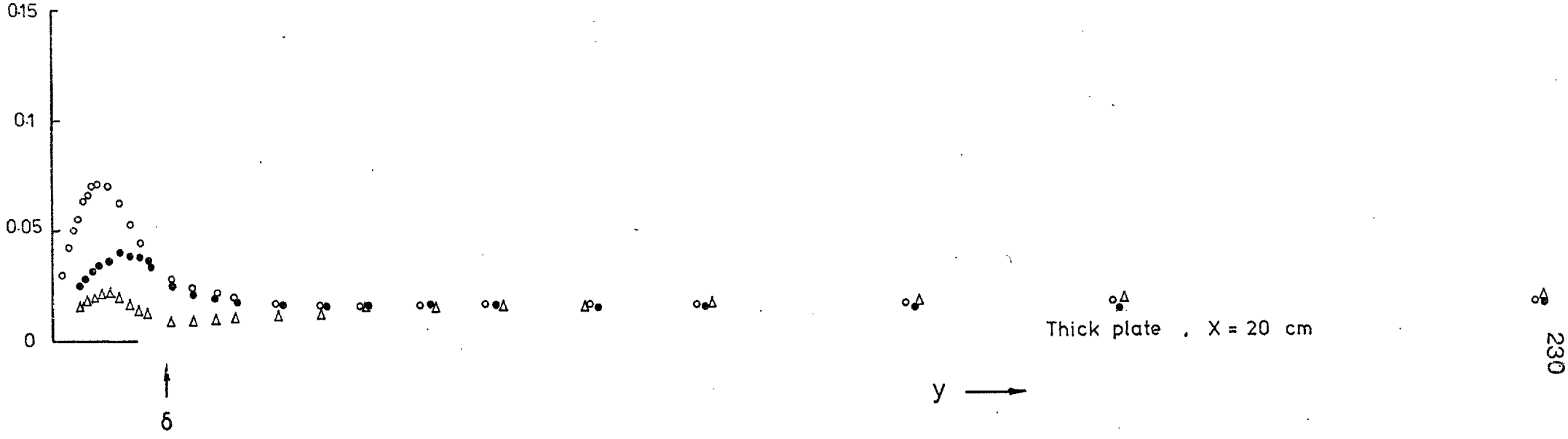
Fig. 4.13



$\sqrt{u^2}$, $\sqrt{v^2}$ & $\sqrt{w^2}$ profiles in the laminar region over the two plates.

(noses 1&2)

Fig. 4.14



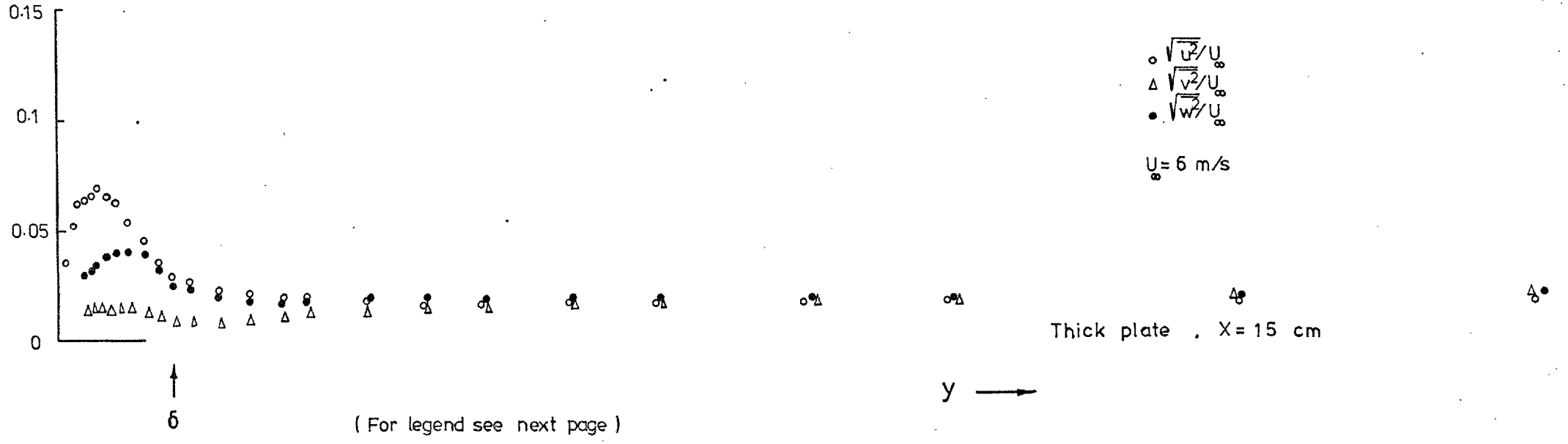


Fig. 4.15

(For legend see next page)

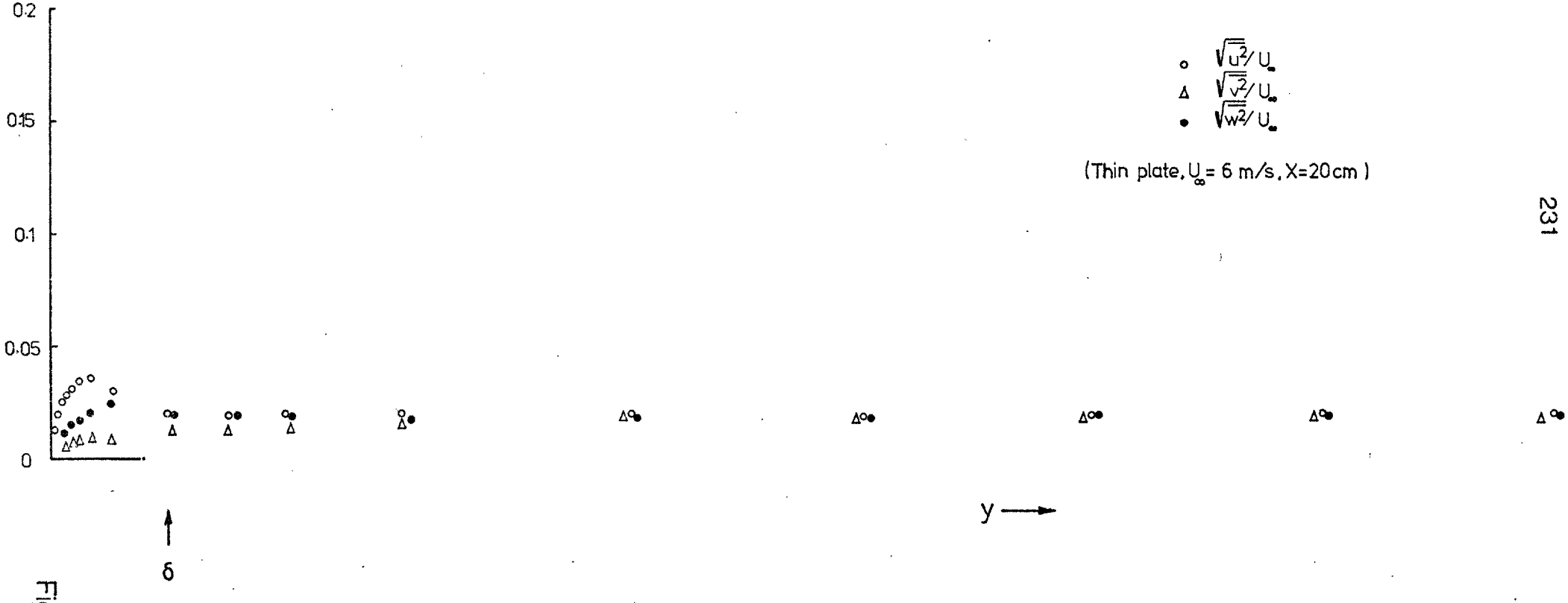


Fig. 4.15 (cont.)

$\sqrt{\overline{u^2}}$, $\sqrt{\overline{v^2}}$ & $\sqrt{\overline{w^2}}$ profiles over the two plates within the laminar region

(noses 1 & 2)

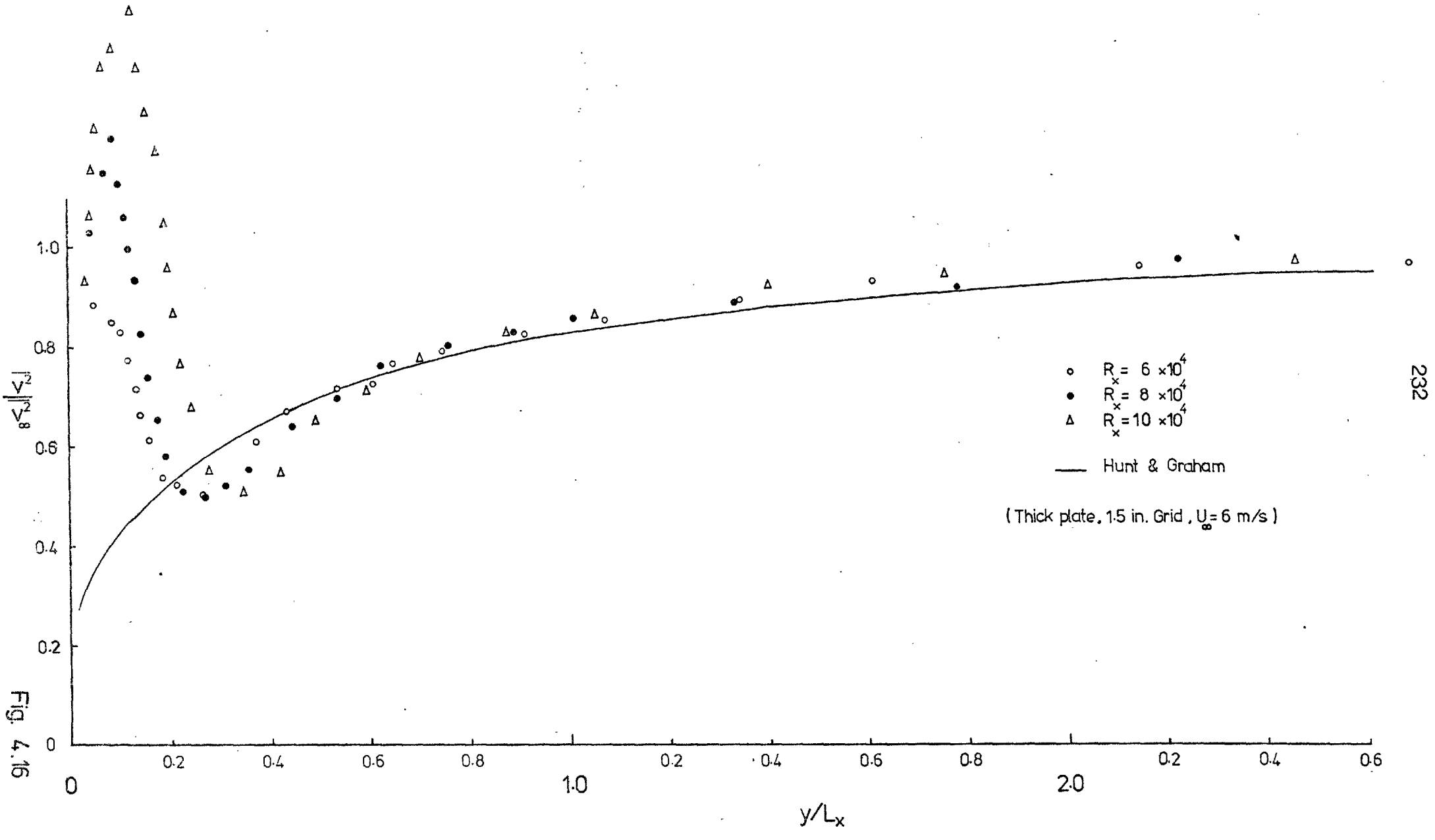


Fig. 4.16

Theoretical and experimental $\overline{v^2}$ profiles over the plate (nose 2).

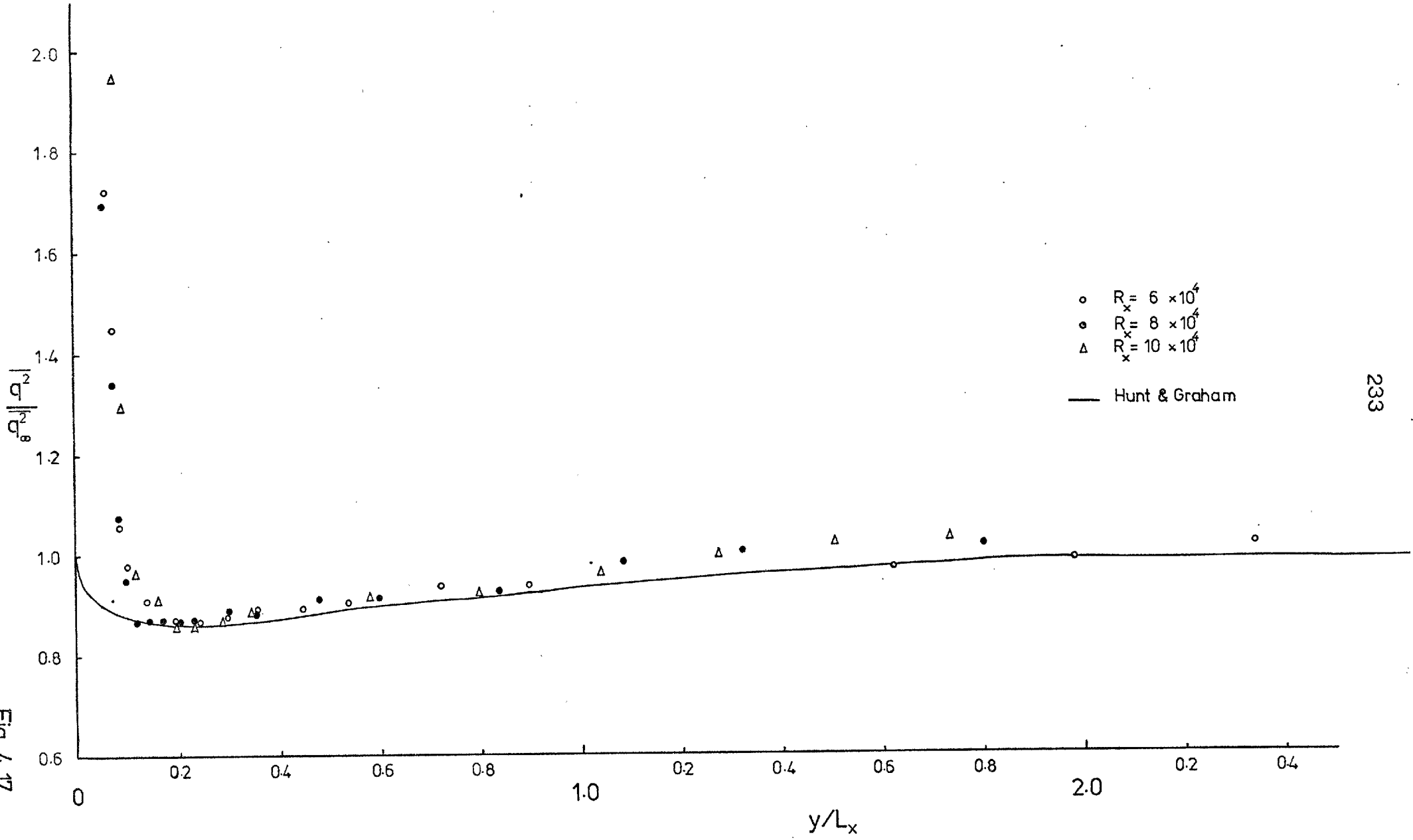


Fig. 4.17

Theoretical and experimental $\overline{q^2}$ profiles over the plate (nose 2).

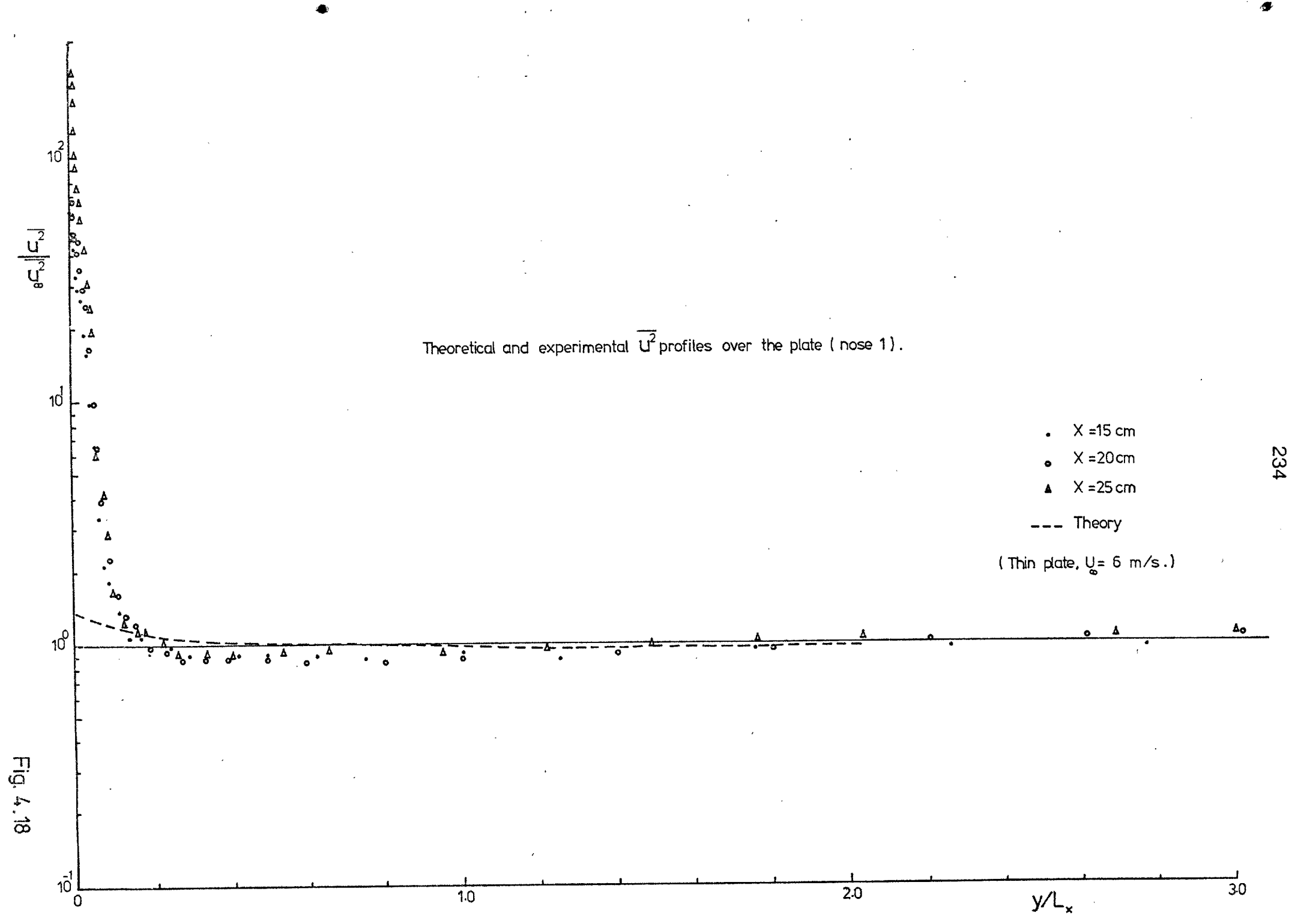

Theoretical and experimental $\overline{u^2}$ profiles over the plate (nose 1).
$\frac{\overline{u^2}}{U_\infty^2}$
10^2
10^1
10^0
10^{-1}
0
1.0
2.0
3.0
y/L_x
X =15 cm
X =20 cm
X =25 cm
Theory
(Thin plate, U_∞ = 6 m/s.)

Fig. 4.18

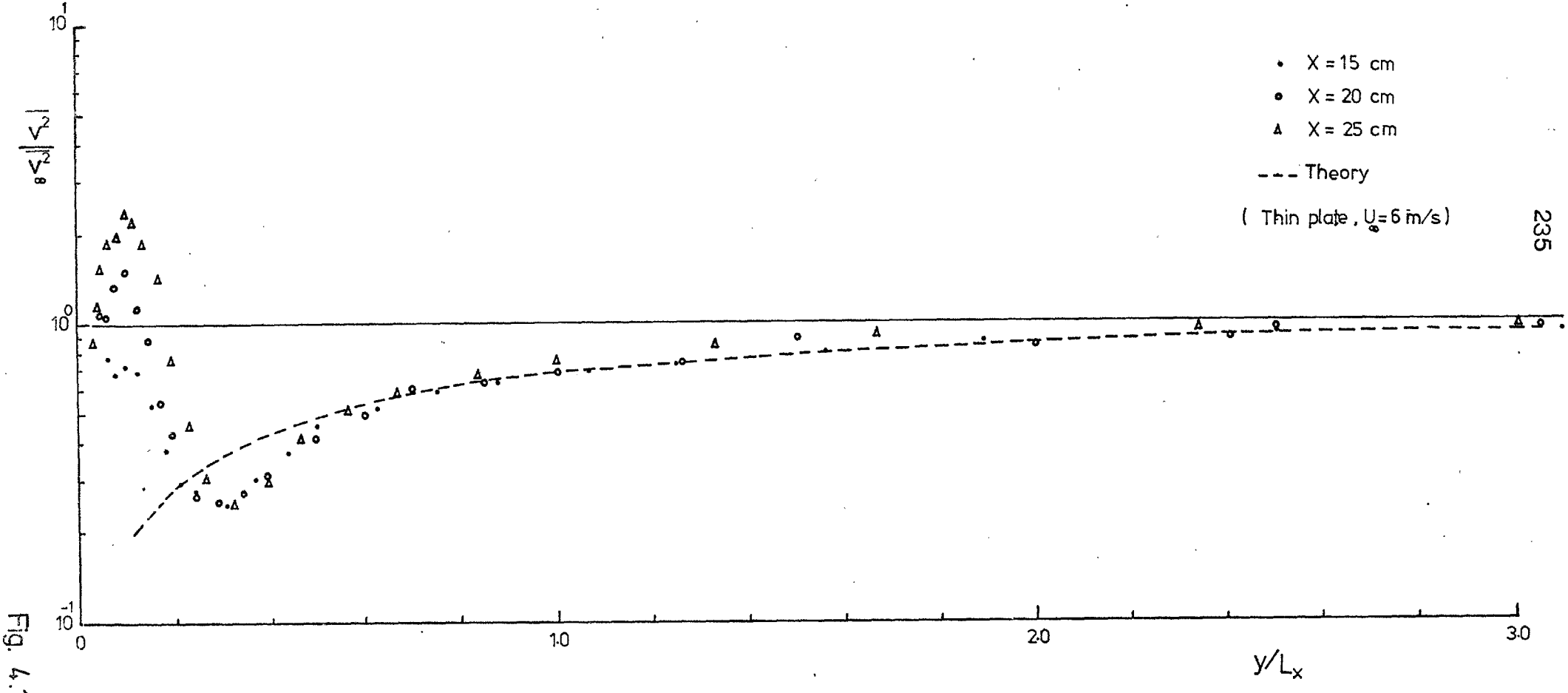


Fig. 4.19

Theoretical and experimental $\overline{V^2}$ profiles over the plate (nose 1).

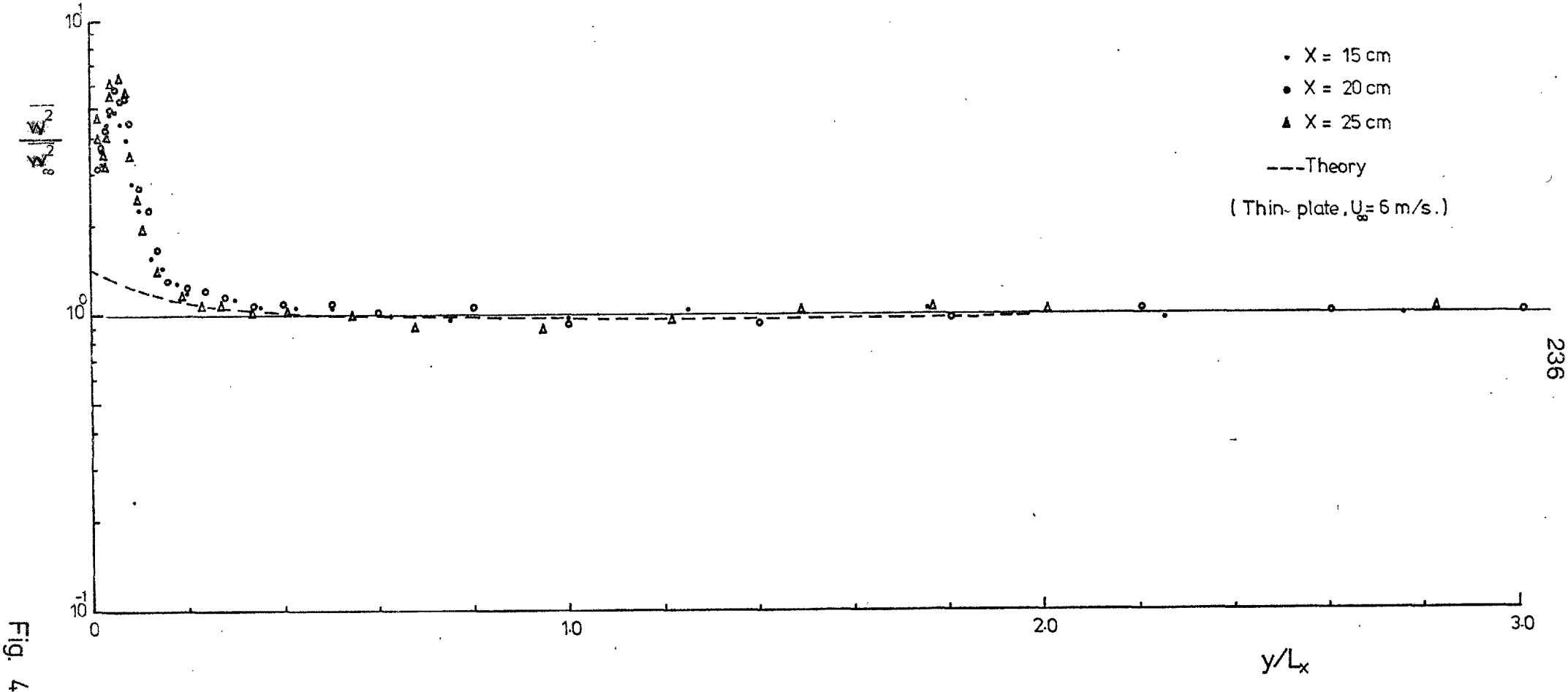


Fig. 4.20

Theoretical and experimental $\overline{w^2}$ profiles over the plate (nose 1).

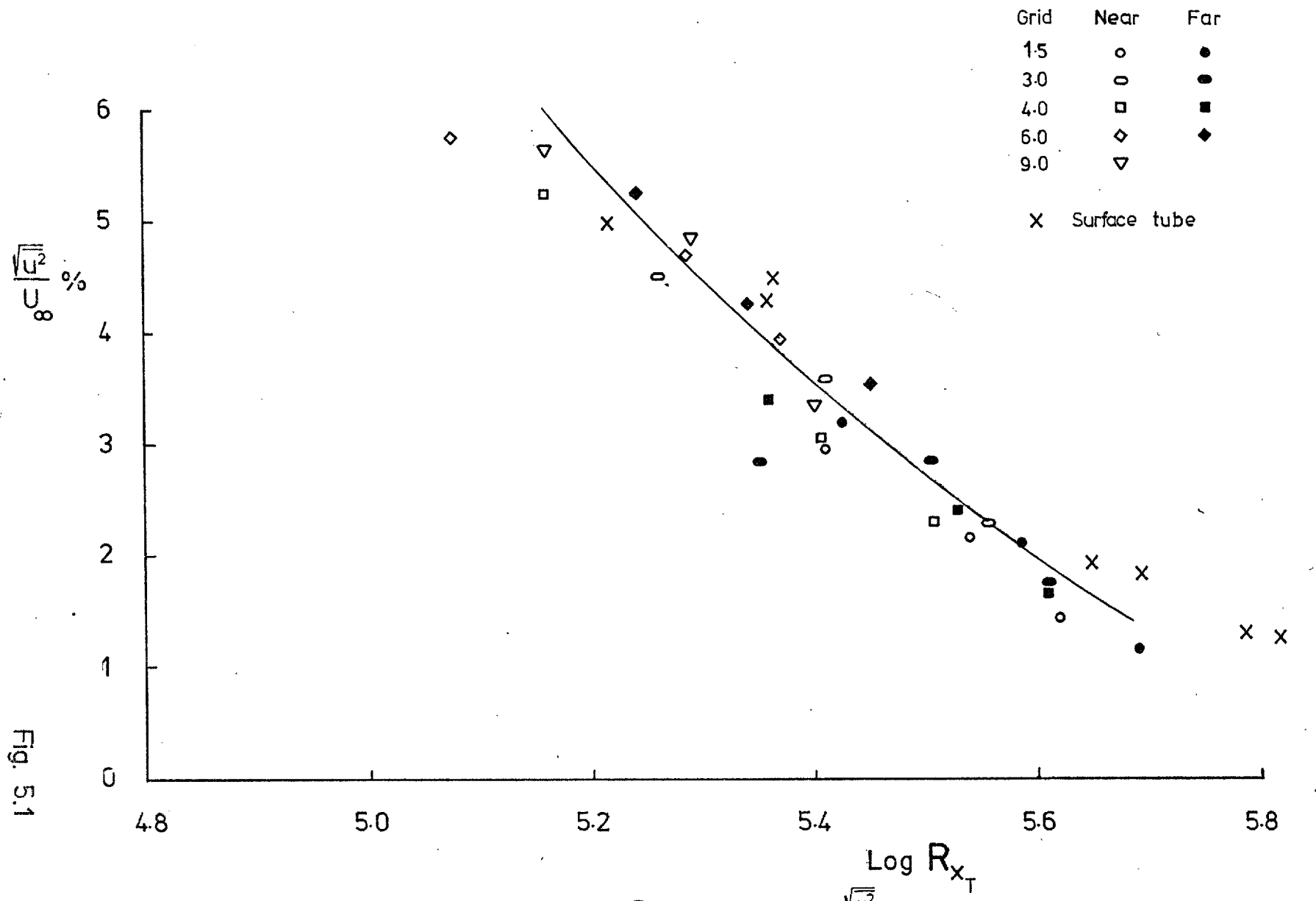


Fig. 5.1

Transition R_x as a function of $\frac{\sqrt{u^2}}{U}$ · (nose 1).

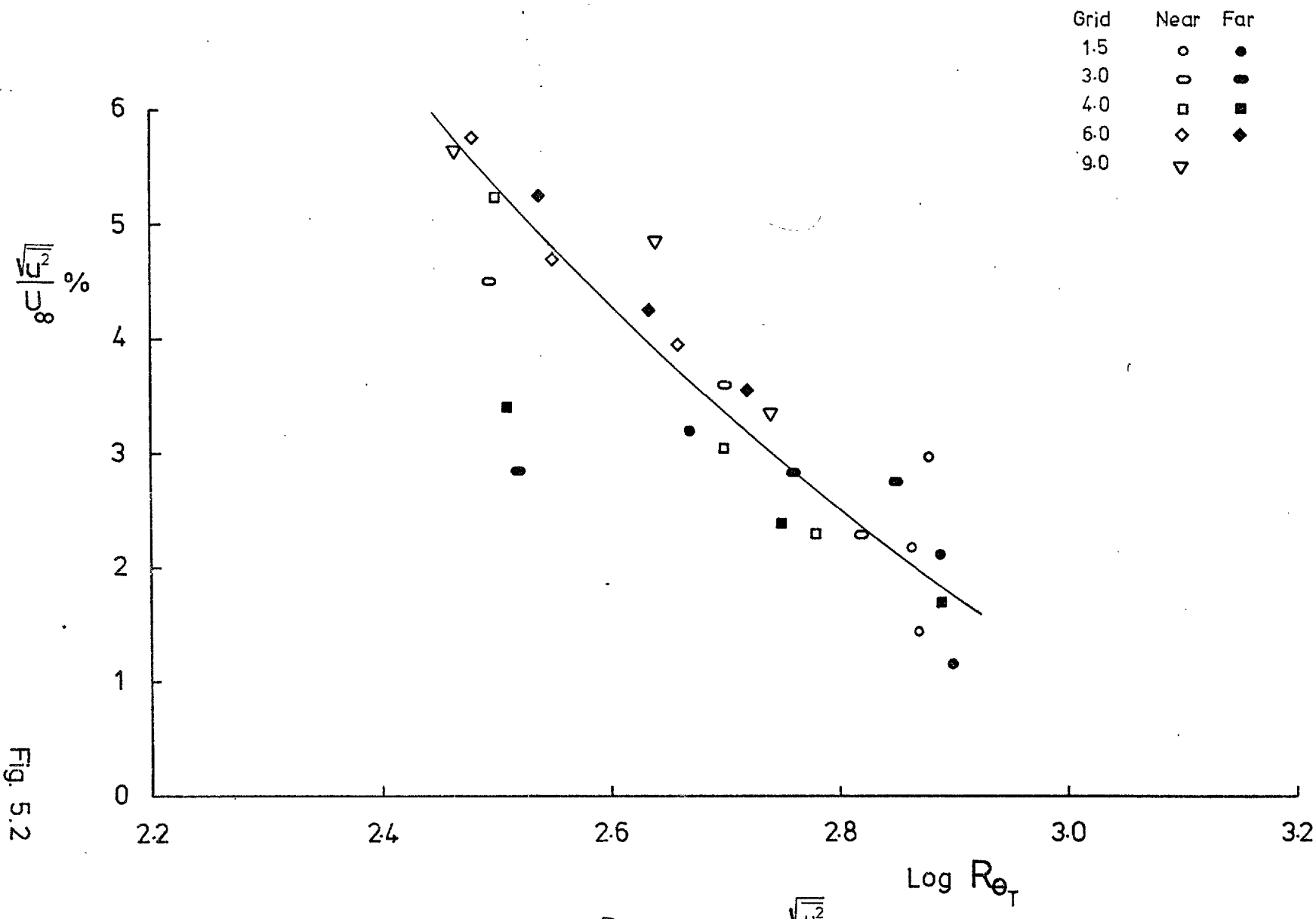


Fig. 5.2

Transition R_θ as a function of $\frac{\sqrt{u^2}}{U}$ (nose 1).

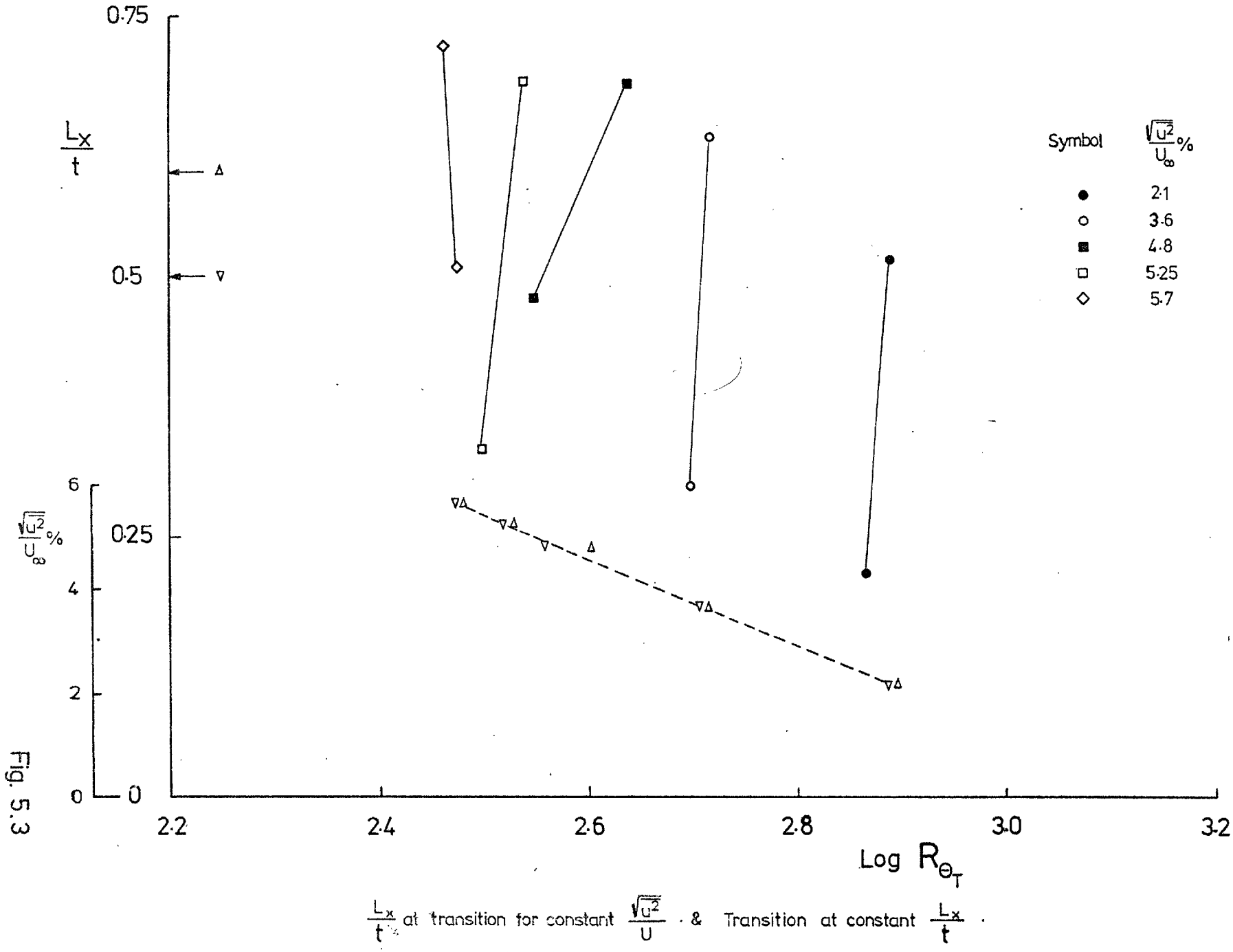


Fig. 5.3

$\frac{L_x}{t}$ at transition for constant $\frac{\sqrt{u^2}}{U}$ · & Transition at constant $\frac{L_x}{t}$ ·

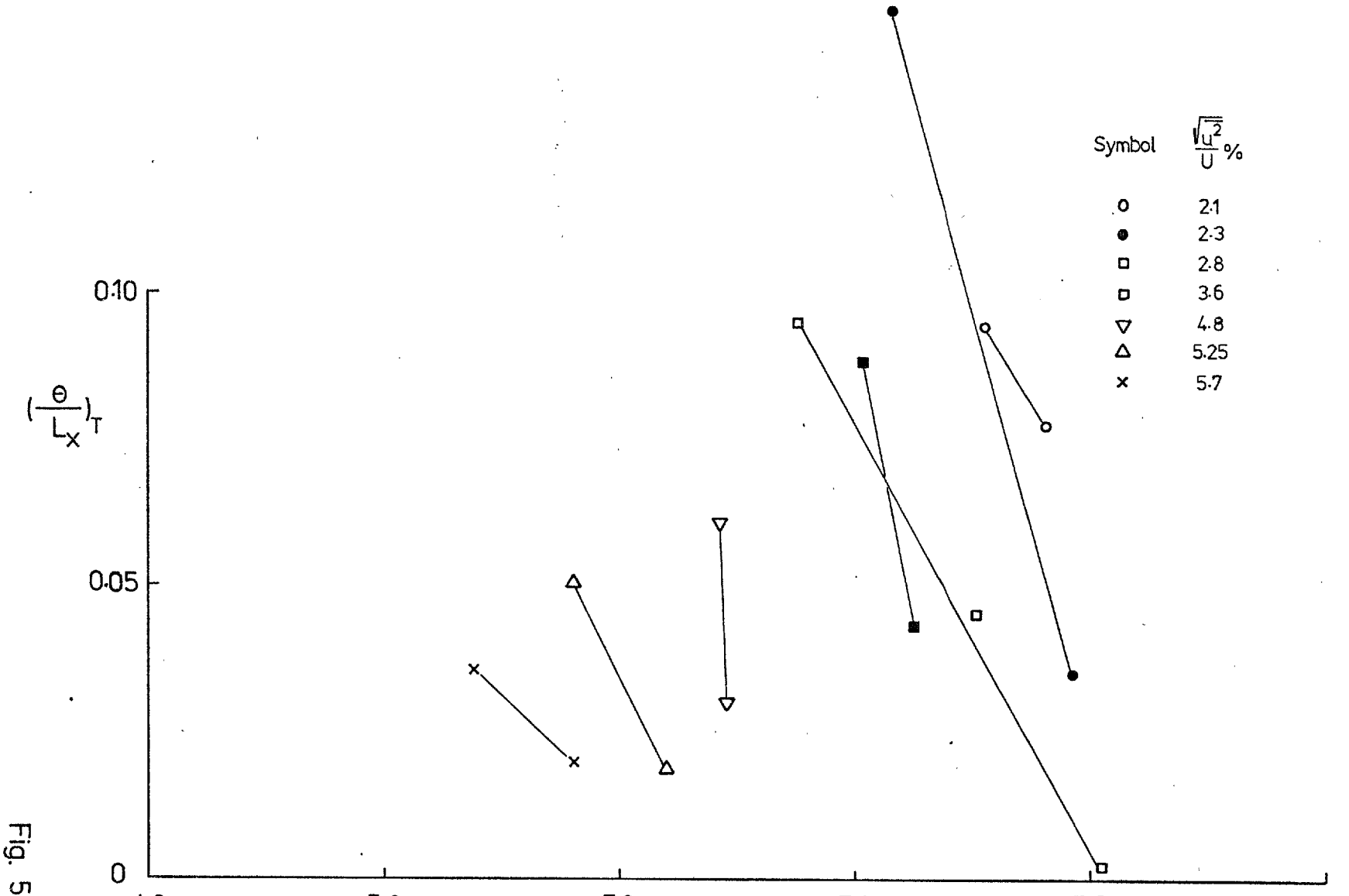


Fig. 5.4

$\frac{\theta}{L_x}$ at transition for constant $\frac{\sqrt{\overline{u^2}}}{U}$ (nose 1).

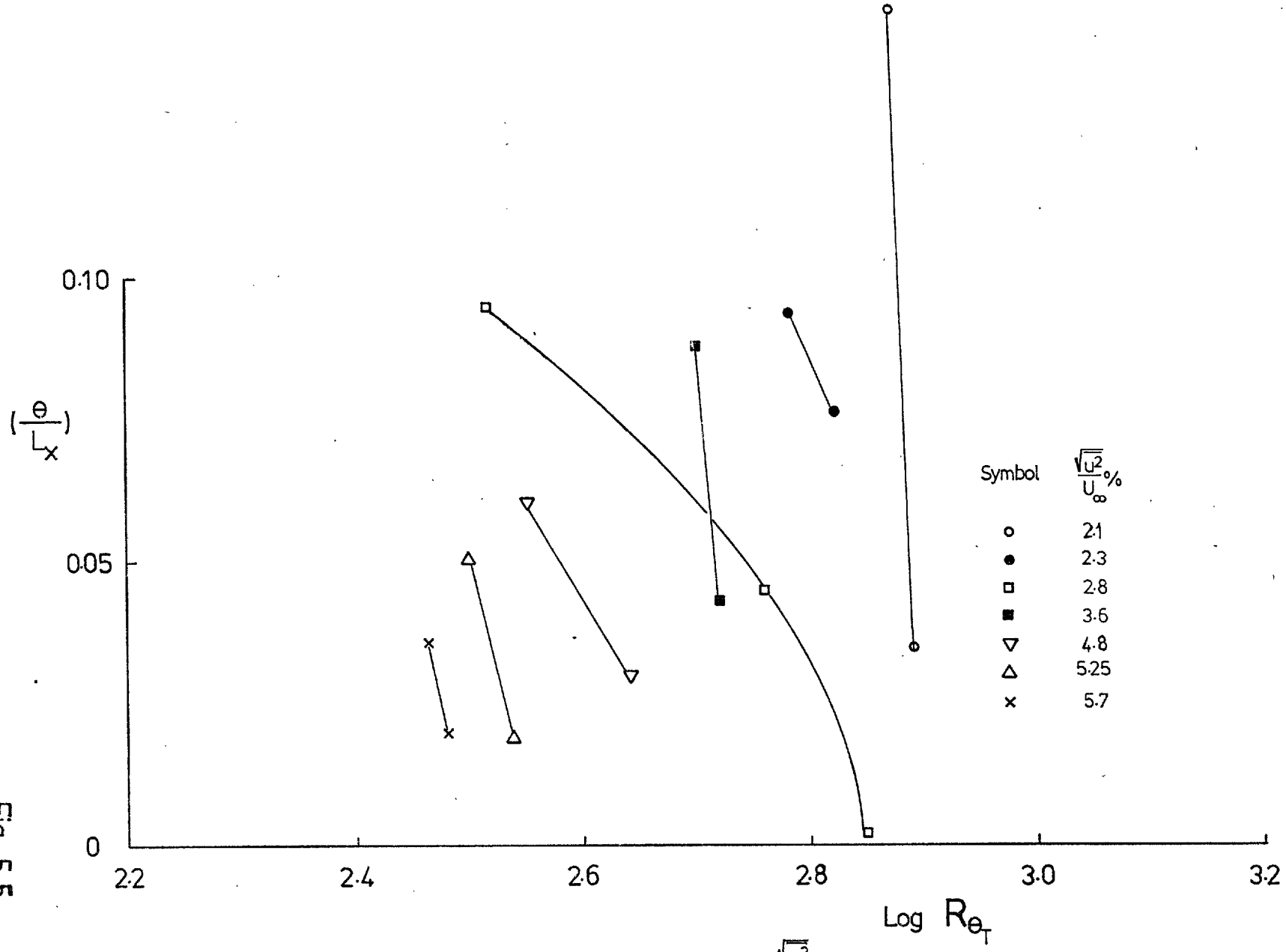


Fig. 5.5

$\frac{\theta}{L_x}$ at transition for constant $\frac{\sqrt{u^2}}{U}$ (nose 1).

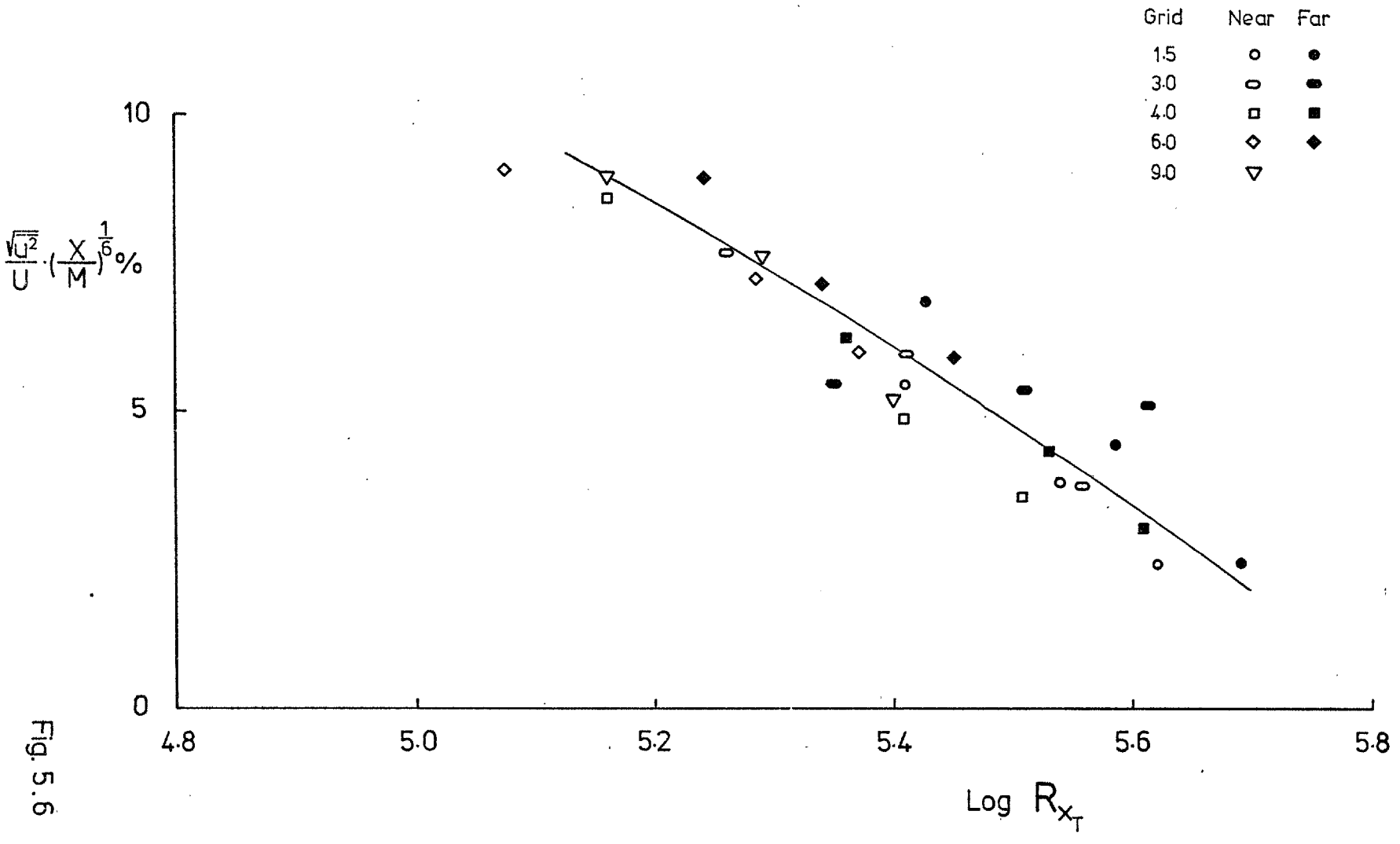


Fig. 5.6

Transition as a function of the modified Taylor's parameter (nose 1).

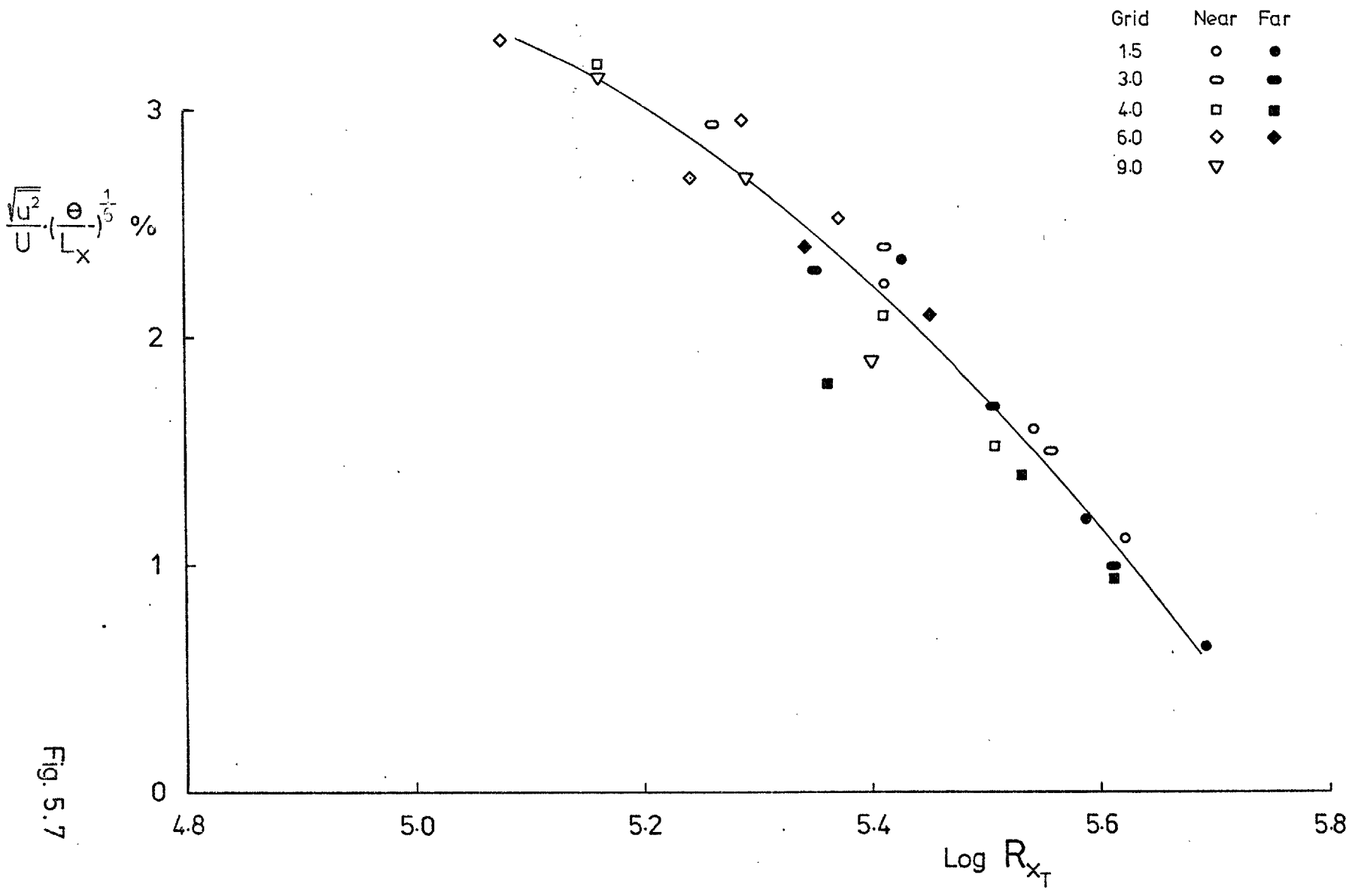


Fig. 5.7

Transition as a function of the modified Taylor's parameter in terms of $\frac{\theta}{L_x}$ (nose 1).

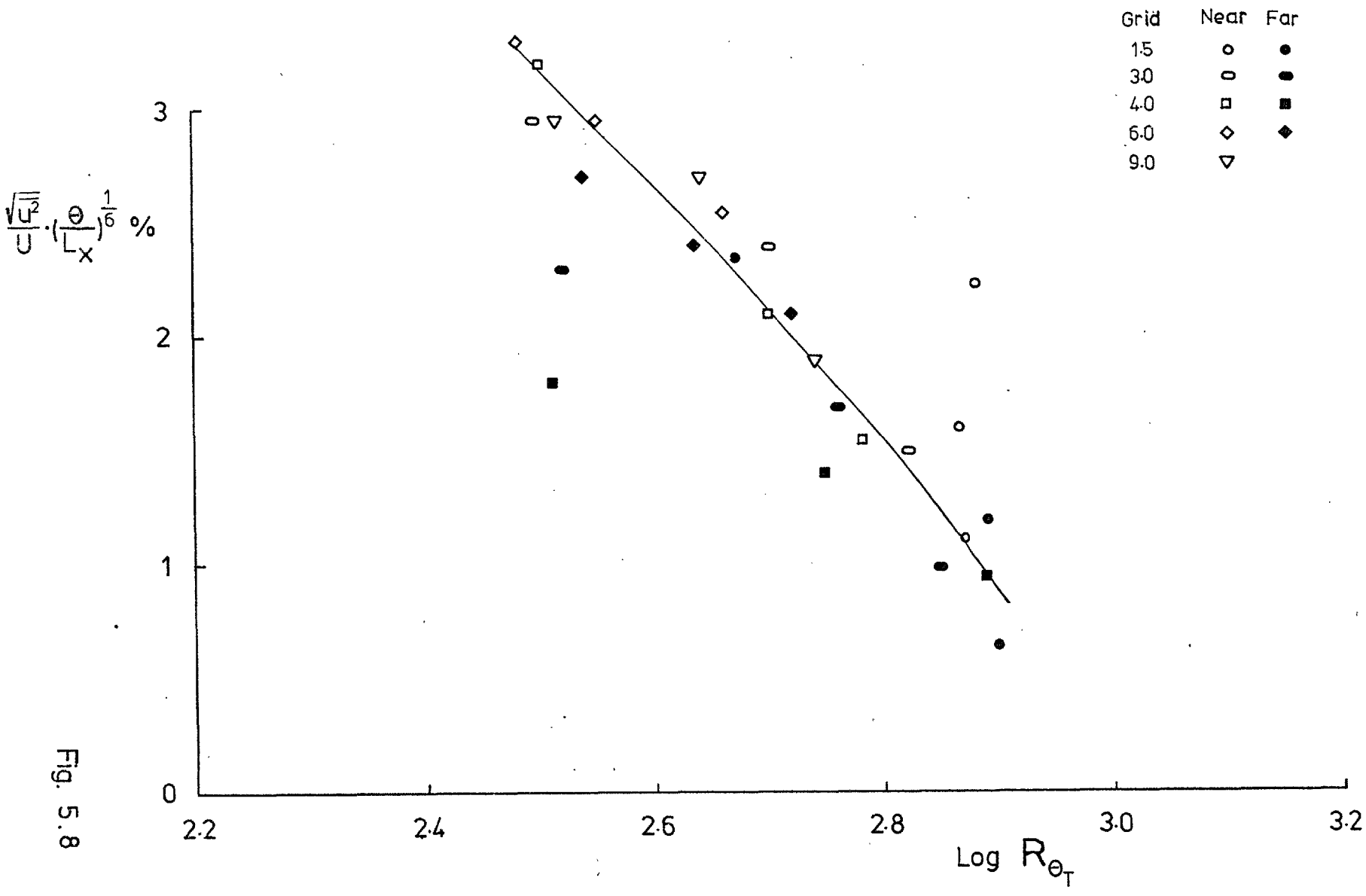


Fig. 5.8

Transition as a function of the modified Taylor's parameter in terms of $\frac{\theta}{L_x}$ (nose 1).

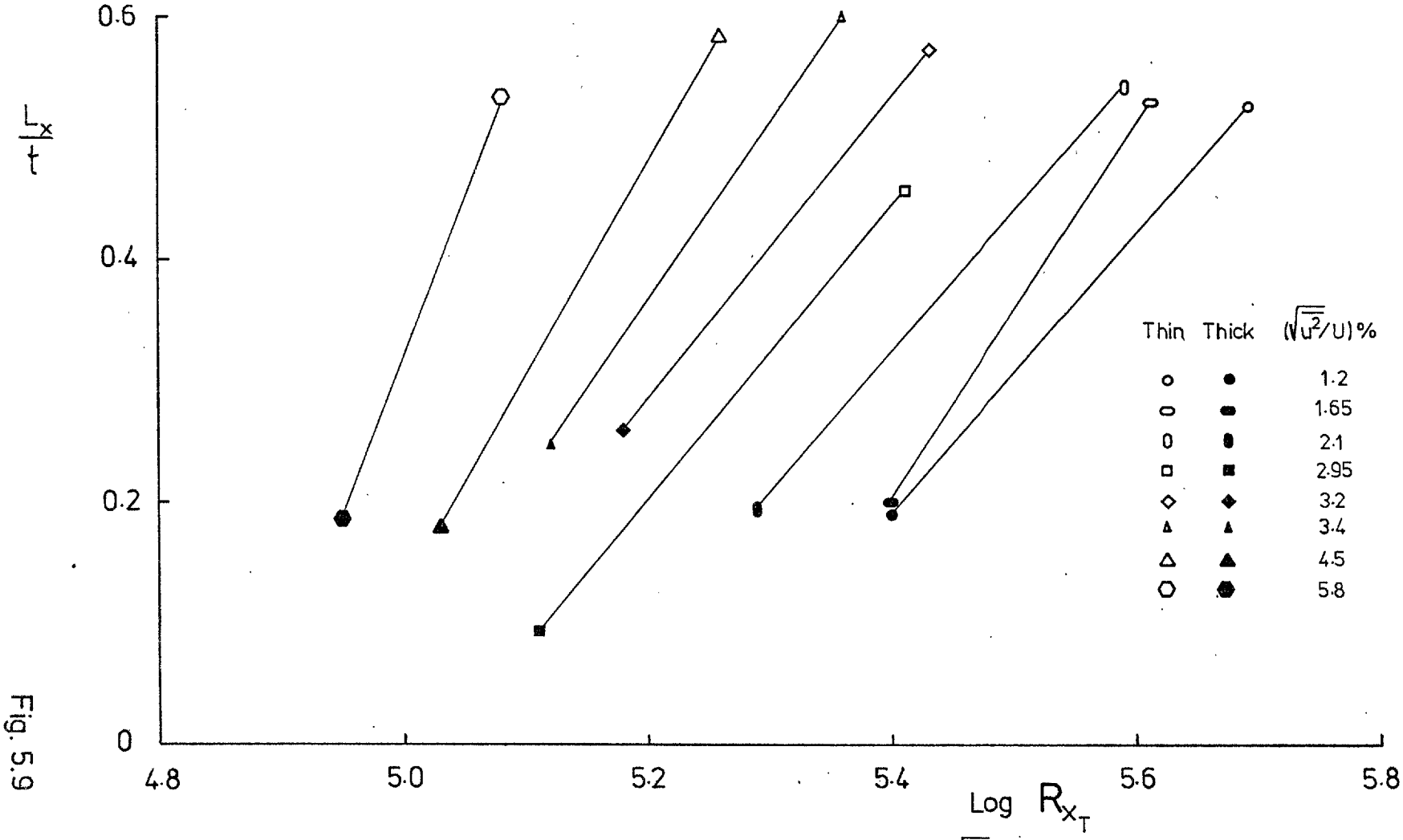


Fig. 5.9

Effect of changes in $\frac{L_x}{t}$ on transition for constant $\frac{\sqrt{u^2}}{U}$ (noses 1&2).

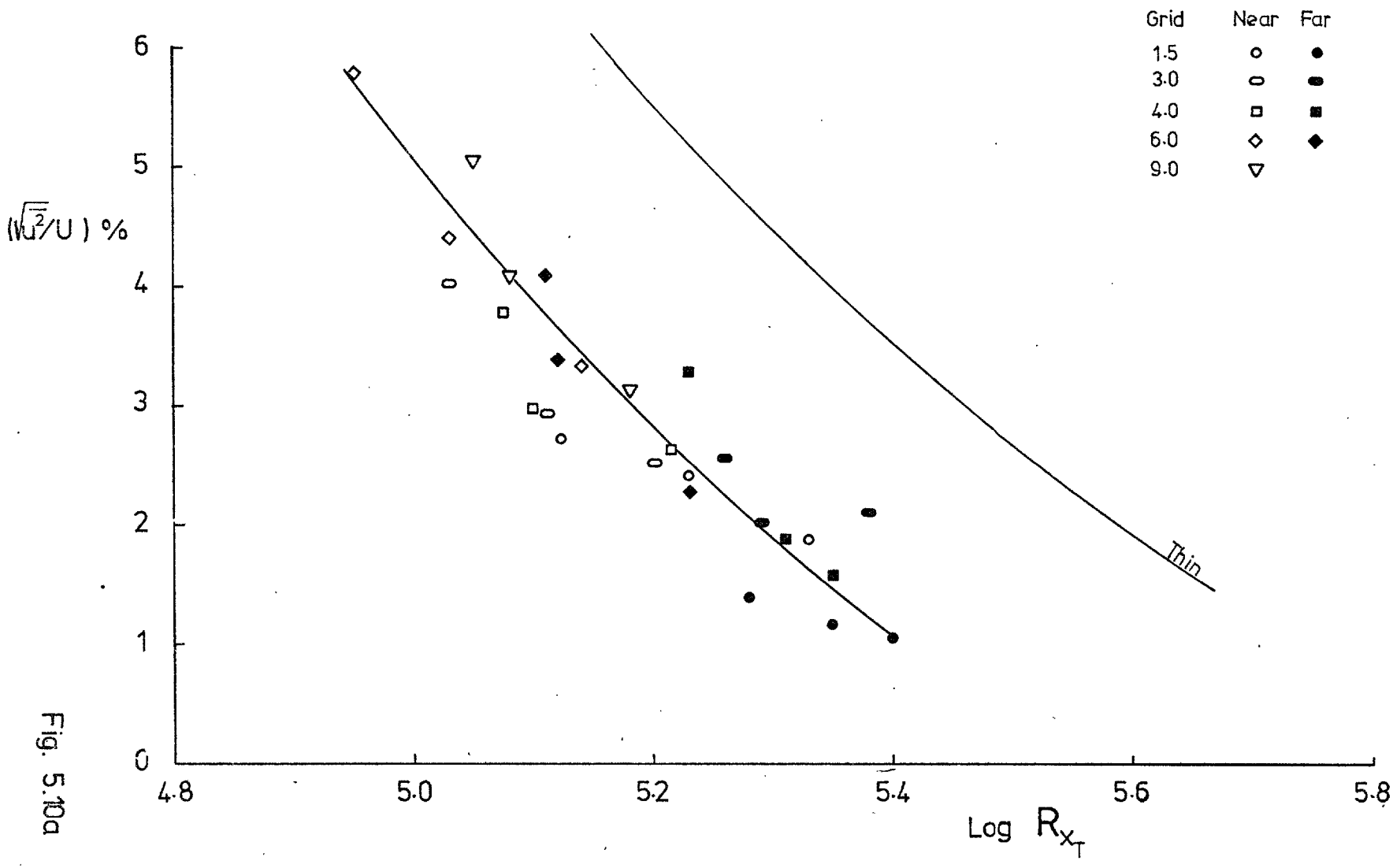


Fig. 5.10a

Transition over the thick plate (nose 2) compared with that over the thin plate (nose 1) reported earlier .

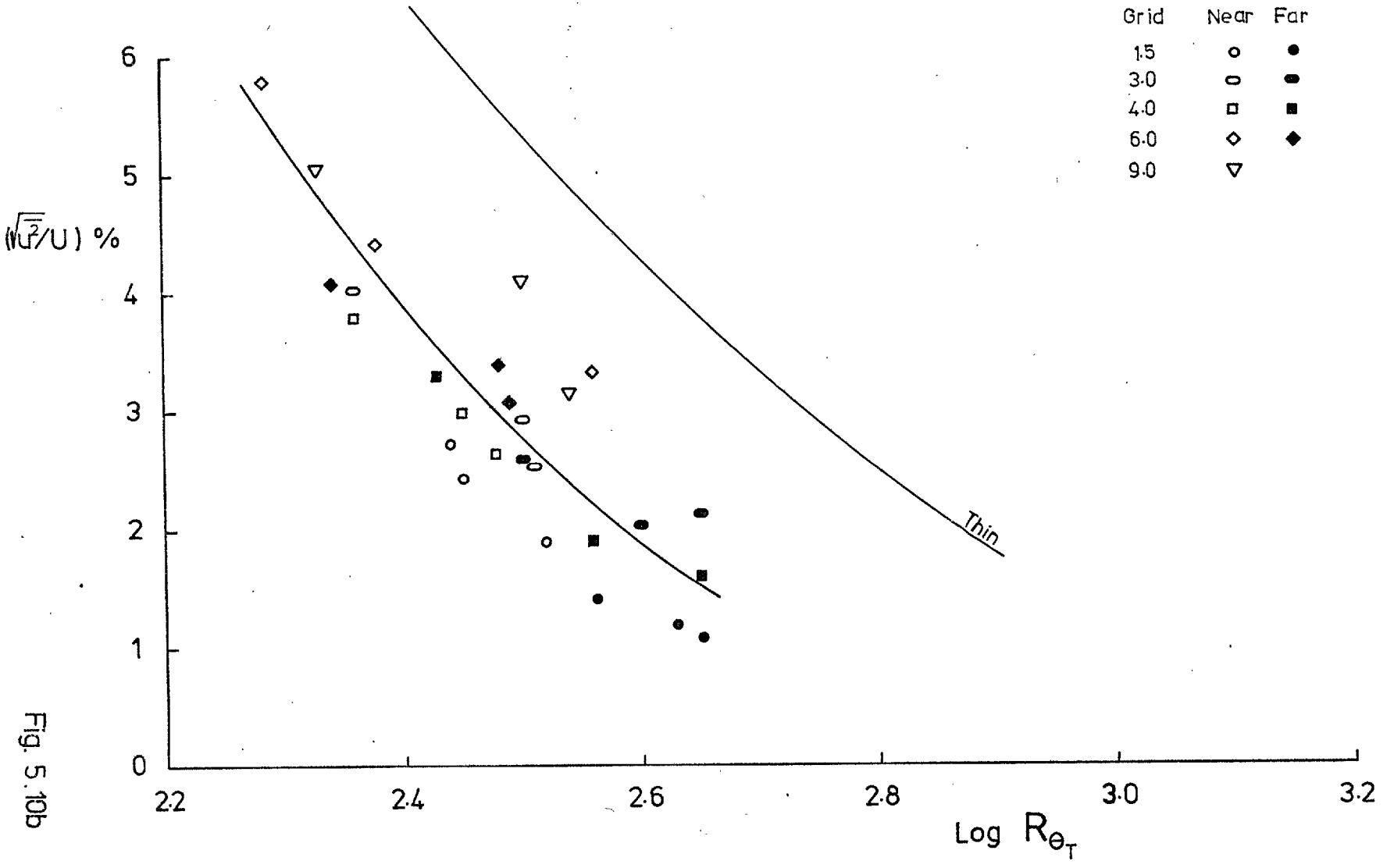


Fig. 5.10b

(For legend see fig. 5.10.A)

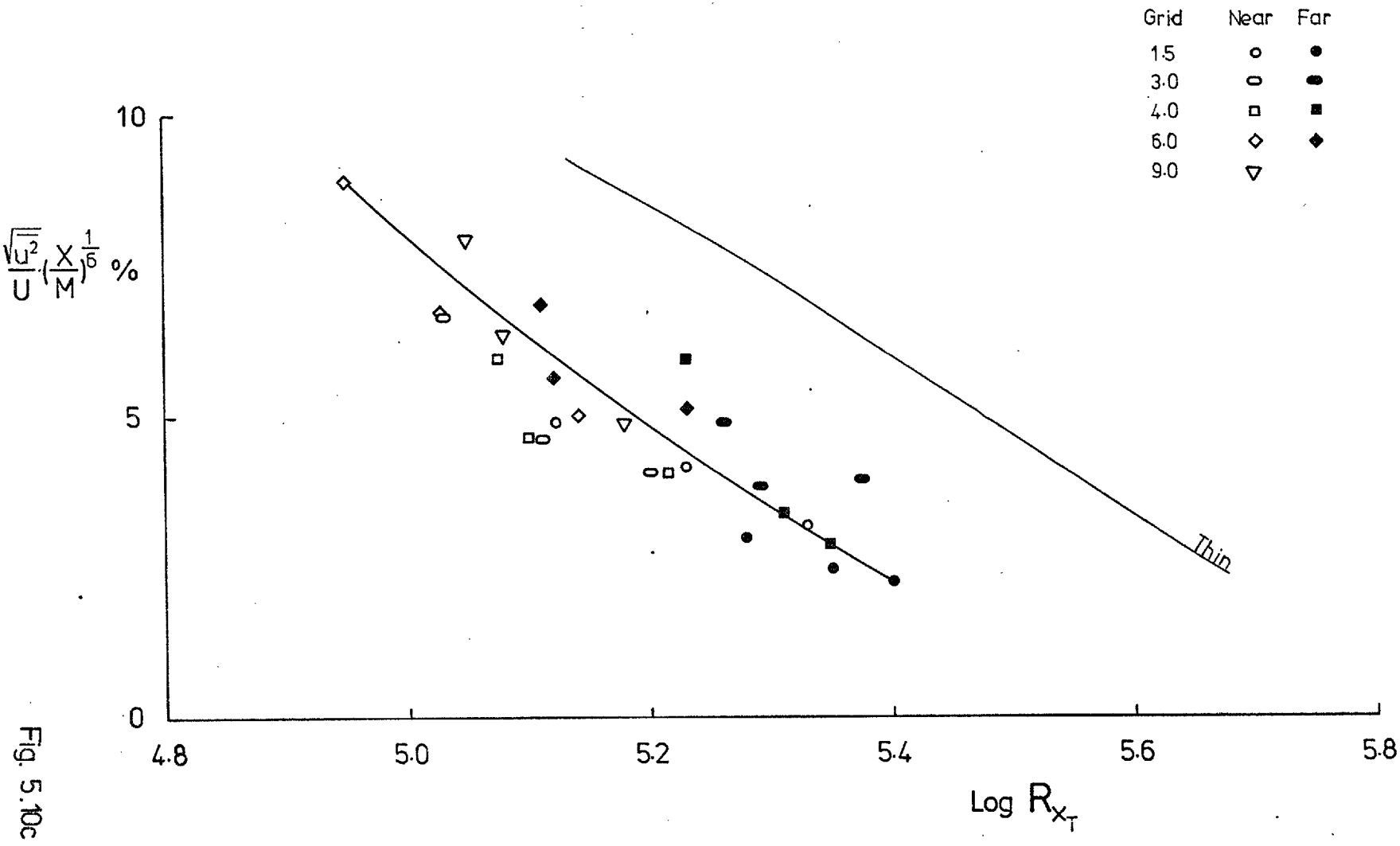


Fig. 5.10c

(For legend see fig. 5.10.A)

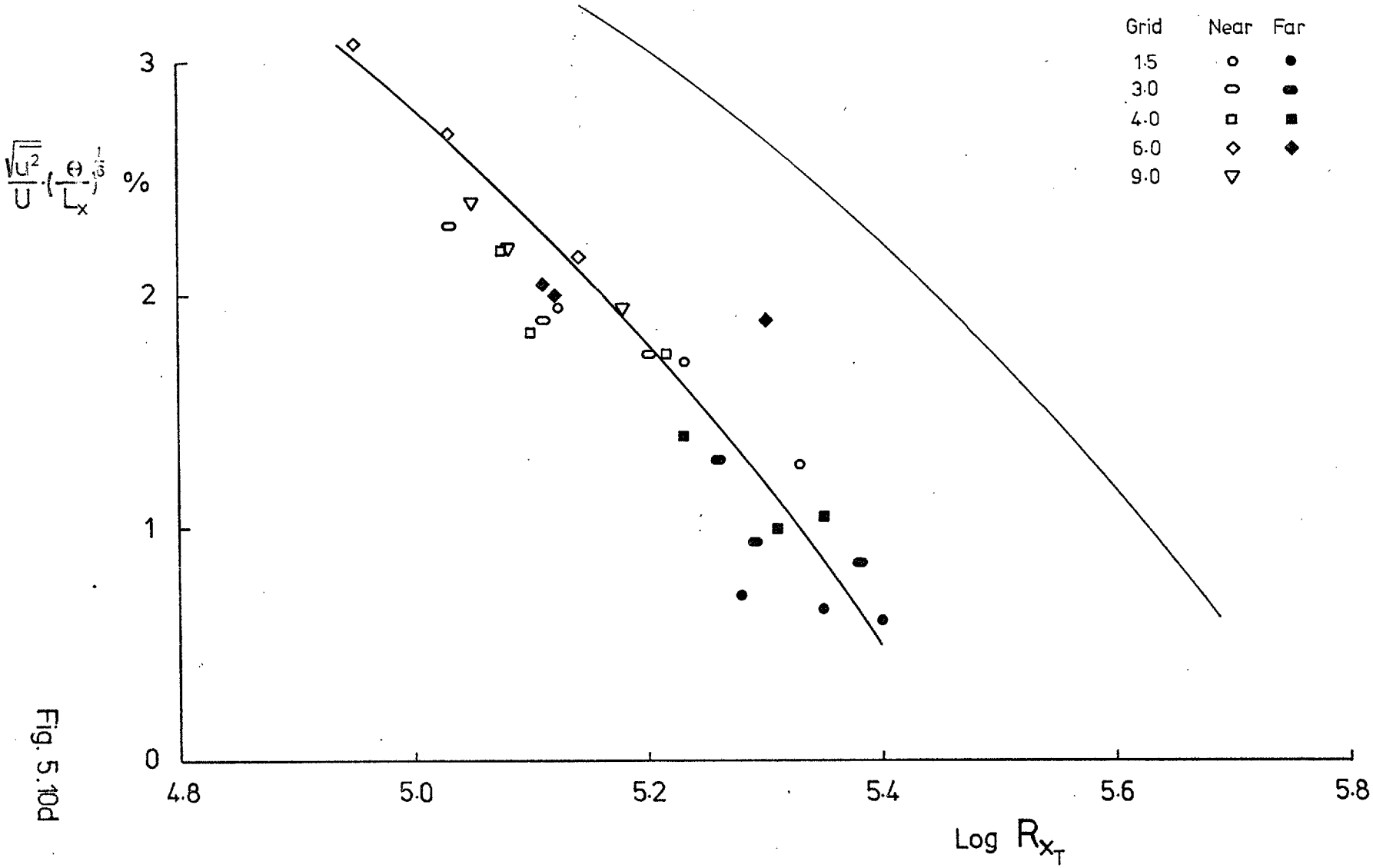


Fig. 5.10d

(For legend see fig. 5.10.A)

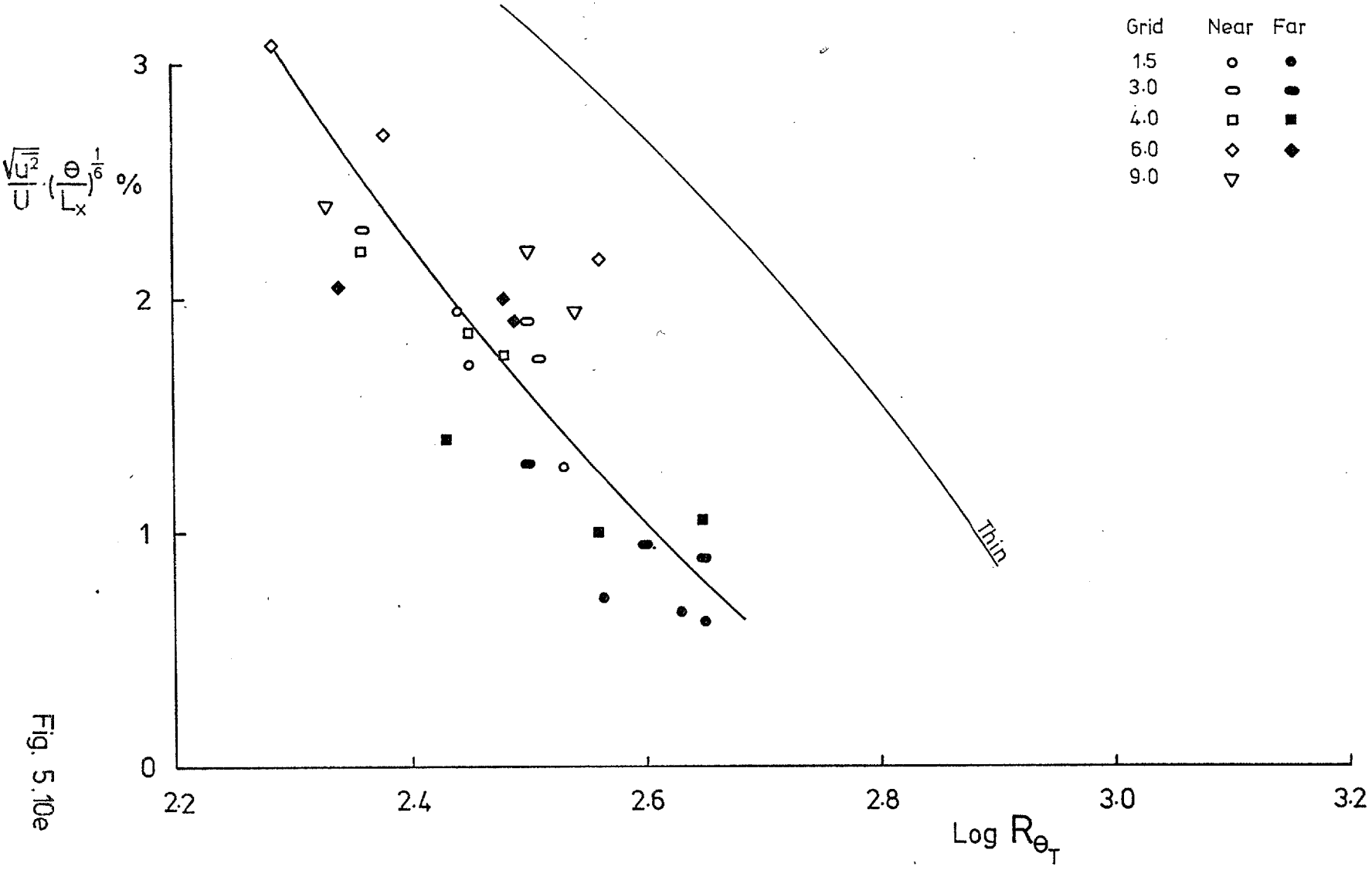


Fig. 5.10e

(For legend see fig. 5.10.A)

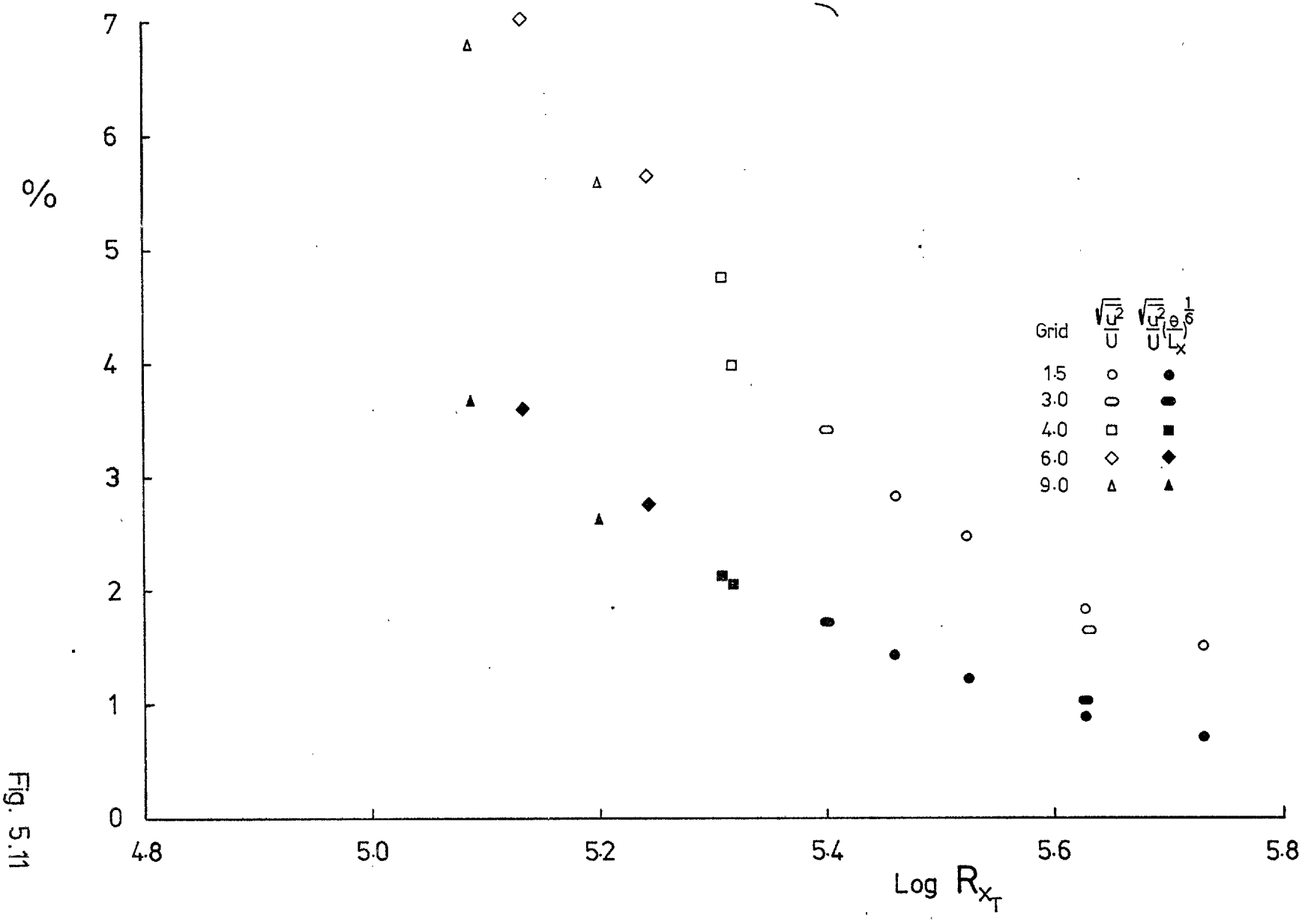


Fig. 5.11

Transition R_x detected at a constant X (nose 1).

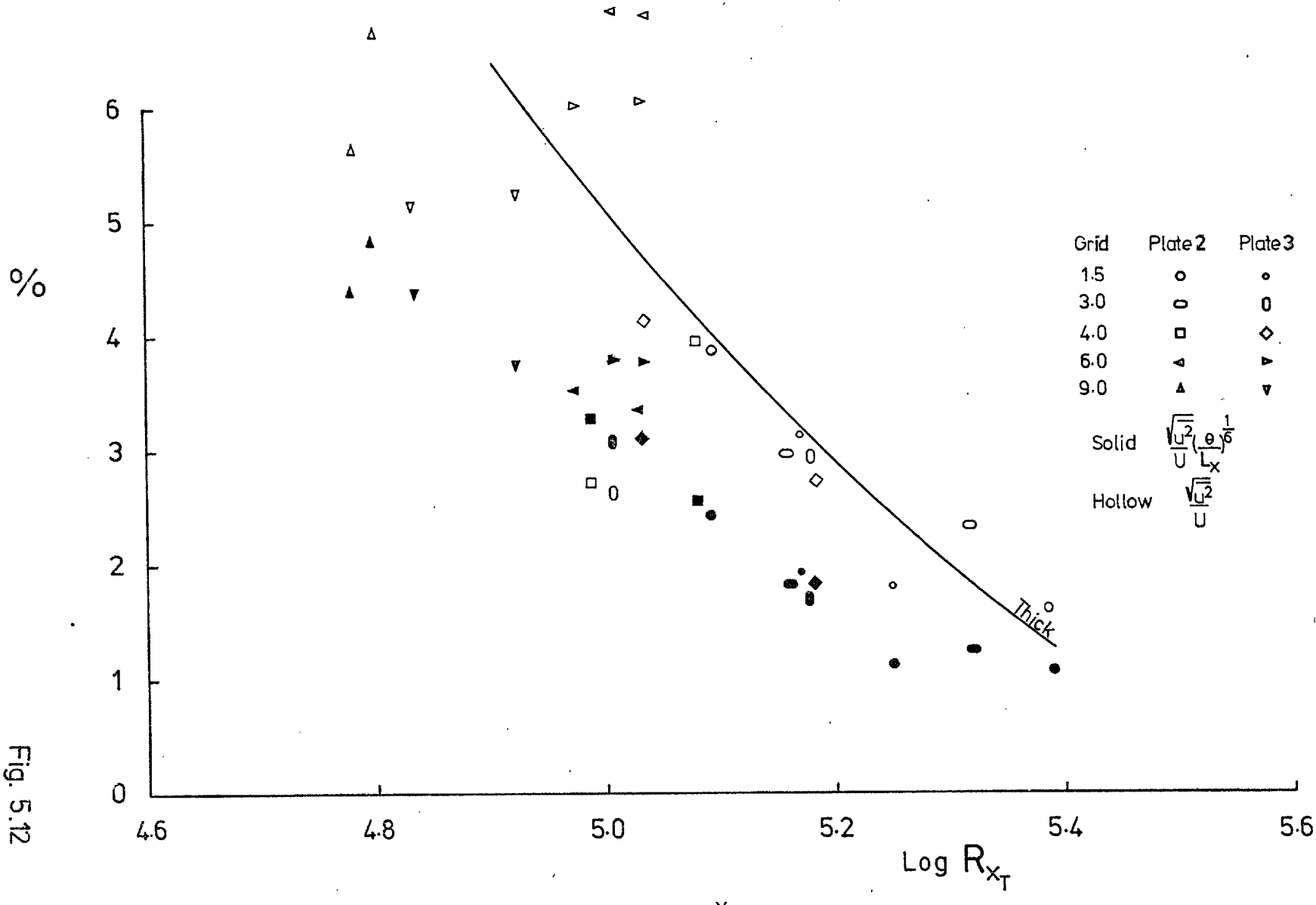


Fig. 5.12

Transition R_x detected at the same $\frac{X_T}{X_n}$ over the two plate (noses 2 & 3).

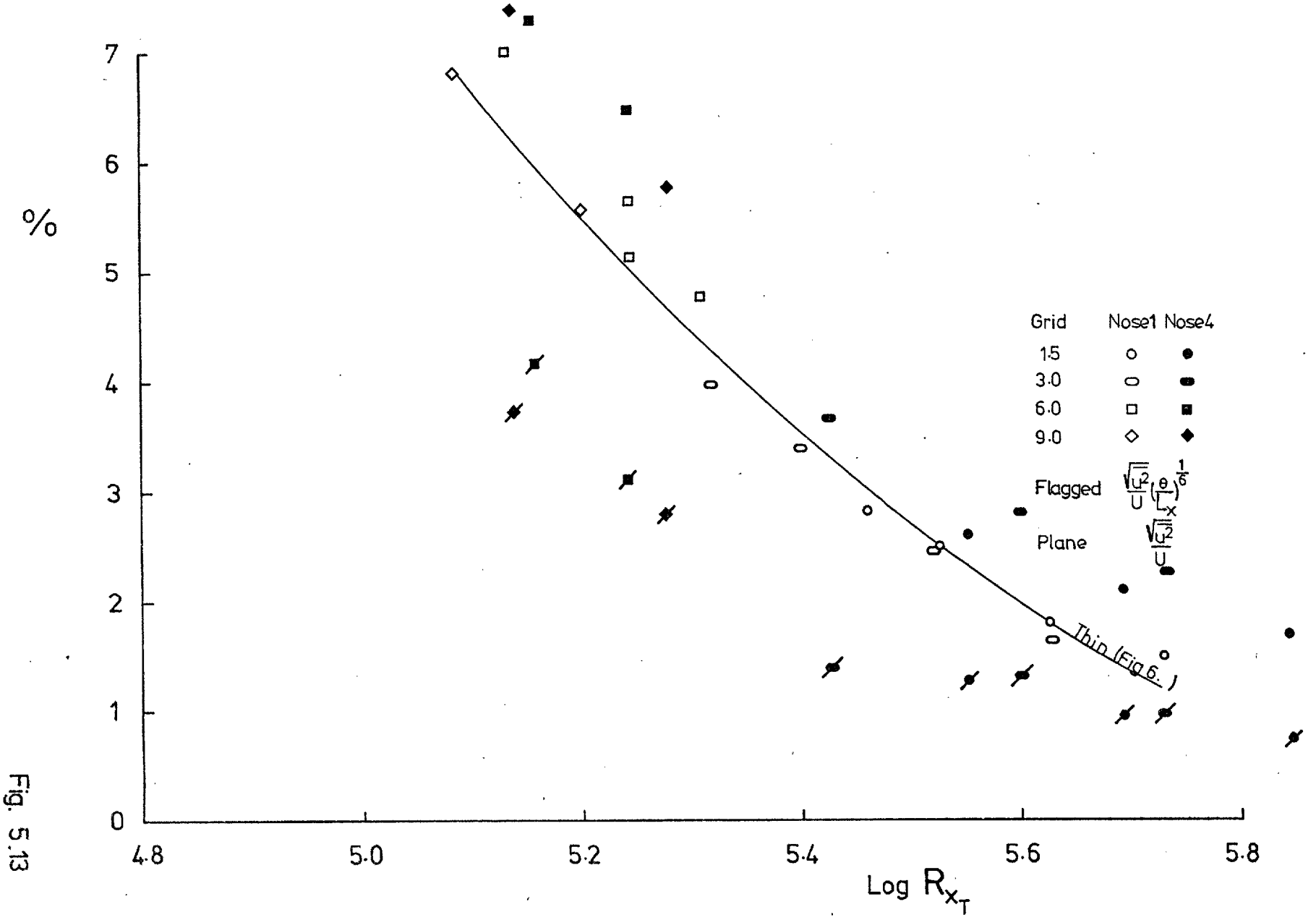


Fig. 5.13

Effect of changing the pressure gradient around the nose on transition (noses 1&4).

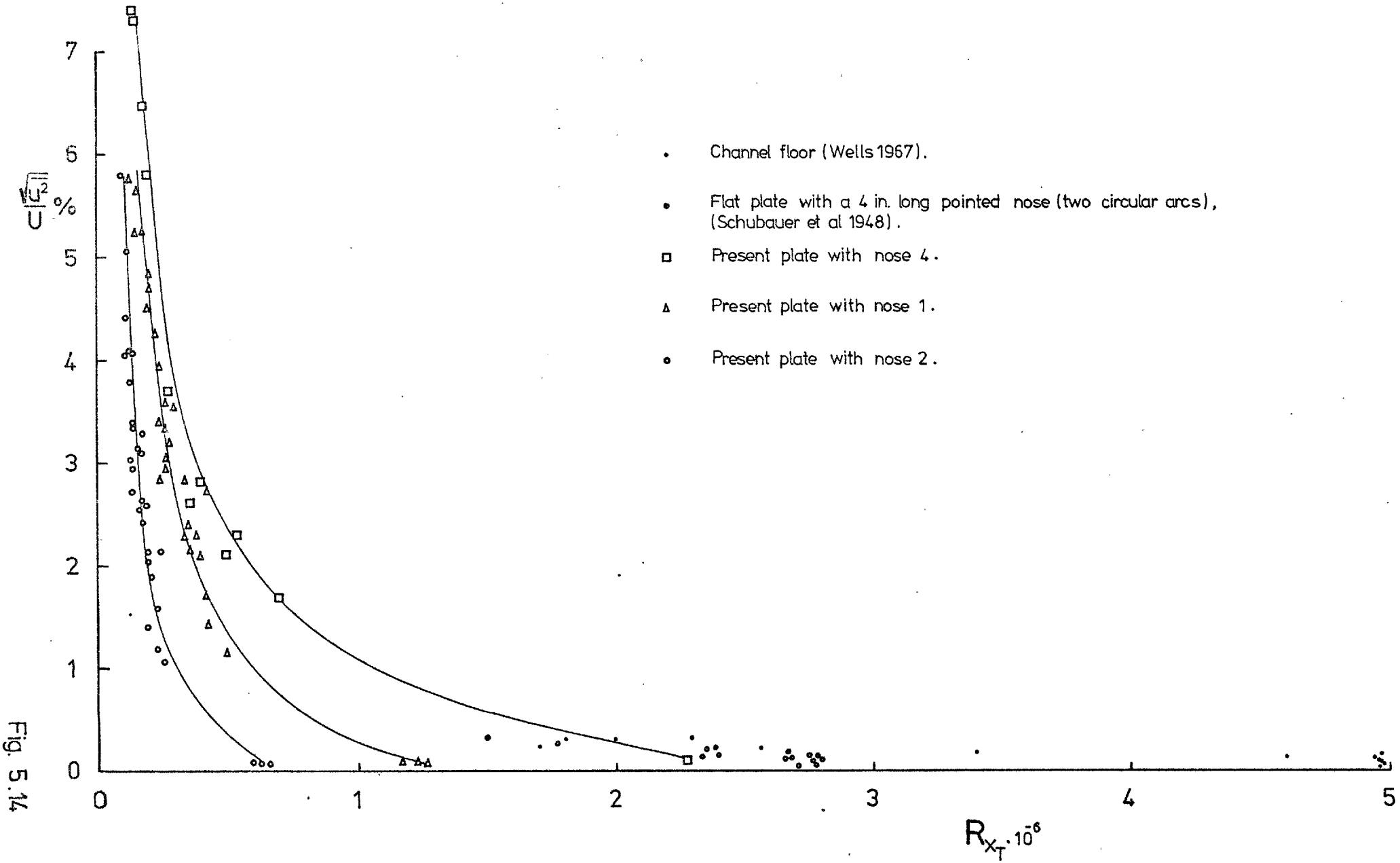
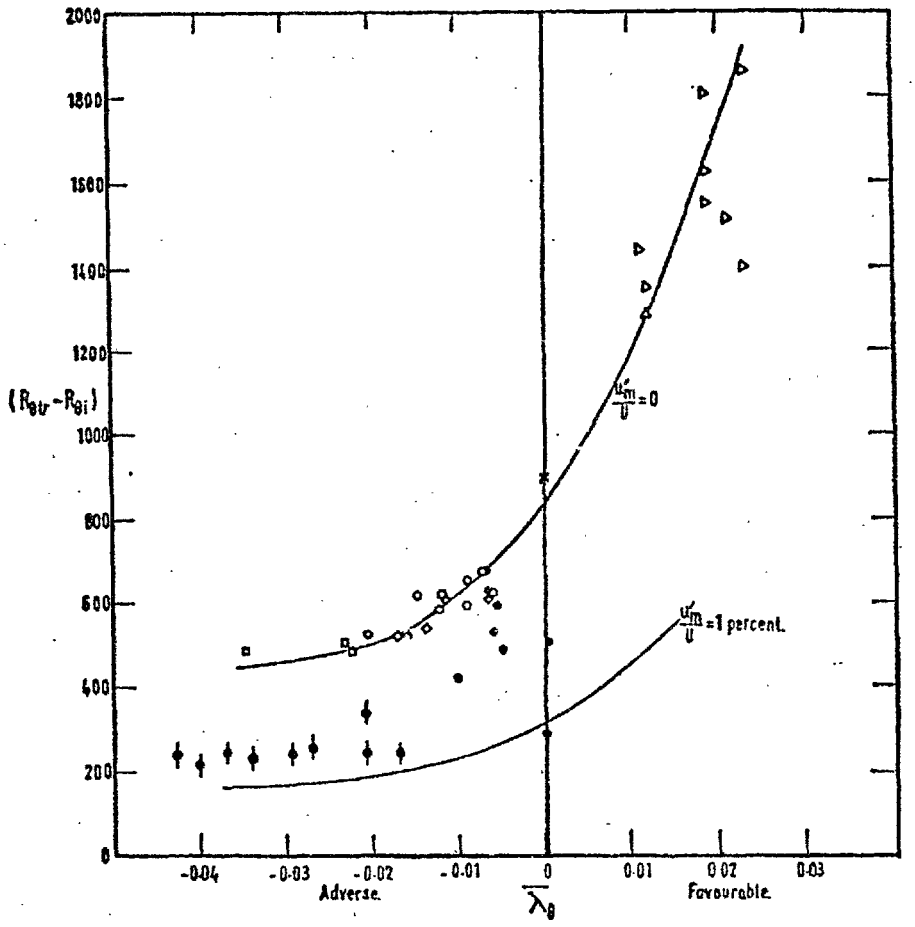


Fig. 5.14

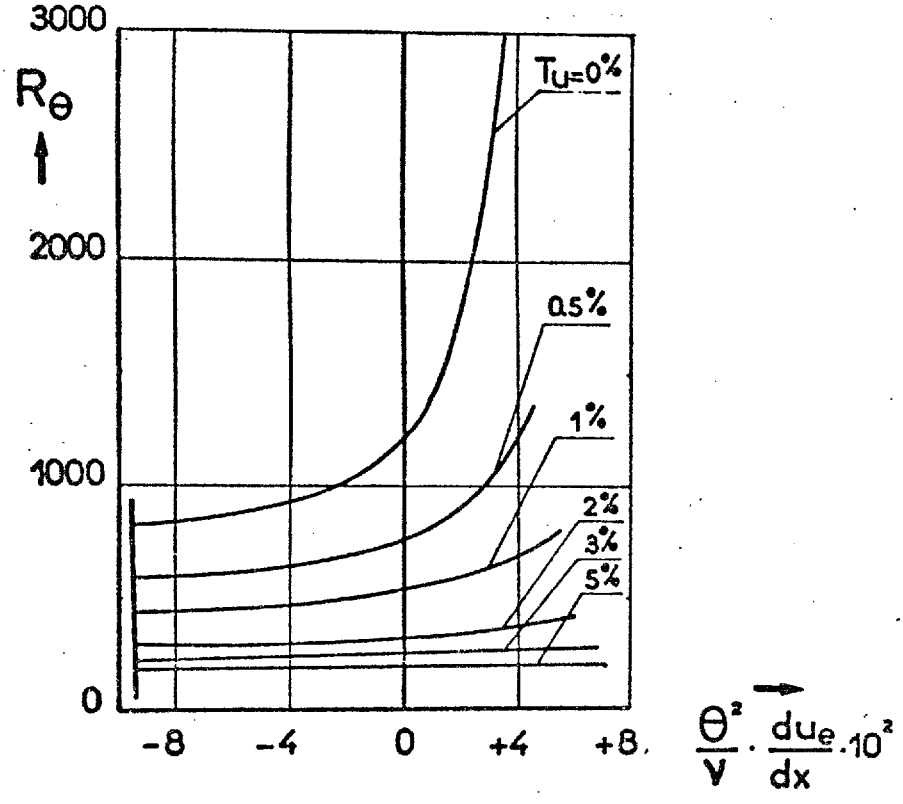
Transition for different pressure gradients around the leading edge.



Plot of $(R_{\theta tr} - R_{\theta i})$ against λ_θ for natural transition, from Granville [7].
Start of transition.

After Hall (1968)

Fig. 5.15



Transition R for different $\frac{\sqrt{\overline{u^2}}}{U}$ and $\lambda_\theta = \frac{\theta^2}{\nu} \cdot \frac{dU_\infty}{dX}$

(After Michel 1974)

Fig. 5.16

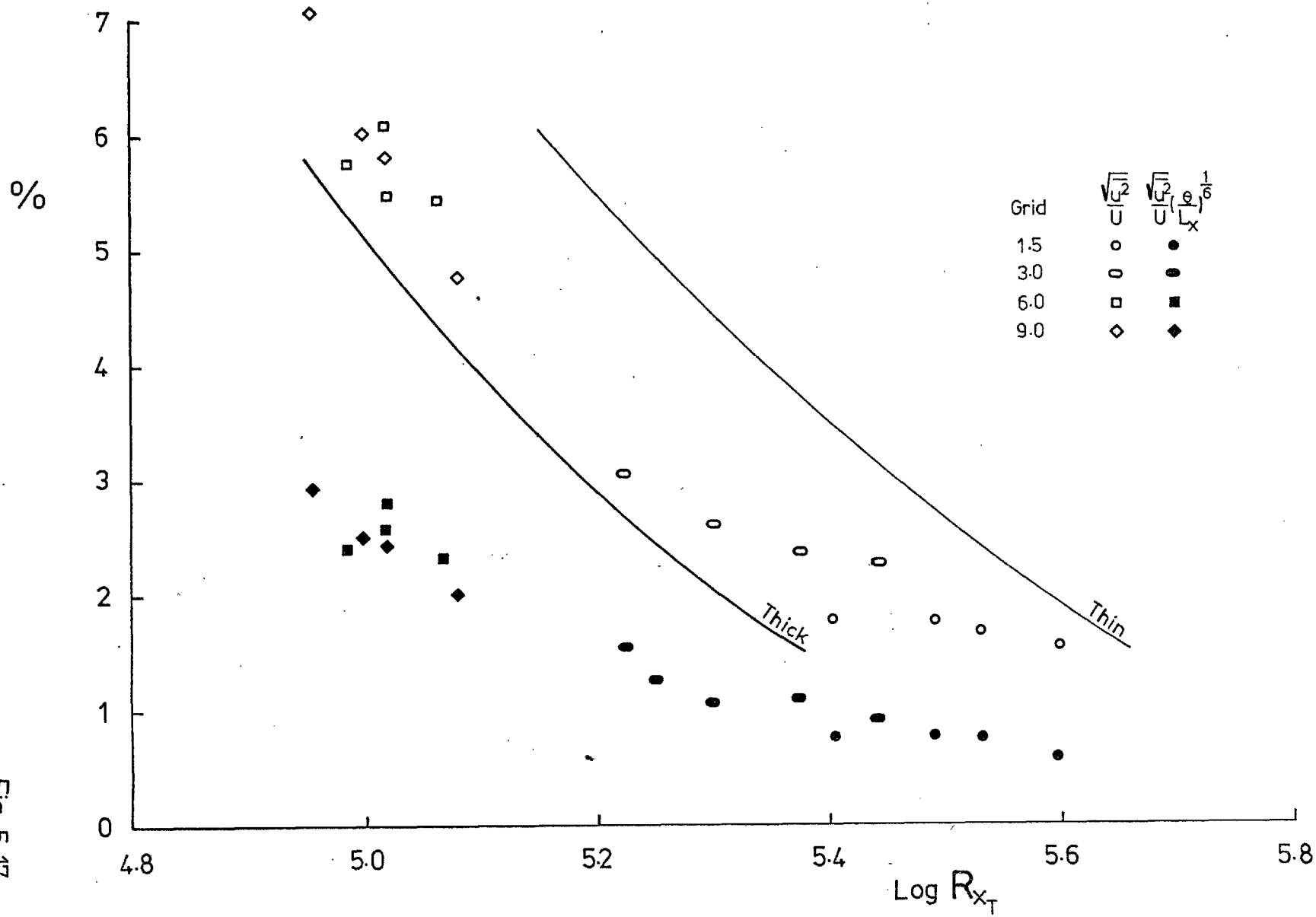
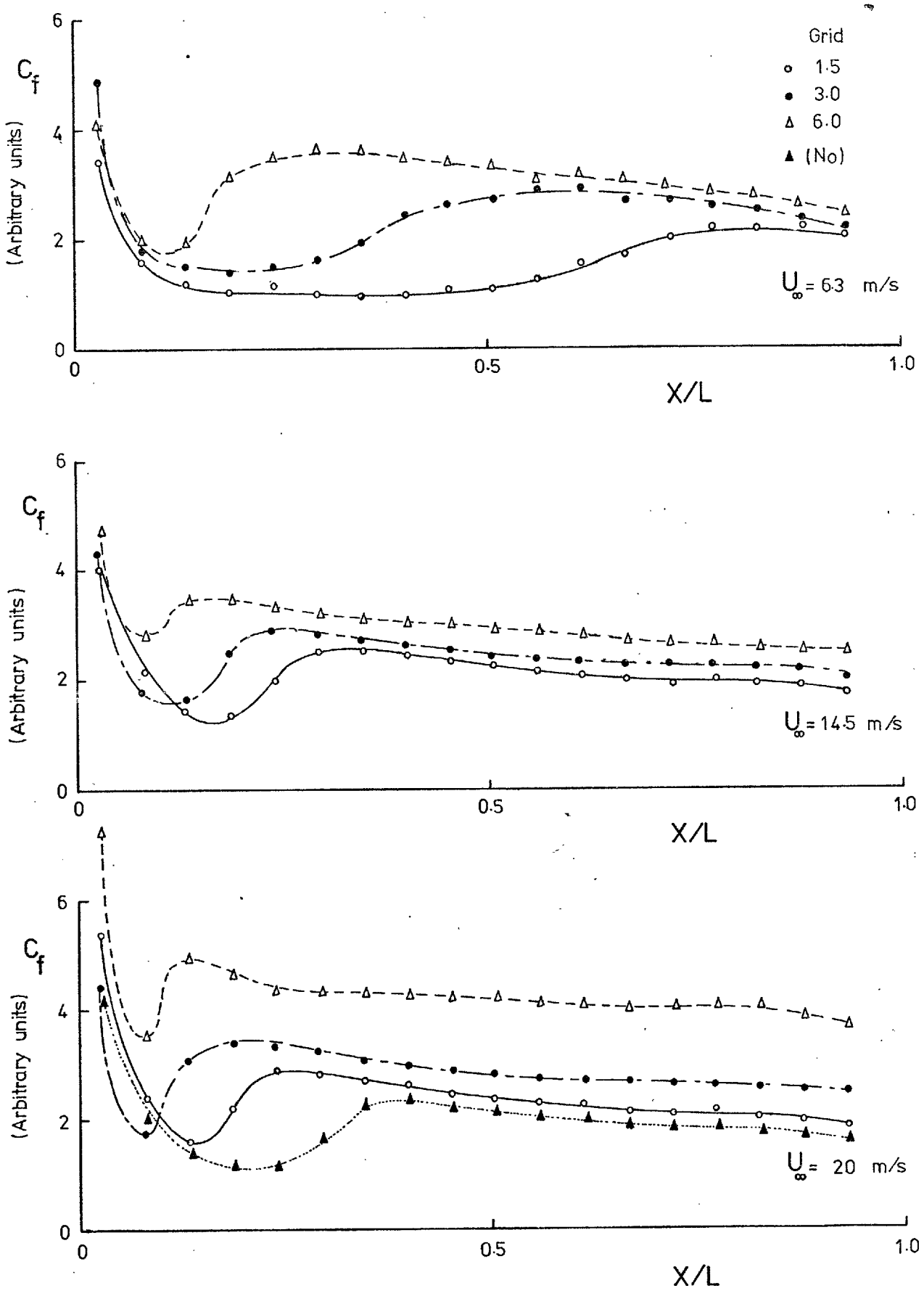


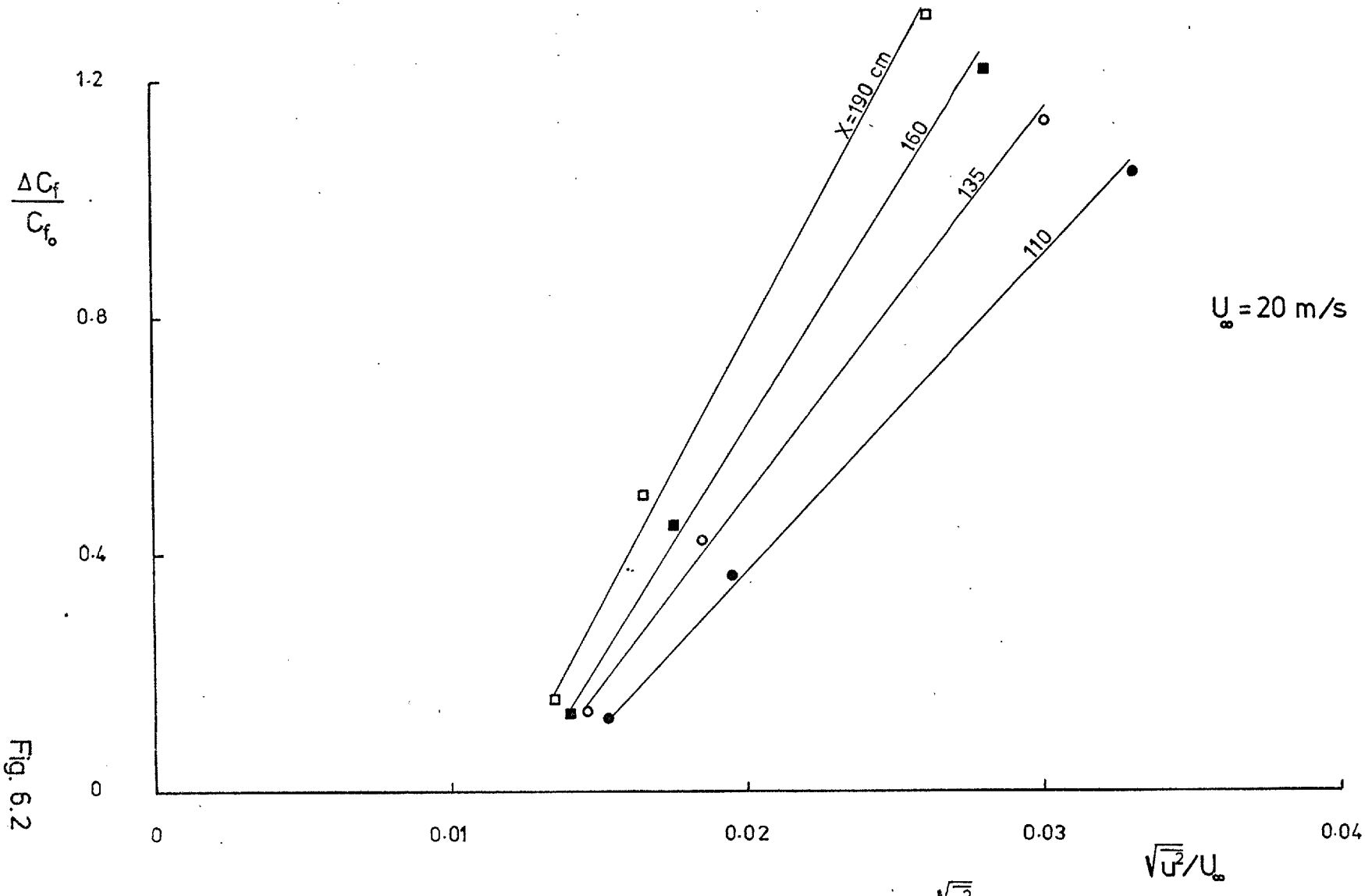
Fig. 5.17

Transition R_x over the plate with nose 5 (no +ve P.G. over the nose) .



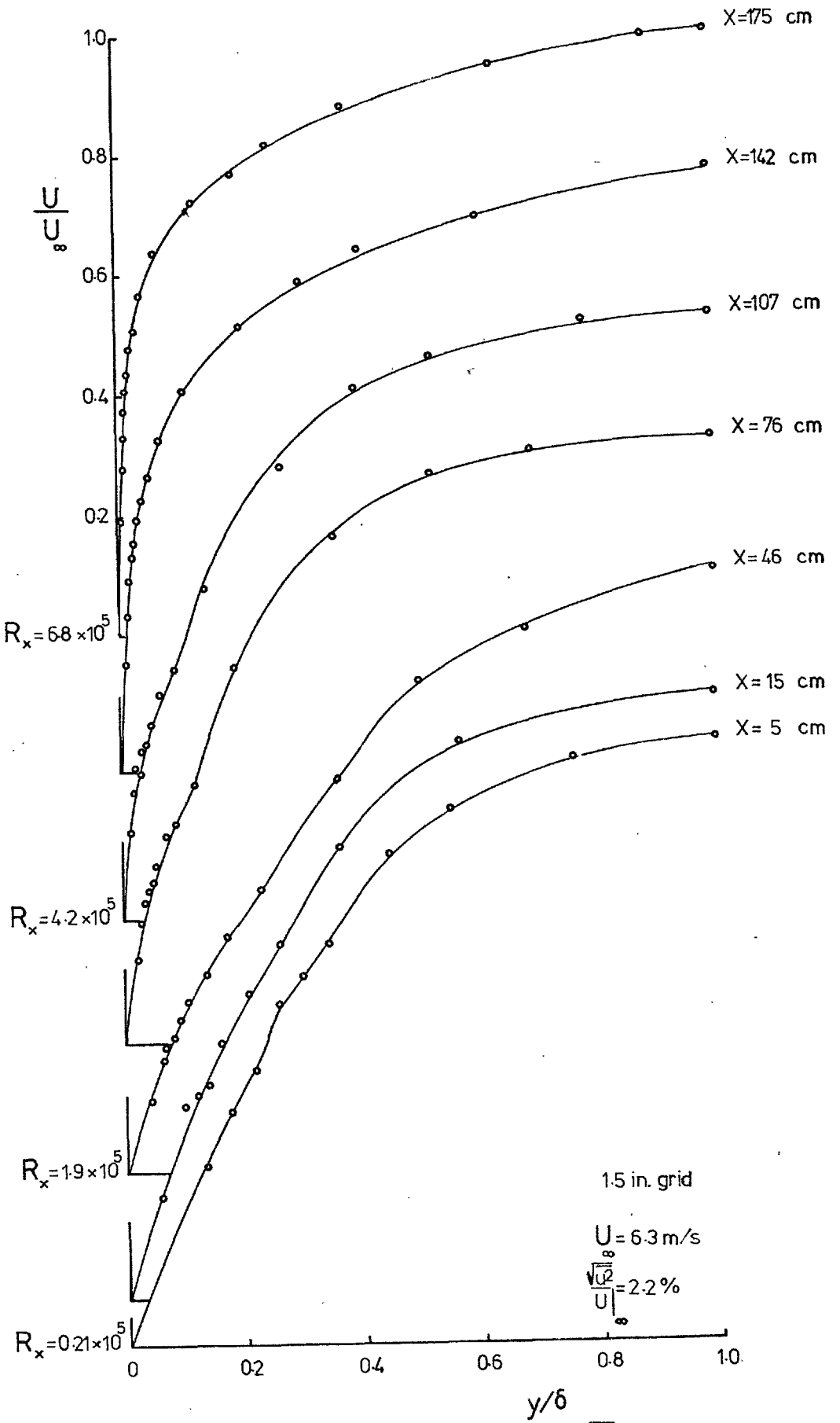
C_f distribution over the plate (nose 1).

Fig. 6.1



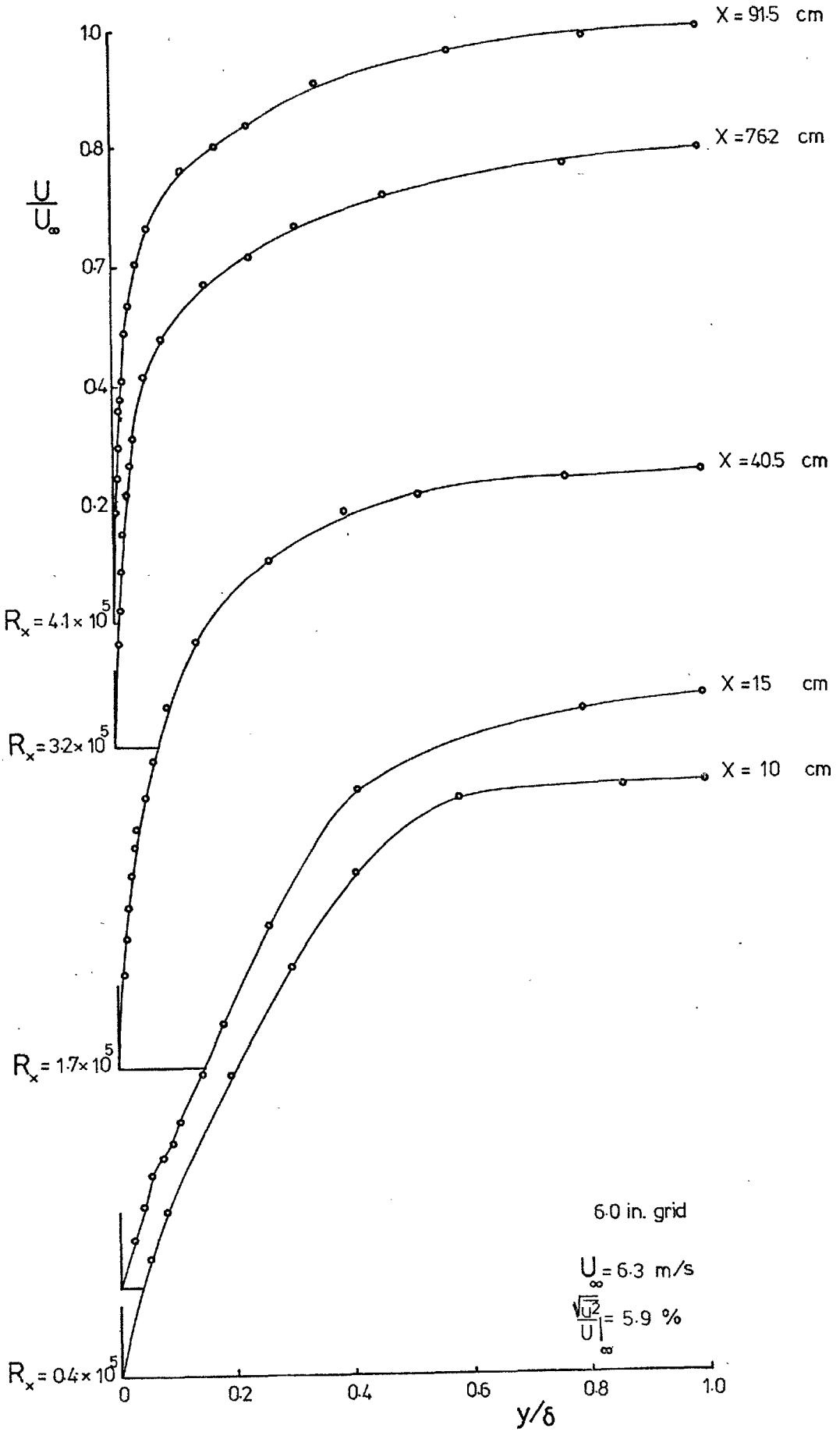
Changes in C_f caused by changes in $\frac{\sqrt{\overline{u^2}}}{U}$.

Fig. 6.2



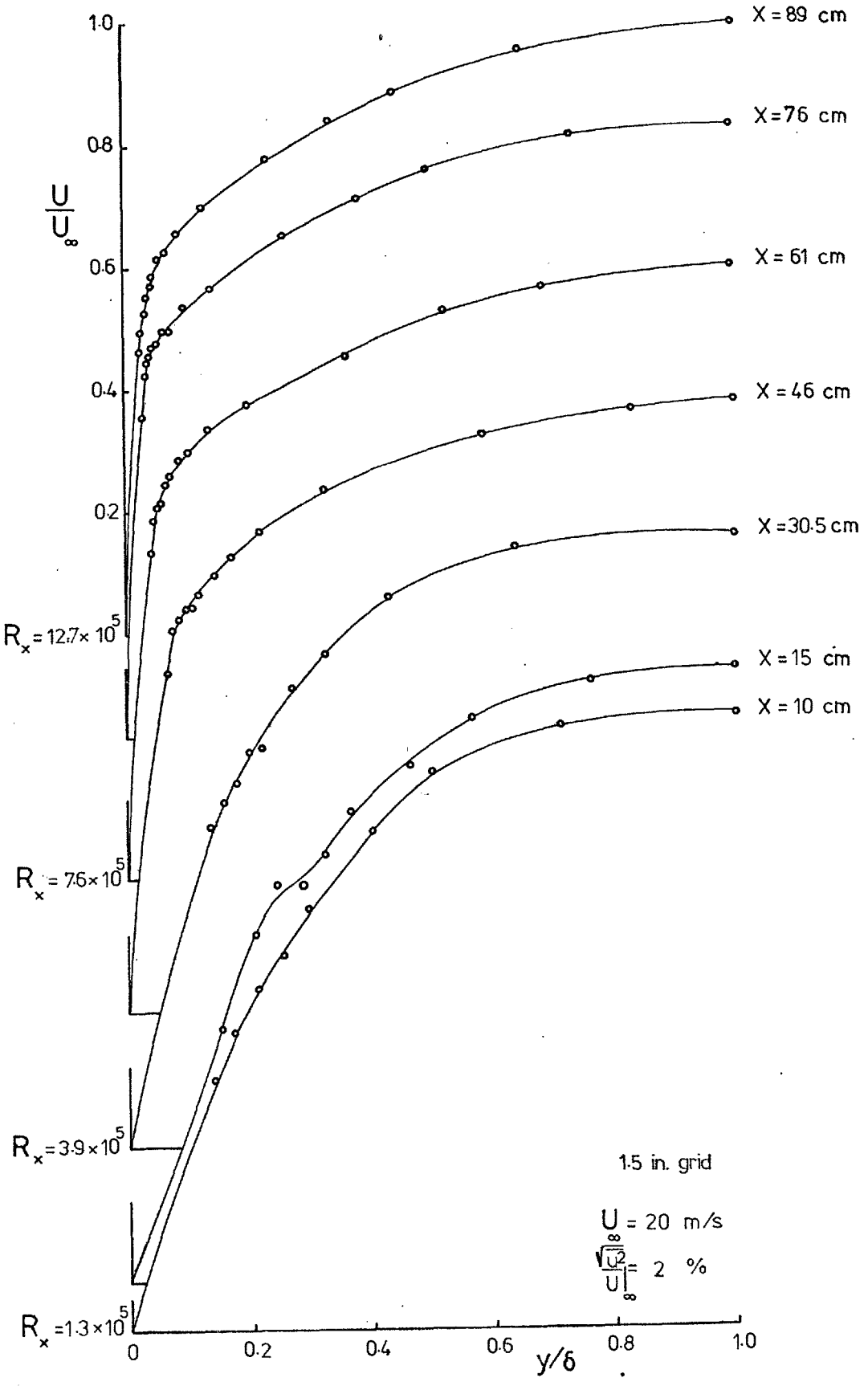
The U-profiles over the plate (for different $\frac{\sqrt{\overline{u^2}}}{U}\Big|_\infty$ "nose1")

Fig. 6.3



(For legend see fig. 6.3)

Fig. 6.4



(For legend see fig. 6.3)

Fig. 6.5

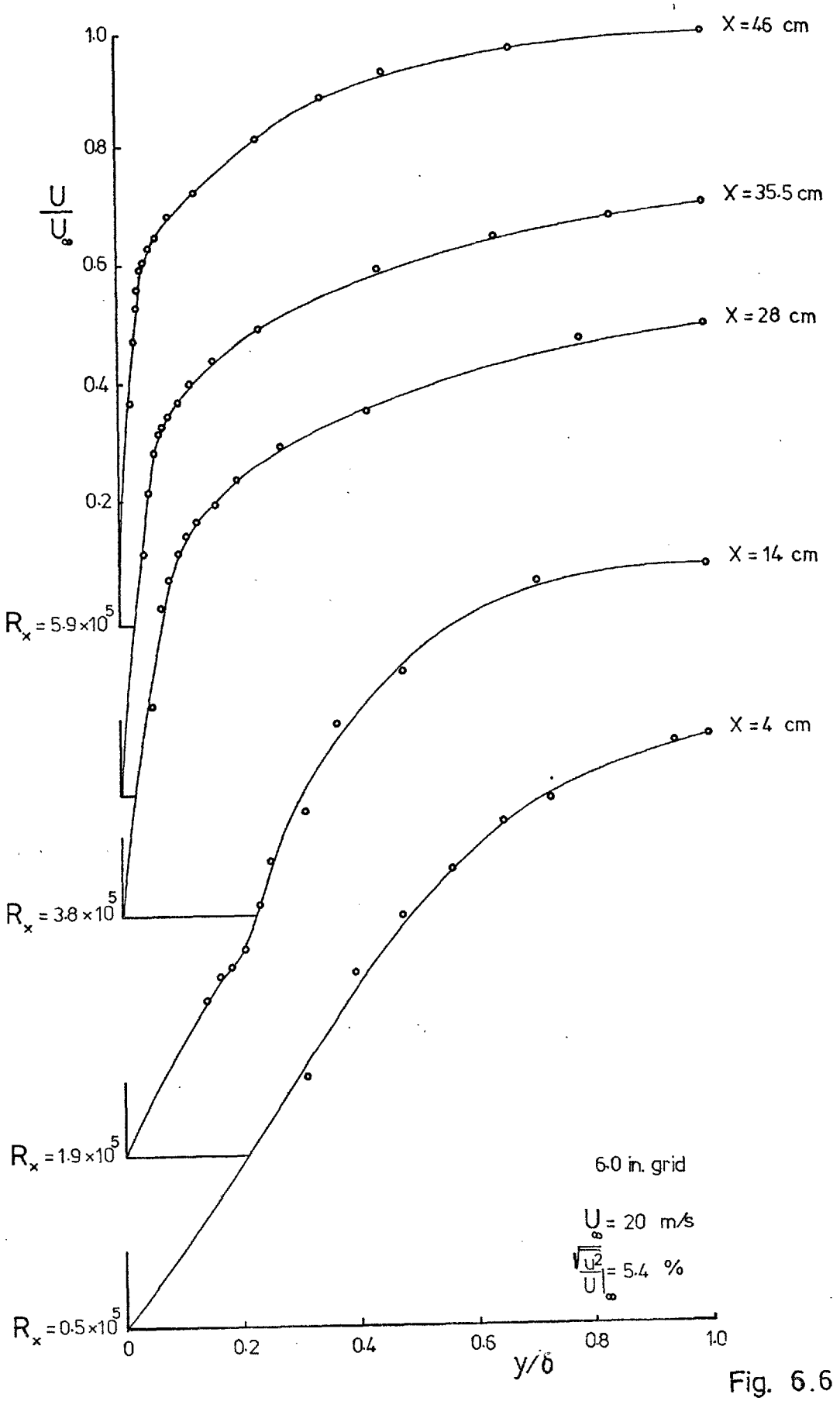
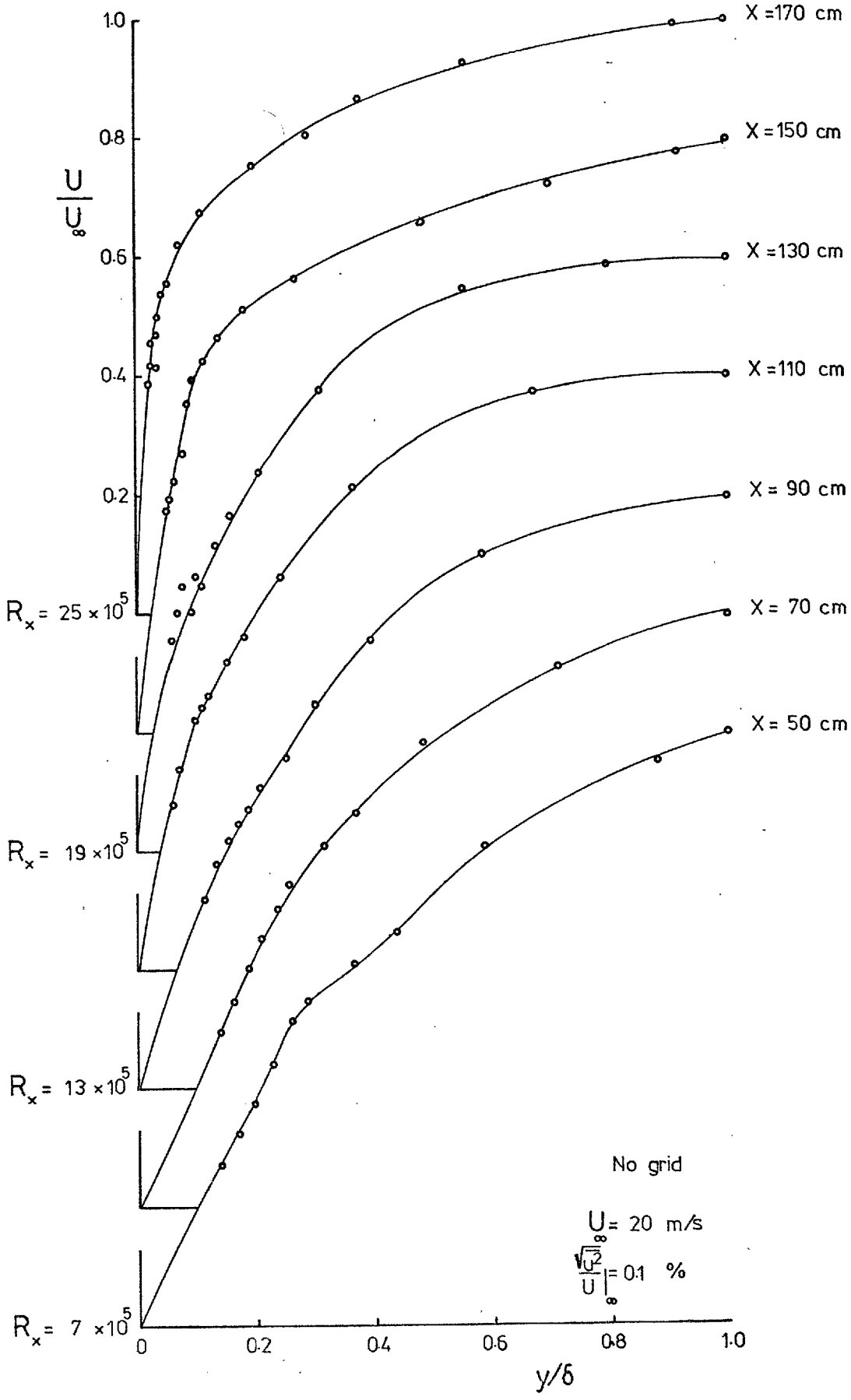


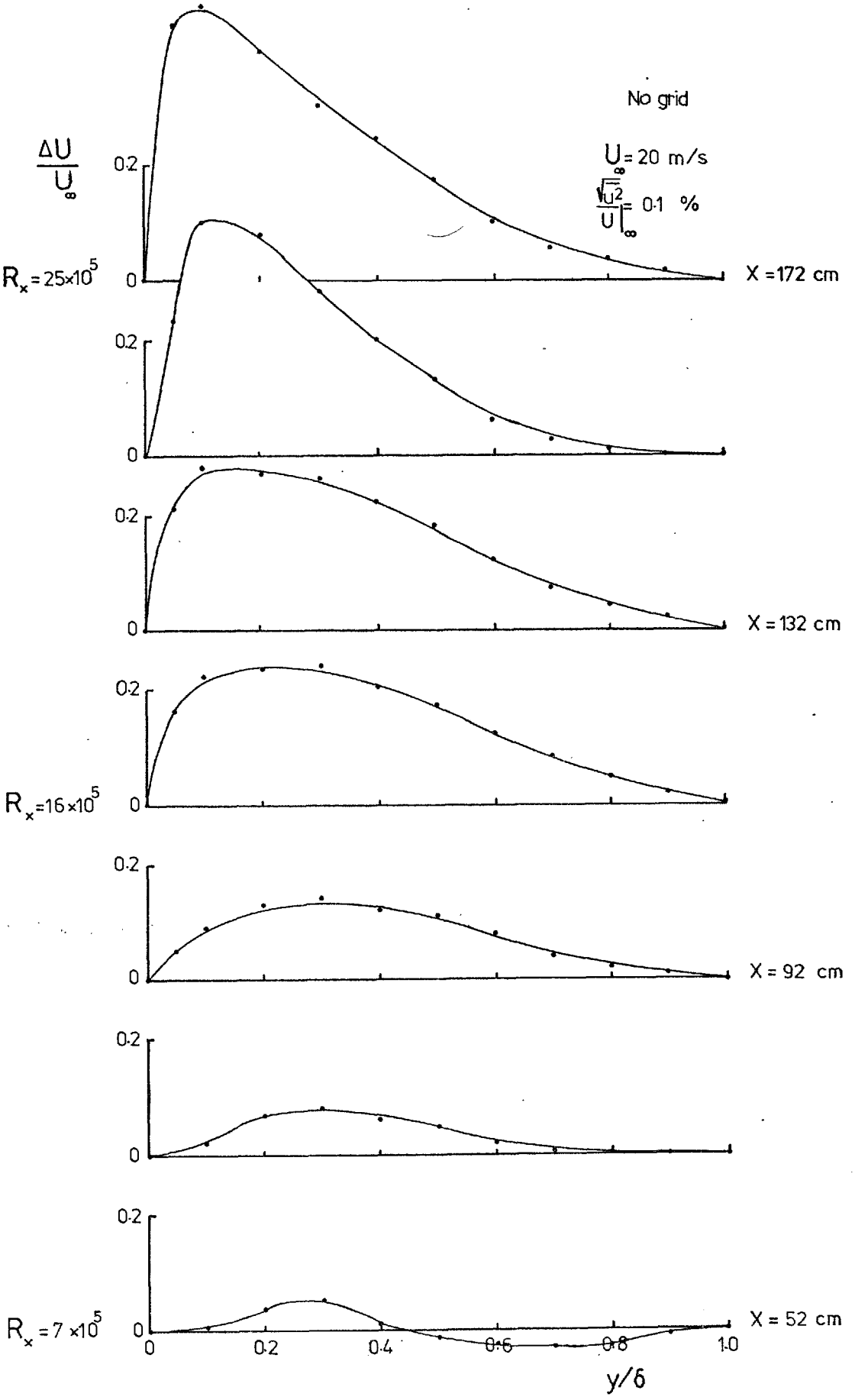
Fig. 6.6

(For legend see fig. 6.3)



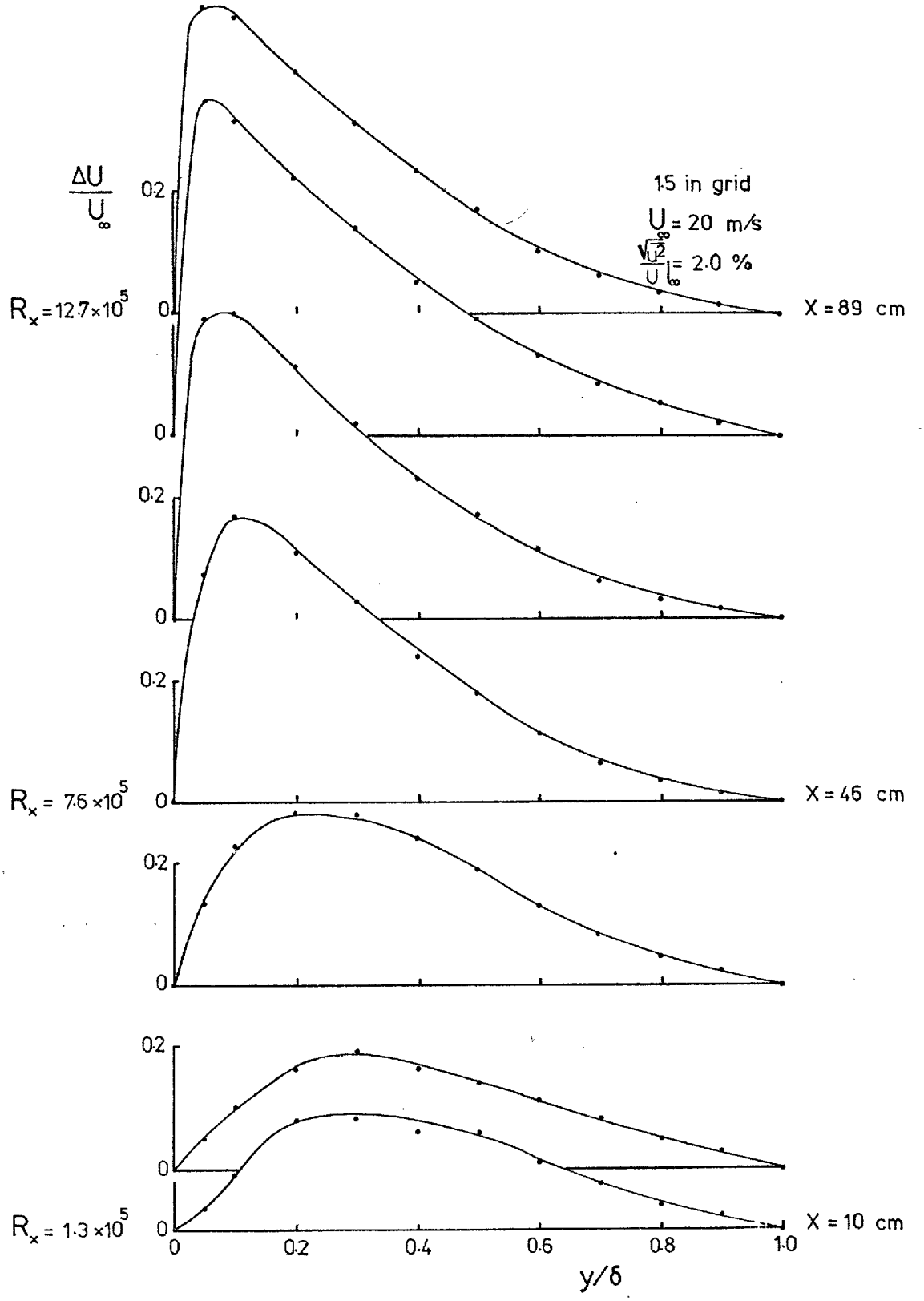
(For legend see fig. 6.3)

Fig. 6.7



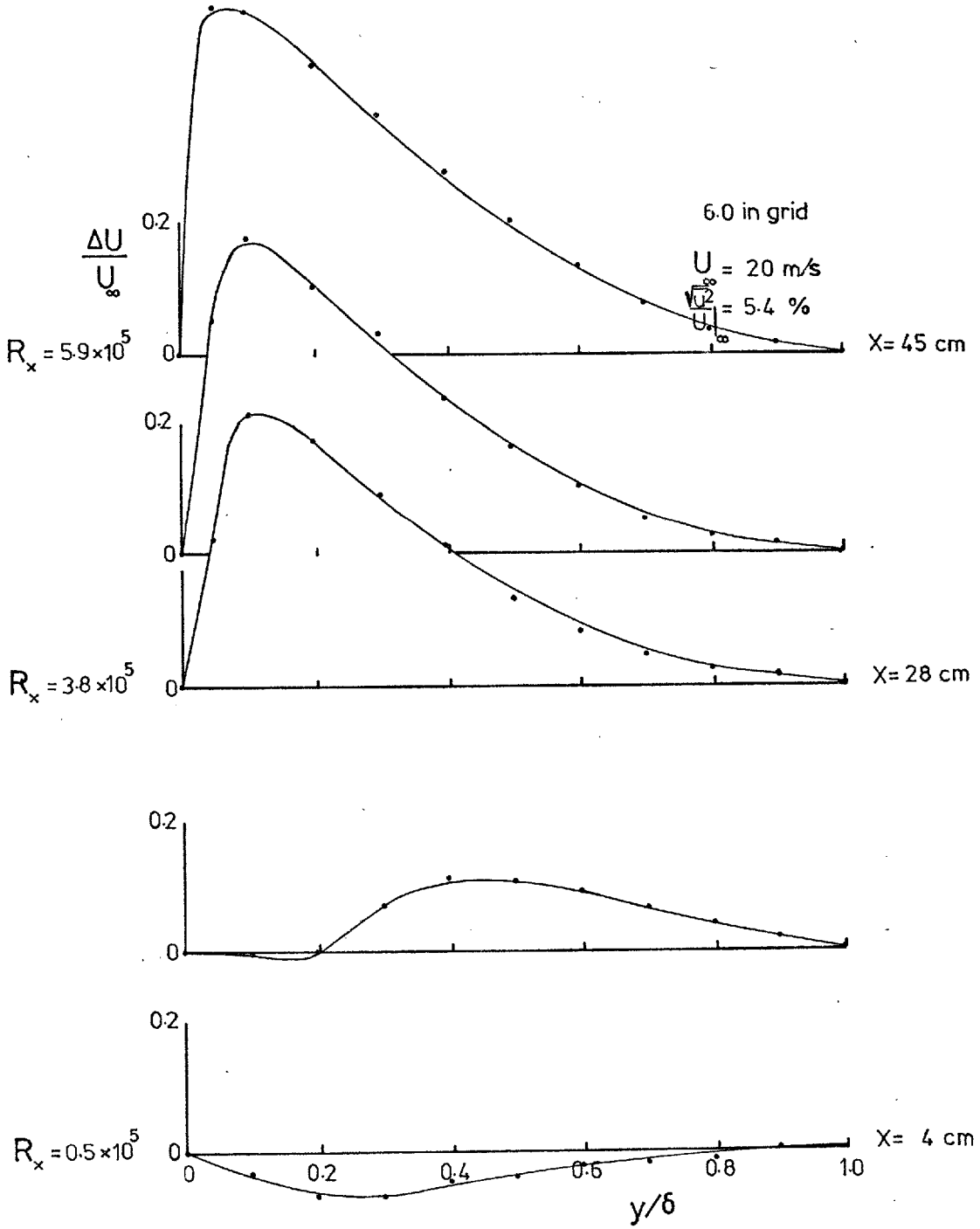
The deviation of the U-profiles from the Blasius profile.

Fig. 6.8



(For legend see fig. 6.8)

Fig. 6.9



(For legend see fig. 6.8)

Fig. 6.10

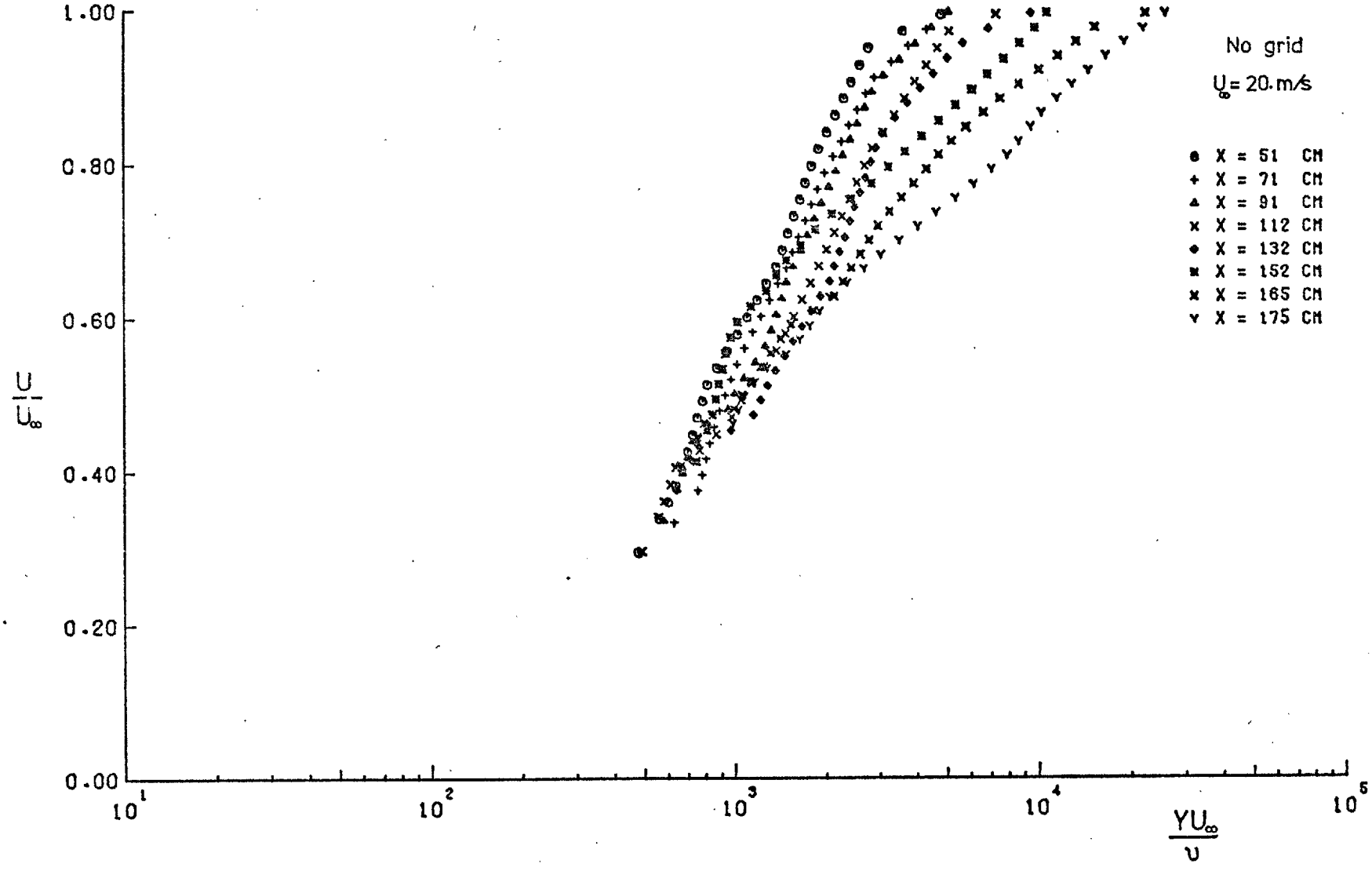
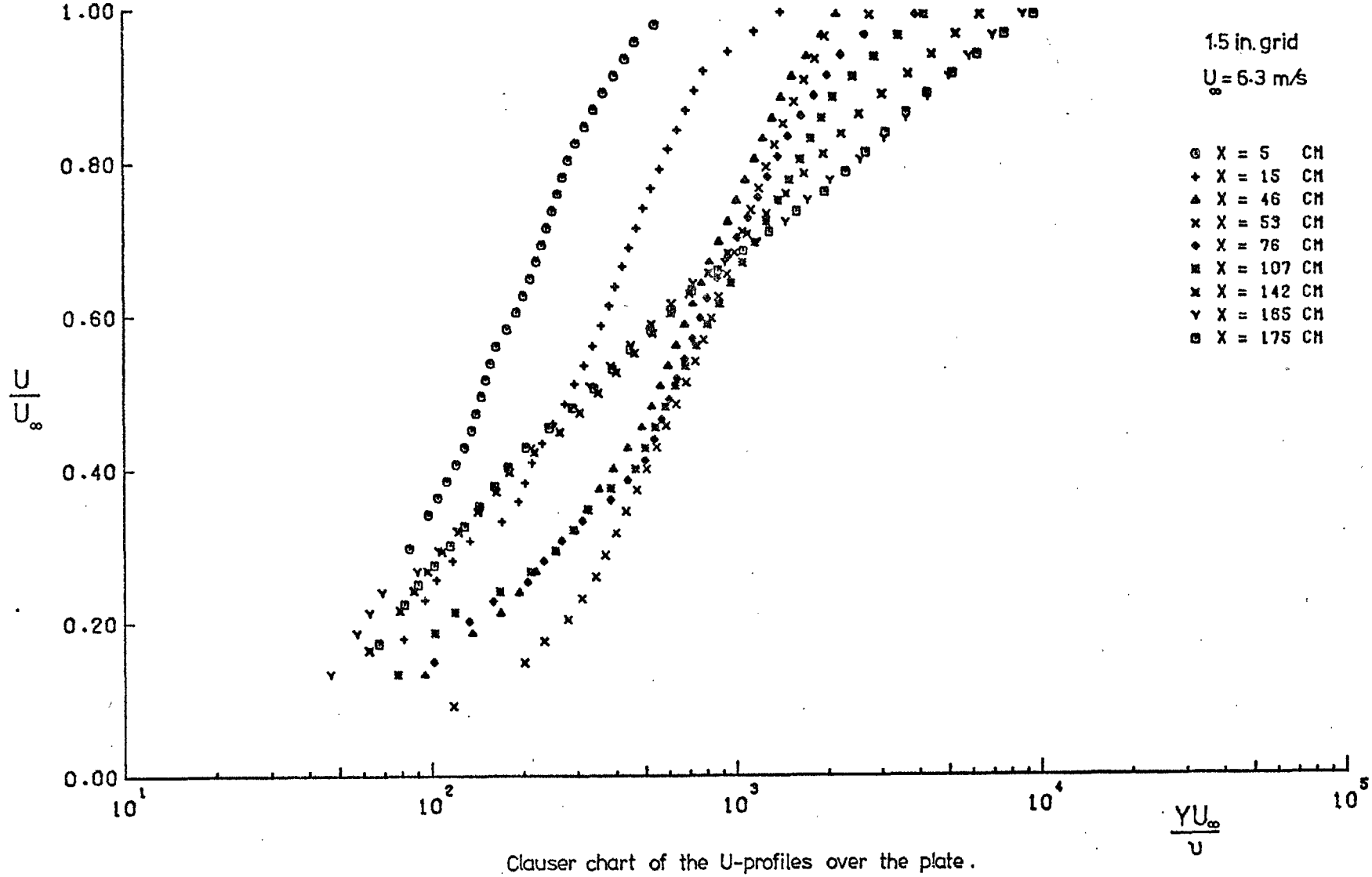


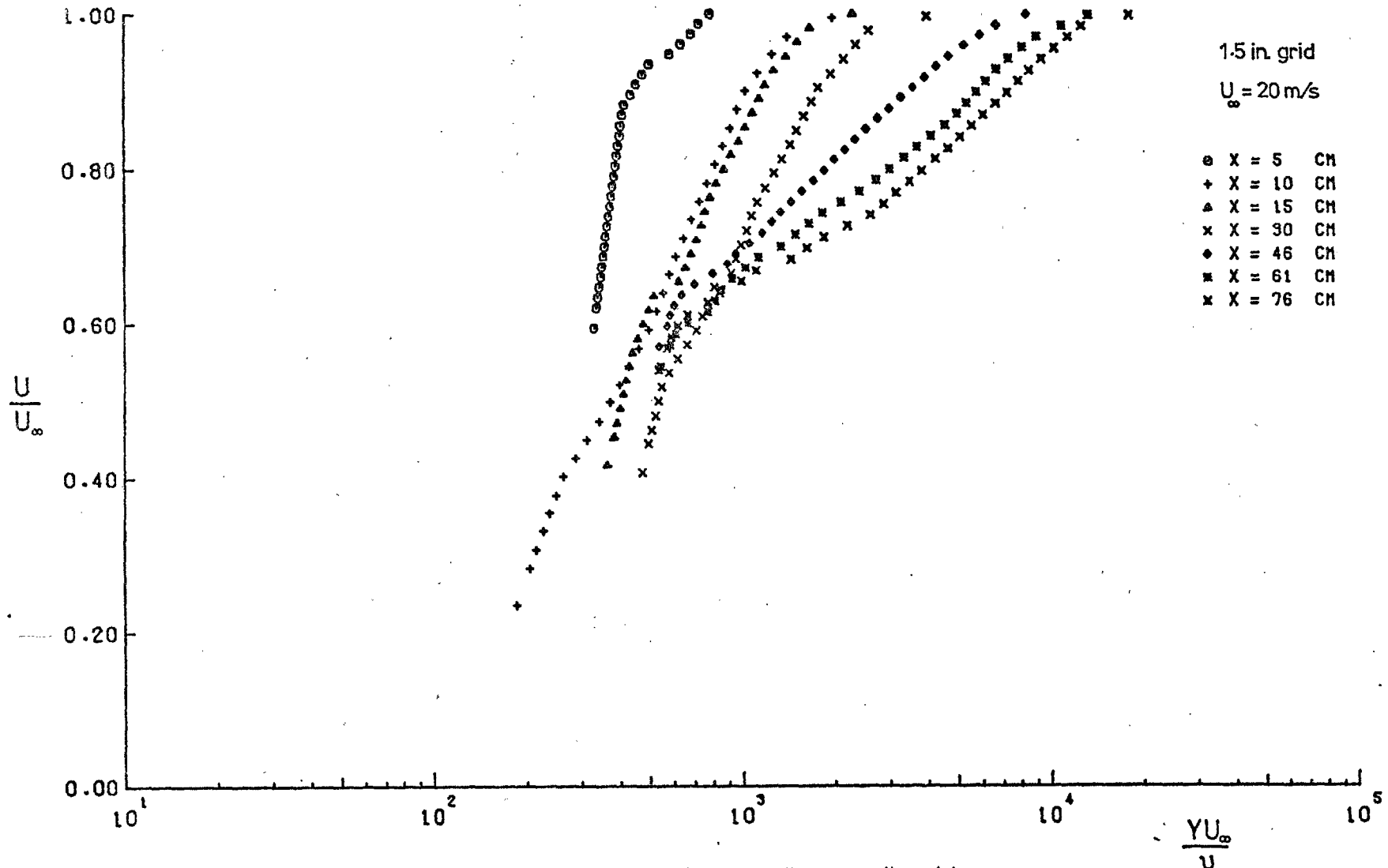
Fig. 6.11

Clauser chart of the U-profiles over the plate .



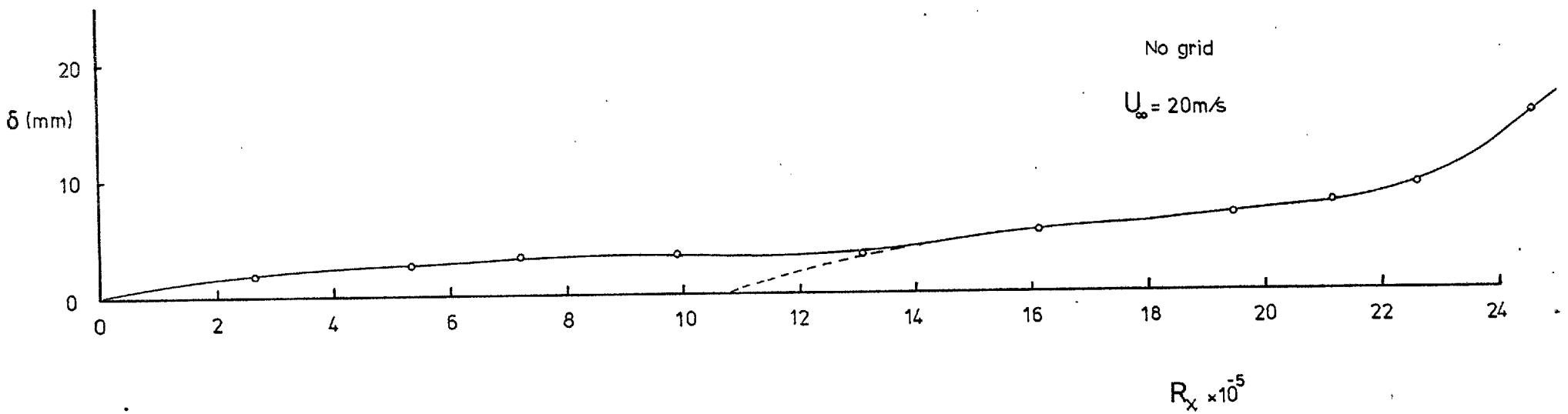
Clauser chart of the U-profiles over the plate.

Fig. 6.12



Clauser chart of the U-profiles over the plate .

Fig. 6.13



Boundary layer growth over the plate.

Fig. 6.14

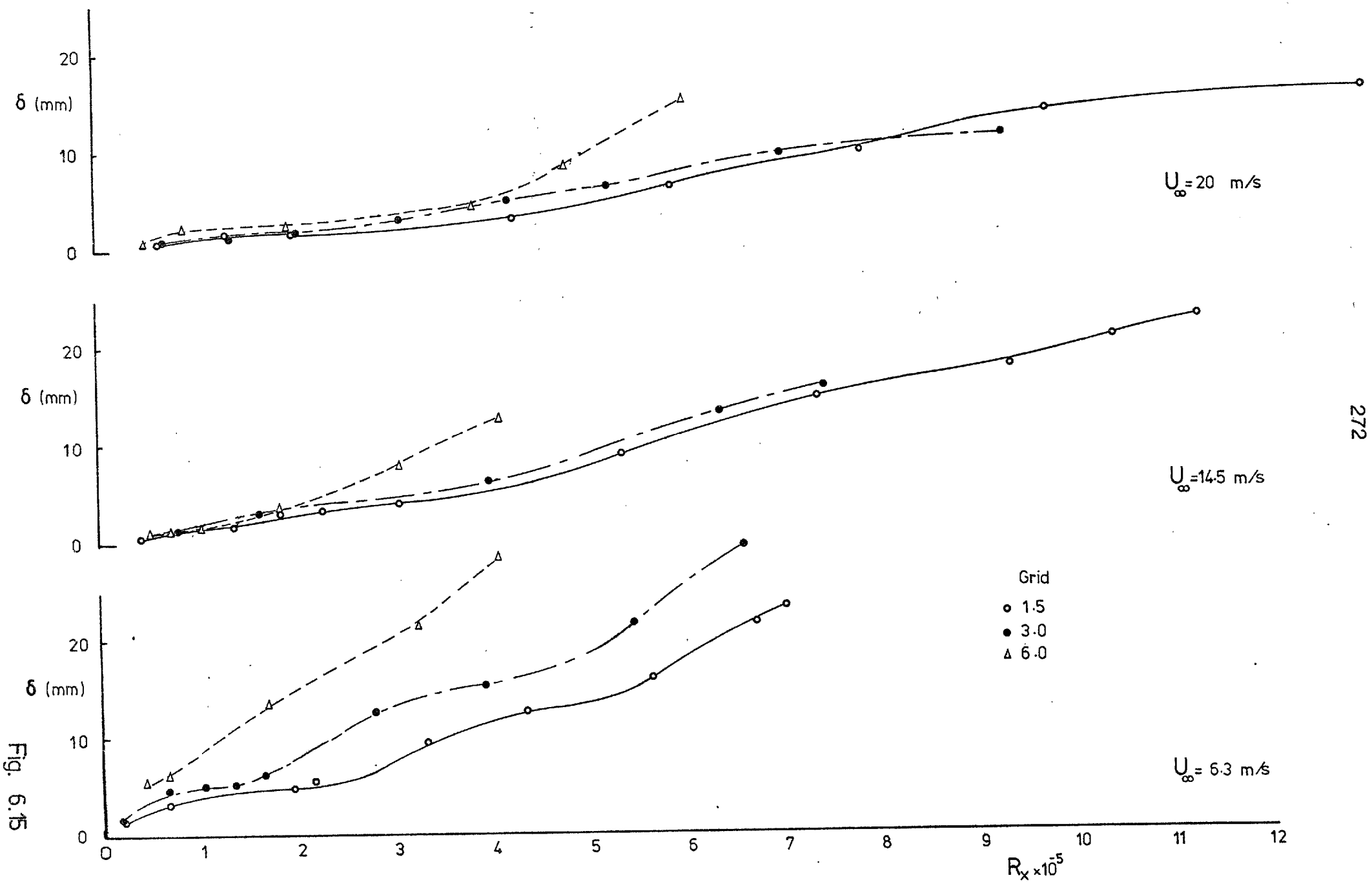


Fig. 6.15

Boundary layer growth over the plate.

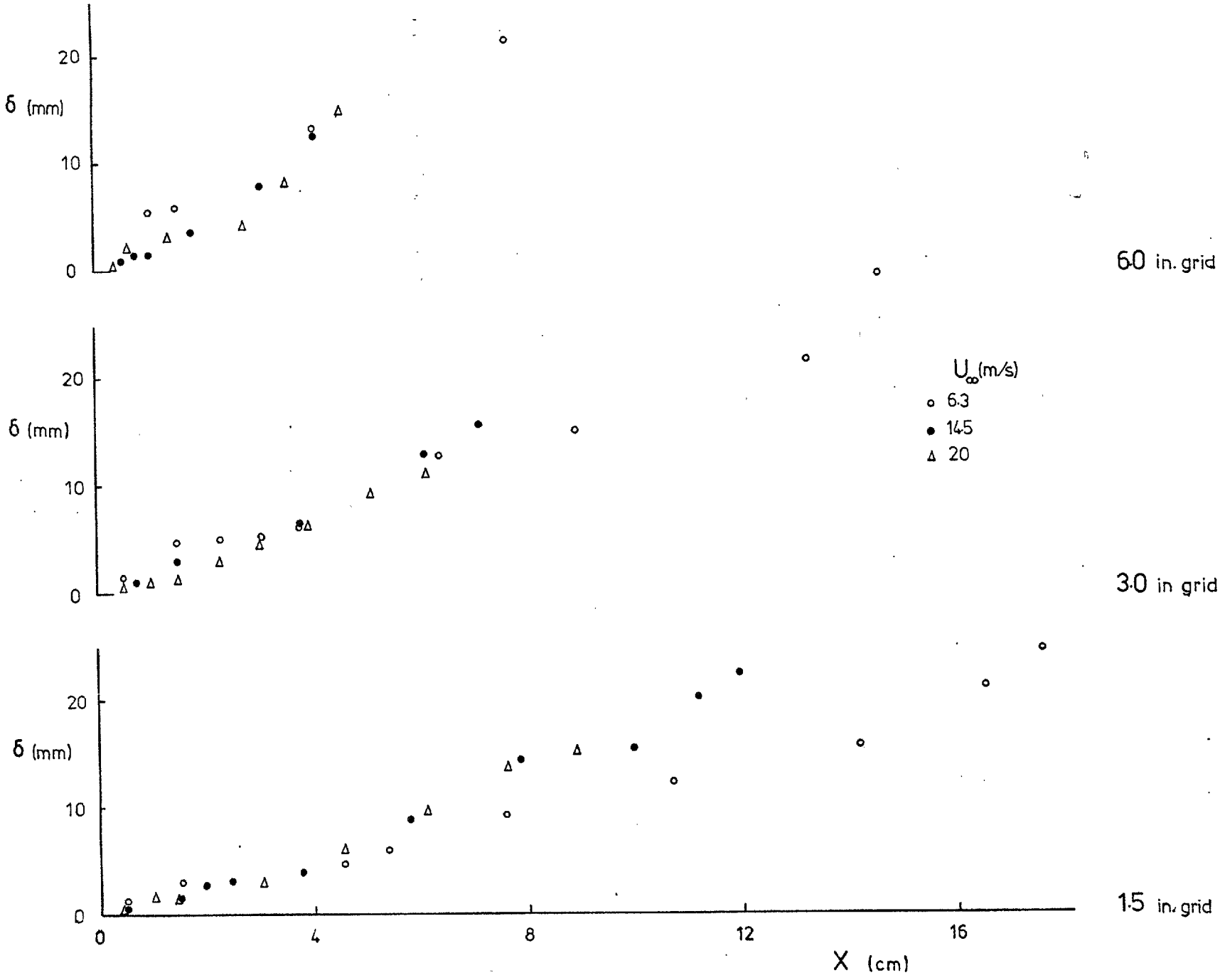
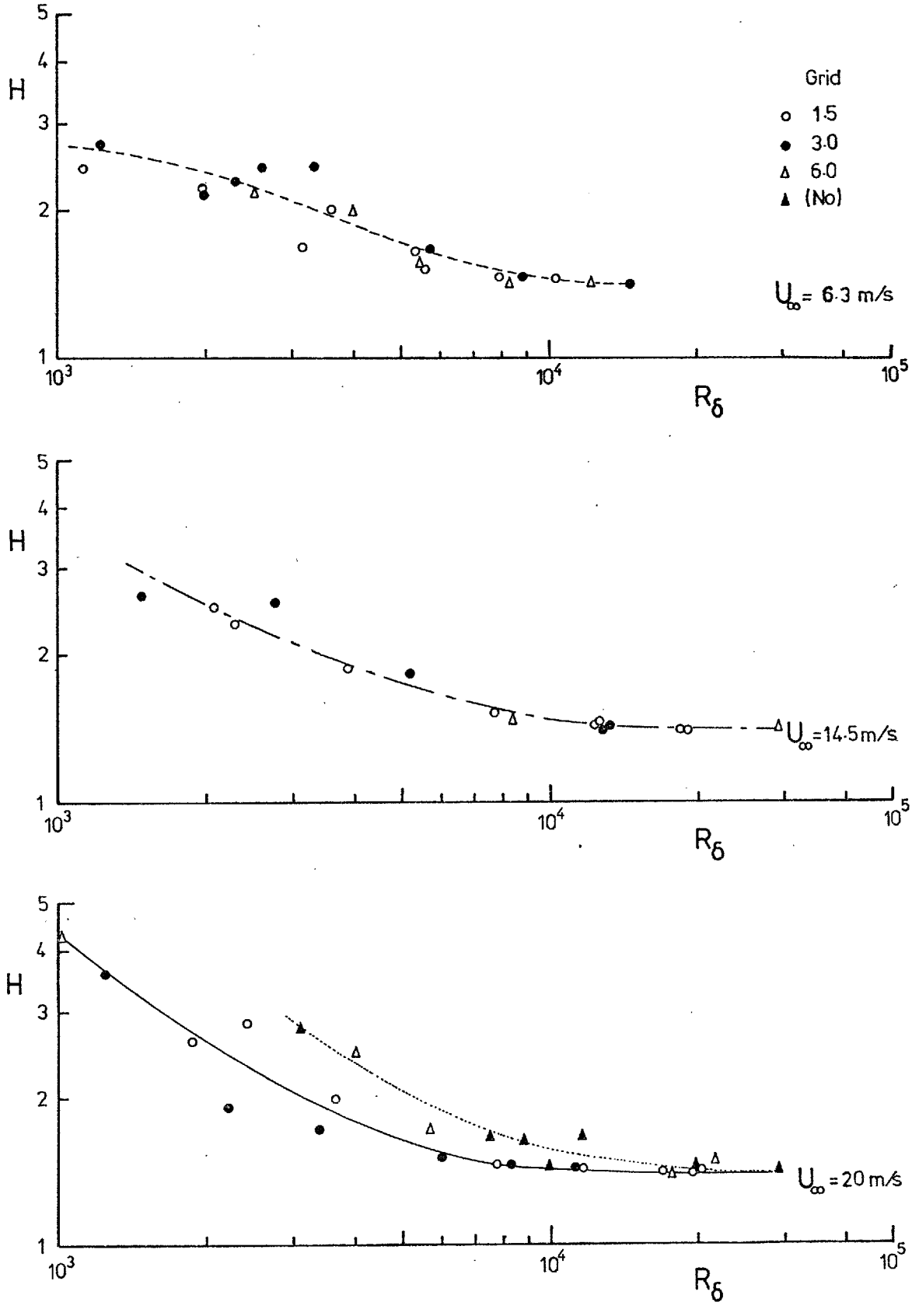


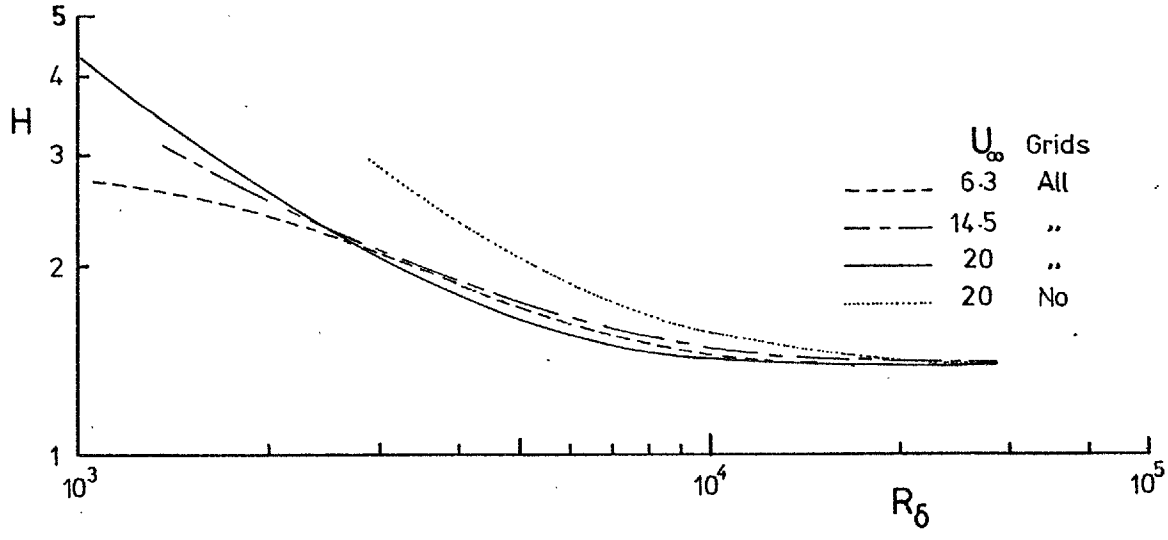
Fig. 6.15

Boundary layer growth over the plate.



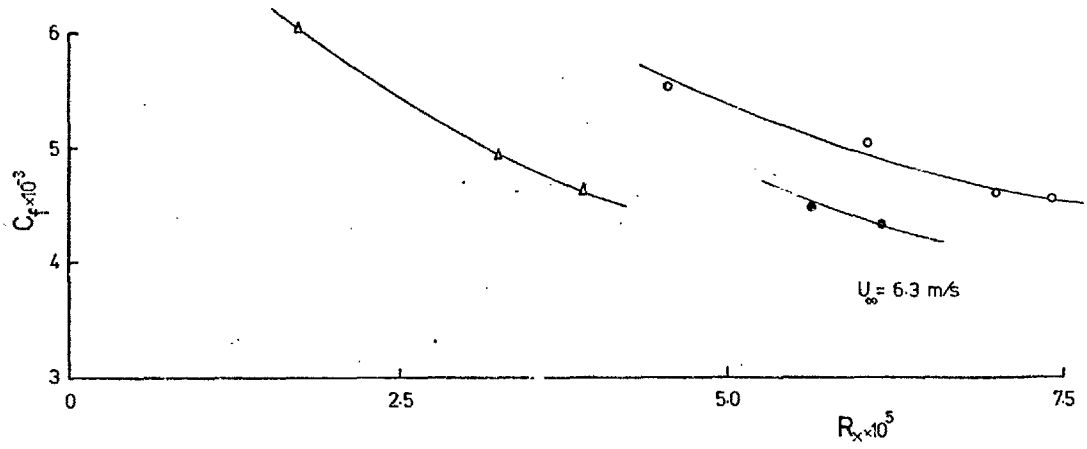
The effect of changes in $\frac{\sqrt{\overline{u^2}}}{U}$ on the boundary layer shape factor.

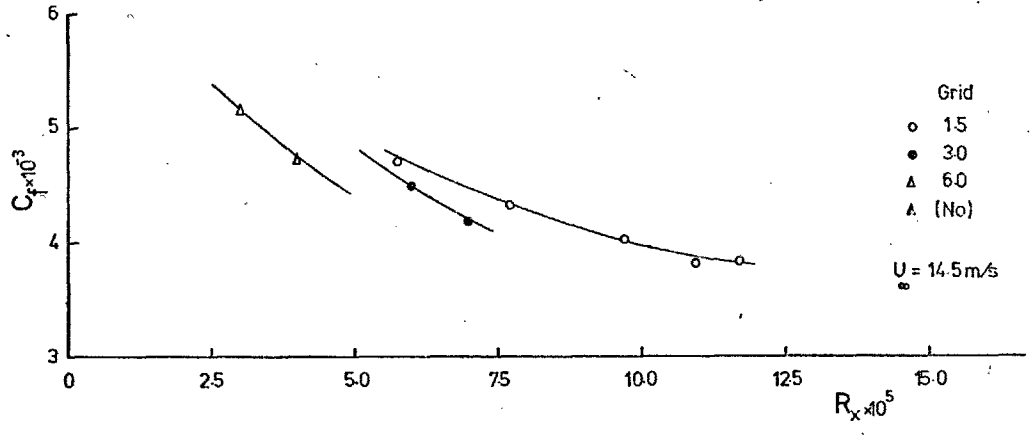
Fig. 6.17

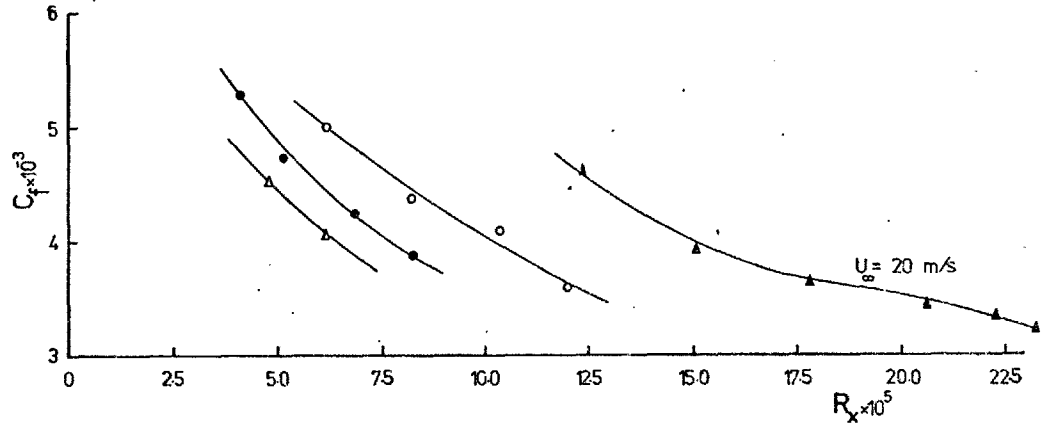


Curve presentation of the data in fig. 6.17

Fig. 6.18







C_f computed from the U-profiles.

Fig. 6.19

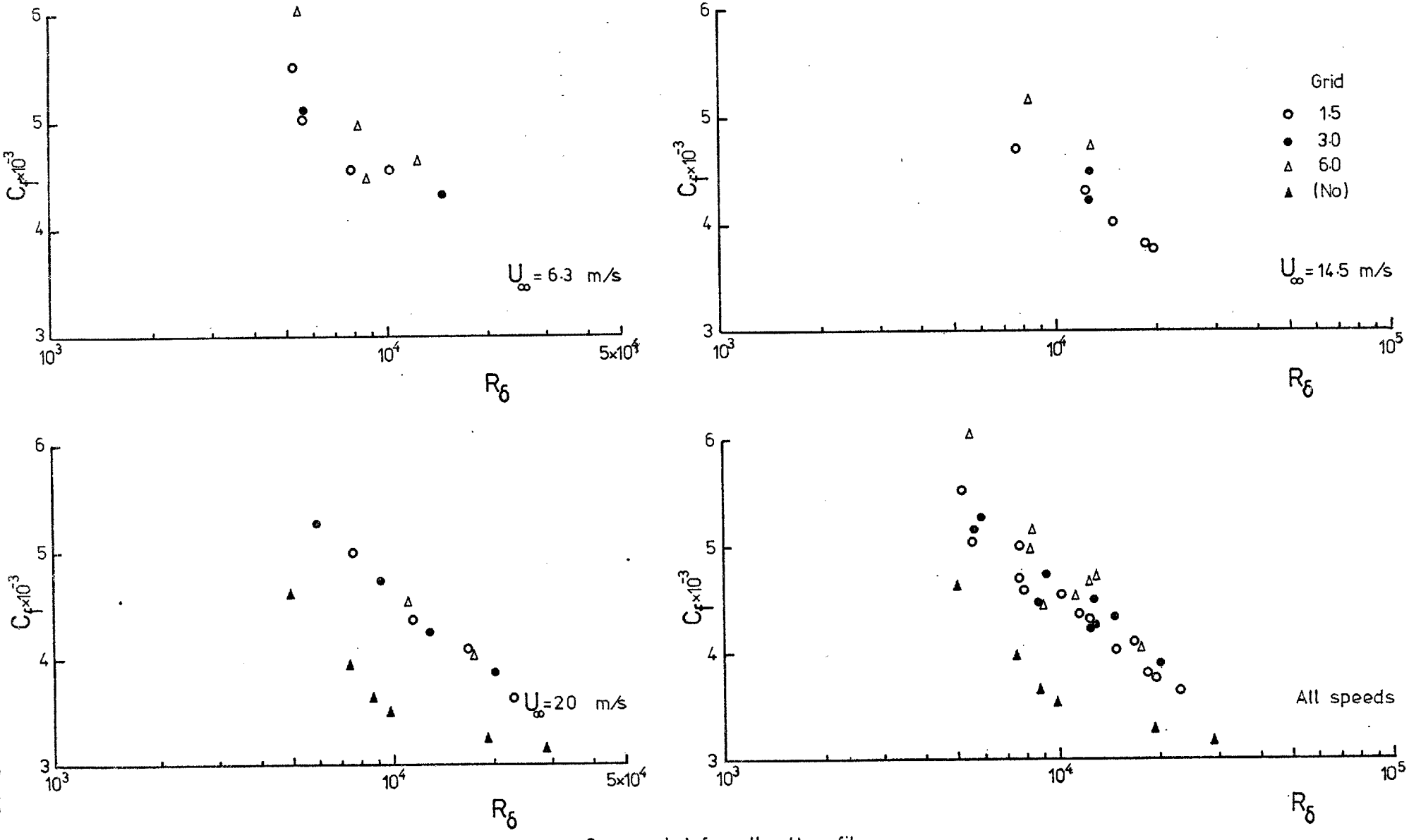


Fig. 6.20

C_f computed from the U-profiles.

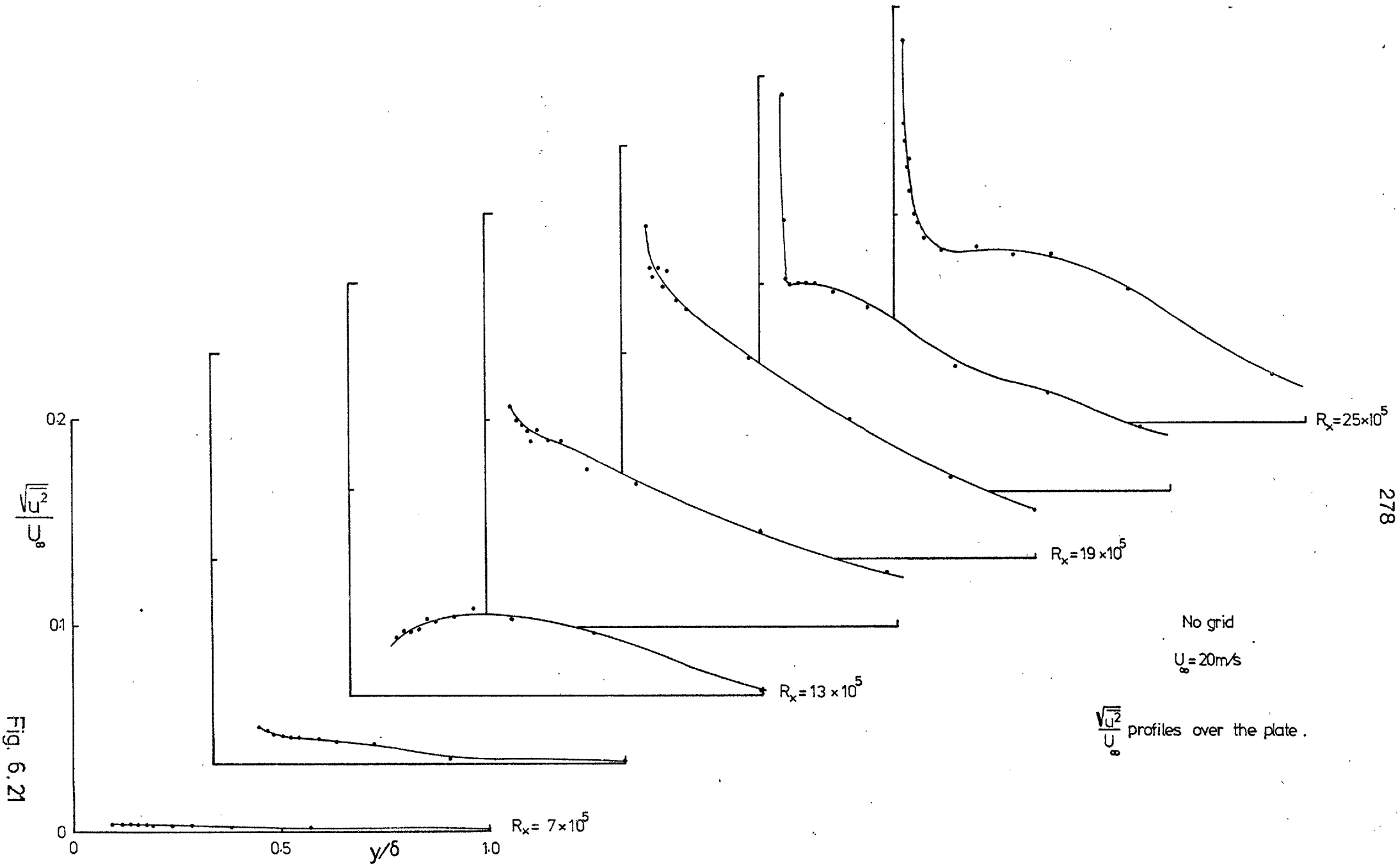


Fig. 6.21 $\frac{\sqrt{\overline{u^2}}}{U_\infty}$ profiles over the plate.

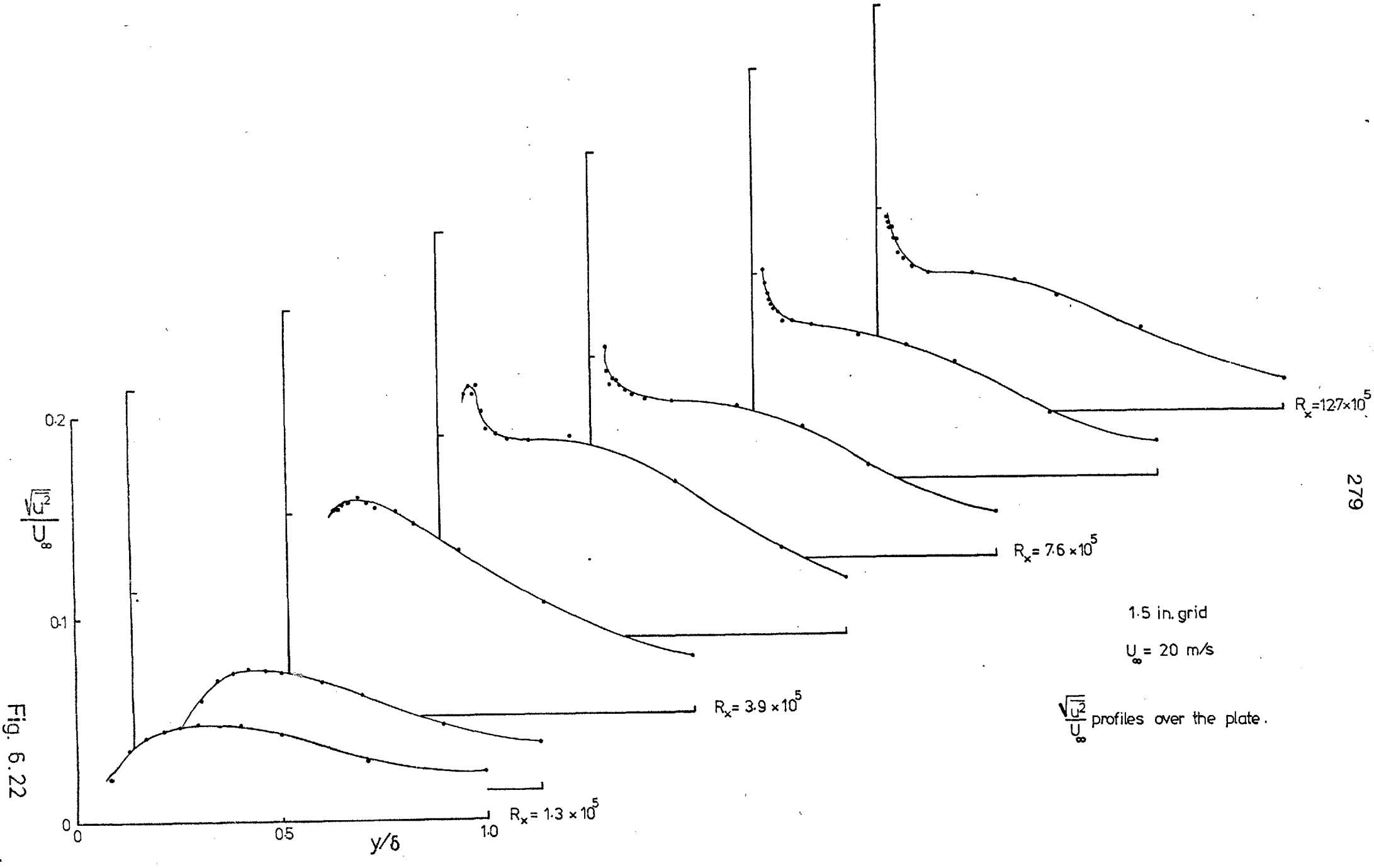

0·2
0·1
0
0
0·5
1·0
y/δ
$\frac{\sqrt{\overline{u^2}}}{U_\infty}$
$R_x = 1·3 \times 10^5$
$R_x = 3·9 \times 10^5$
$R_x = 7·6 \times 10^5$
$R_x = 12·7 \times 10^5$
1·5 in. grid
U_∞ = 20 m/s
$\frac{\sqrt{\overline{u^2}}}{U_\infty}$ profiles over the plate.

Fig. 6.22

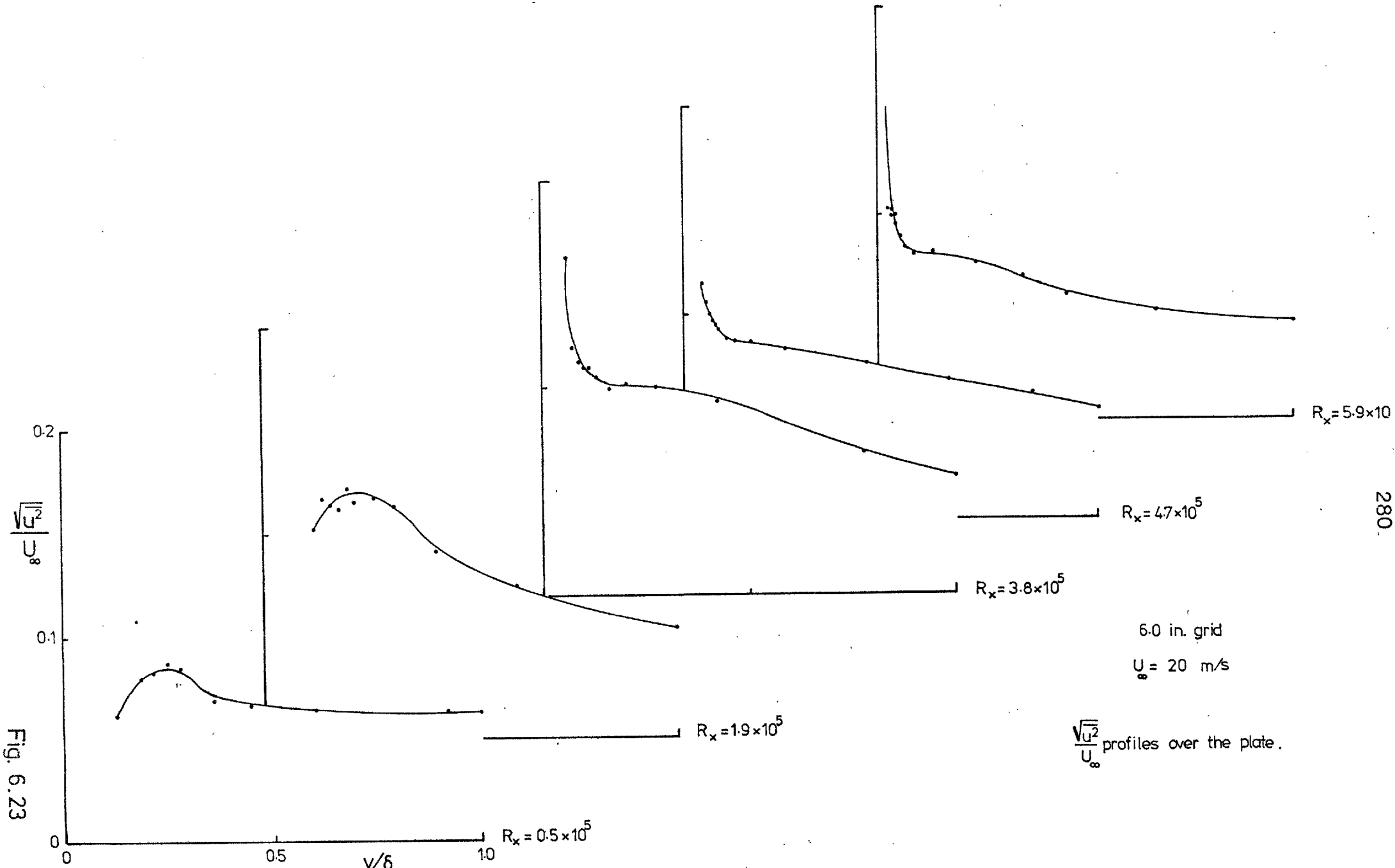


Fig. 6.23 $\frac{\sqrt{\overline{u^2}}}{U_\infty}$ profiles over the plate.

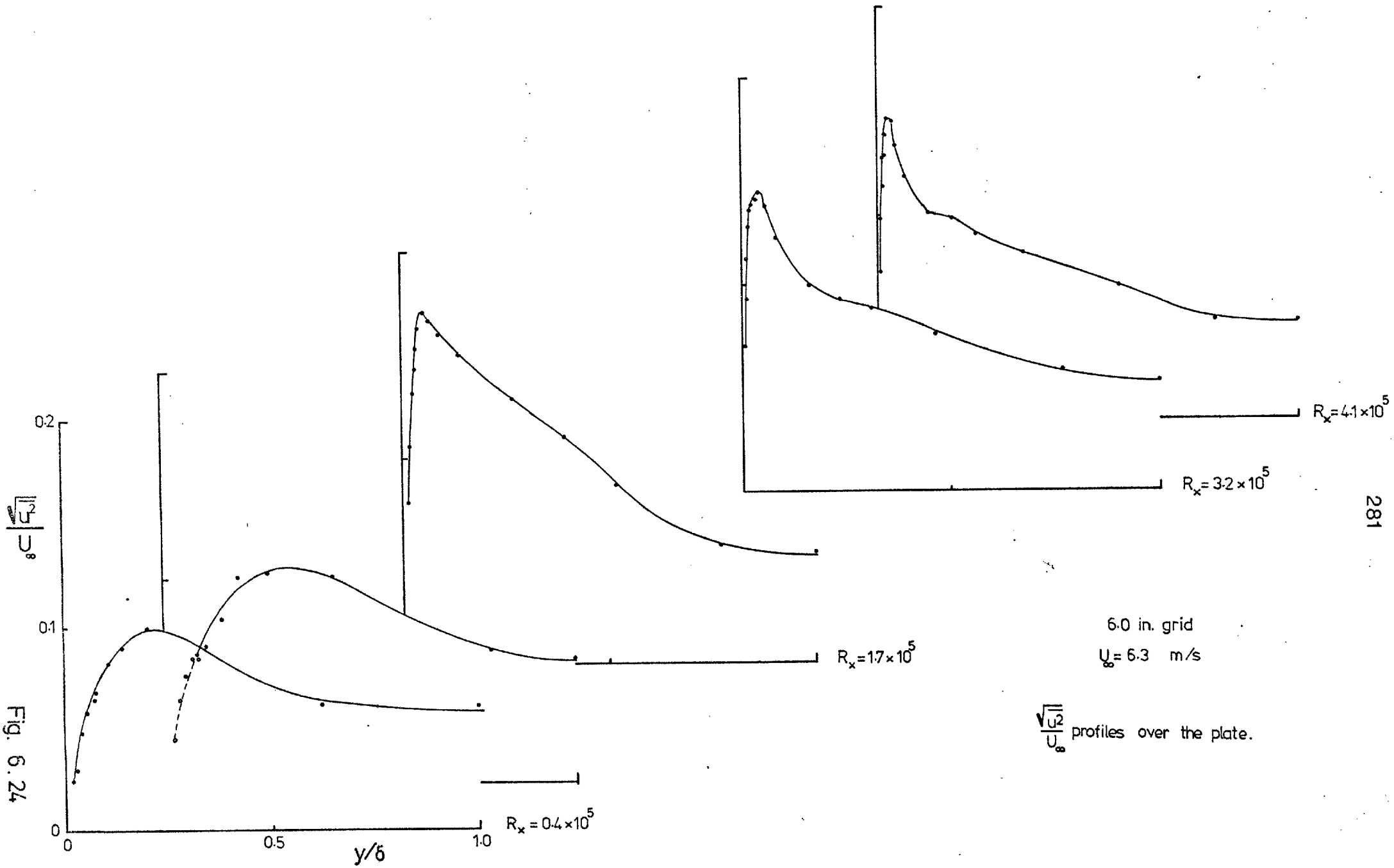
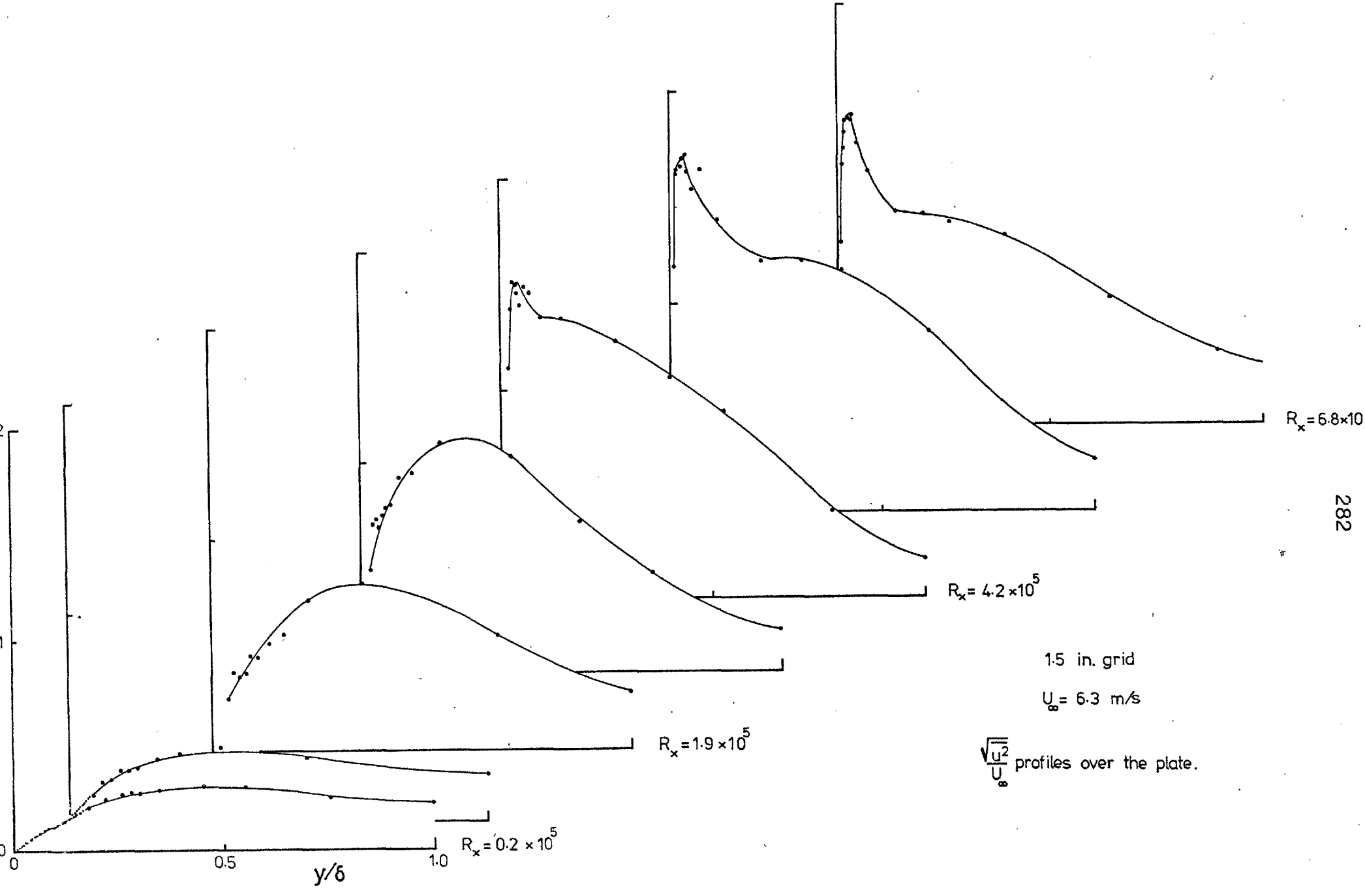


Fig. 6.24

6·0 in. grid

U_∞ = 6.3 m/s

$\frac{\sqrt{u^2}}{U_\infty}$ profiles over the plate.

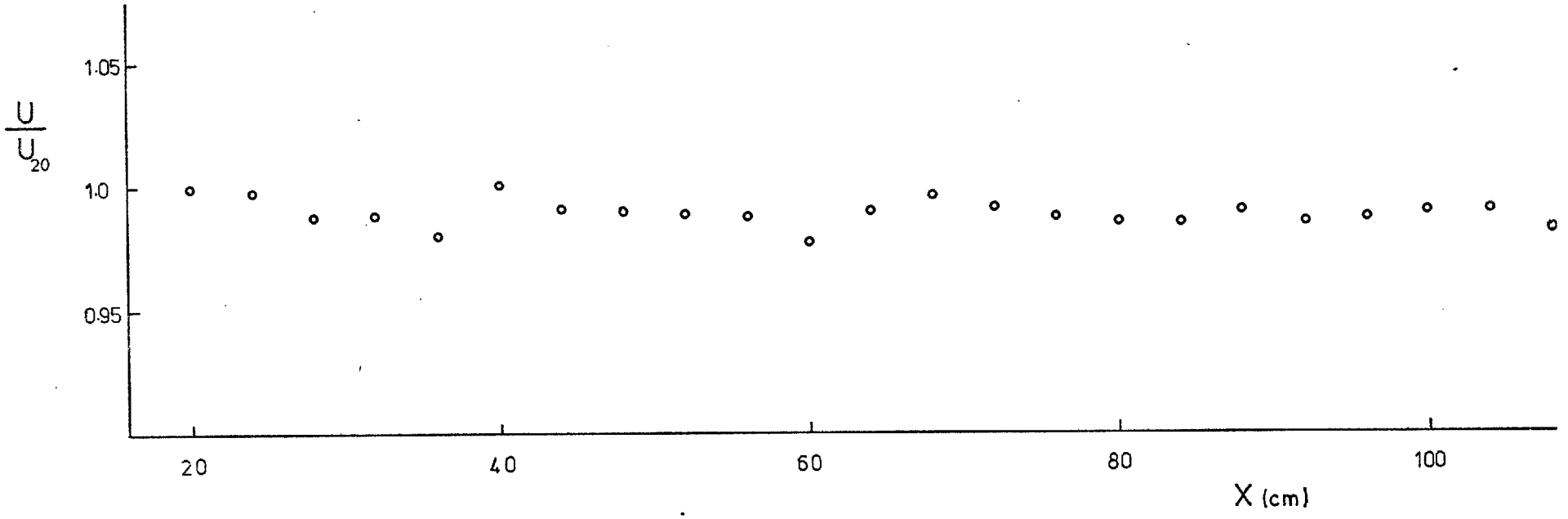


1.5 in. grid

U_∞ = 6.3 m/s

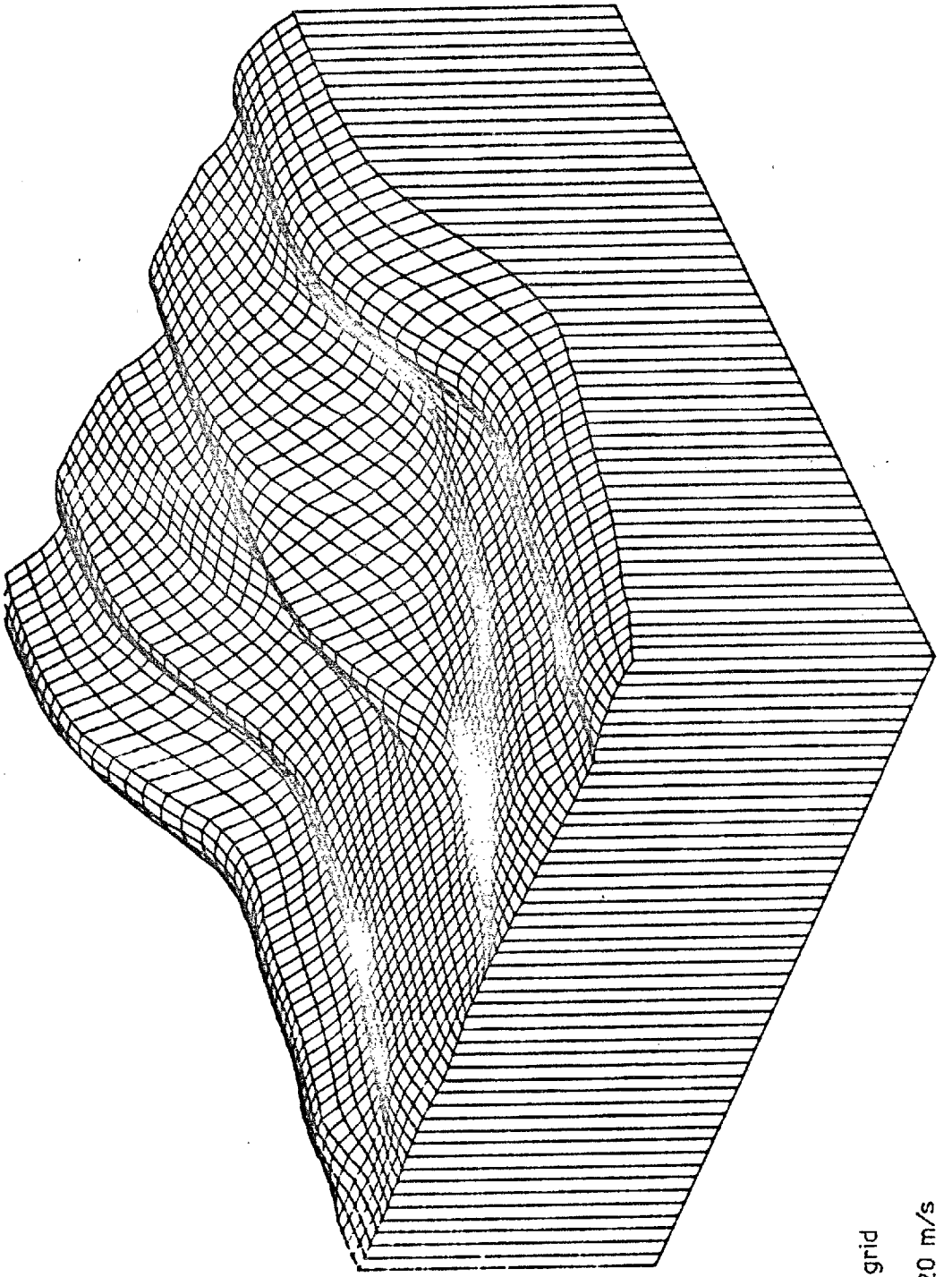
$\frac{\sqrt{u^2}}{U_\infty}$ profiles over the plate.

Fig. 6.25



U_∞ along the plate (1.5 in. grid , U_{20} = 8.5 m/s)

Fig. 6.26

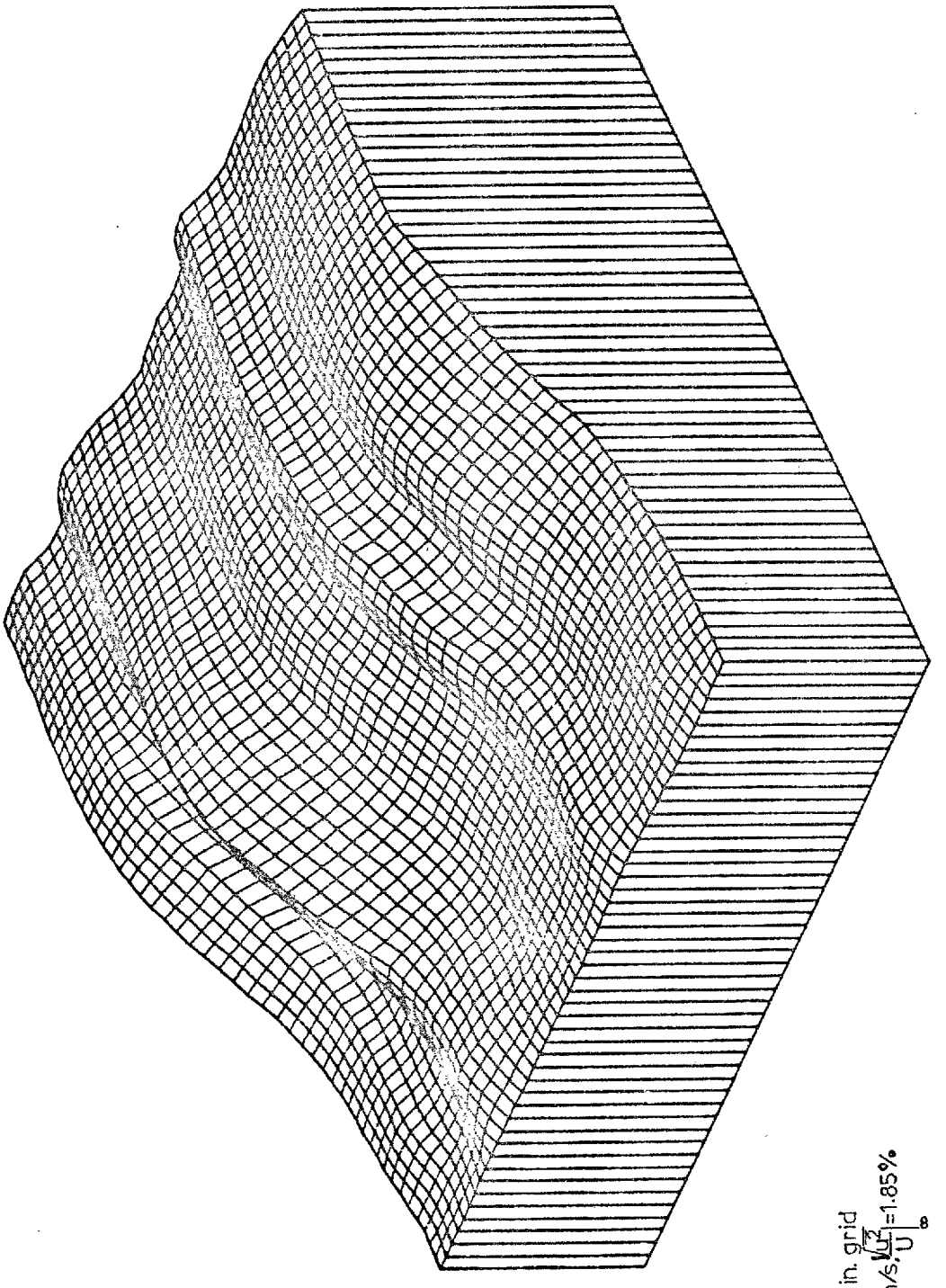


No grid

U_∞ = 20 m/s

C_f around transition.

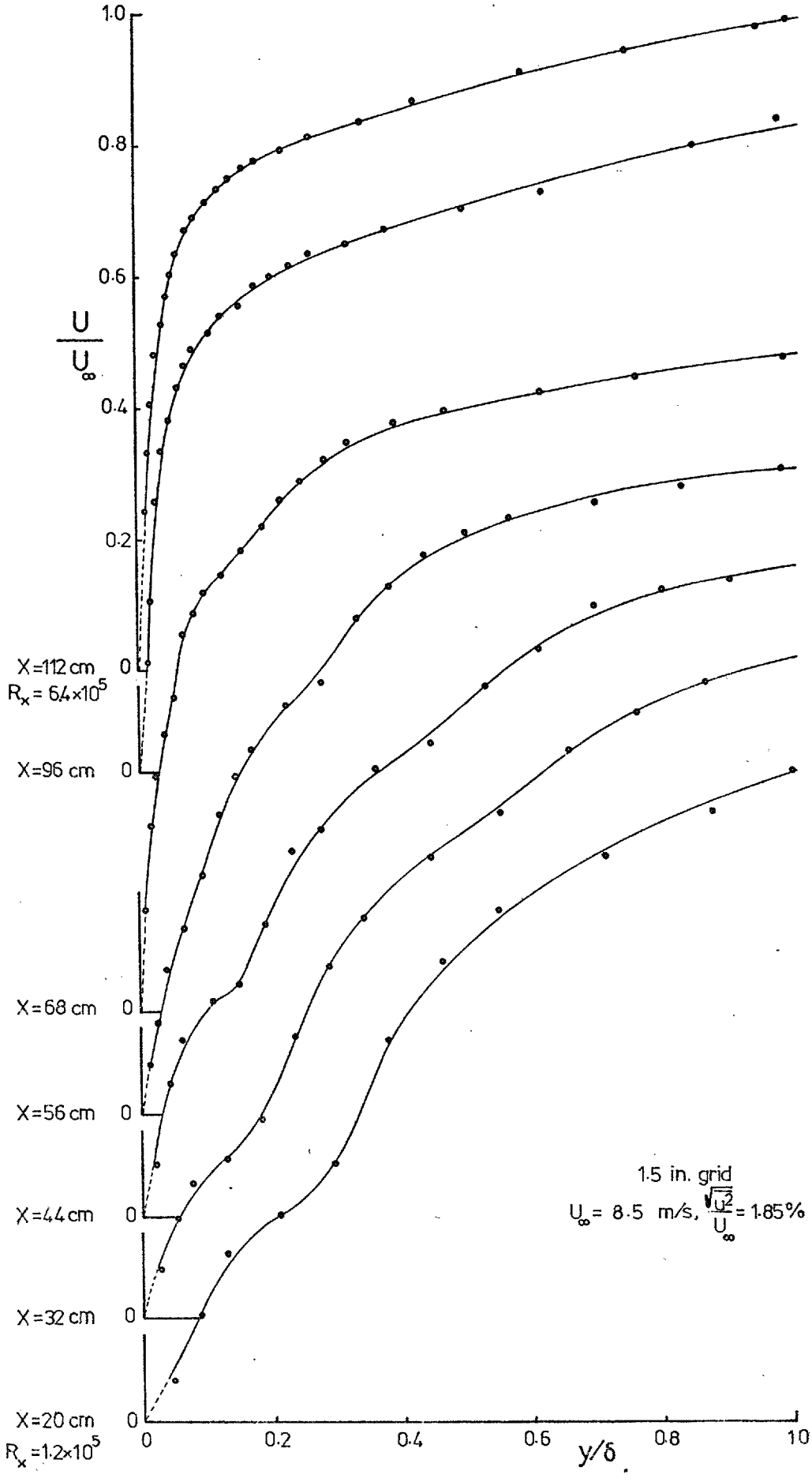
Fig. 6.27



1.5 in. grid
U_∞=8.5 m/s, $\frac{\sqrt{u^2}}{U}\Big|_\infty$=1.85%

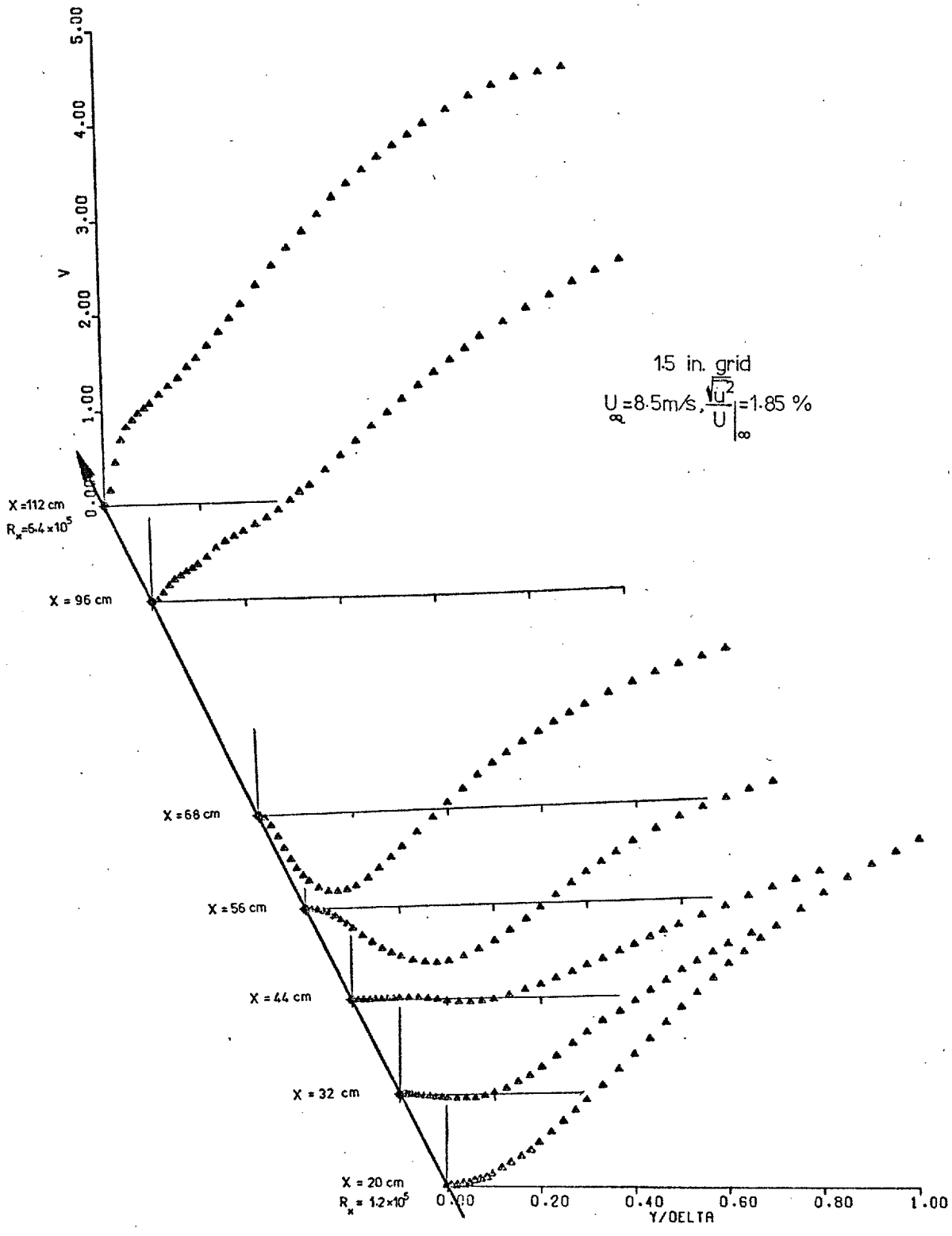
C_f around transition.

Fig. 6.28



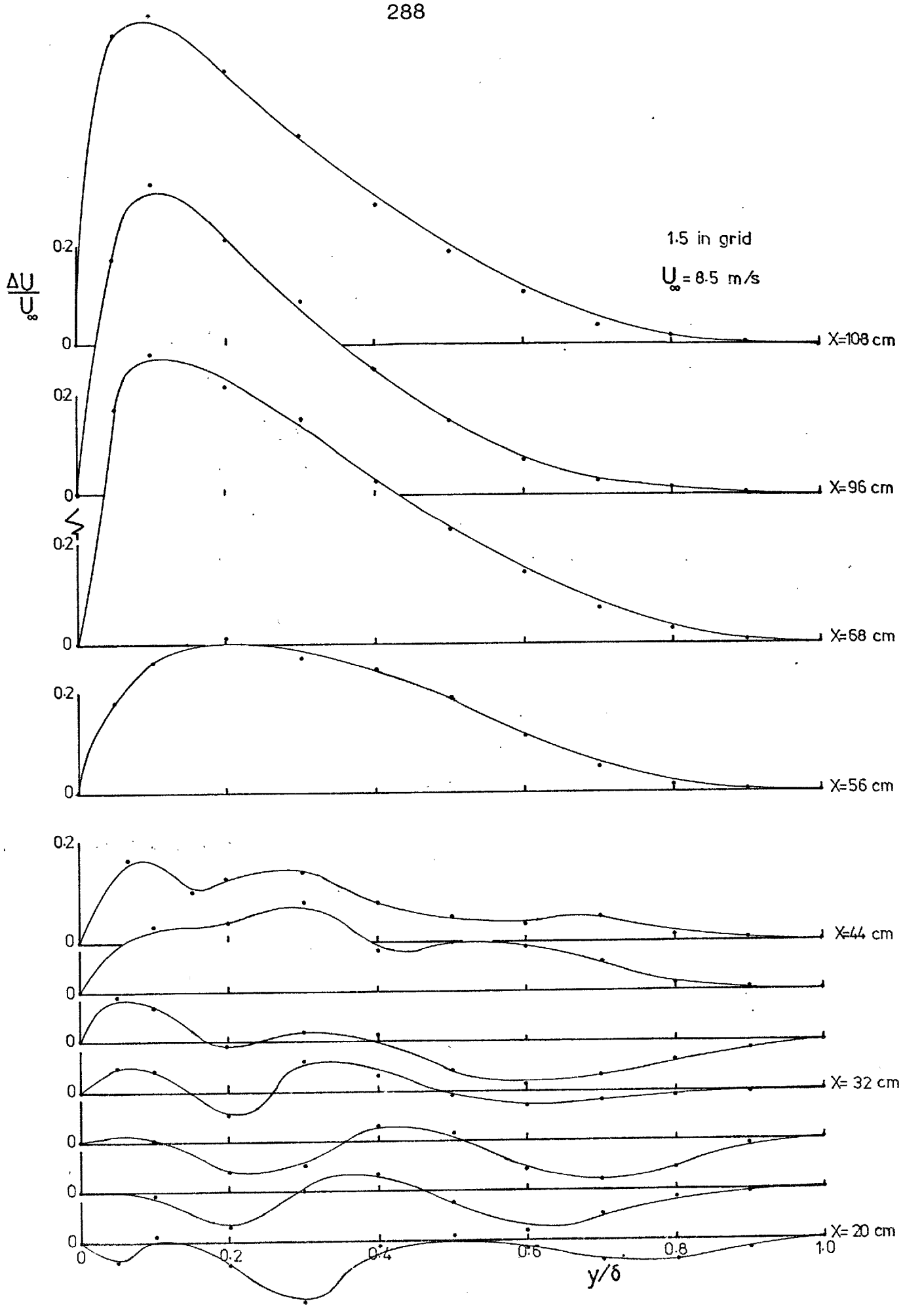
U-profiles within the laminar-transitional boundary layer.

Fig. 6.29



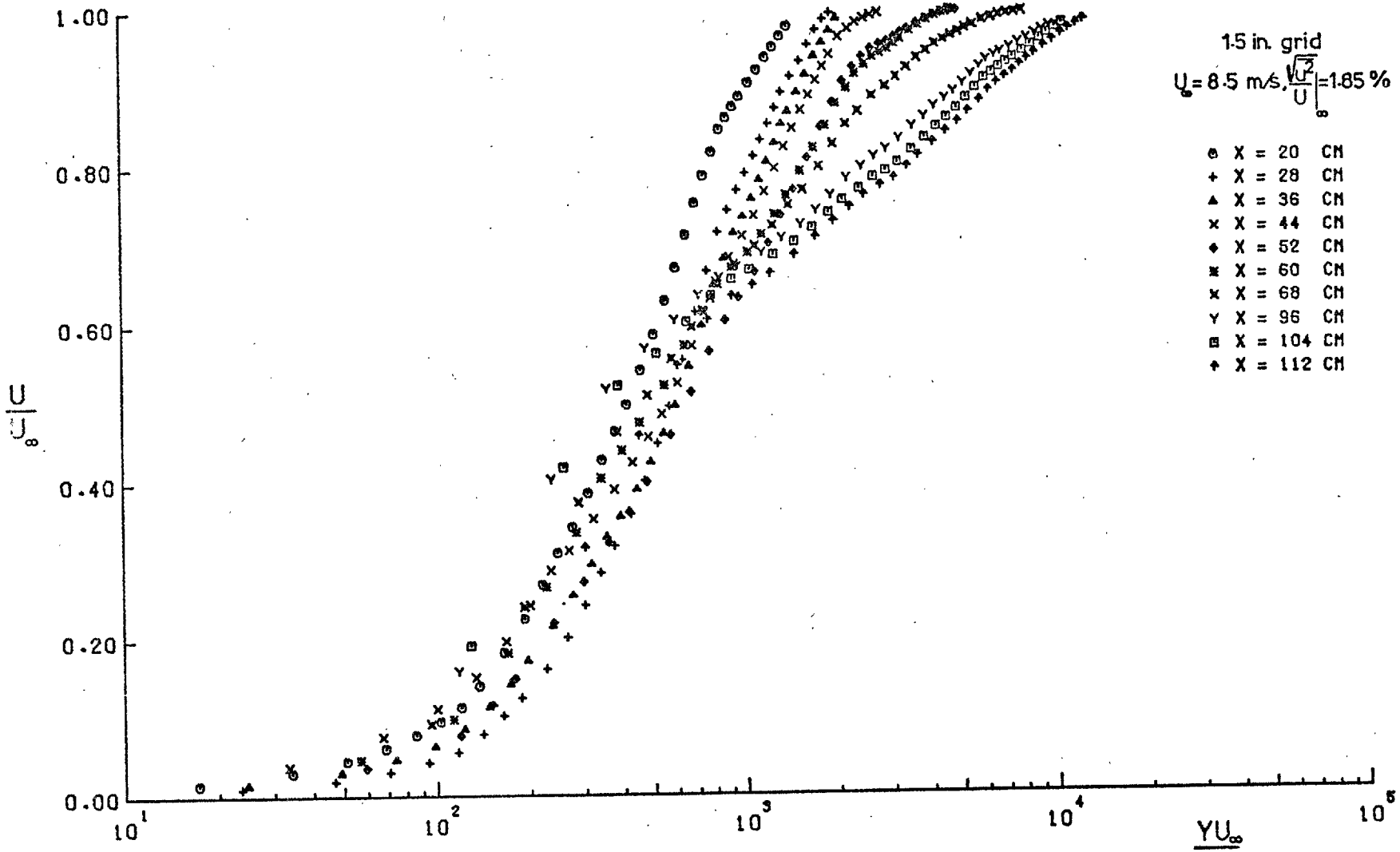
V-profiles within the laminar-transitional boundary layer.

Fig. 6.30



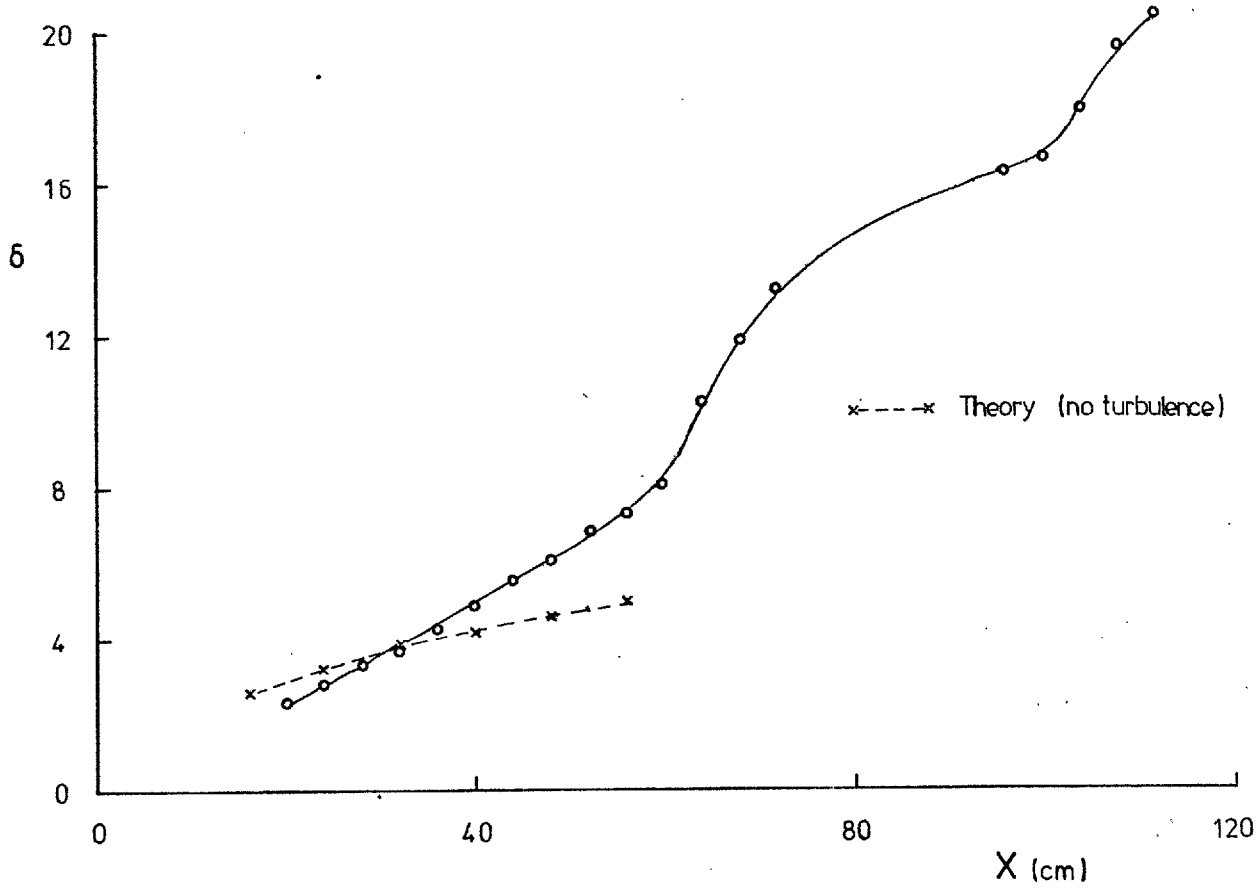
The deviations of the U-profiles (fig. 6.29) from the Blasius profile .

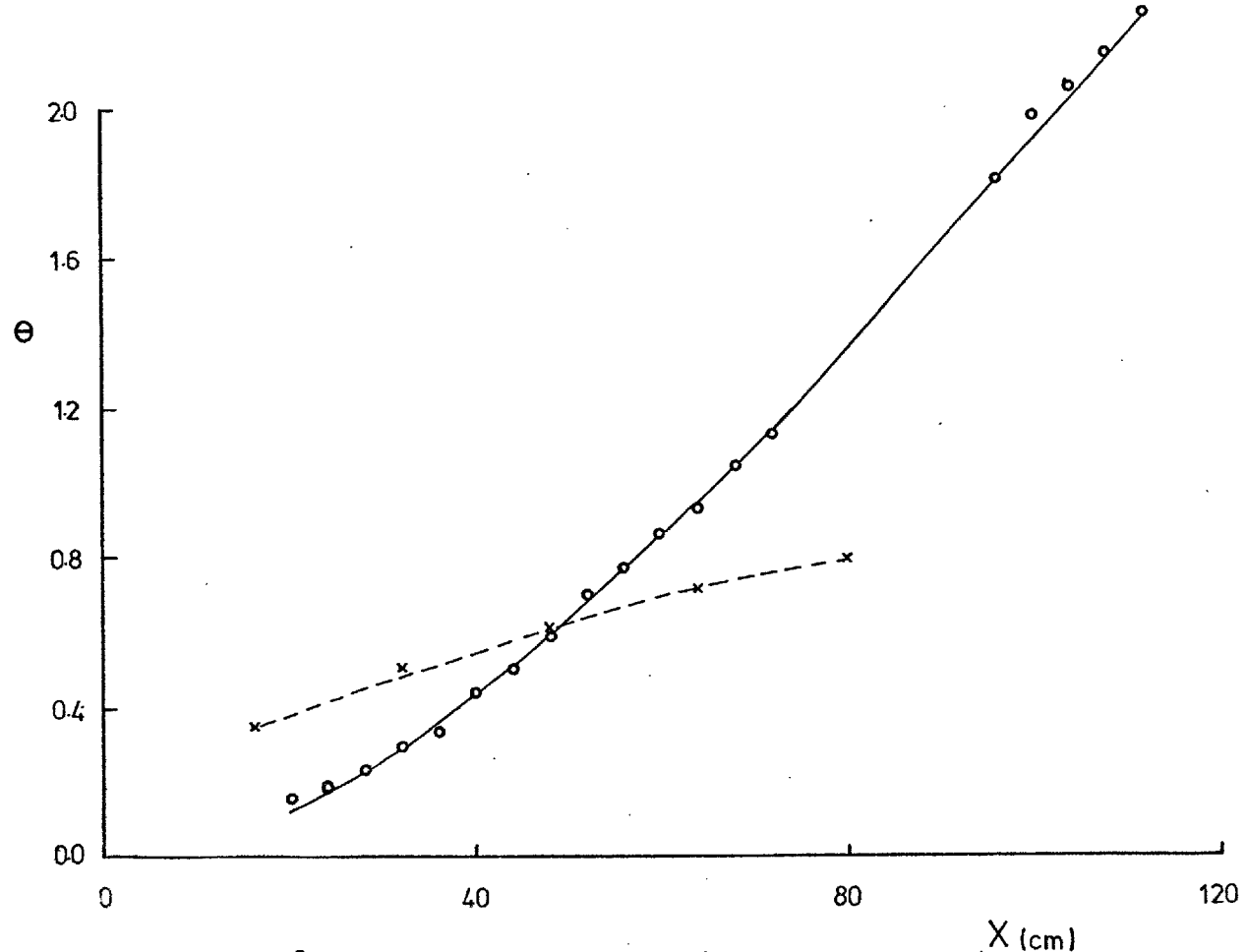
Fig. 6.31



Clauser chart of the U-profiles (fig. 6.29) over the plate.

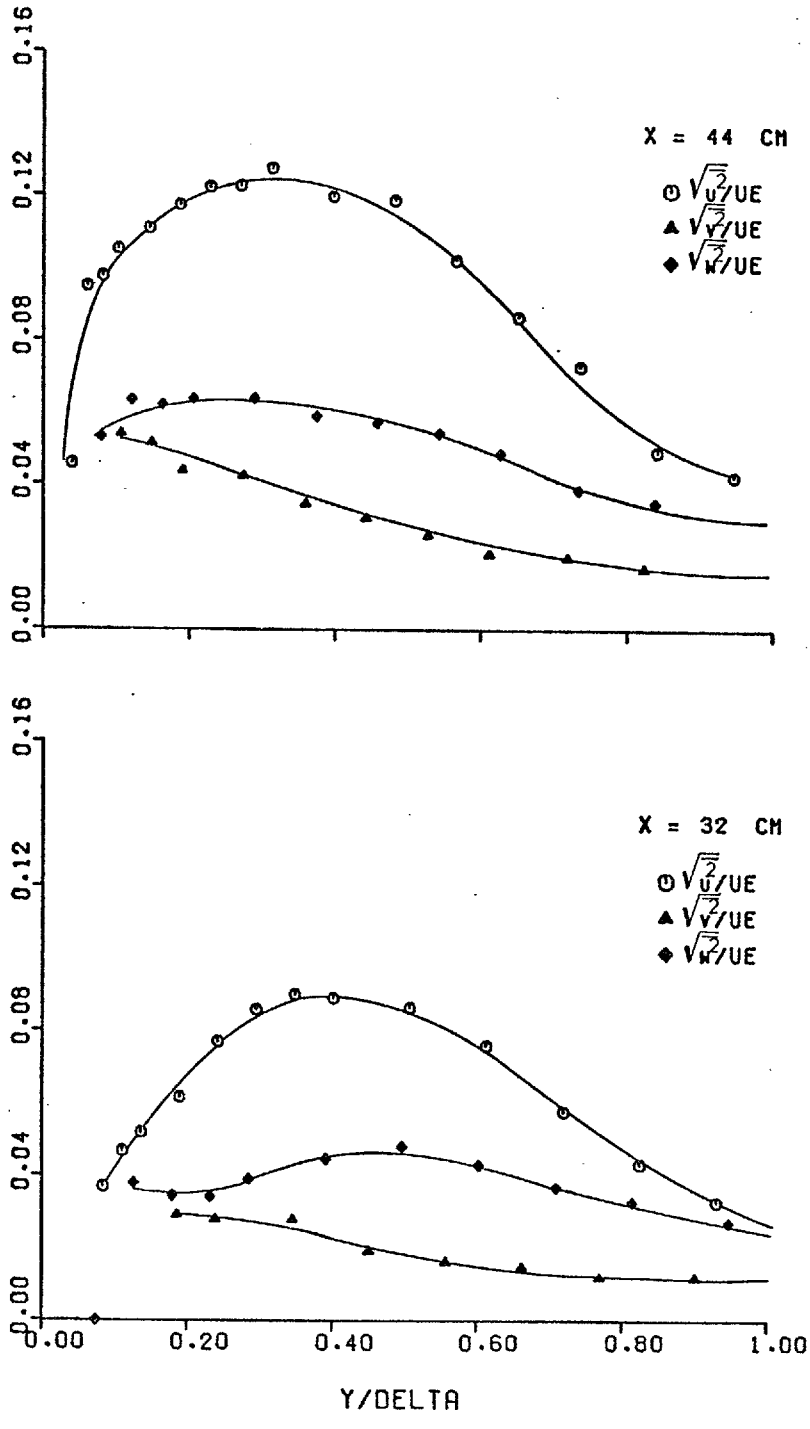
Fig. 6.32





δ & Θ development over the plate (1.5 in. grid, U_∞ = 8.5 m/s)

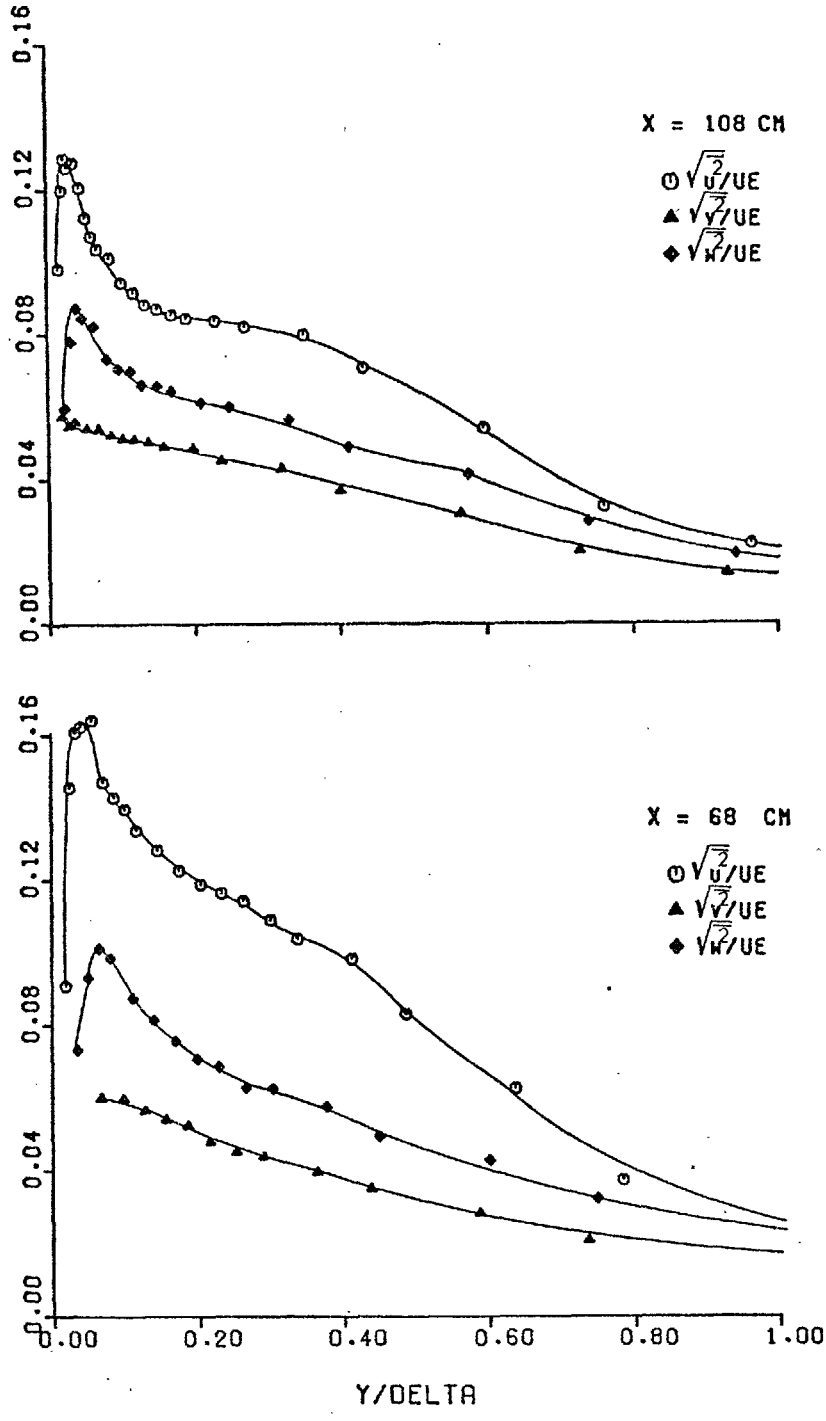
Fig. 6.33



$\sqrt{\overline{u^2}}, \sqrt{\overline{v^2}}, \sqrt{\overline{w^2}}$ profiles within the laminar-transitional region .

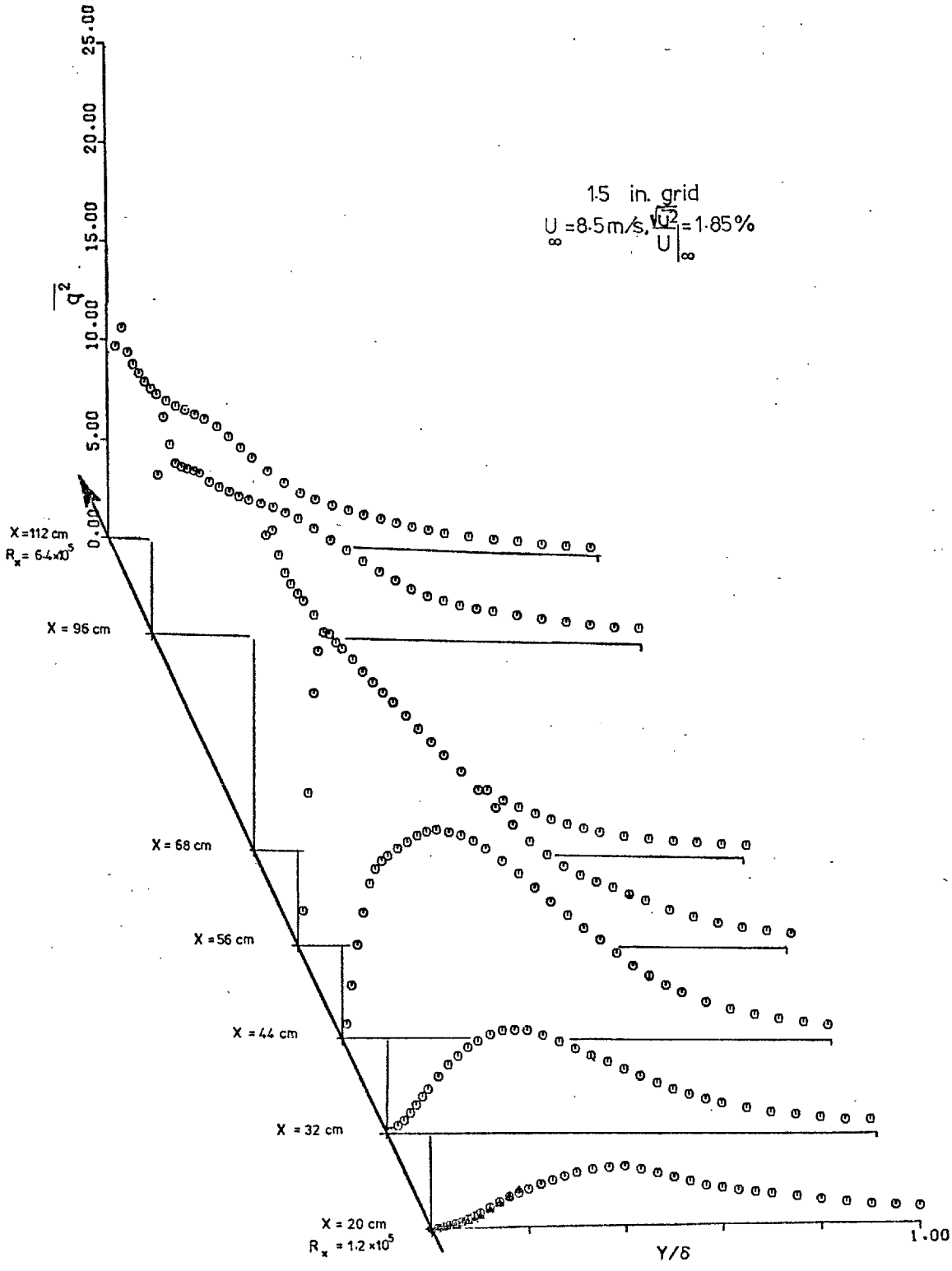
$\left(\left. \frac{\sqrt{\overline{u^2}}}{U} \right|_\infty = 1.85\% \right)$

Fig. 6.34



(continued)

Fig. 6.34



$\overline{q^2}$-profiles within the laminar-transitional boundary layer.

Fig. 6.35

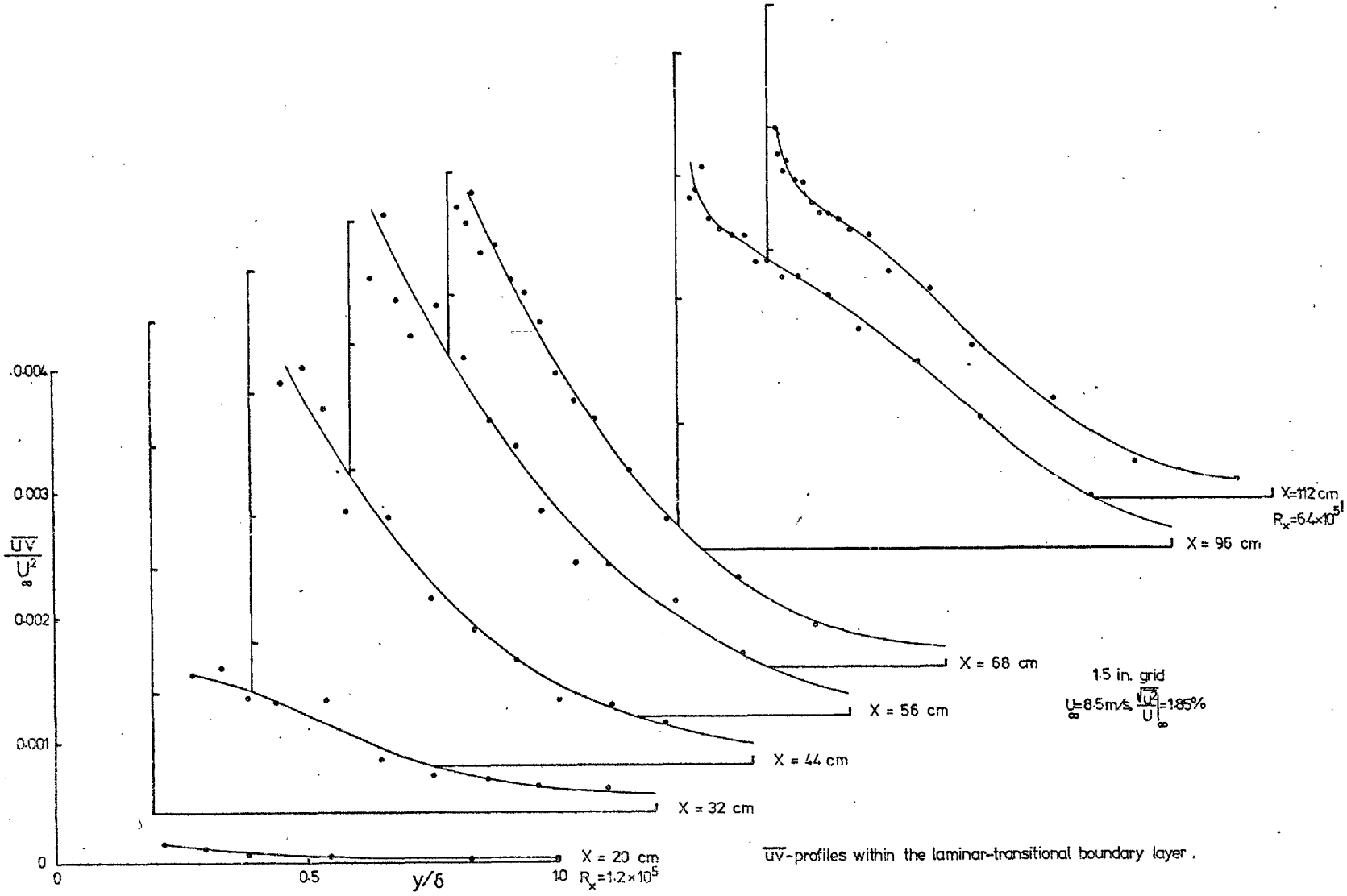


Fig. 6.36 $\overline{uv}$-profiles within the laminar-transitional boundary layer.

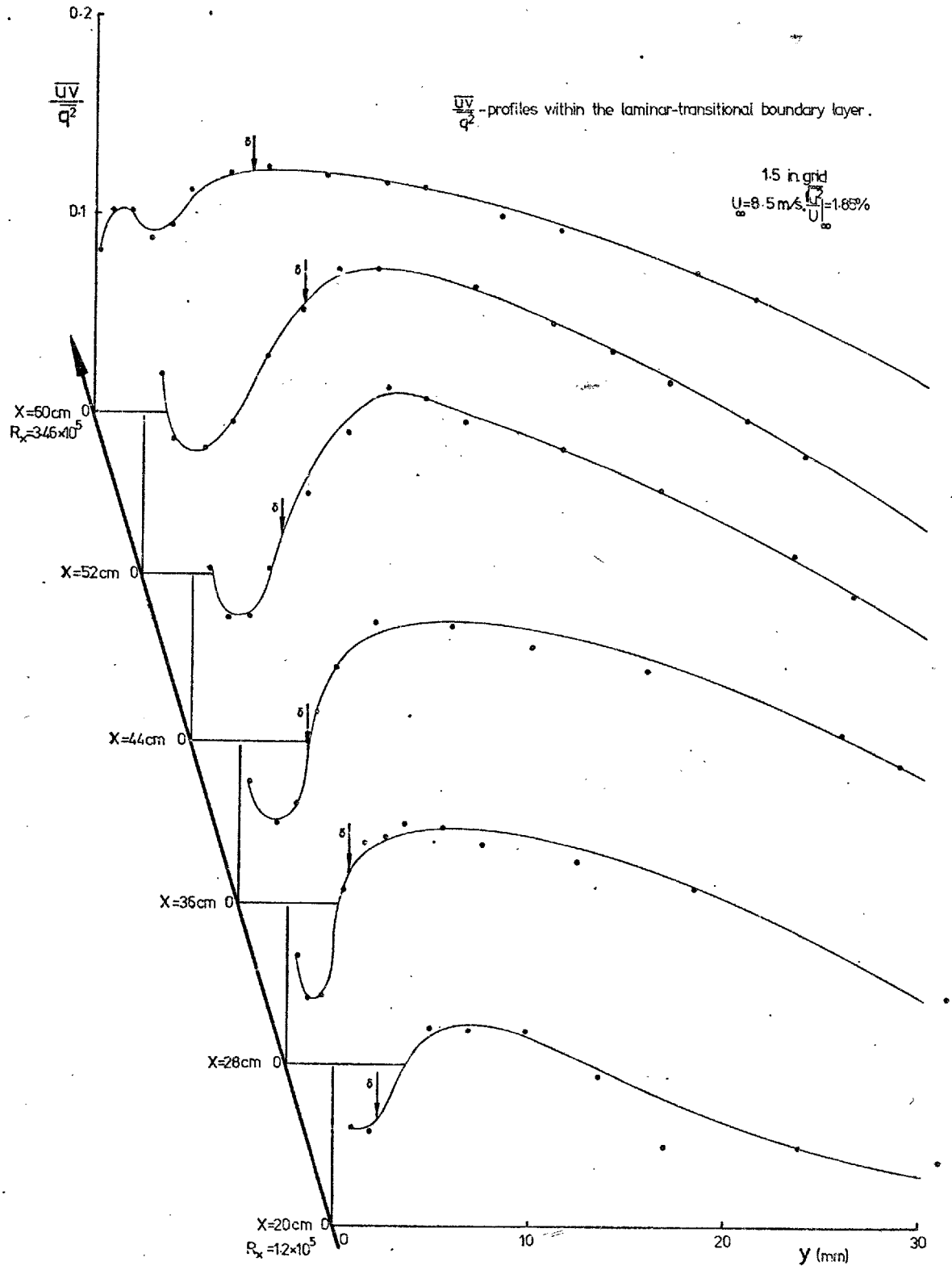
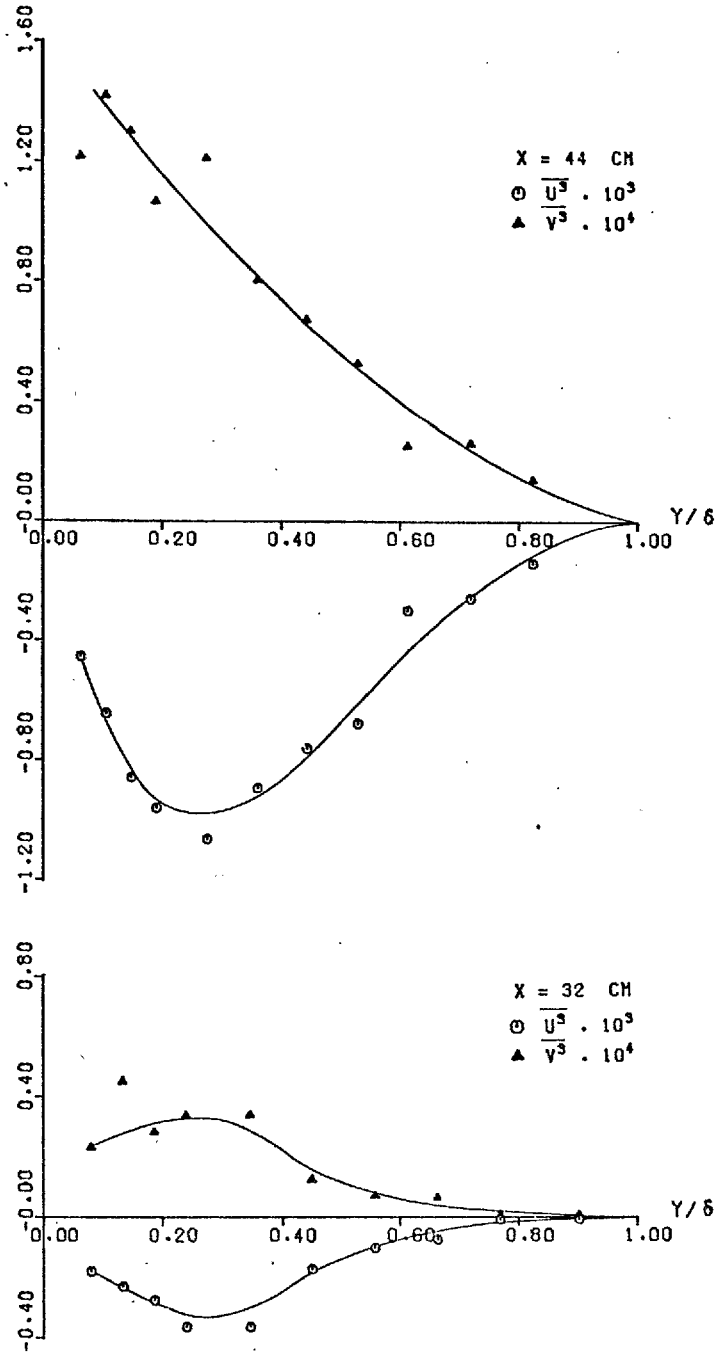
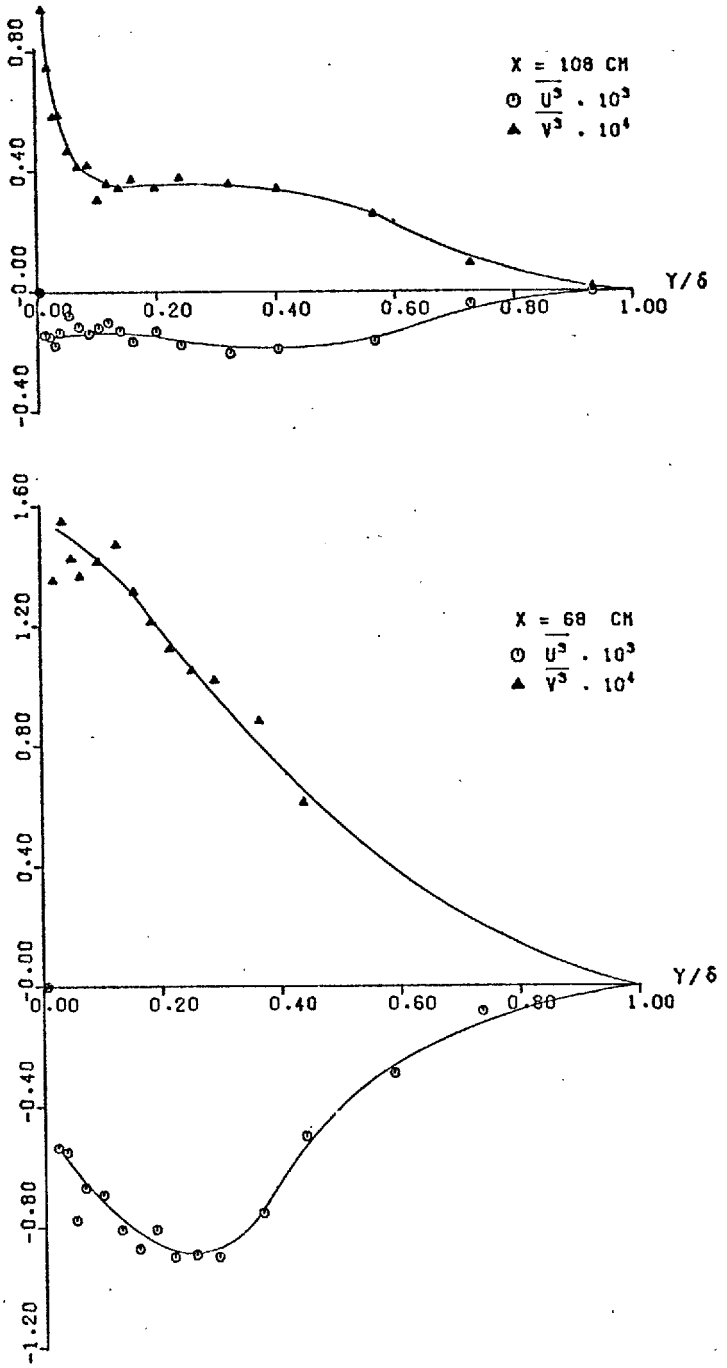

0·2
$\frac{\overline{uv}}{q^2}$
0·1
$\frac{\overline{uv}}{q^2}$-profiles within the laminar-transitional boundary layer.
1·5 in grid
U_∞=8·5 m/s. $\frac{\sqrt{u^2}}{U_\infty}$=1·65%
δ
X=60cm 0
R_x=3·46×10^5
X=52cm 0
X=44cm 0
X=36cm 0
X=28cm 0
X=20cm 0
R_x=1·2×10^5
0
10
20
30
y (mm)

Fig. 6.37



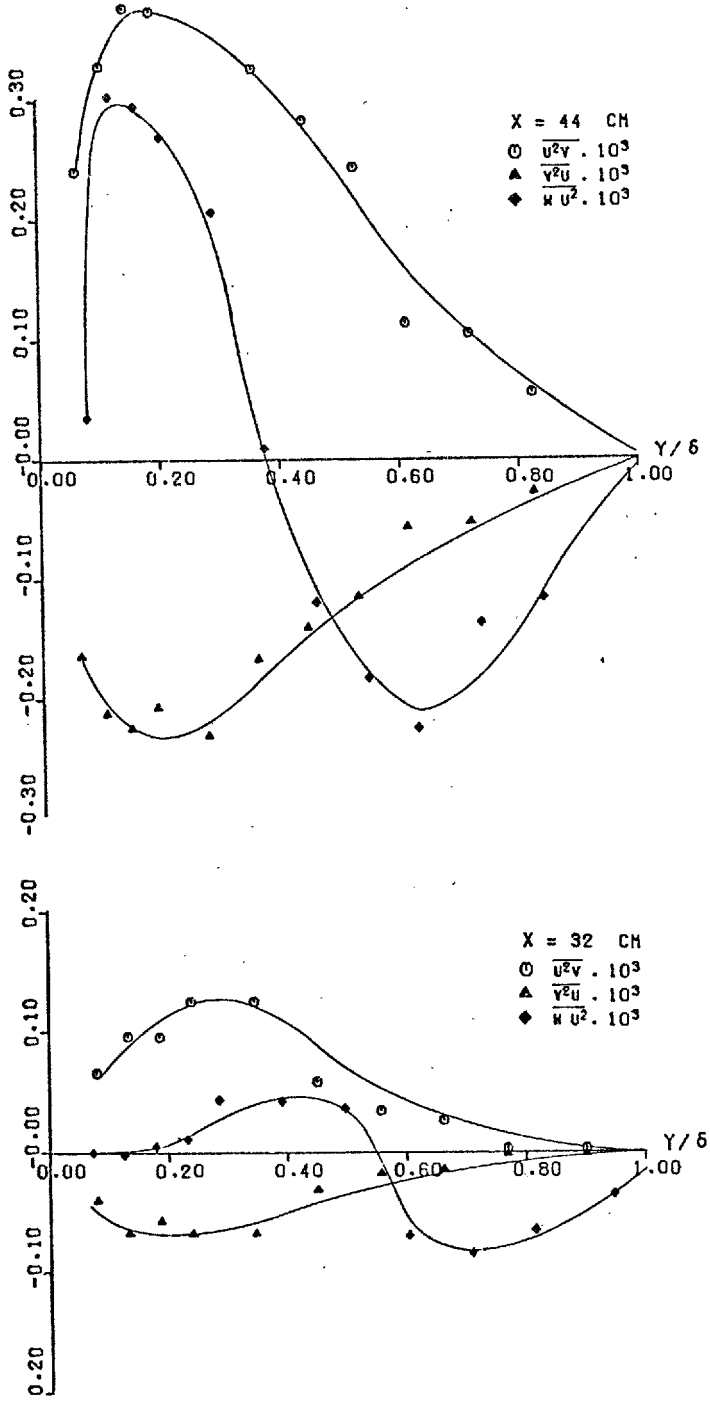
$\overline{u^3}$&$\overline{v^3}$ profiles within the laminar-transitional region

Fig. 6.38



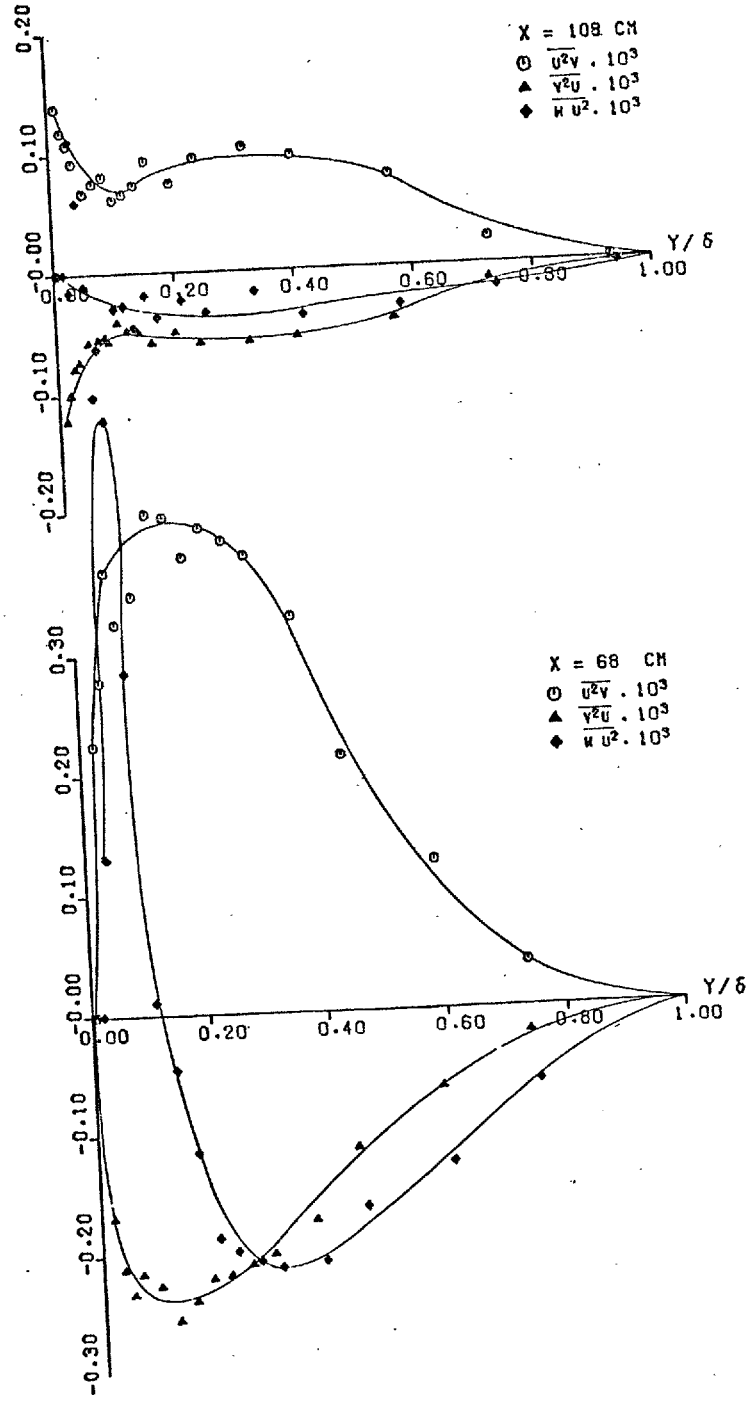
(continued)

Fig. 6.38



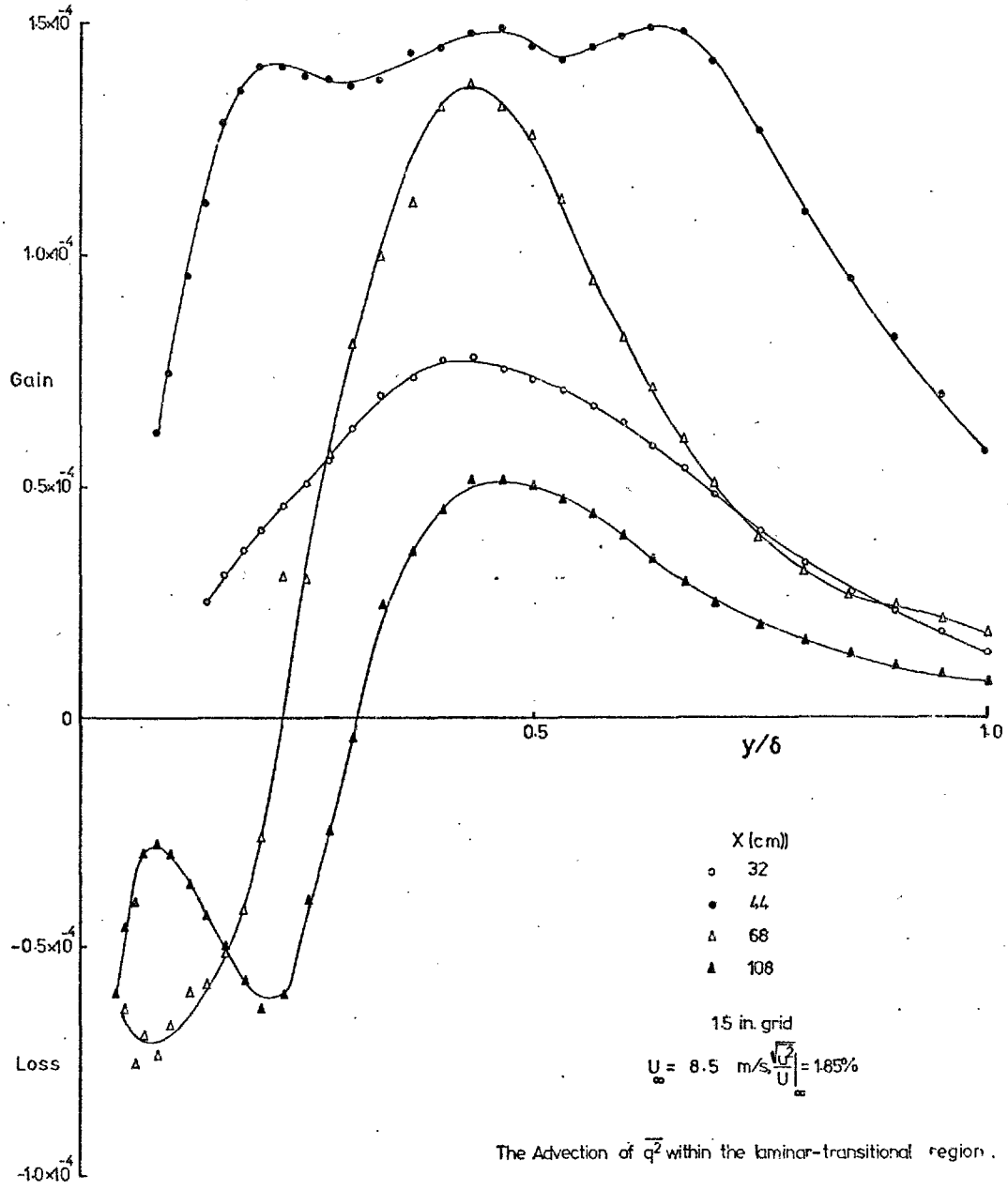
Triple-product profiles within the laminar-transitional region .

Fig. 6.39



(continued)

Fig. 6.39



The Advection of $\overline{q^2}$ within the laminar-transitional region.

Fig. 6.40

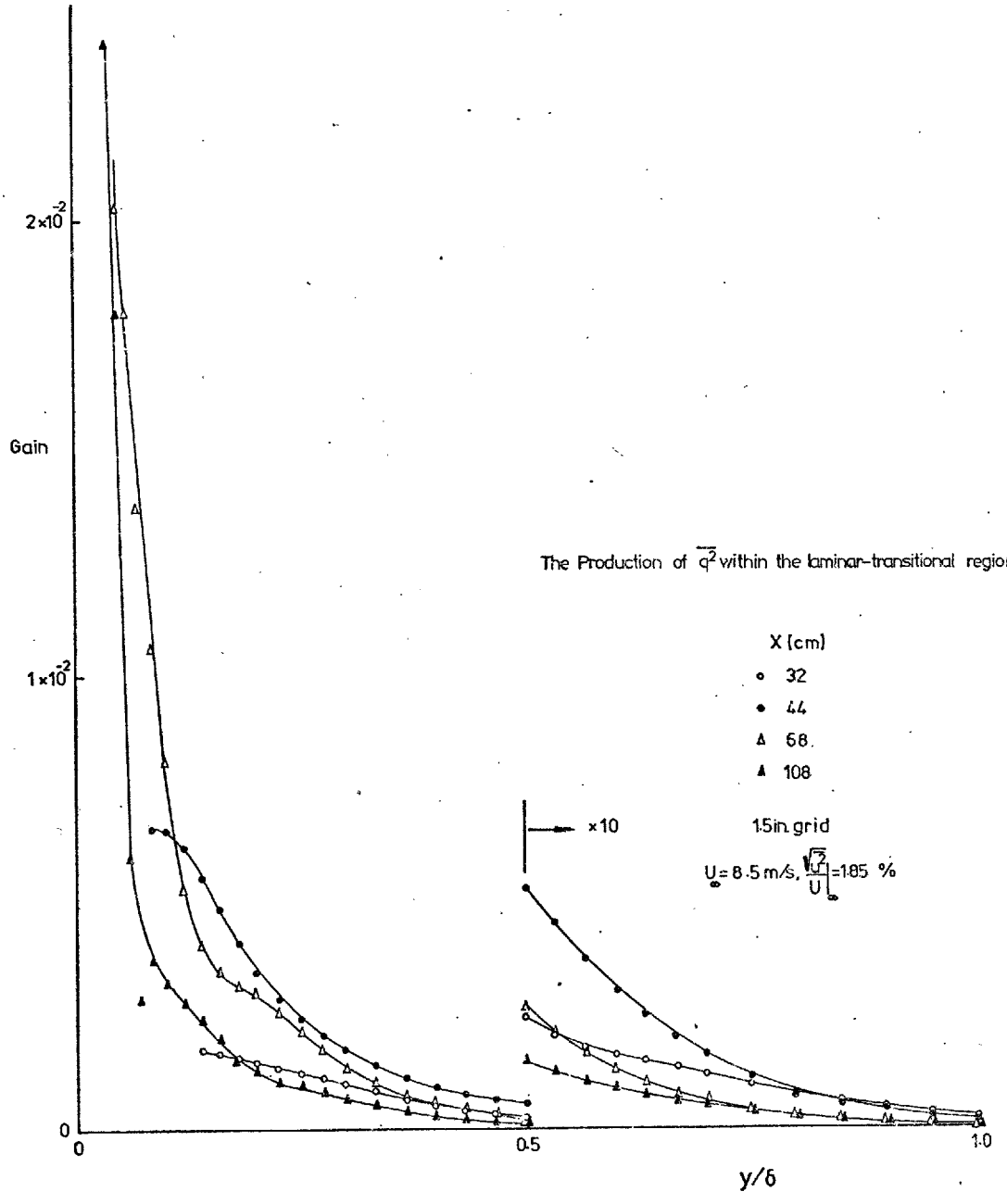
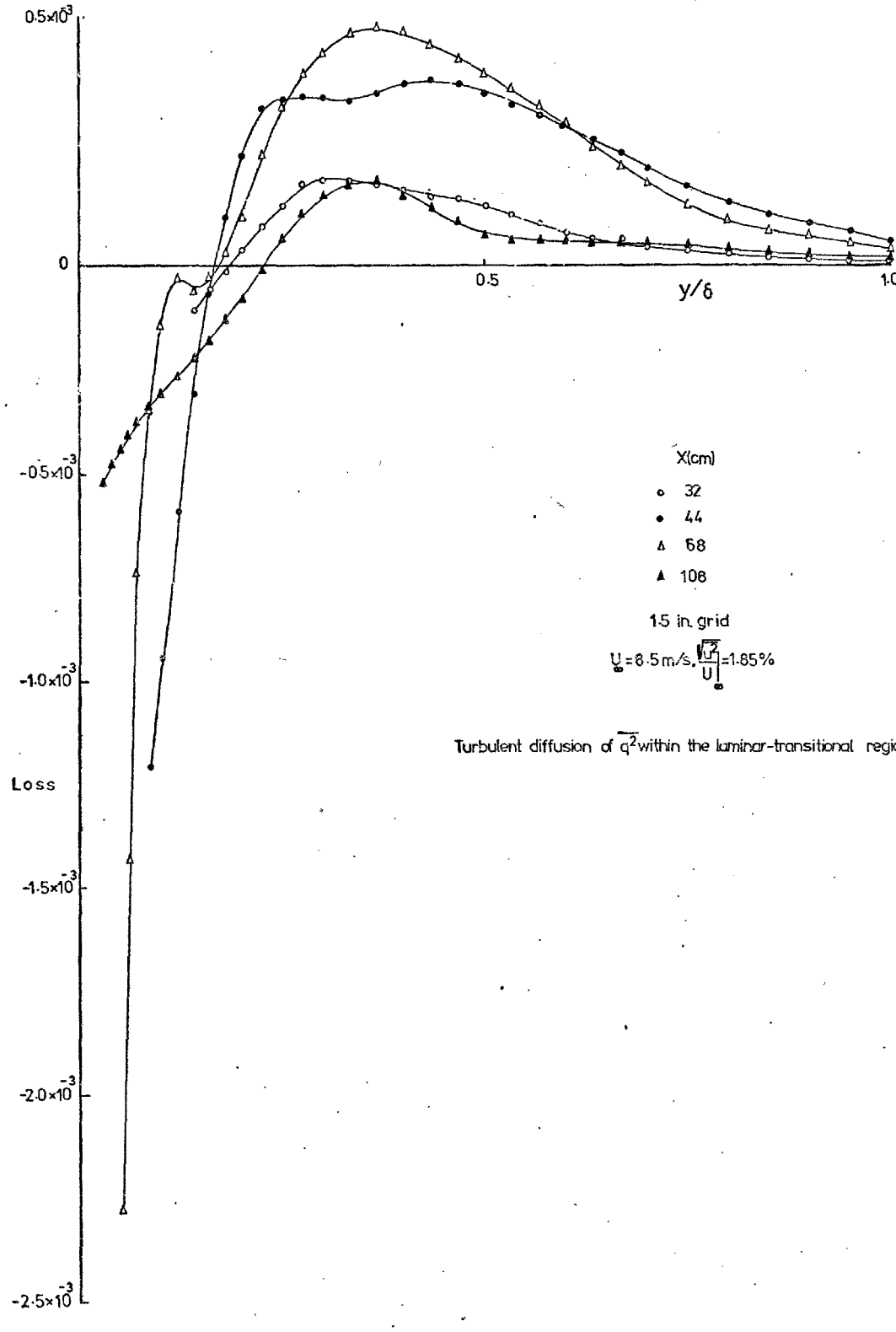
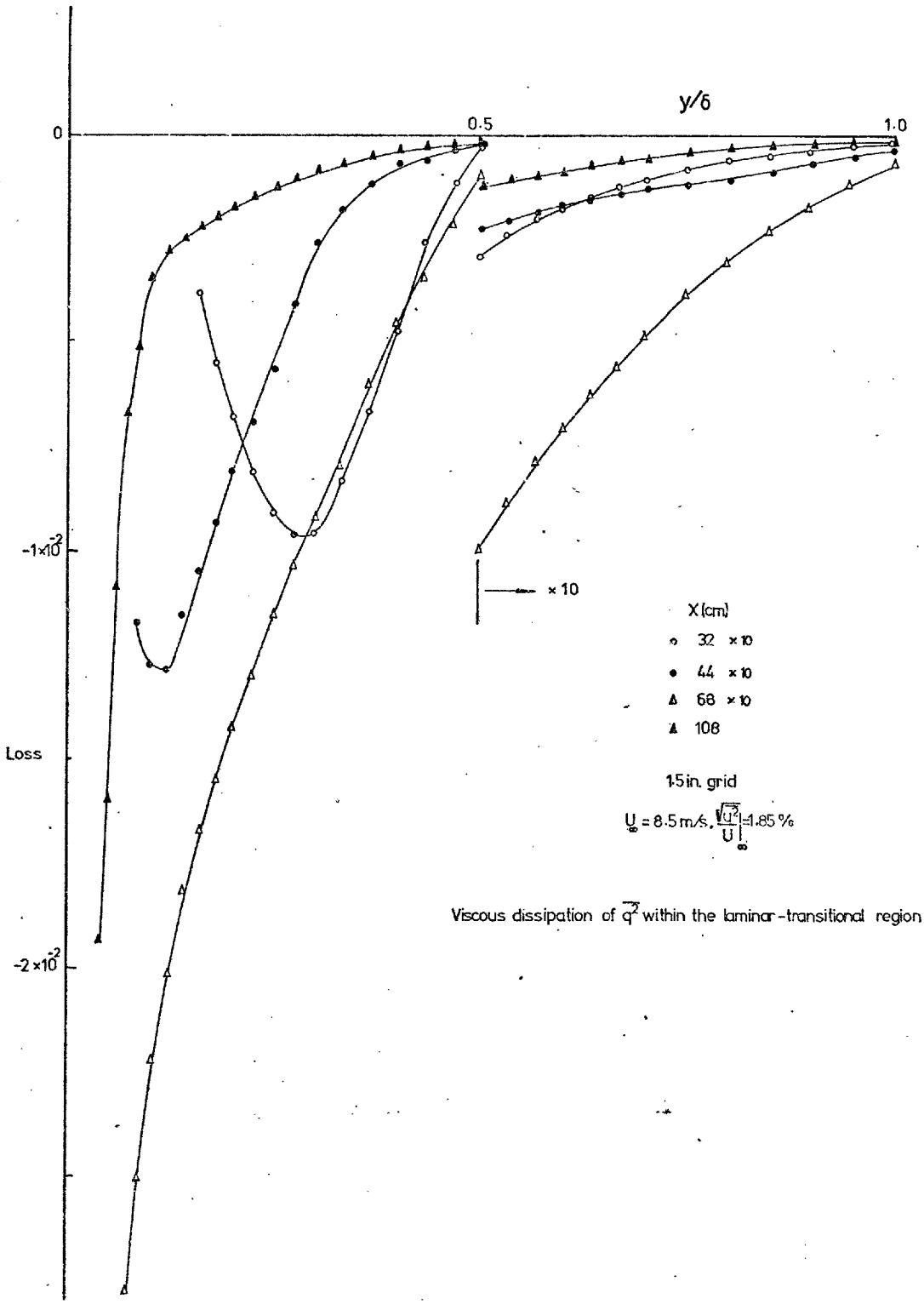

Gain
2×10⁻²
1×10⁻²
0
0
0.5
1.0
y/δ
The Production of $\overline{q^2}$ within the laminar-transitional region.
X (cm)
32
44
68
108
×10
1.5in. grid
U_∞ = 8.5 m/s, $\frac{\sqrt{u^2}}{U_\infty}$ = 1.85 %

Fig. 6.41



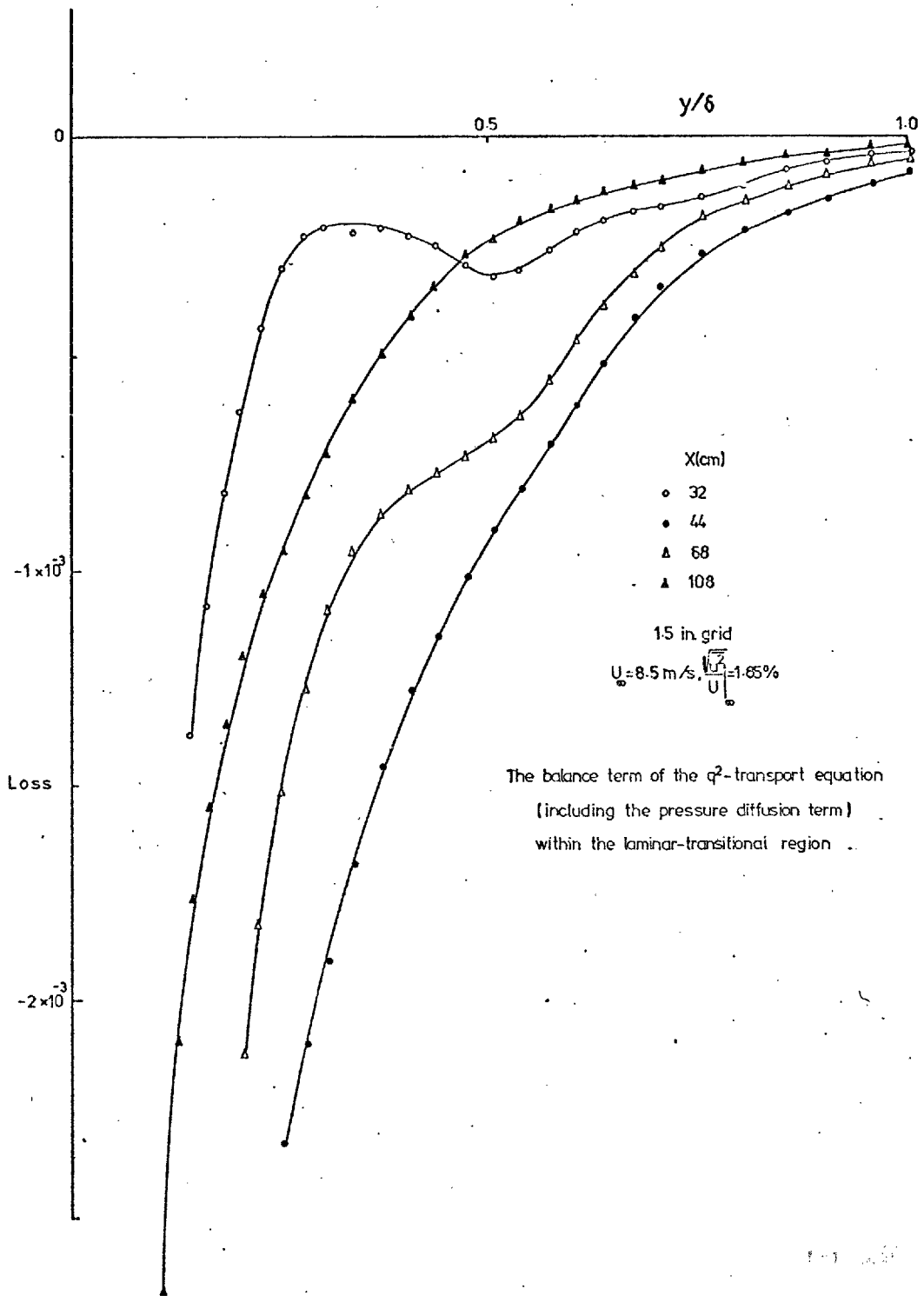
Turbulent diffusion of $\overline{q^2}$ within the laminar-transitional region.

Fig. 6.42



Viscous dissipation of $\overline{q^2}$ within the laminar-transitional region.

Fig. 6.43



The balance term of the q^2-transport equation (including the pressure diffusion term) within the laminar-transitional region .

Fig. 6.44

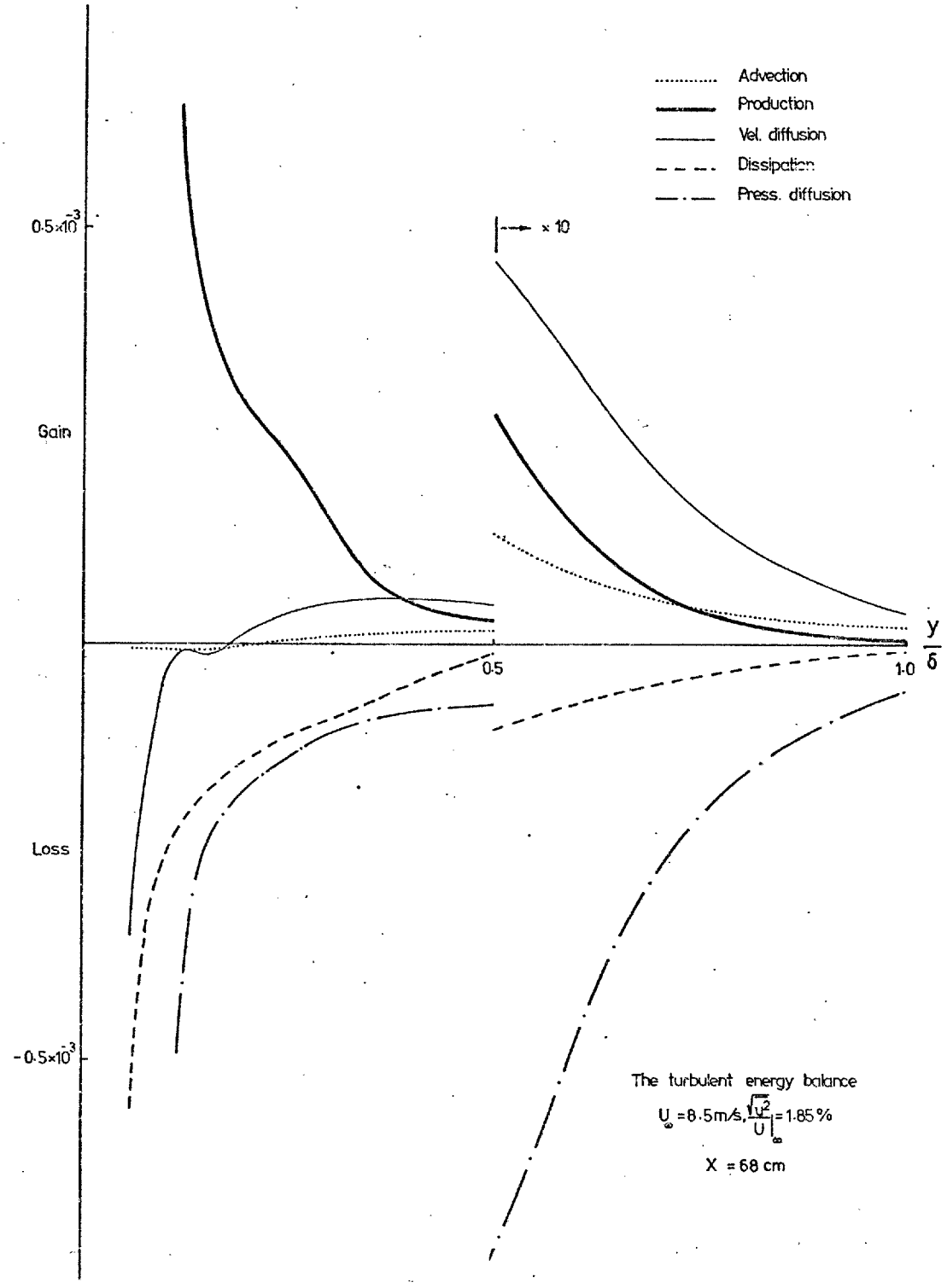
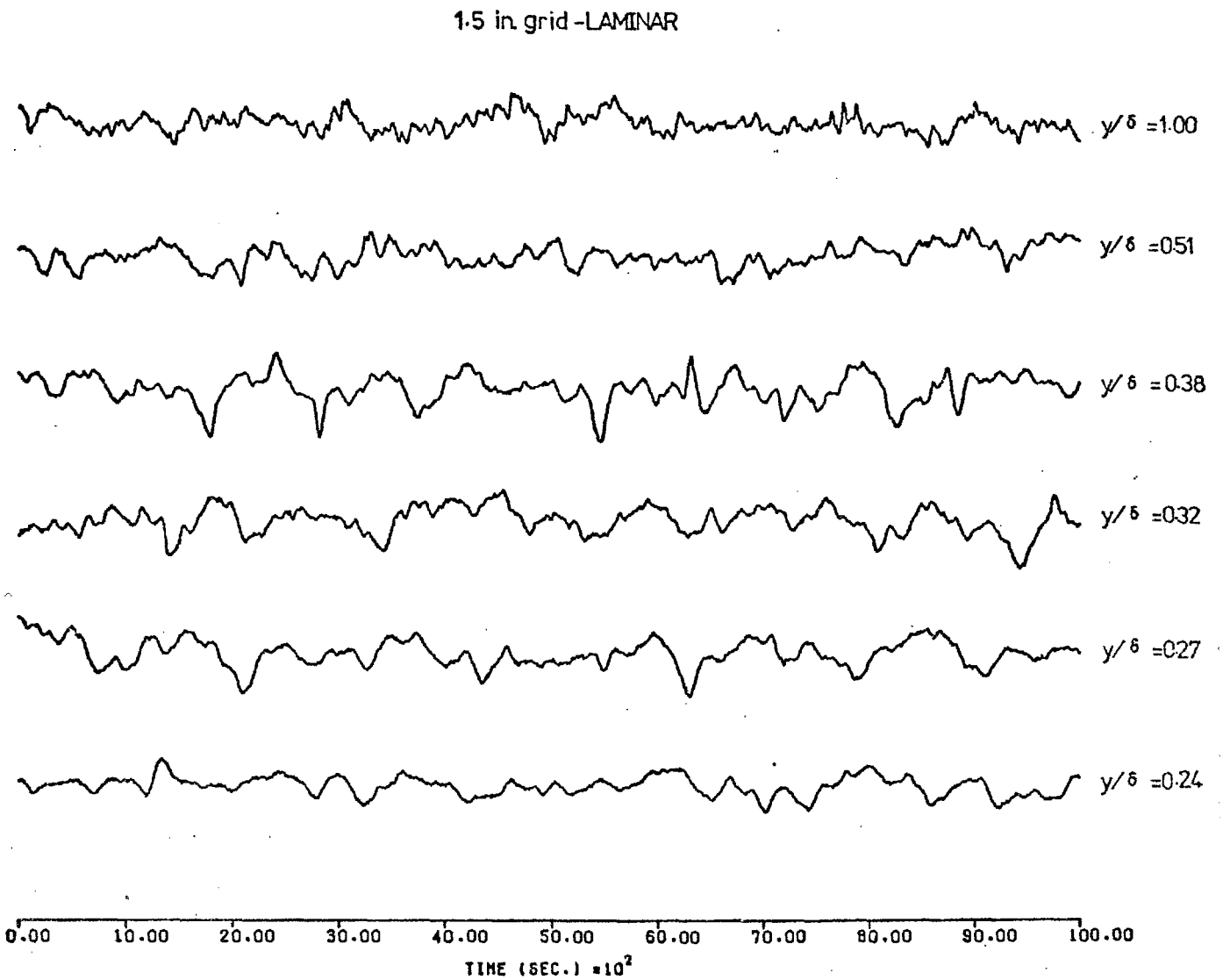

Advection
Production
Vel. diffusion
Dissipation
Press. diffusion
0·5×10⁻³
× 10
Gain
Loss
-0·5×10⁻³
0·5
1·0
y/δ
The turbulent energy balance
U∞ = 8·5 m/s, √u²/U∞ = 1·85 %
X = 68 cm

Fig. 6.45

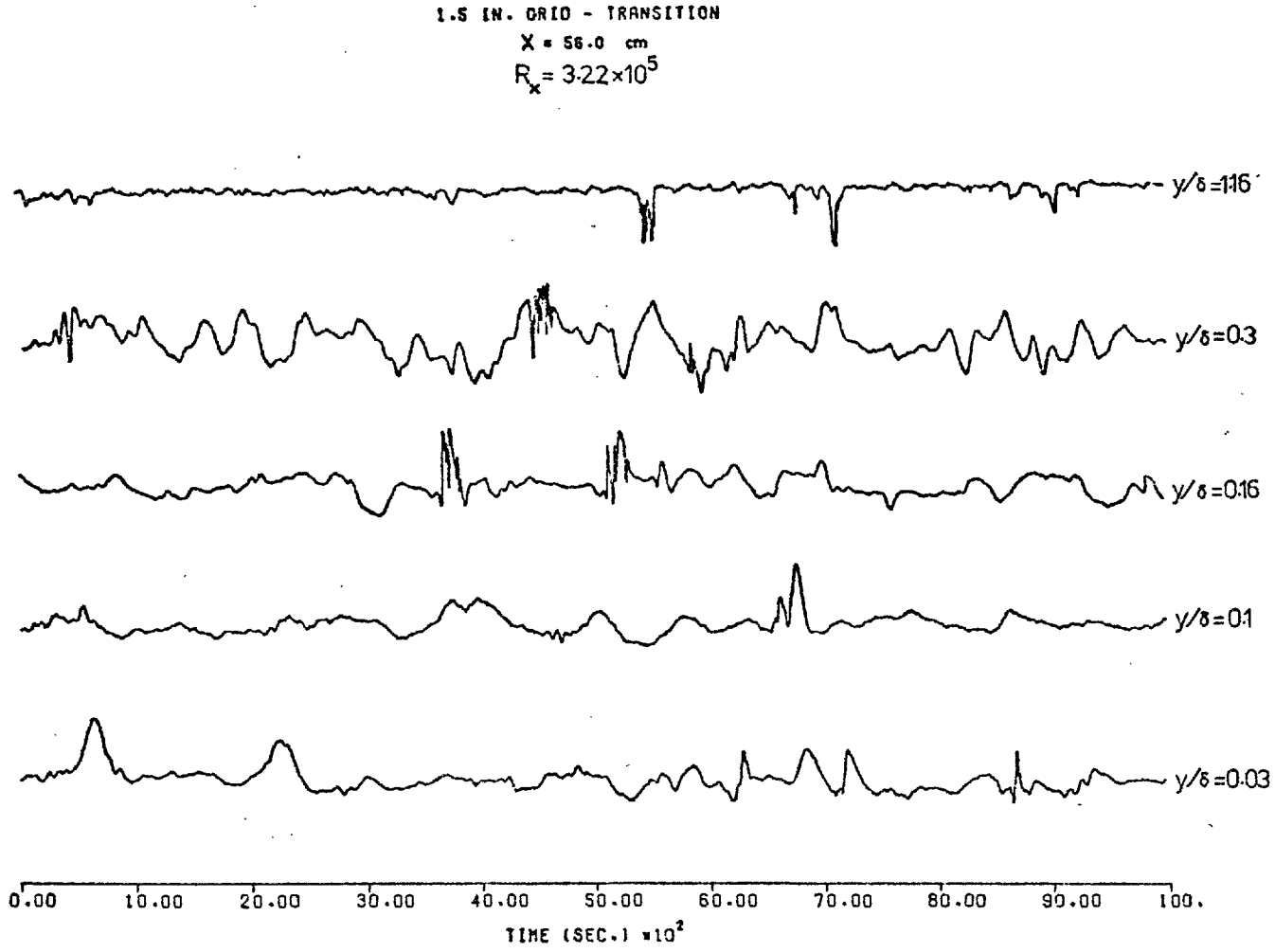


X = 32 cm

$R_x = 1.84 \times 10^5$

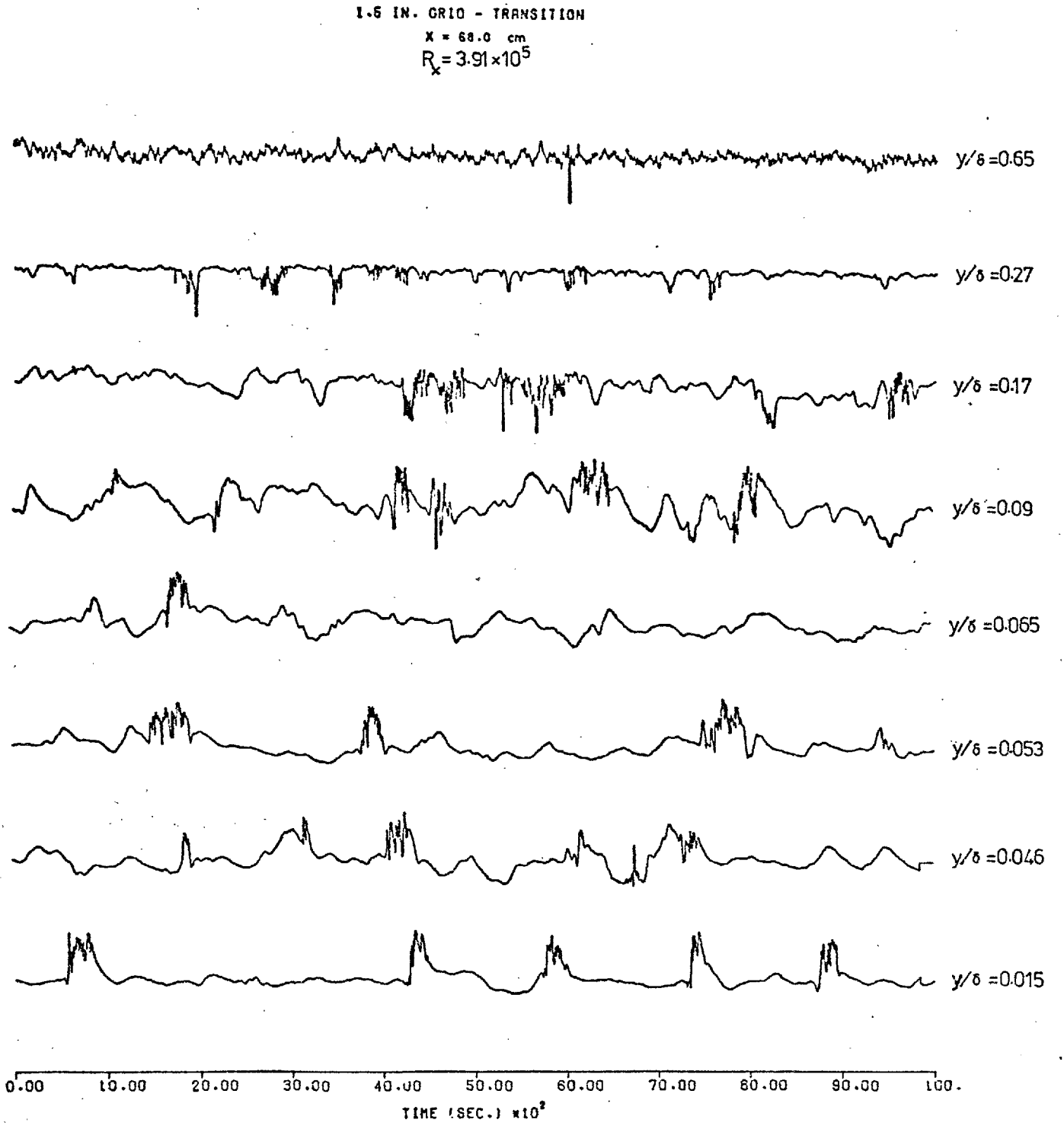
u-records at different x &y positions within the laminar & the transition regions .

Fig. 7.1a



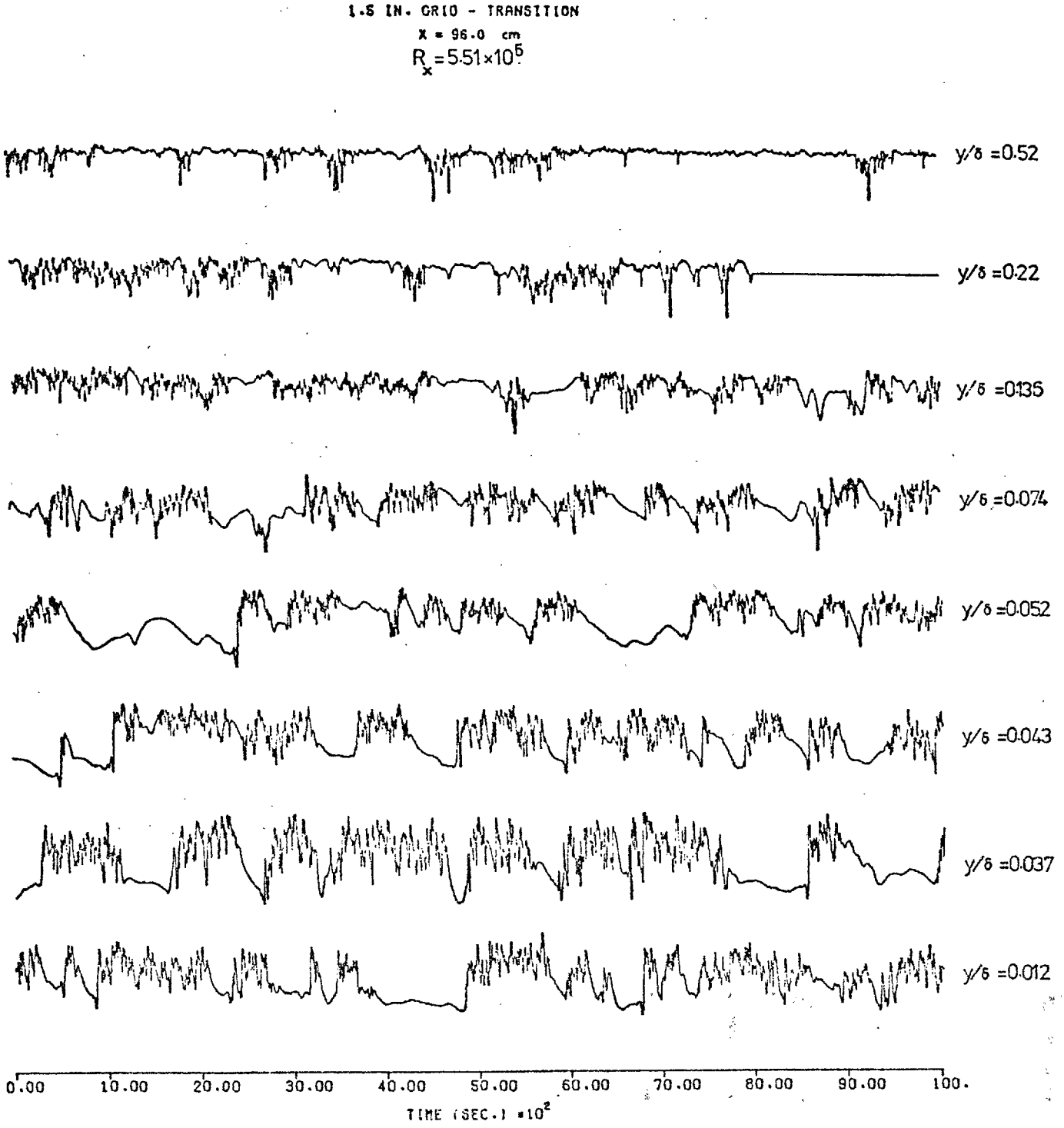
(For legend see fig. 7.1.A)

Fig. 7.1b



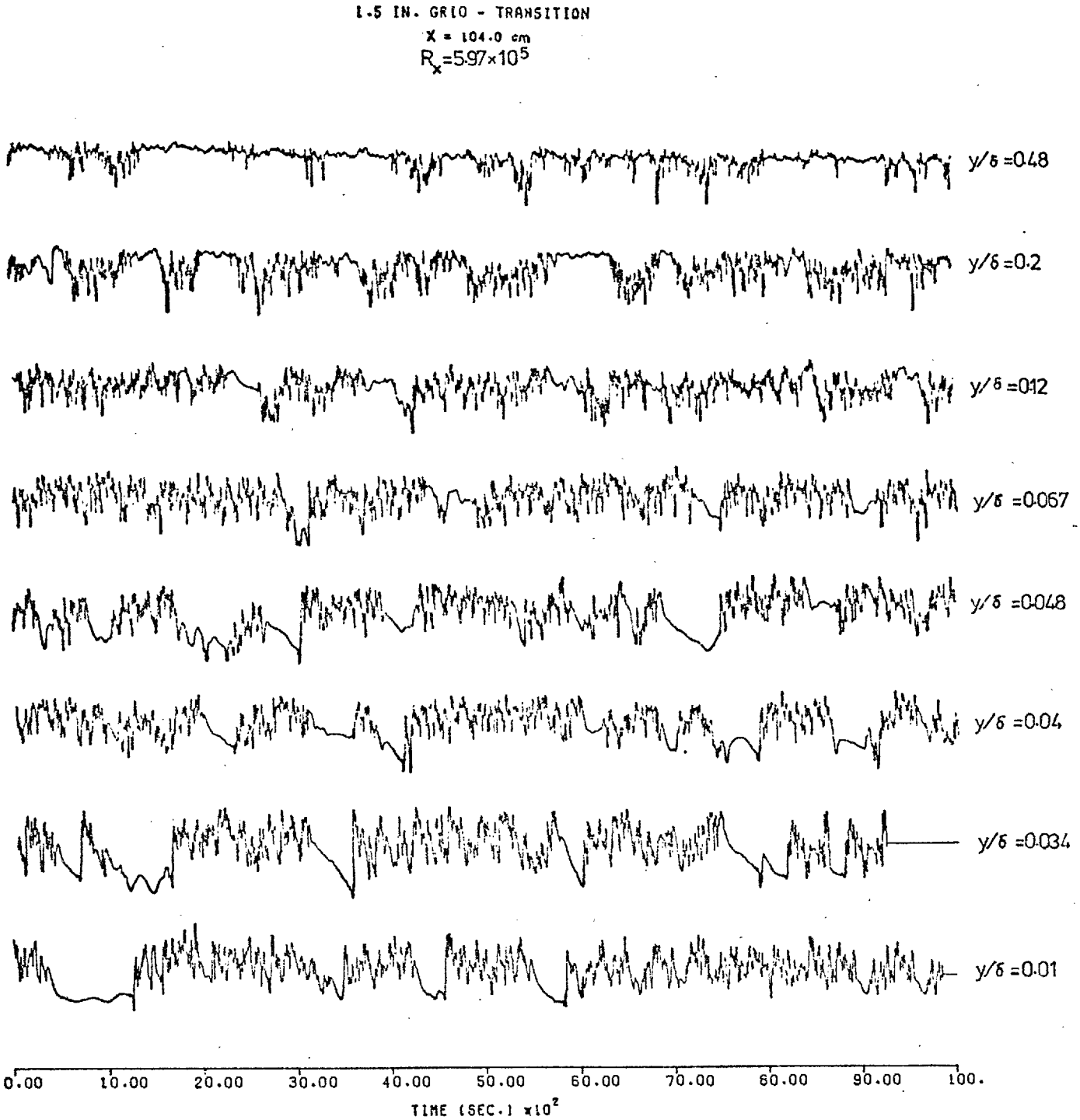
(For legend see fig. 7.1.A)

Fig. 7.1c



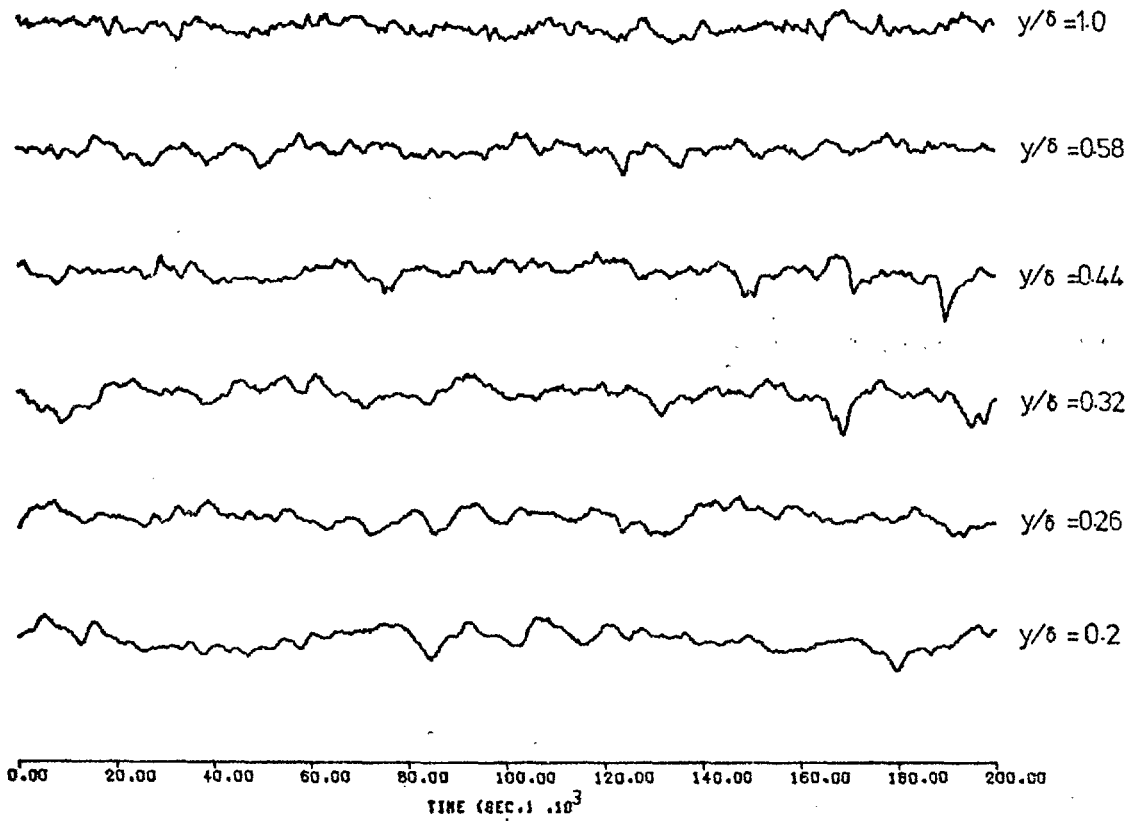
(For legend see fig. 7.1.A)

Fig. 7.1d



(For legend see fig. 7.1.A)

Fig. 7.1e



3.0 IN. GRID - LAMINAR BL

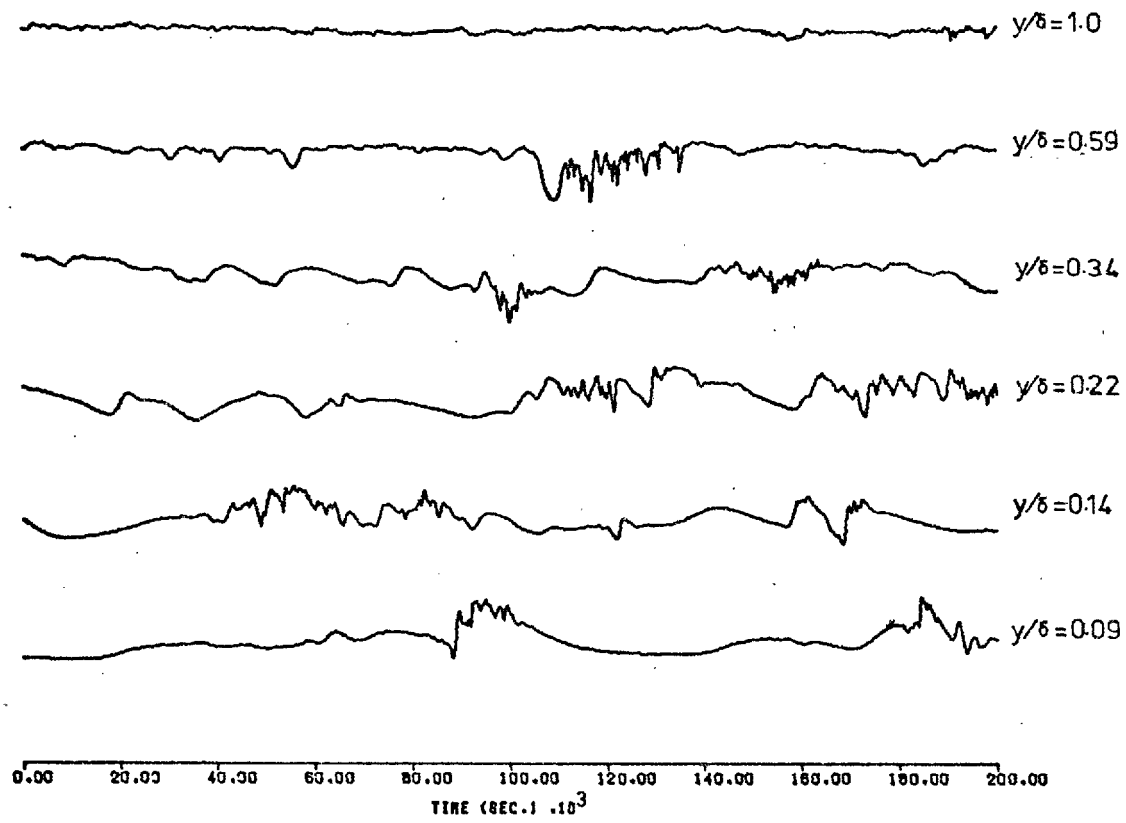
X=20 cm

$R_x = 1.24 \times 10^5$

(Relatively scaled)

(For legend see fig. 7.1.A)

Fig. 7.2a



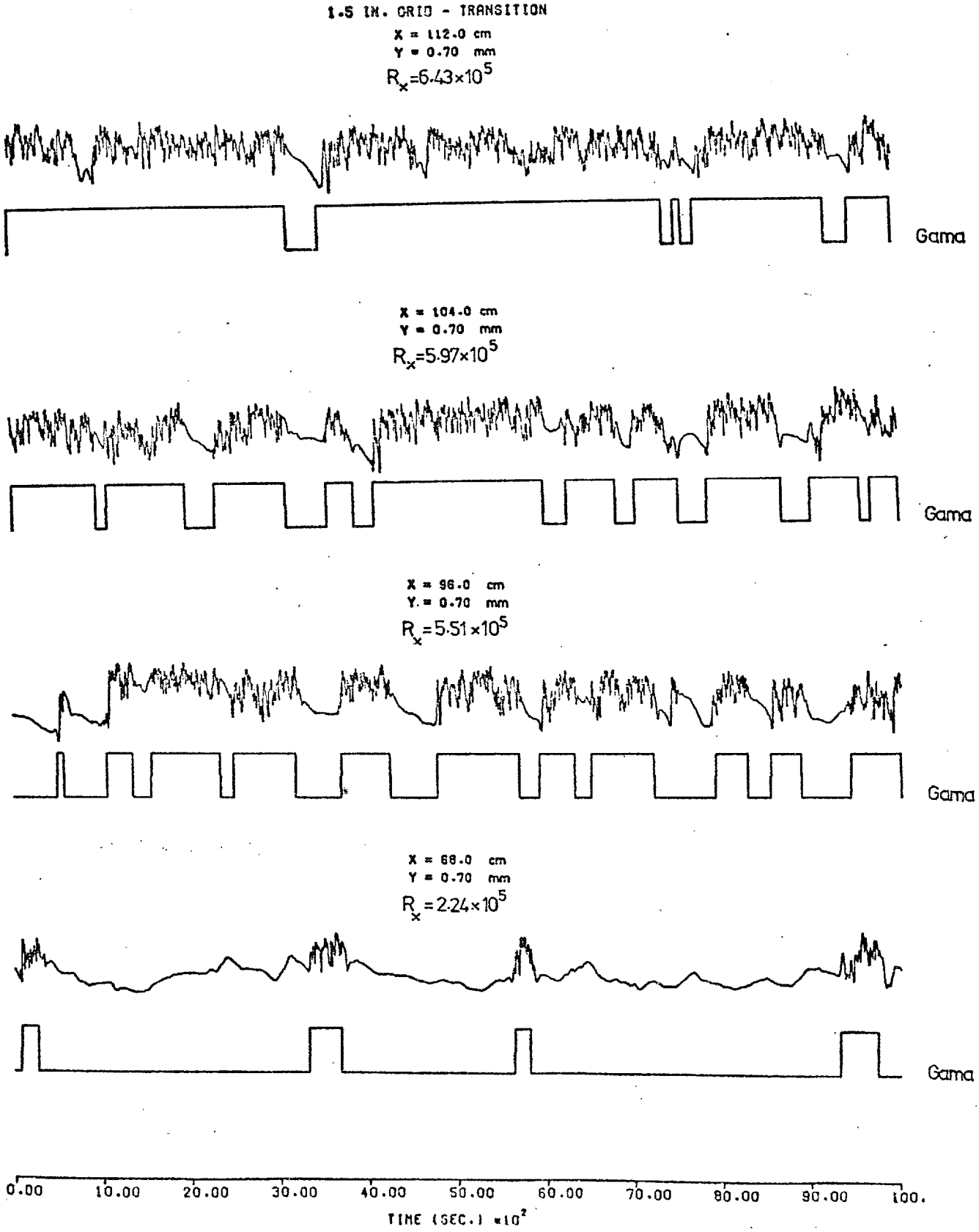
3.0 IN. GRID - TRANSITION

X = 36 cm

$R_x = 2.24 \times 10^5$

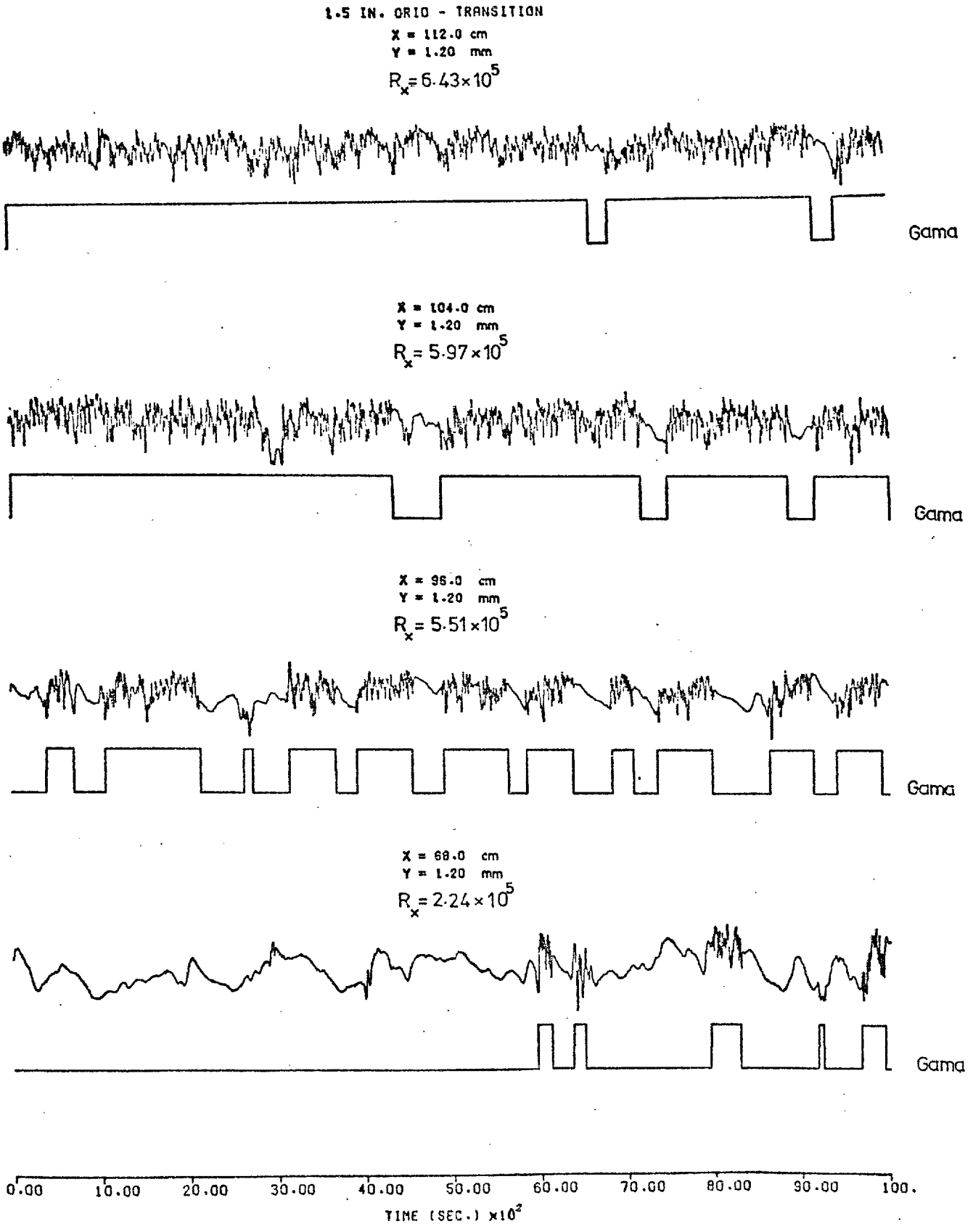
(For legend see fig. 7.1.A)

Fig. 7.2b



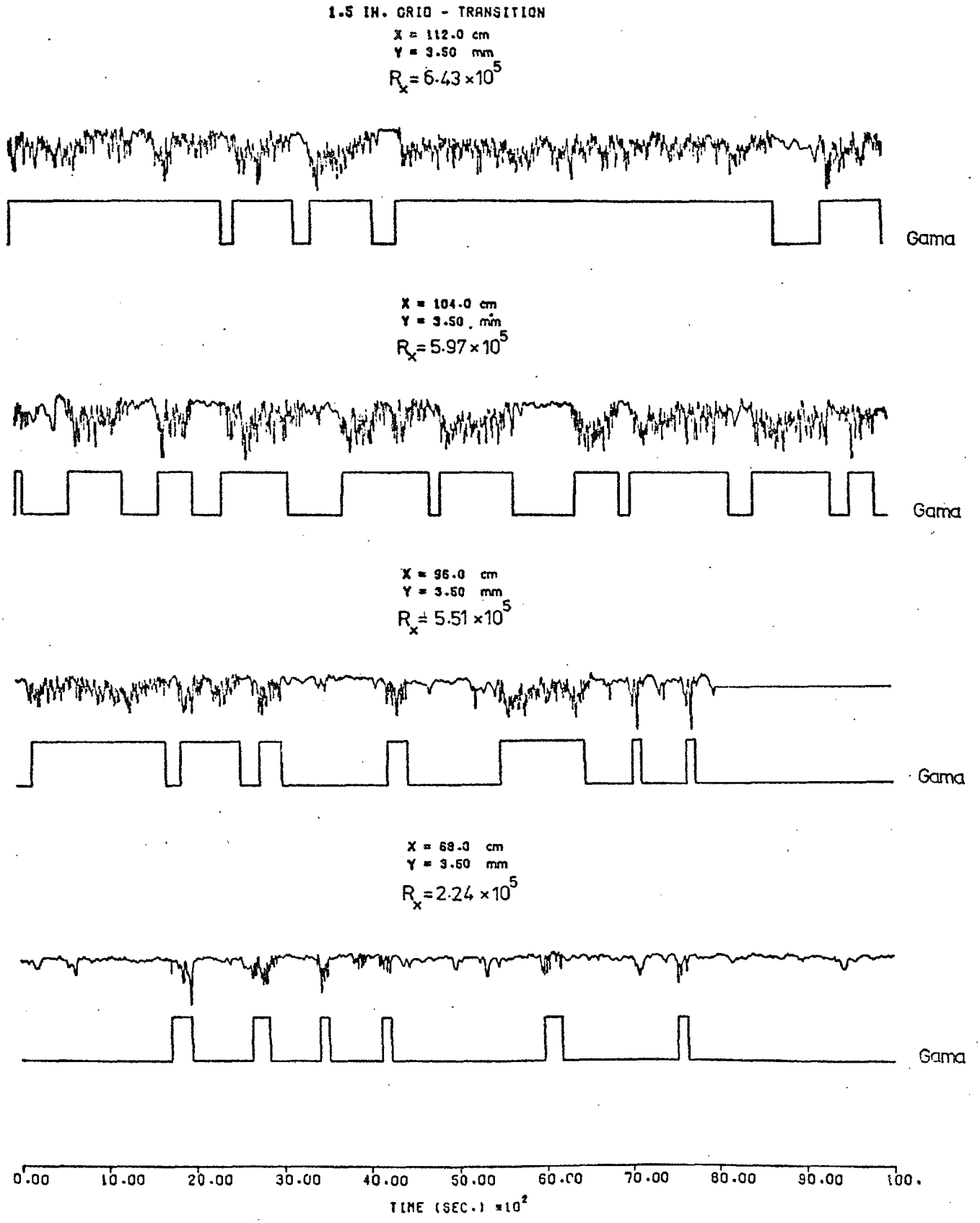
Bursting within the transition region (y=constant).

Fig. 7.3a



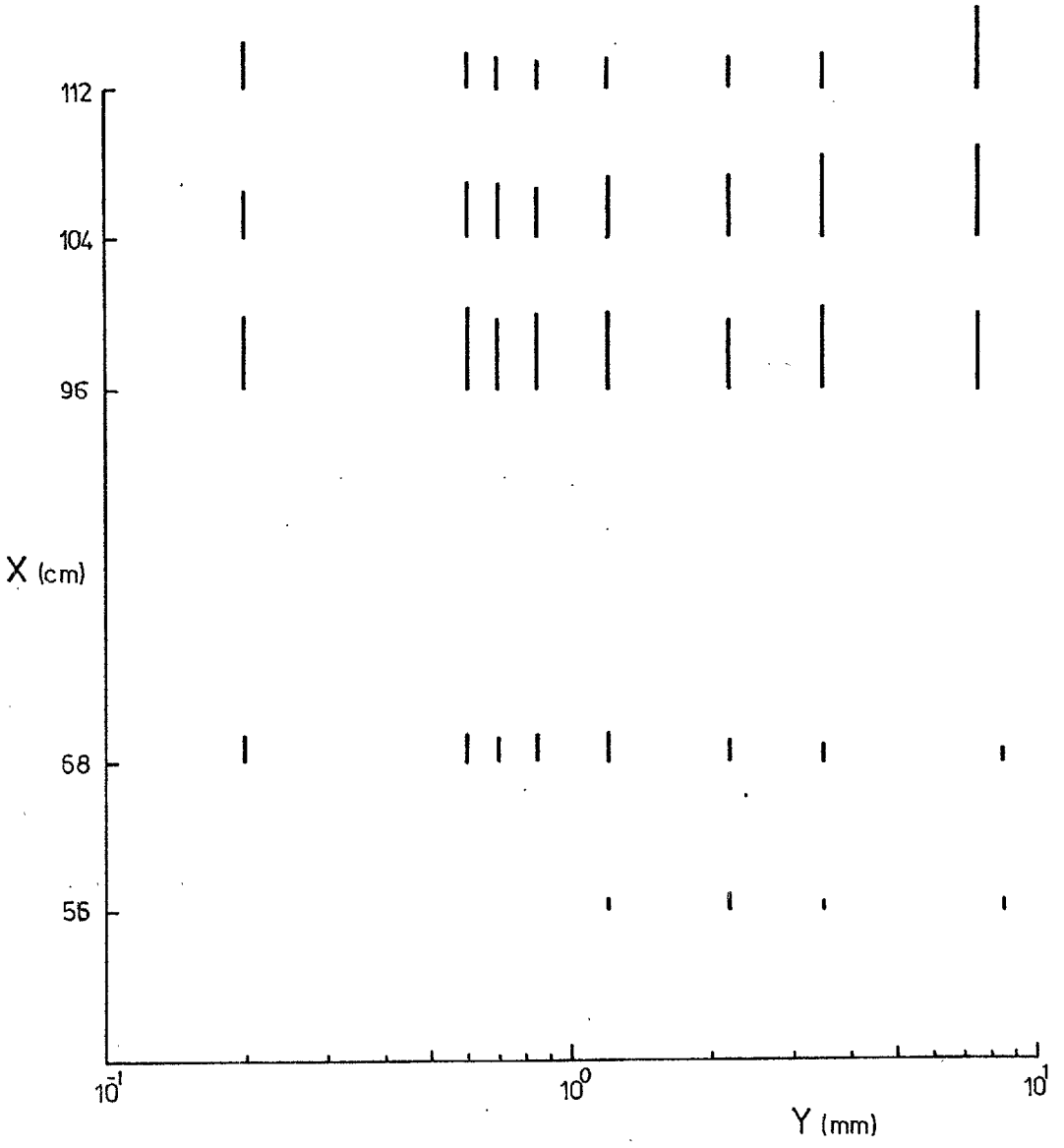
Bursting within the transition region (y=constant).

Fig. 7.3b



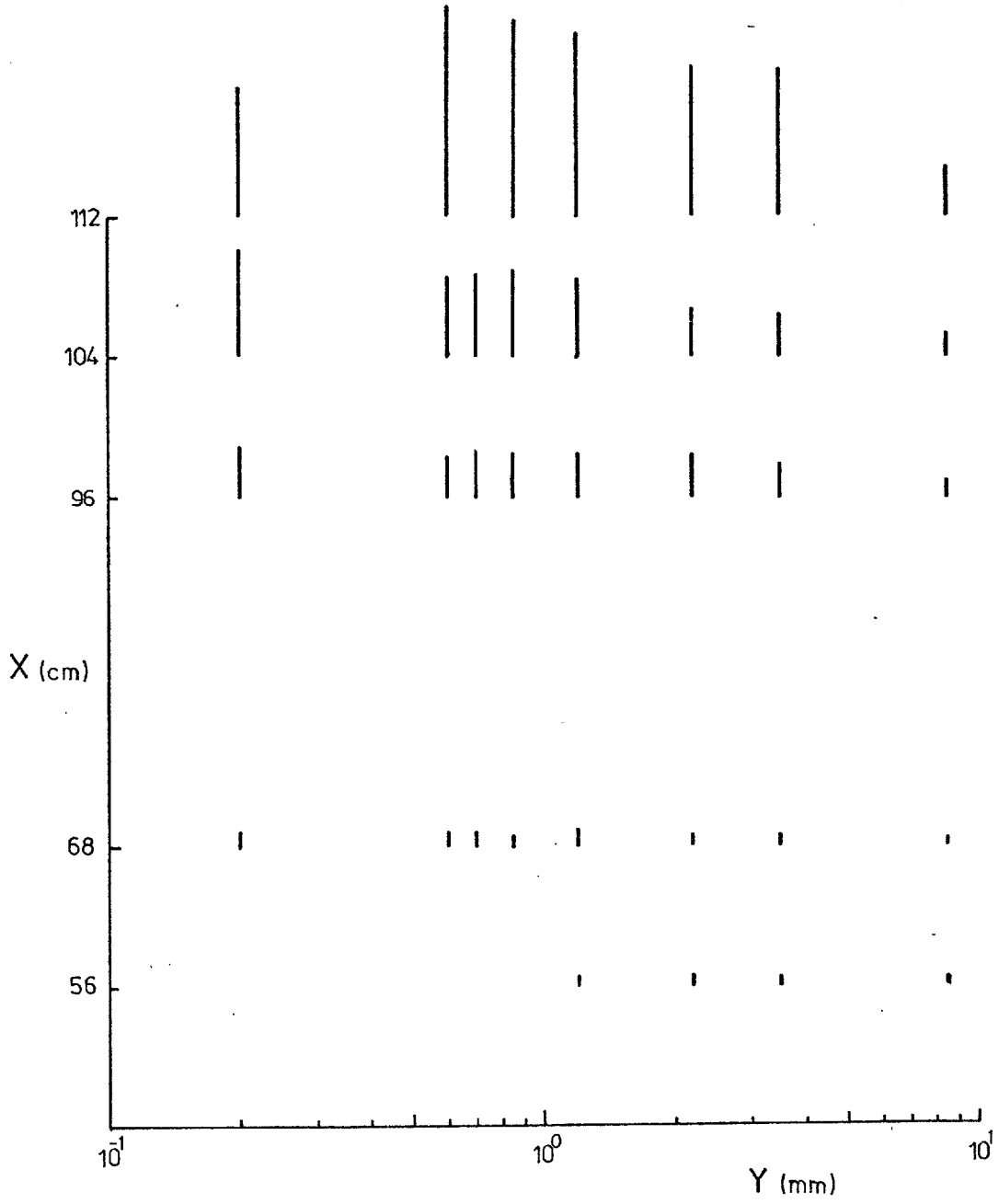
Bursting within the transition region (y=constant).

Fig. 7. 3c



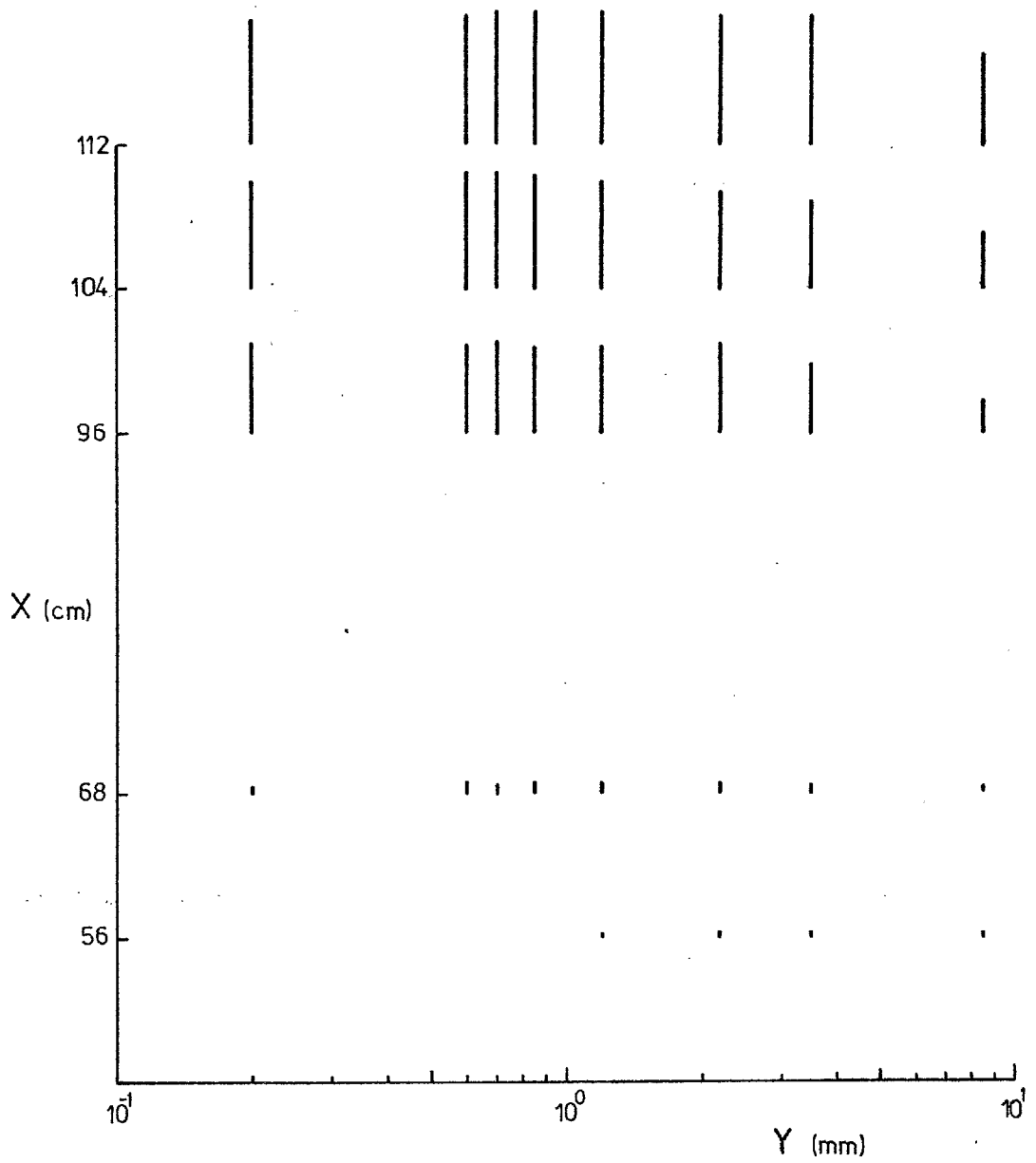
Relative rate of bursting within the transition region .

Fig. 7.4



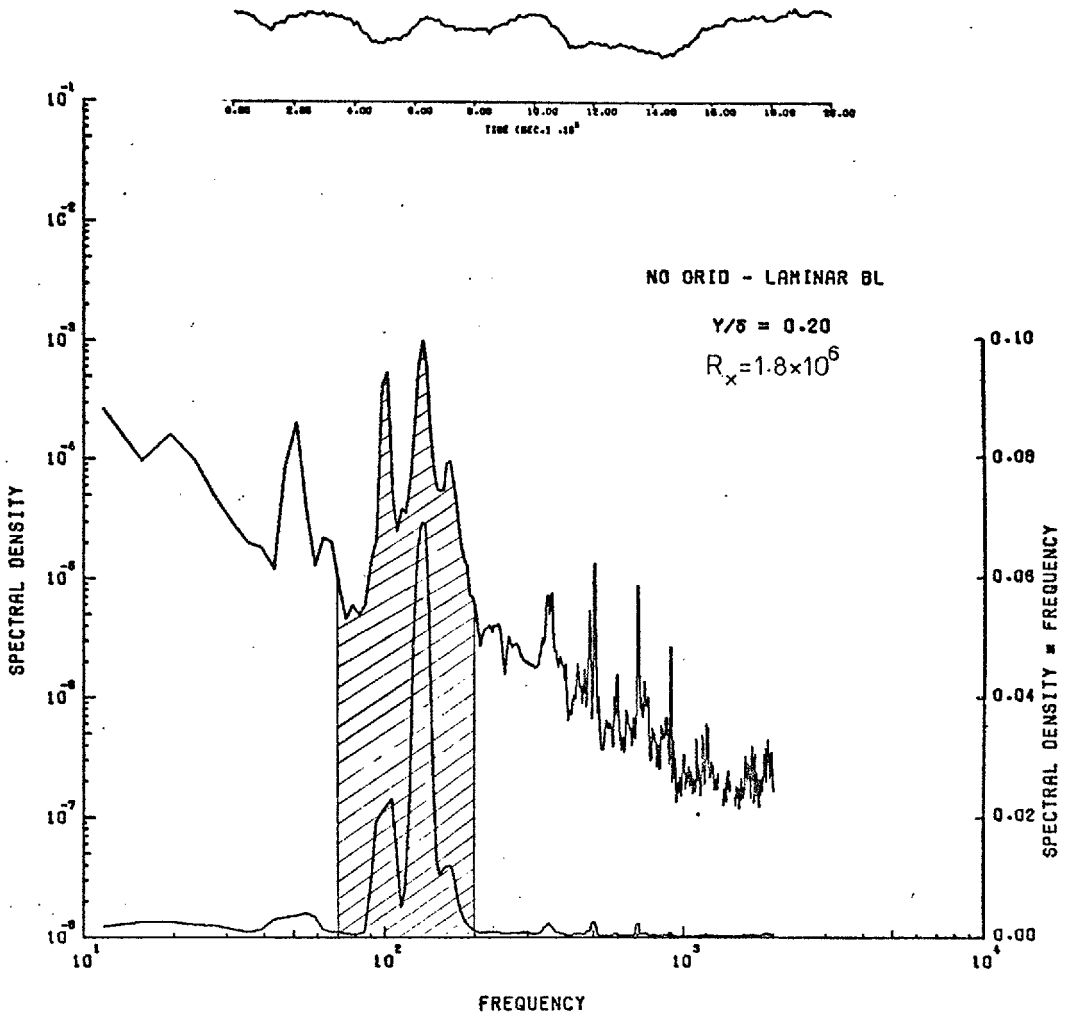
Relative width of the turbulent bursts within the transition region.

Fig. 7.5



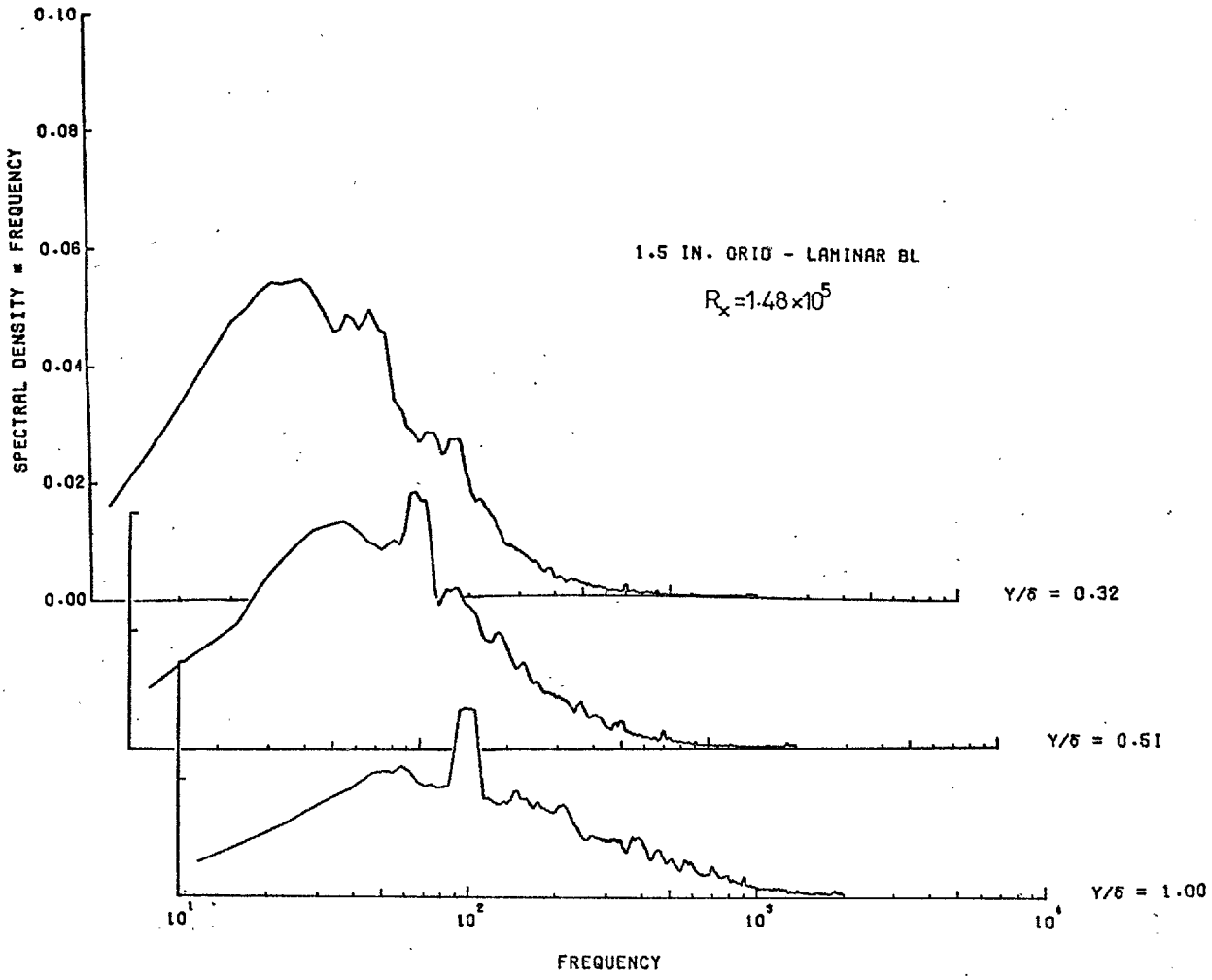
Burst intermittency within the transition region .

Fig. 7.6



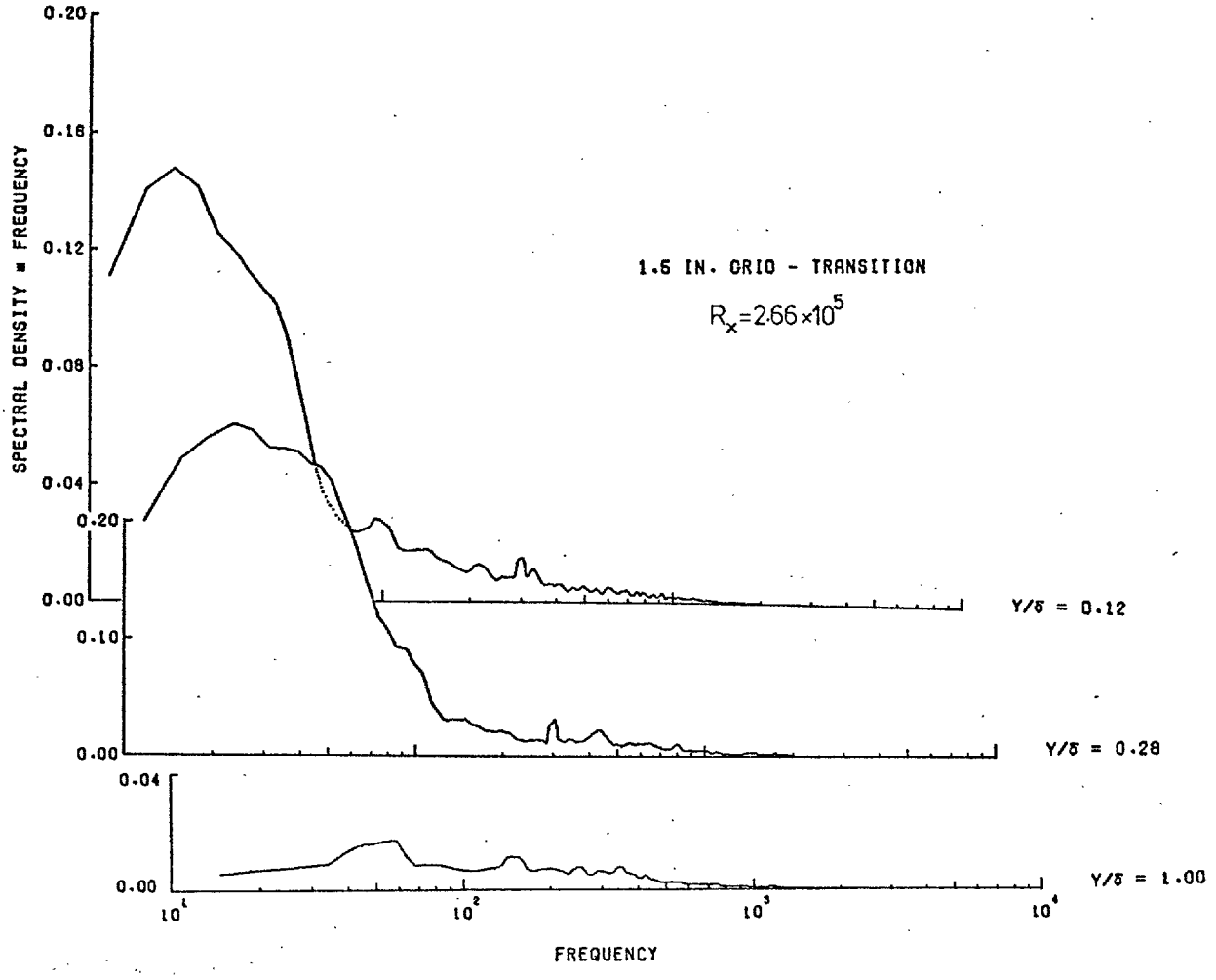
The spectrum of (u) for $\frac{\sqrt{\overline{u^2}}}{U}\Big|_\infty$=0.1% within the unstable laminar boundary layer .

Fig. 7.7



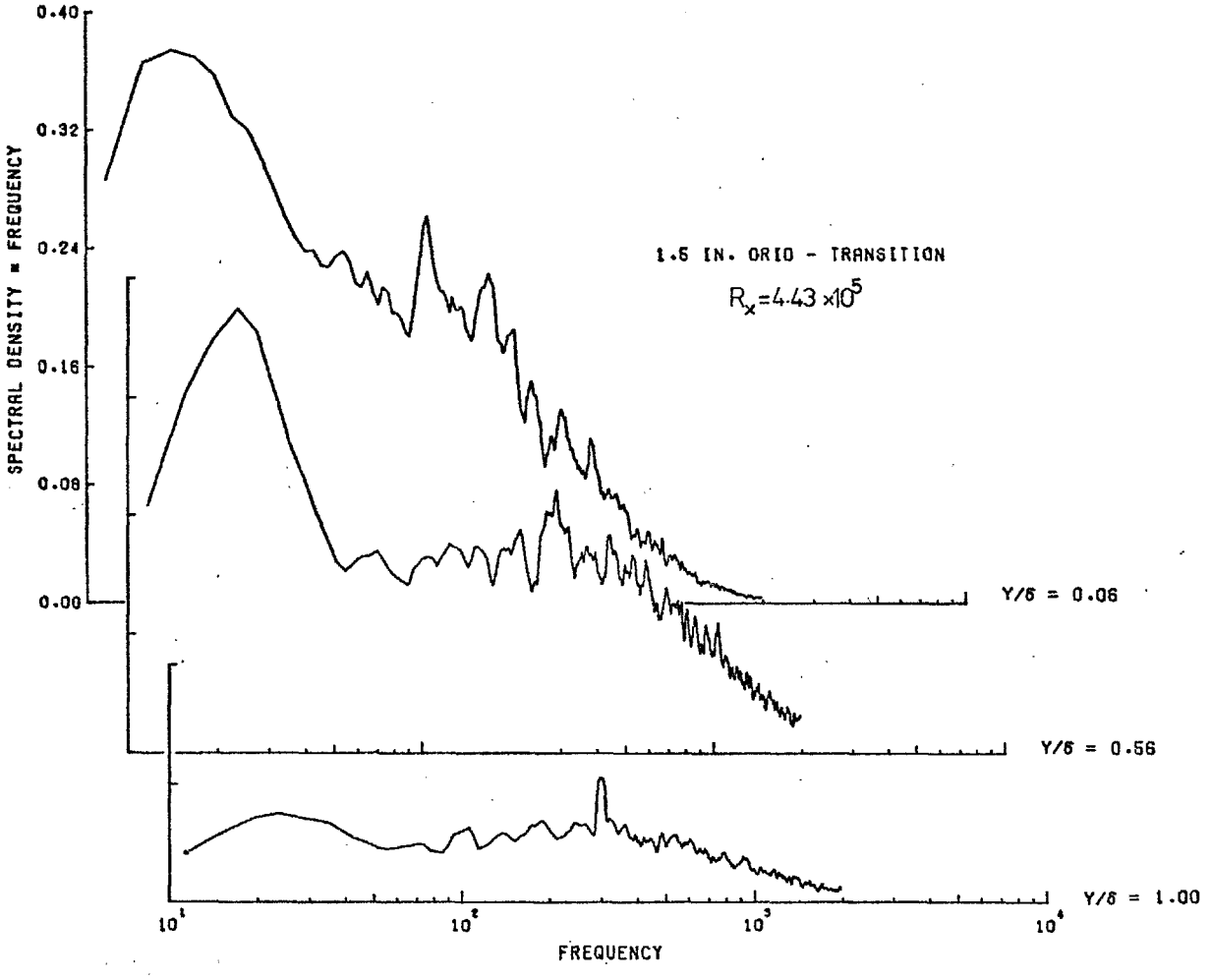
u-spectra within the laminar boundary layer at constant (X).

Fig. 7.8a



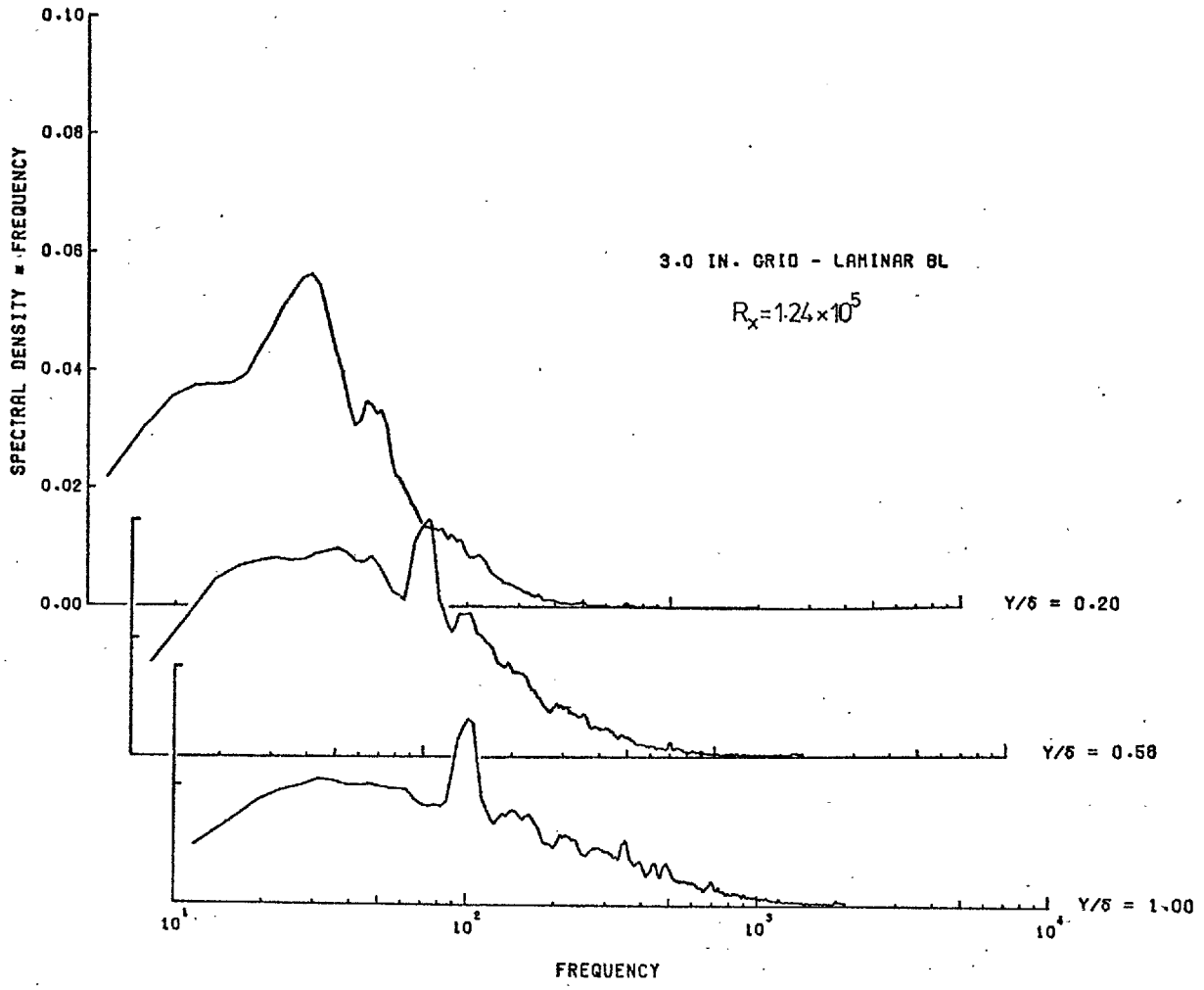
u-spectra at constant X (transition).

Fig. 7. 8b



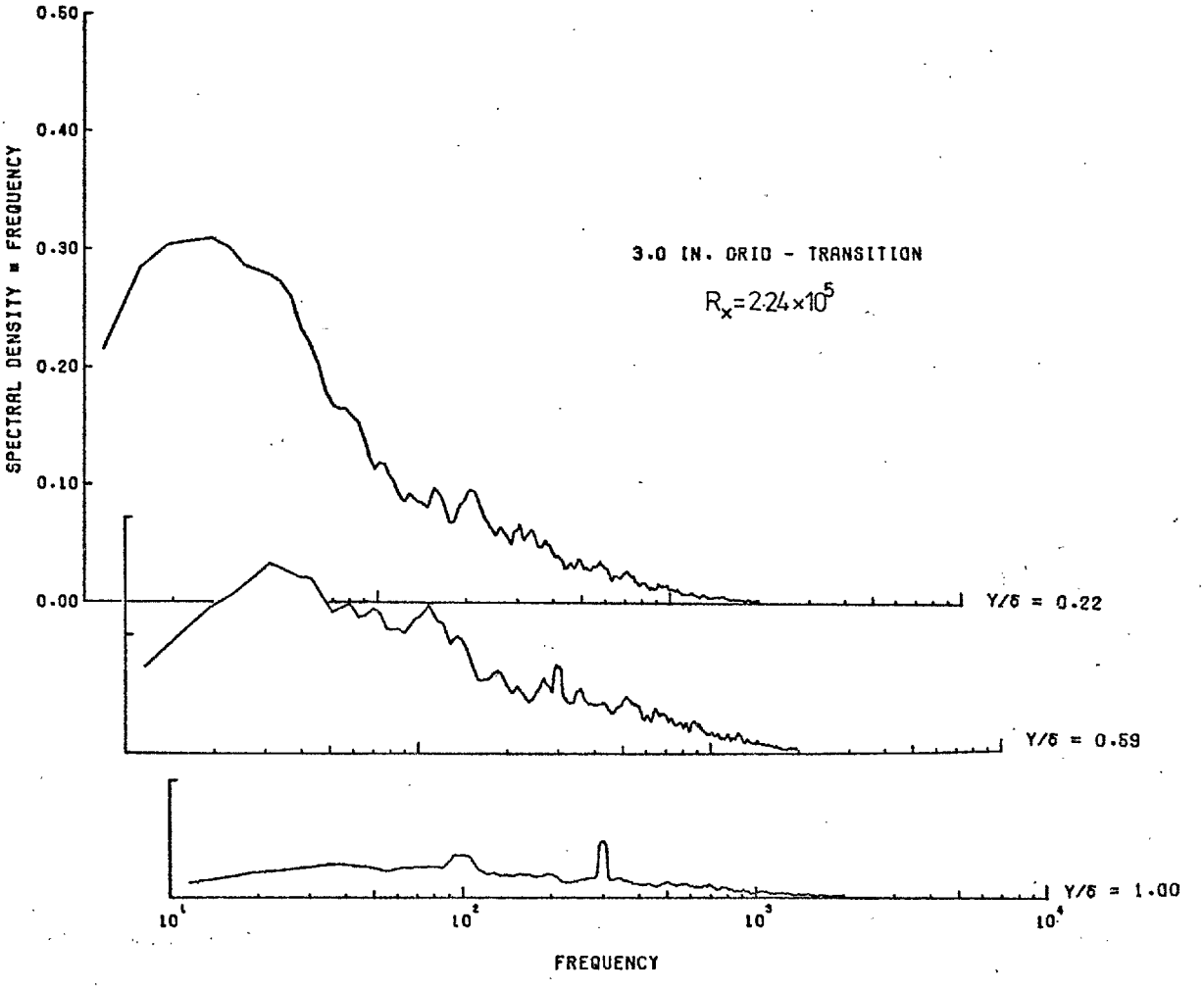
u-spectra at constant X (transition).

Fig. 7.8c



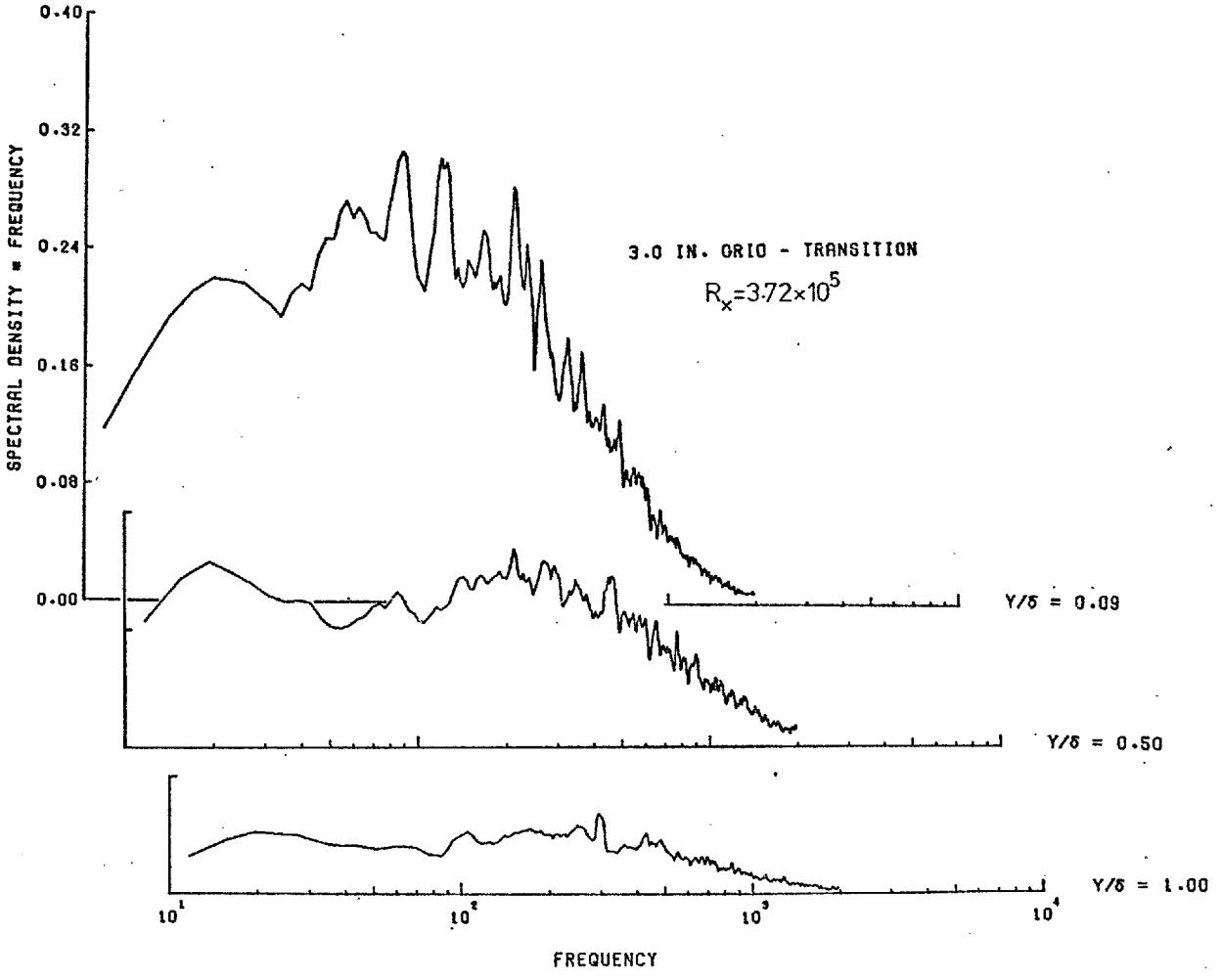
u-spectra within the laminar region at constant (X).

Fig. 7.9a



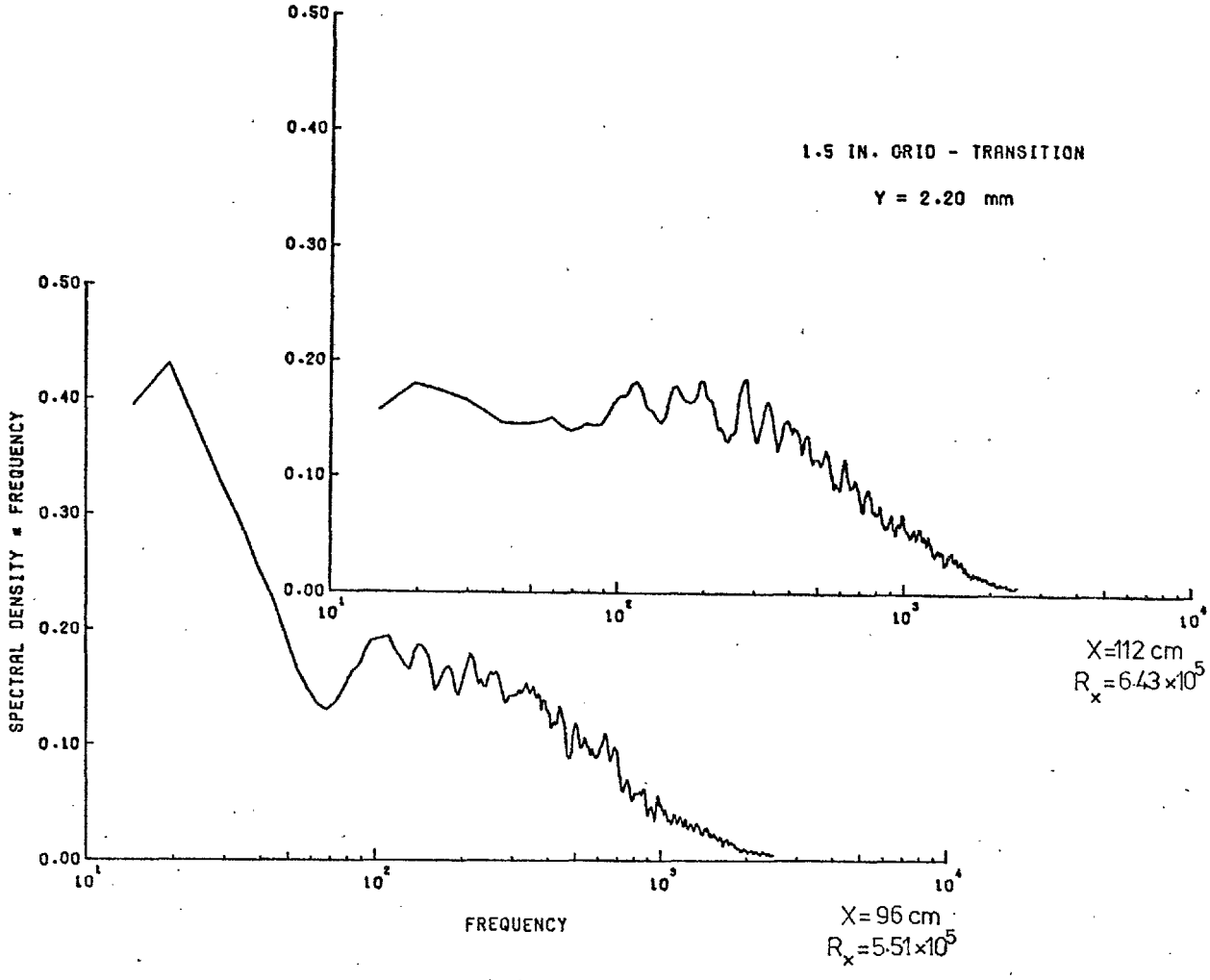
u-spectra at constant X (transition).

Fig. 7.9b



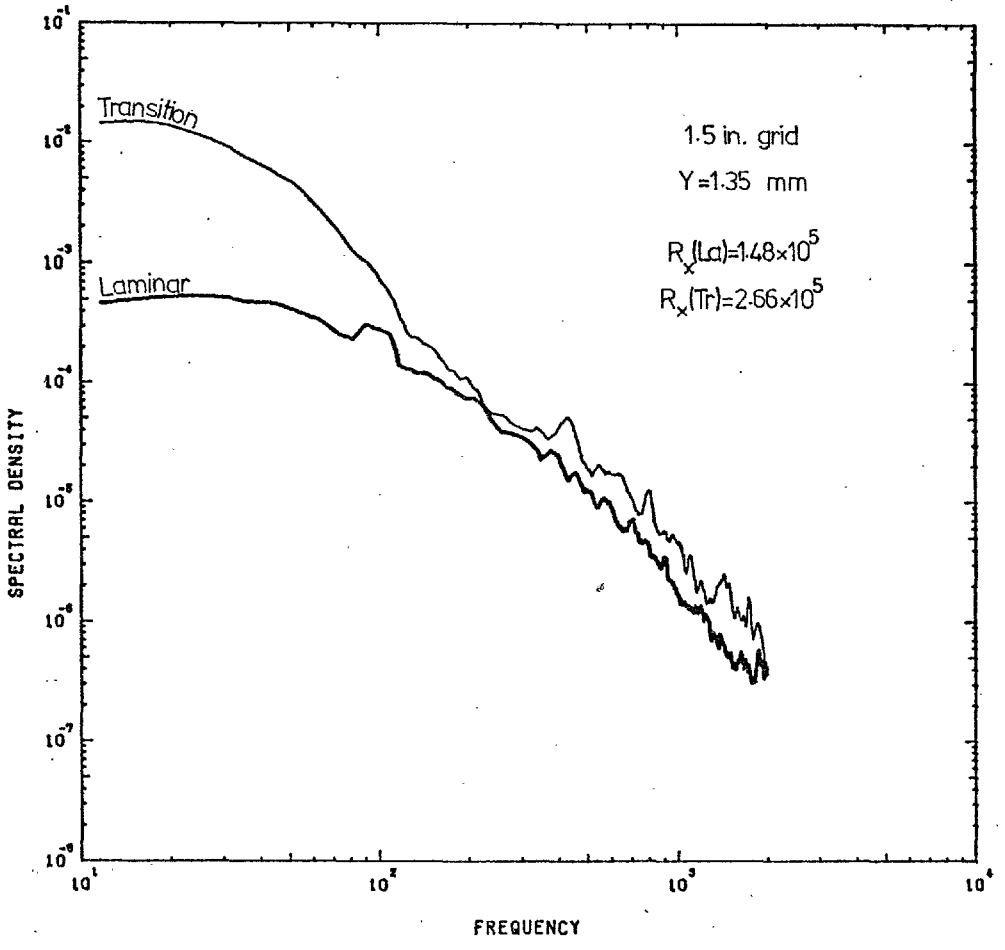
u-spectra at constant X (transition).

Fig. 7. 9c



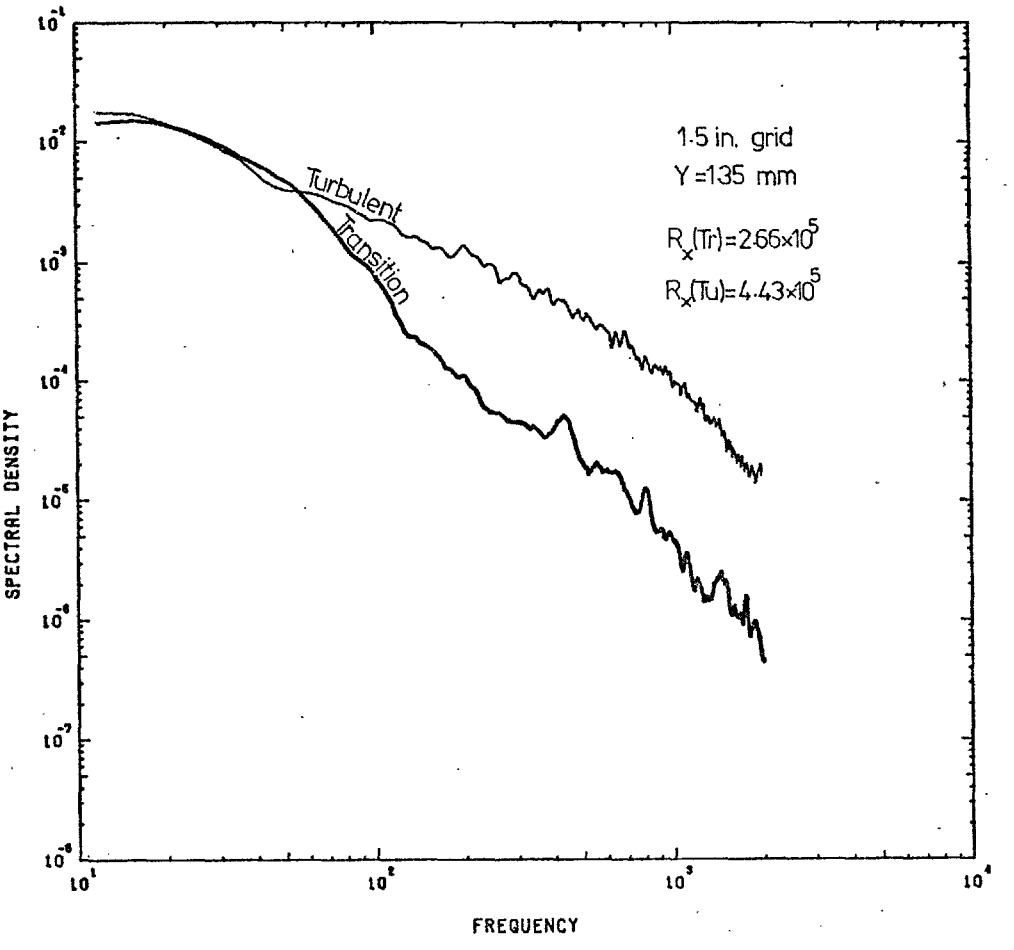
Evolution of the large scale motion inside the boundary layer near the end of transition.

Fig. 7.10



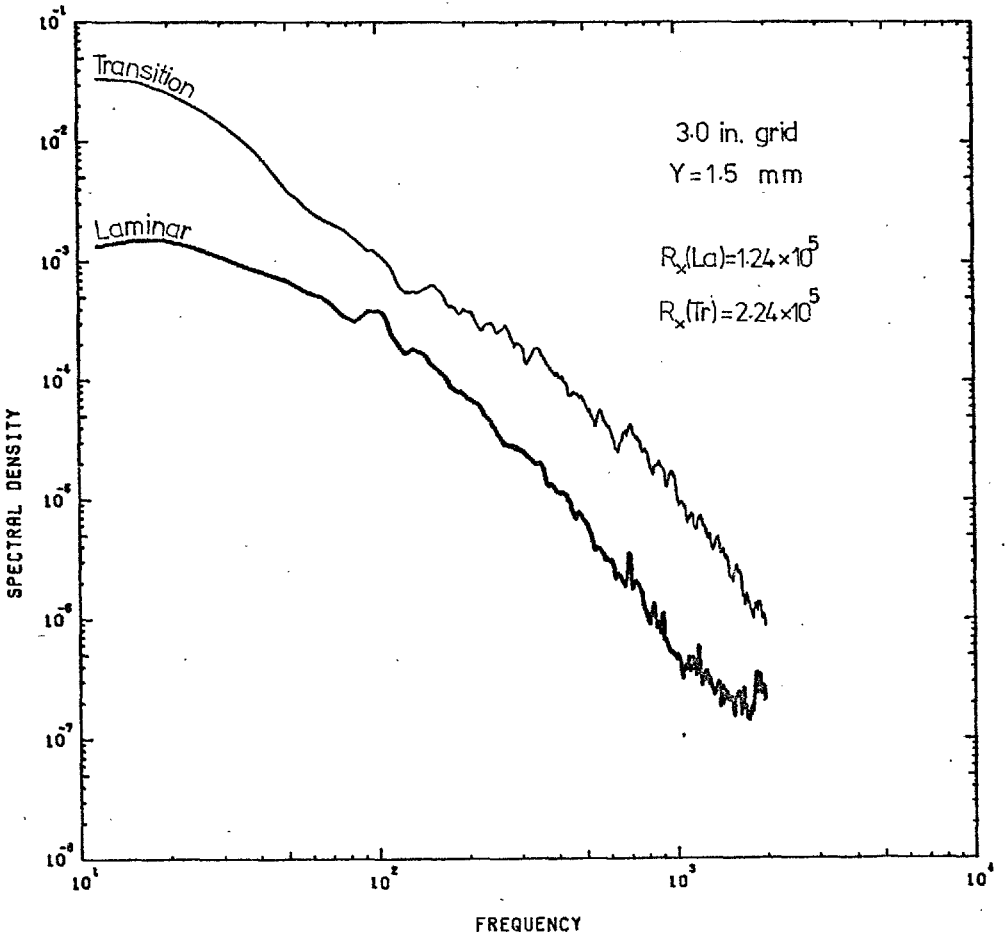
u-spectra at constant Y in the laminar and the transitional regions.

Fig. 7.11a



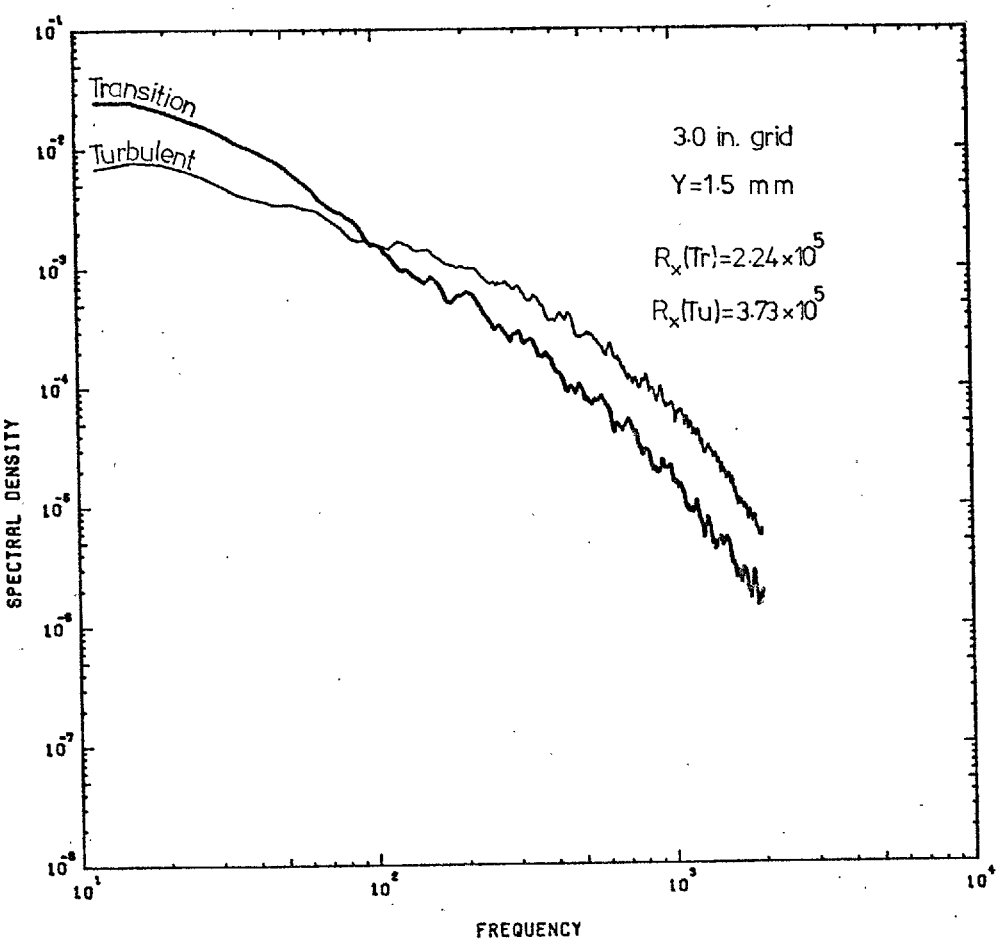
u-spectra at constant Y in the transitional and the turbulent regions.

Fig. 7.11b



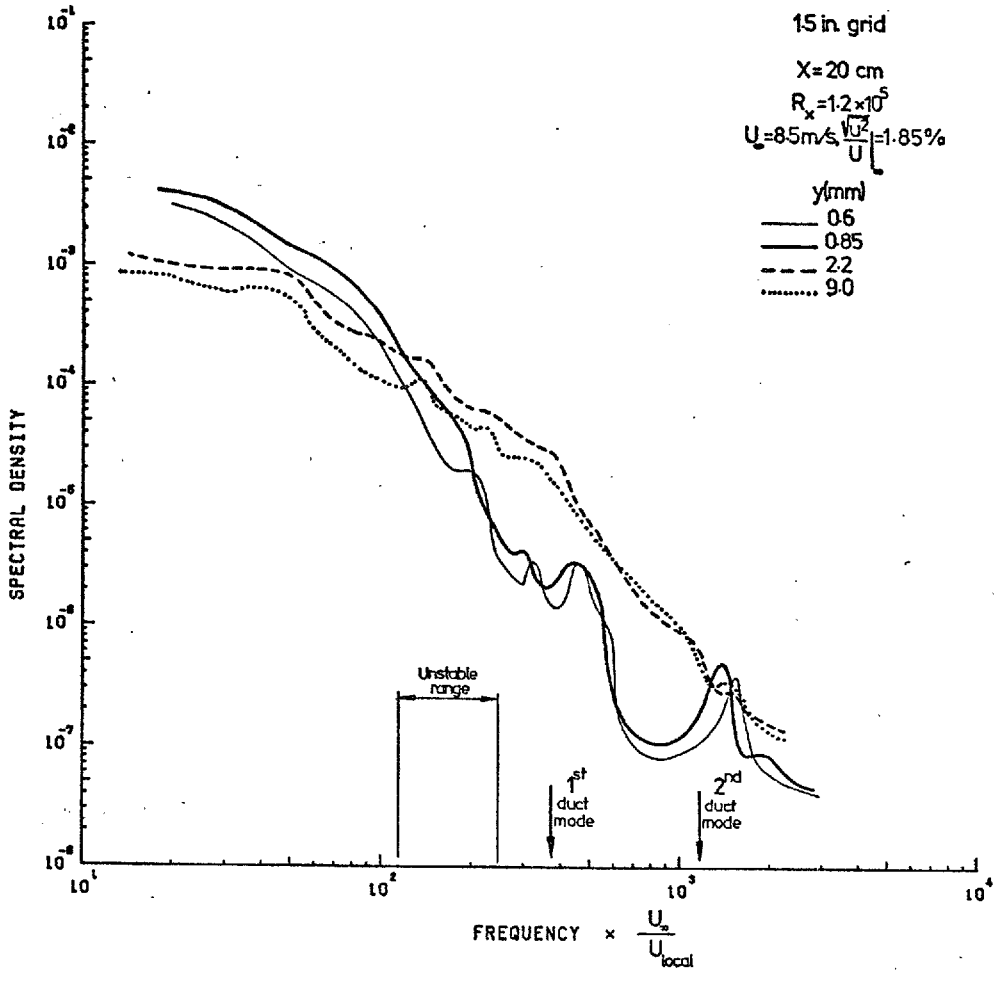
u-spectra at constant Y in the laminar and the transitional regions .

Fig. 7.12a



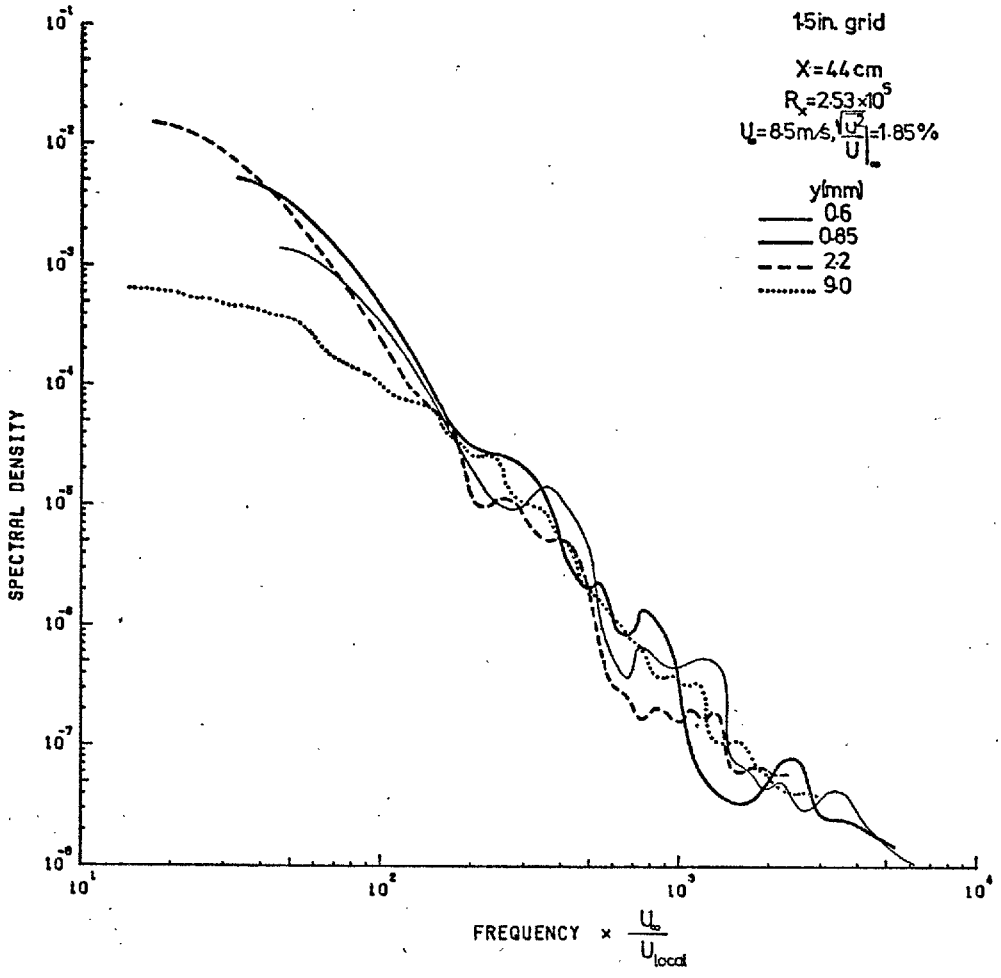
u-spectra at constant Y in the transitional and the turbulent regions.

Fig. 7.12b



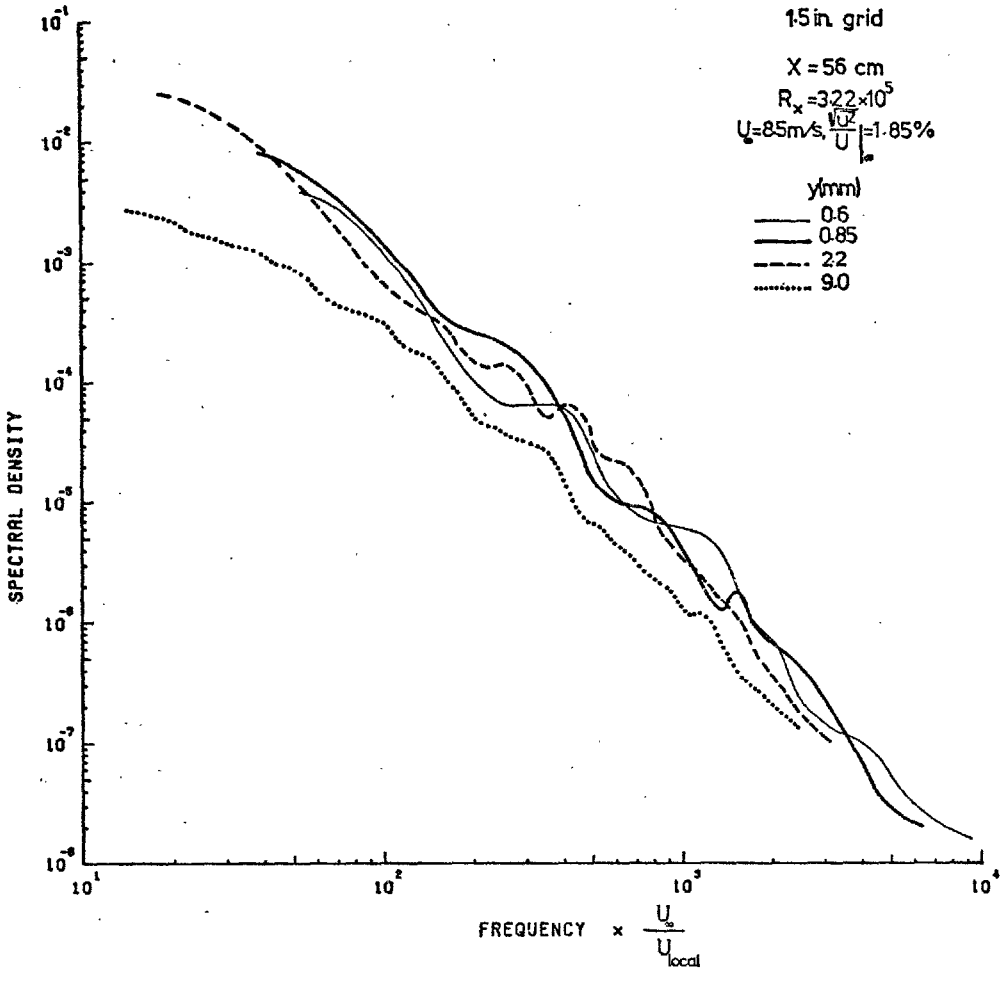
u-spectra at constant X (taking $U_c = U_{local}$)

Fig. 7.13a



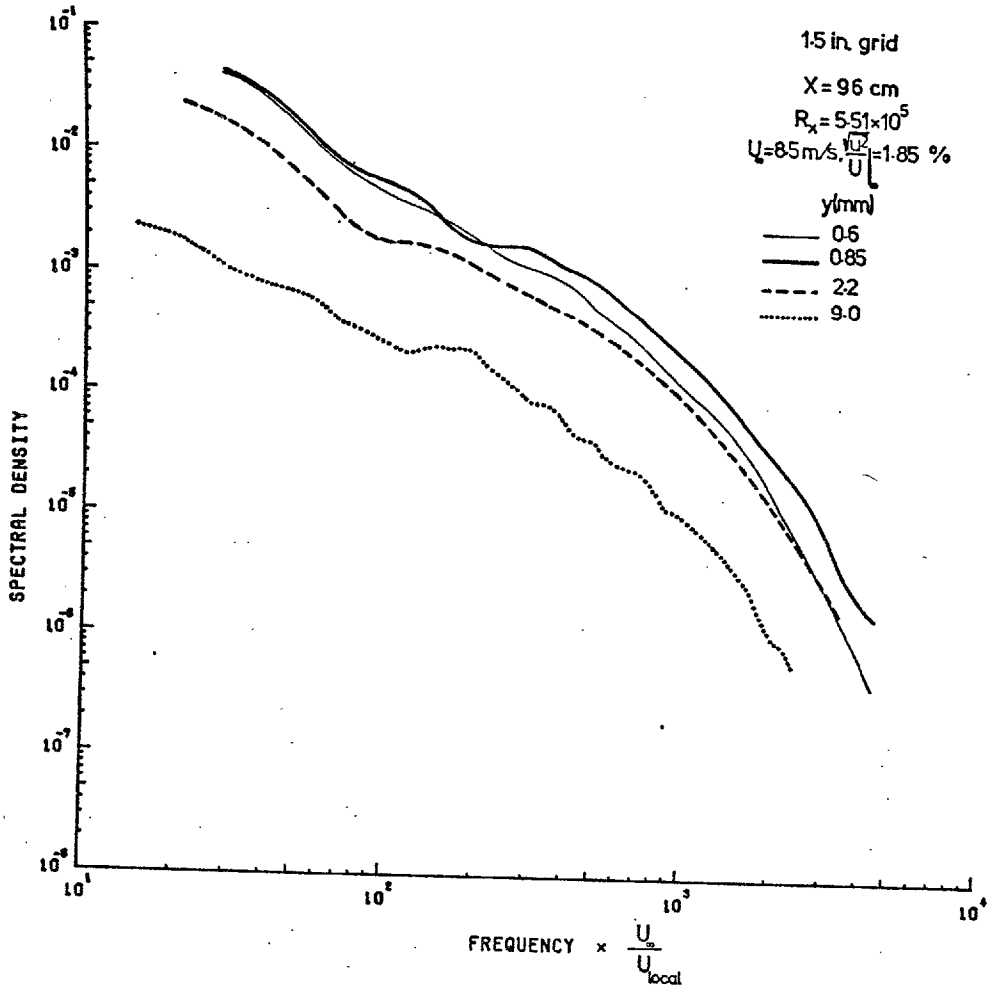
u-spectra at constant X (taking $U_c = U_{local}$)

Fig. 7.13b



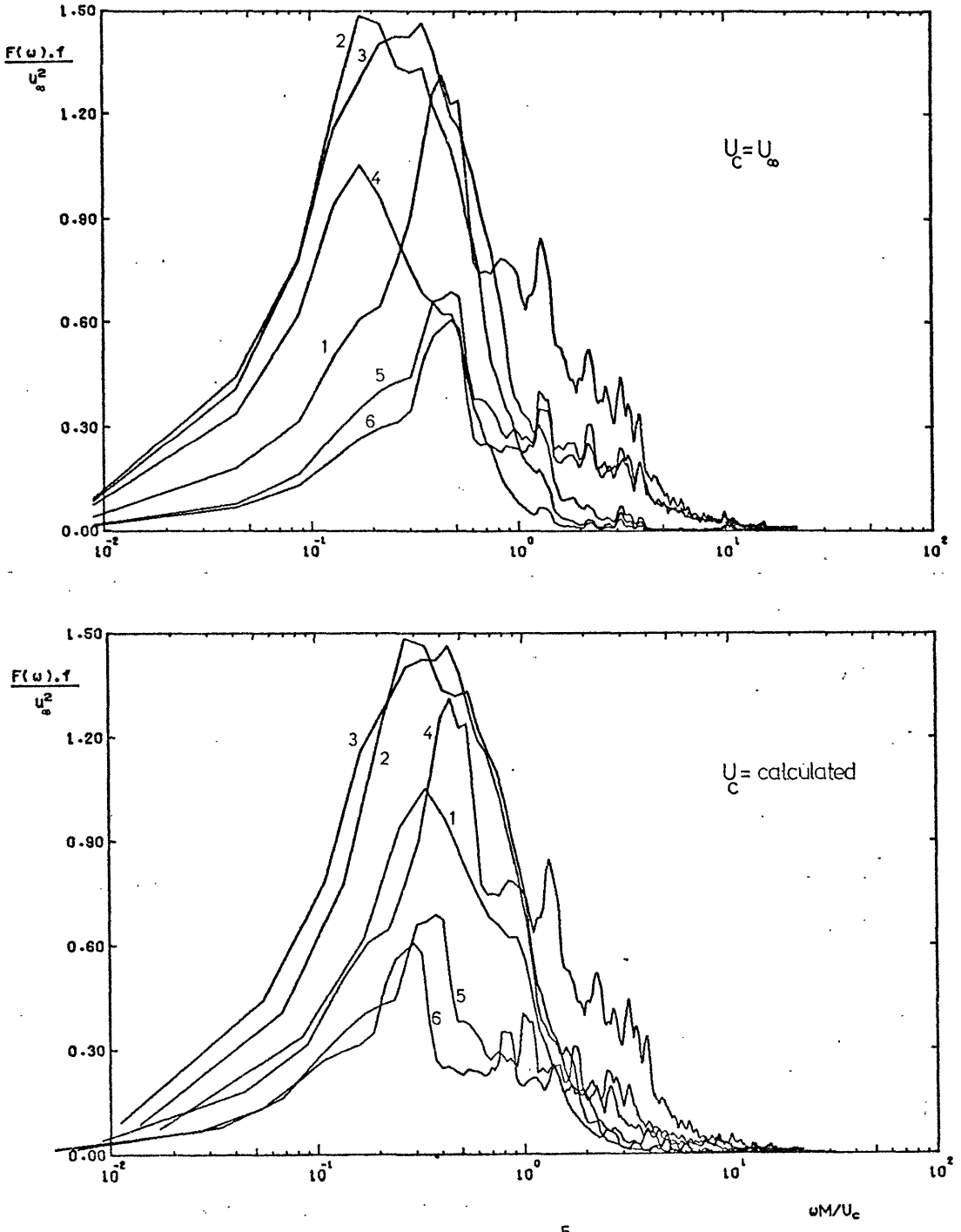
u-spectra at constant X (taking $U_c = U_{local}$)

Fig. 7.13c



u-spectra at constant X (taking $U_c = U_{local}$)

Fig. 7.13d

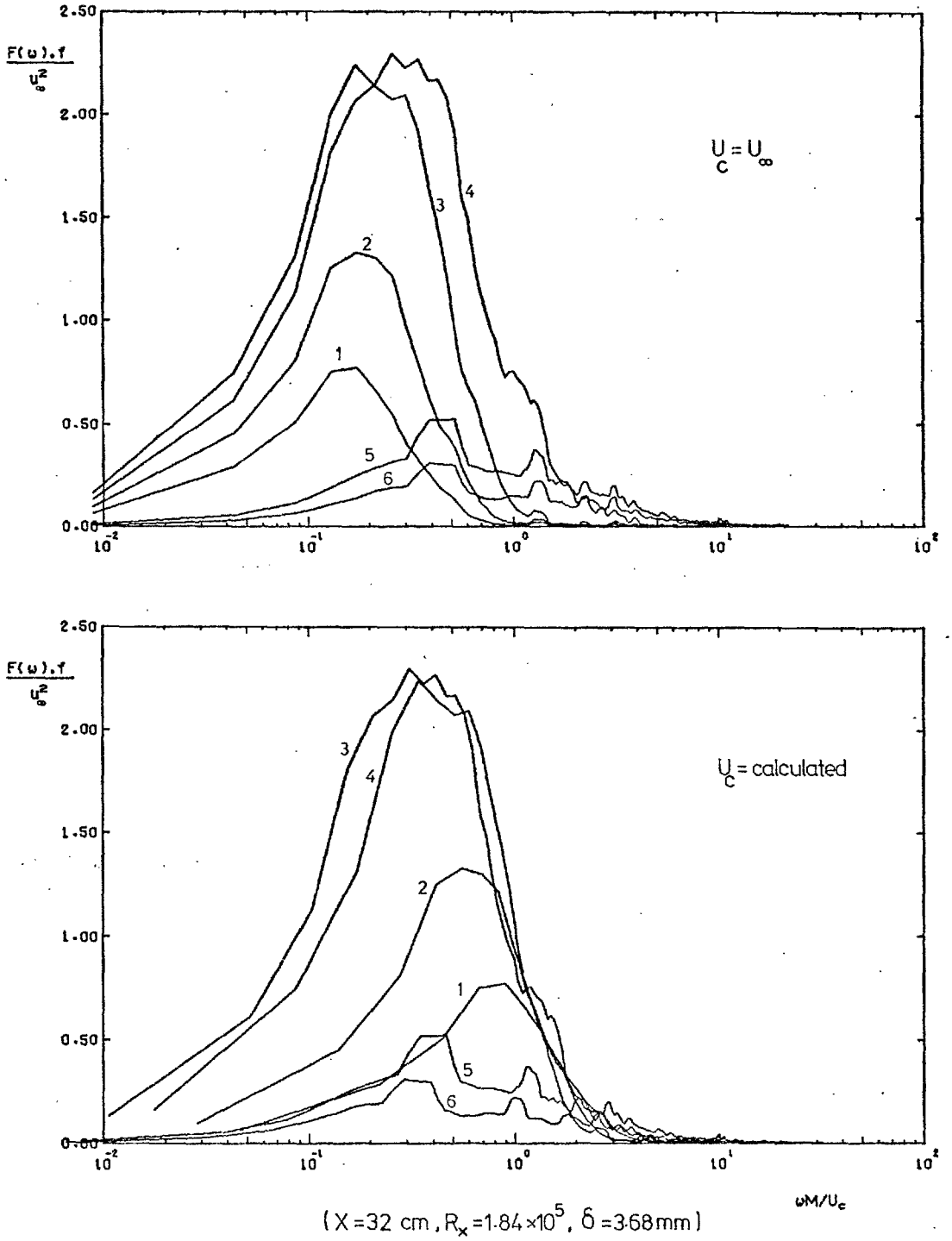


(X = 20 cm , $R_x = 1.2 \times 10^5$, δ = 2.32 mm)

u-spectra at constant X corrected for the differences in the convection speed ($U_c(\omega)$)

	y(mm)
1	0.6
2	0.85
3	1.2
4	2.2
5	9.0
6	17.0

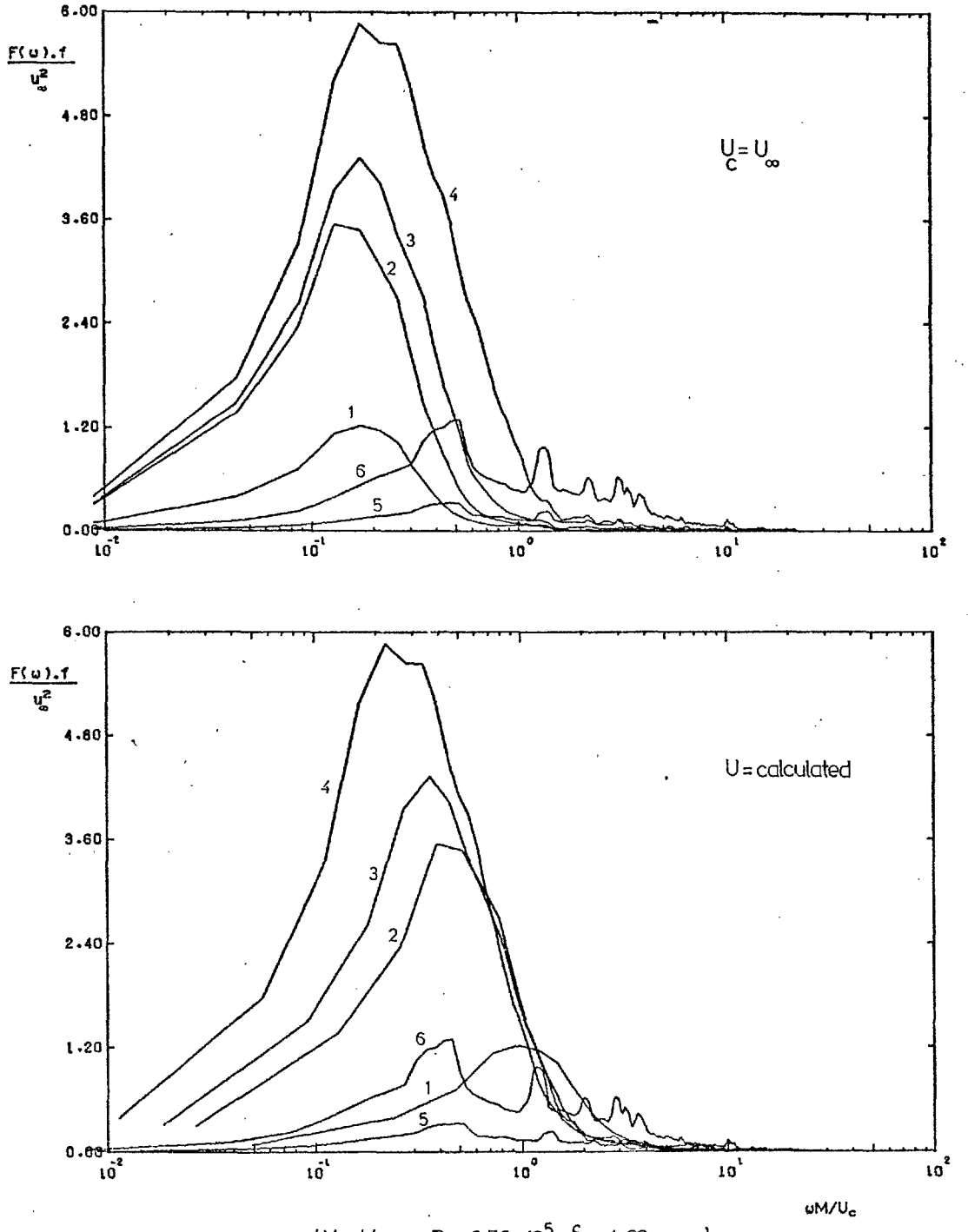
Fig. 7.14a



(X = 32 cm , $R_x = 1.84 \times 10^5$, $\delta = 3.68$ mm)

(For legend see fig. 7.14.a)

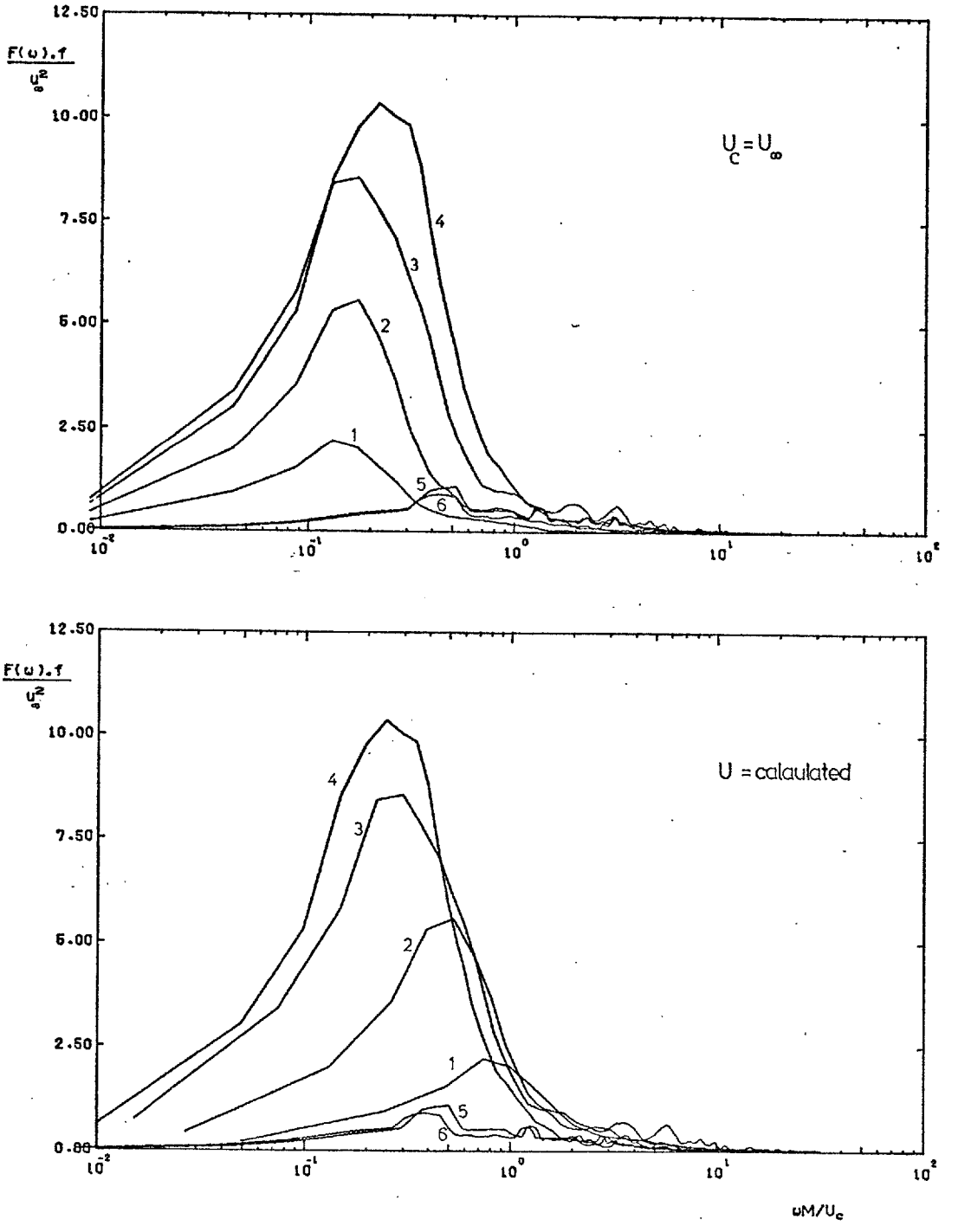
Fig. 7.14b



(X = 44 cm , $R_x = 2.53 \times 10^5$, δ = 4.62 mm)

(For legend see fig. 7.14.a)

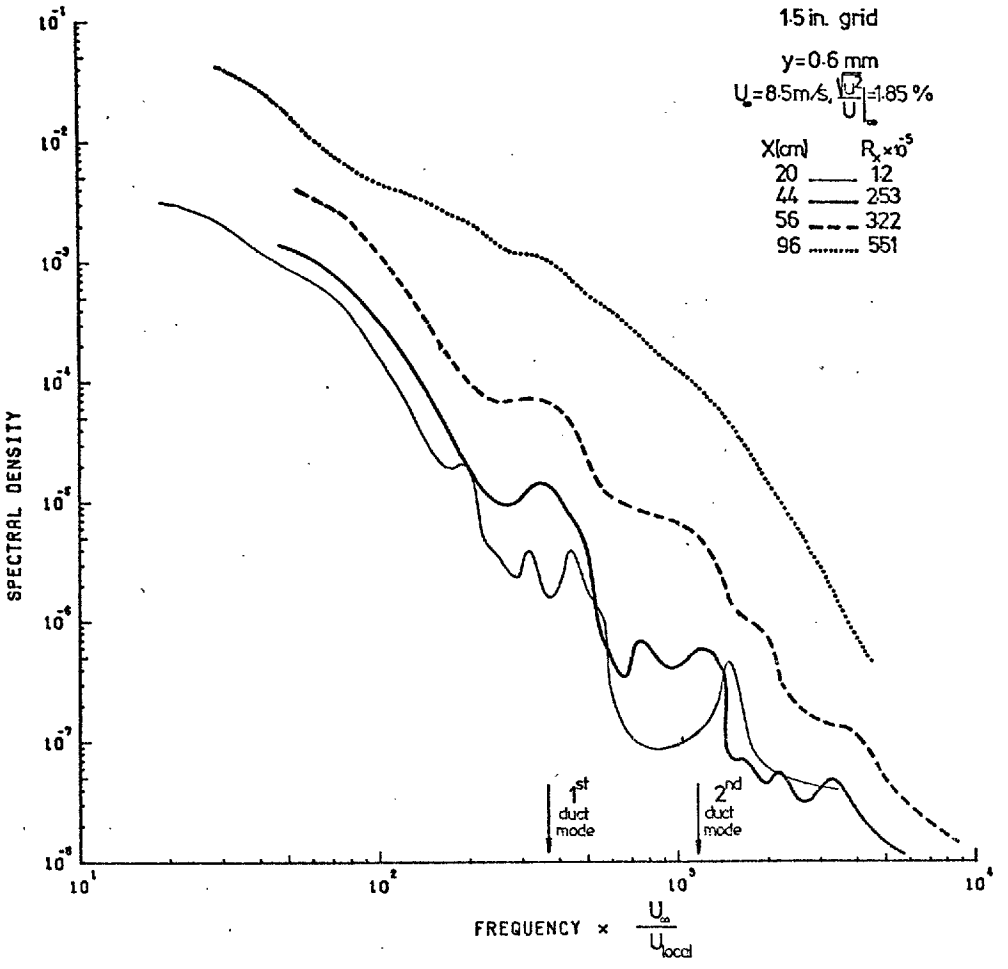
Fig. 7.14c



(X = 56 cm , $R_x = 3.22 \times 10^5$, δ = 7.35 mm)

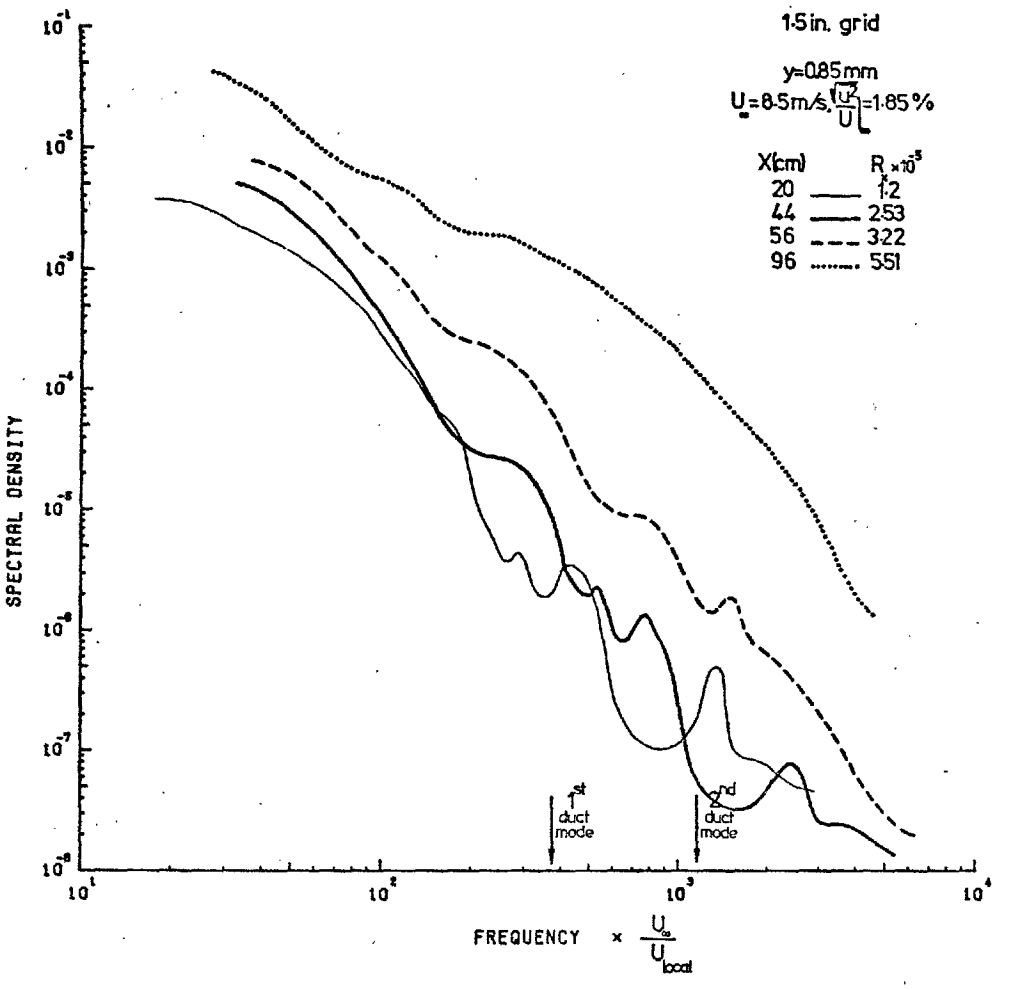
(For legend see fig. 7.14.a)

Fig. 7.14d



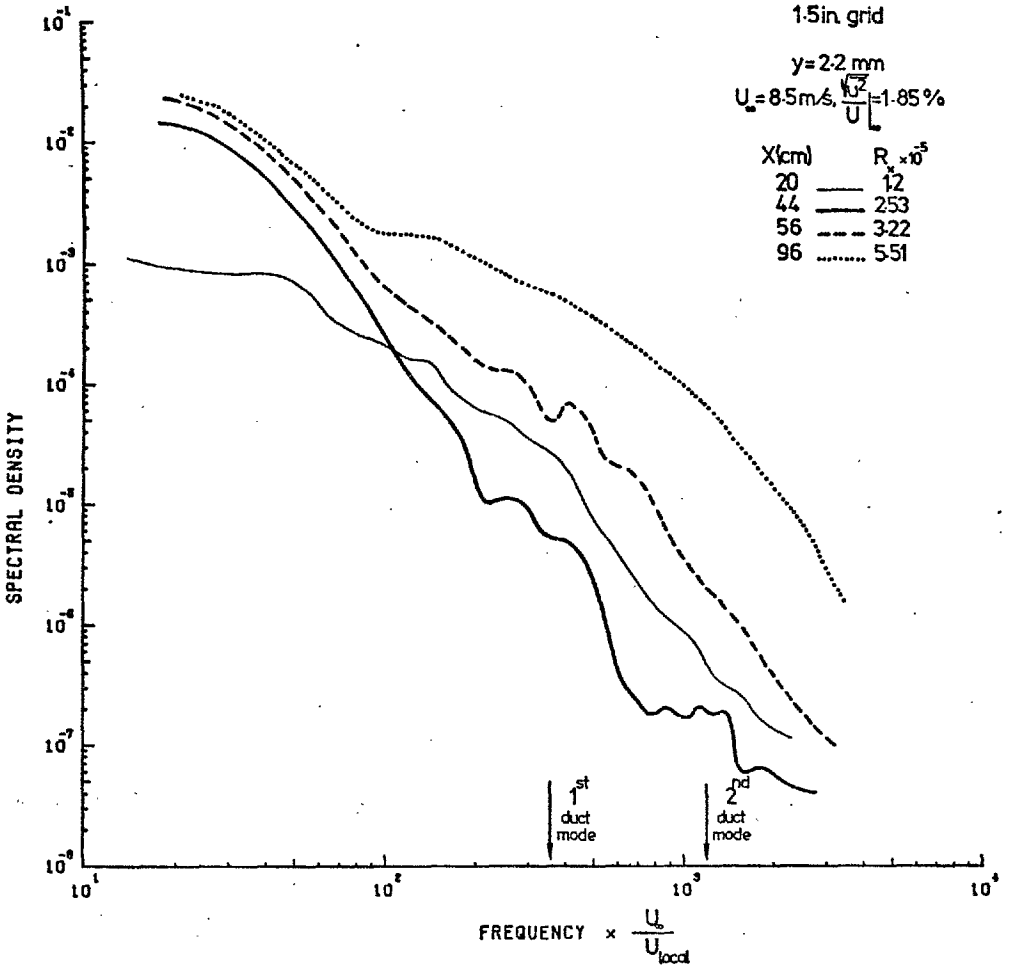
u-spectra inside the boundary layer at constant (y)

Fig. 7.15a



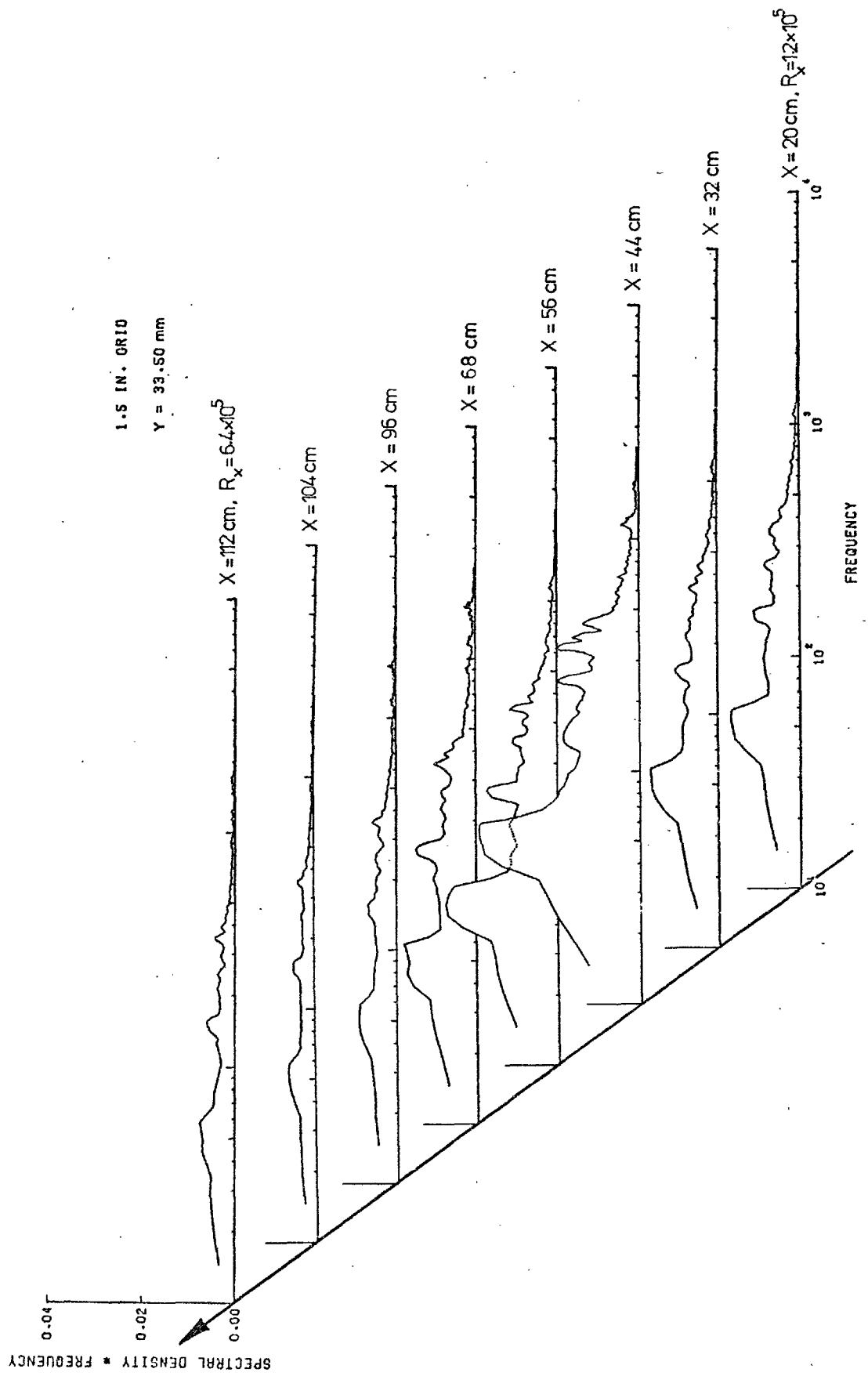
u-spectra inside the boundary layer at constant (y).

Fig. 7.15b



u-spectra inside the boundary layer at constant (y)

Fig. 7.15c



u-spectra outside the boundary layer at constant (y).

Fig. 7.16